

# Chiroptically-Active Quantum Nanostructures



**Trinity College Dublin**  
Coláiste na Tríonóide, Baile Átha Cliath  
The University of Dublin

A thesis submitted to the School of Chemistry,  
Trinity College, the University of Dublin,  
for the degree of Doctor of Philosophy

Alexander Loudon

Under the supervision of Professor Yurii K. Gun'Ko

December 2017

# Abstract

In this research a wide variety of fluorescent nanoparticles have been synthesised and analysed through the lens of optical activity and potential chiroptical applications. Cadmium and cadmium-free fluorescent nanoparticles were synthesised using a range of synthetic approaches including aqueous co-precipitation, hot-injection and heating up techniques. While the majority of the particles analysed in this research were spherical (quantum dots), efforts were taken to produce several different shapes such as nanoplatelets, dot-in-rods and nanotetrapods.

Using ligand exchange techniques, and the inclusion of chiral stabilising ligands in the synthesis of these particles, optical activity was induced and subsequently analysed using circular dichroism spectroscopy. The resultant chiral nanoparticles were tested for potential applications in a series of experiments including enantio-cytotoxicity, enantioselective quenching, and enantioselective biological imaging.

While producing particles which demonstrated ligand induced optical activity was the primary focus of this research, many of the tested applications demonstrated clear differences in the behaviour of nanoparticles stabilised with opposite enantiomer ligands.

# Summary

Chapter 1 of the thesis provides the introduction and describes the background theory and literature review relevant to quantum dot research.

Chapter 2 provides experimental details for all procedures including the protocols of synthesis and modification of quantum nanostructures, the methods used and the sample preparations for characterisation. It also describes principles of the main instrumental characterisation techniques and relevant equipment used in this research.

Chapter 3 is dedicated to the development and characterisation of new cadmium free chiral ZnS and ZnS:Mn quantum dots. It explores the development of ligand exchange processes to exchange the lipophilic organic ligands for biocompatible water soluble chiral ligands such as cysteine and penicillamine and studies of their optical properties. In addition, glutathione capped ZnSe QDs were synthesised in the aqueous phase and were tested for enantioselectivity when using D- and L-penicillamine as a quenching molecule.

Chapter 4 presents the synthesis and characterisation of new optically active anisotropic quantum nanostructures such as luminescent CdSe-CdS dot in rods and CdSe-CdS tetrapods. The 1- $\beta$ -D-thioglucose functionalised dot in rods were subsequently used for chiral sensing of Naproxen enantiomers.

Chapter 5 describes the preparation of chiroptically active CdS QDs and 2D CdSe nanostructures. The synthetic approaches involved: firstly, a 1 step aqueous synthesis and secondly, a two-step process using initial hot injection synthesis followed by a ligand exchange. The chiroptical properties of these materials were then examined. Chapter 5 also reports the synthesis of CdSe nanoplatelets of various thicknesses. These nanoplatelets were transferred into the aqueous phase using chiral ligands and their optical activity was investigated.

Chapter 6 describes the exploration of selected applications of some of our chiral quantum dot based nanomaterials and techniques. Specifically, it describes the use of cation exchange on our CdS QDs and CdSe nanoplatelets to convert them to optically active  $\text{Cu}_2\text{S}$  and  $\text{Cu}_{2-x}\text{Se}$  respectively. This chapter also describes the use of the phase transfer approach to prepare luminescent CdZnSeS/ZnS alloyed QDs with varying degrees of glycosylation on the surface. These materials were used for in vitro cellular imaging using confocal microscopy to investigate a relationship between cellular interaction and the degree of QD glycosylation.

Finally, chapter 7 presents the conclusions and main outcomes of this research. It also discusses the future research that would follow on from this work.

We believe that this research has contributed to the further development of the preparation and analysis of a variety of new optically active fluorescent nanomaterials. It is expected that these nanomaterials might find applications in many areas ranging from photonics to biomedicine.

# Declaration

This thesis is submitted for the degree of Doctor of Philosophy to the University of Dublin, Trinity College and has not been submitted before for any degree or examination to this or any other university. Other than where acknowledged, all work described herein is original and carried out by the author alone. Permission is granted so that the Library may lend or copy this thesis upon request. This permission covers only single copies made for study purposes, subject to normal conditions of acknowledgement.

---

Alexander Loudon

# Acknowledgements

This research would not have been possible without the support of several people who I would like to sincerely thank.

Most importantly, I would like to thank my supervisor, Professor Yurii Gun'ko. His exceptional knowledge and thoughtful guidance have been invaluable throughout this research and without it none of this would have been possible. By extension, I would like to thank the Gun'ko research group, my academic family. Through constant support and expertise, they made every day enjoyable and allowed me to grow both as a scientist and a person during my PhD. In particular I thank Dr. Finn Purcell-Milton, my post-doctoral supervisor and close friend. Thank you for your time and patience over the years to help me extract the most out of my research and academic experience.

I would like to thank Vera Kutznetzova and the Scanlan group for contributing their expertise in biochemistry and organic chemistry for this project also.

I would like to extensively thank Olan Cleary, my flat mate of 4 years and fellow chiroptical nanomaterial researcher. Our time spent together, in and out of the lab, will leave an indelible mark on me as some of the greatest memories I've had to date.

Finally, I would like to extend a huge thanks to my parents, Paul and Frances, my sister Bridget, and my grandparents Robert and Shirl. Their confidence in my ability to complete this research when at times I struggled to see it myself is commendable. When I fell ill towards the end of my PhD you lifted me up and helped me get over the line, thank you.

# Contents

<b>Chapter 1: Introduction</b> .....	<b>1</b>
1.1 <i>Introduction to band structure and semiconductors</i> .....	1
1.2 <i>Quantum Dots</i> .....	2
1.3 <i>Synthesis of quantum dots</i> .....	5
1.3.1 <i>The development of colloidal quantum dot synthesis</i> .....	6
1.3.2 <i>Organometallic synthesis of colloidal quantum dots</i> .....	6
1.3.3 <i>Core-shell quantum dots</i> .....	10
1.3.4 <i>Aqueous synthesis of Quantum dots</i> .....	12
1.4 <i>Anisotropic Nanostructures</i> .....	14
1.5 <i>Quantum Rods and Dot-in-Tetrapods</i> .....	15
1.6 <i>Applications of QDs in optoelectronics</i> .....	16
1.6.1 <i>Quantum dot light emitting diodes</i> .....	19
1.6.2 <i>Quantum dot based solar cells</i> .....	21
1.7 <i>Biological applications of QDs</i> .....	24
1.8 <i>Chirality in nanoscience</i> .....	27
1.8.1 <i>Chirality of nanomaterial macro-assemblies</i> .....	29
1.8.2 <i>Ligand-induced chirality</i> .....	30
1.8.3 <i>Intrinsic chirality</i> .....	31
1.9 <i>Chiral Quantum Dots</i> .....	32
1.10 <i>Thiosugars as ligands for QDs</i> .....	34
1.11 <i>Cation exchange in quantum nanostructures</i> .....	35
1.12 <i>Aims and objectives of the project</i> .....	36
1.13 <i>References</i> .....	38
<b>Chapter 2 Experimental</b> .....	<b>49</b>

2.1	<i>Starting materials and general equipment.....</i>	49
2.2	<i>Experimental details for chapter 3.....</i>	50
2.2.1	Synthesis of ZnS and ZnS:Mn quantum dots .....	50
2.2.2	Phase transfer of ZnS:Mn doped QDs by precipitation technique .....	51
2.2.3	Phase transfer of Mn Doped ZnS QDs using ethylenediamine (EDA) .....	51
2.2.4	Synthesis of L-glutathione capped ZnSe QDs.....	52
2.2.5	Chiral recognition of penicillamine by ZnSe-GSH QDs .....	52
2.3	<i>Experimental details for chapter 4.....</i>	53
2.3.1	Synthesis of wurtzite CdSe QDs .....	53
2.3.2	Synthesis of zinc blende CdSe QDs .....	54
2.3.3	Preparation of solutions for synthesis of CdSe/CdS DiRs and TPs .....	54
2.3.4	Synthesis of CdSe/CdS dot in rods .....	55
2.3.5	Synthesis of CdSe/CdS tetrapods.....	55
2.3.6	Phase Transfer of CdSe-CdS DiR using thioglucose.....	56
2.4	<i>Experimental details for chapter 5.....</i>	56
2.4.1	Synthesis of CdS quantum dots .....	56
2.4.2	Phase transfer for CdS QDs with penicillamine .....	57
2.4.3	Synthesis of small CdSe QDs .....	57
2.4.4	Aqueous synthesis of L- and D- penicillamine stabilised QDs.....	58
2.4.5	Reverse phase transfer using dodecanethiol (DDT) on aqueous CdS QDs .....	58
2.4.6	Synthesis of 1.5 nm size CdSe nanoplatelets capped with myristic acid .....	58
2.4.7	Synthesis of 1.5 nm size CdSe nanoplatelets capped with decanoic acid .....	59
2.4.8	Synthesis of both 1.5 nm and 1.2 nm size CdSe nanoplatelets capped with Myristic Acid ...	59
2.4.9	Synthesis of 1.2 nm size CdSe nanoplatelets capped with decanoic acid .....	59
2.4.10	Synthesis of Mn doped CdSe nanoplatelets of size 1.5 nm .....	60
2.4.11	Phase transfer of 1.5 nm size CdSe QPs.....	60
2.4.12	Phase transfer of 1.2 nm size CdSe QPs.....	60



2.5	<i>Experimental details for chapter 6</i> .....	60
2.5.1	Cation exchange from pen capped CdS to pen capped Cu <sub>2</sub> S.....	60
2.5.2	Cation exchange from CdSe:Mn platelets to Cu <sub>2</sub> Se:Mn platelets.....	61
2.5.3	Synthesis of CdSe@ZnS/ZnS QDs.....	61
2.5.4	Phase transfer of the above QDs using thiolactose and penicillamine.....	62
2.6	<i>Characterisation techniques</i> .....	62
2.6.1	UV-Vis spectroscopy .....	62
2.6.2	Photoluminescence Spectroscopy .....	63
2.6.3	Circular Dichroism Spectroscopy .....	65
2.6.4	X-Ray Diffraction .....	66
2.6.5	Transmission Electron Microscopy .....	67
2.6.6	Energy-dispersive X-Ray Spectroscopy .....	69
2.7	<i>References</i> .....	70
<b>Chapter 3: Synthesis of non-toxic, optically active ZnS, ZnS:Mn and ZnSe QDs</b> .....		<b>71</b>
3.1	<i>Introduction</i> .....	71
3.2	<i>Aims of this chapter</i> .....	72
3.3	<i>Synthesis and characterisation of ZnS and ZnS:Mn quantum dots in chloroform</i> .....	74
3.4	<i>Ligand Exchange on ZnS:Mn quantum dots to produce chiral quantum dots</i> .....	79
3.4.1	Preparation of L- and D- cysteine stabilised ZnS:Mn QDs.....	79
3.4.2	Penicillamine capped ZnS:Mn quantum dots .....	83
3.4.3	Preparation of cysteine and penicillamine capped ZnS:Mn using ethylenediamine as transfer agent .....	86
3.5	<i>Toxicity studies for L and D cysteine capped ZnS:Mn QDs</i> .....	91
3.6	<i>Preparation of ZnSe quantum dots capped with glutathione</i> .....	92
3.7	<i>Conclusions</i> .....	97
3.8	<i>References</i> .....	99

<b>Chapter 4: Synthesis and characterisation of CdSe-CdS dot in rod and tetrapods for sensing applications.....</b>	<b>101</b>
4.1 Introduction.....	101
4.2 Aims of this chapter.....	102
4.3 Synthesis and characterisation of CdSe-CdS DiRs.....	103
4.4 Use of CdSe-CdS DiRs for chiral recognition.....	118
4.5 Synthesis and characterisation of CdSe-CdS dot in tetrapods.....	124
4.6 Conclusions.....	130
4.7 References.....	132
<b>Chapter 5: Chiral cadmium containing 0D dots, and 2D Platelets.....</b>	<b>133</b>
5.1 Introduction.....	133
5.2 Aims.....	135
5.3 Preparation and characterisation of chiral CdS.....	136
5.3.1 Hot injection synthesis and characterisation of CdS.....	136
5.3.2 Effect of injection temperature on the size of CdS nanoparticles.....	137
5.3.3 Phase transfer of CdS QDs using penicillamine ligands.....	139
5.3.4 Investigation of dependance of the optical activity on the size of QDs.....	143
5.4 Synthesis and characterisation of aqueous CdS QDs.....	144
5.5 Synthesis of Cysteine capped CdS.....	157
5.6 Synthesis of optically active CdSe QDs.....	159
5.7 Synthesis and characterisation of CdSe nanoplatelets.....	162
5.8 Conclusions.....	181
5.9 References.....	183
<b>Chapter 6: Applications of chiral nanomaterials.....</b>	<b>185</b>
6.1 Introduction.....	185
6.2 Aims of this chapter.....	186
6.3 Cation exchange experiments.....	186

6.3.1	Cation exchange on CdS QDs .....	187
6.3.2	Cation exchange for CdSe nanoplatelets .....	190
6.4	<i>Biological imaging using CdSe@ZnS-ZnS QDs in HeLa cells</i> .....	193
6.5	<i>Conclusions</i> .....	203
6.6	<i>References</i> .....	204
	<b>Conclusions and future work .....</b>	<b>208</b>
7.1	<i>Conclusions</i> .....	208
7.2	<i>Future Work</i> .....	209
7.2.1	Enantioselective quenching of L- and D- cys stabilised ZnS:Mn by gold NPs.....	210
7.2.2	Sensing of $\beta$ -Galactosidase .....	213
7.3	<i>References</i> .....	214
	<b>Appendix .....</b>	<b>i</b>

# List of figures

Figure 1-1: The conversion of orbitals into bands for bulk materials.....	1
Figure 1-2: Band structure of an insulator, semiconductor and metal. ....	2
Figure 1-3 Effects of nanocrystal size on band gap properties.....	3
Figure 1-4: Theoretical PL spectra demonstrating size-dependent band gap of QDs. .....	4
Figure 1-5: Diagram explaining Mn(II) doping effect on ZnS quantum dots .....	5
Figure 1-6 Hot injection technique for CQD synthesis (reproduced from ref <sup>26</sup> ). ....	7
Figure 1-7 La Mer model for colloidal growth in solution (Reproduced from ref. <sup>26</sup> ). 8	
Figure 1-8 Effect of nanocrystal size on growth rate (reproduced from ref. <sup>29</sup> ). ....	9
Figure 1-9 Band gap alignment in type I, reverse type I and type II core shell QDs.11	
Figure 1-10: Density of states for materials either not confined (A) or confined in (B) 1, (C) 2 or (D) 3 dimensions (reproduced from ref <sup>91</sup> ). ....	15
Figure 1-11 Diagram describing CdSe-CdS dot-in-rod and dot-in-tetrapod. ....	16
Figure 1-12 Optoelectronic applications of quantum dots (reproduced from ref. <sup>119</sup> ). .....	17
Figure 1-13 Spectral range of heavy metal and heavy metal free QDs varying from UV to IR (reproduced from ref. <sup>119</sup> ). ....	18
Figure 1-14 Typical QD LED (reproduced from ref. <sup>134</sup> ). ....	19
Figure 1-15 Graphical description of 3 types of QD solar cells as well as the associated energy diagrams (reproduced from ref. <sup>164</sup> ) .....	23
Figure 1-16: Common water solubilising ligands for QD phase transfers. ....	26
Figure 1-17: General process for phase transfer and stabilising of quantum dots. 26	
Figure 1-18: The numerous uses for quantum dots in biomedical applications. Reproduced from ref. <sup>212</sup> ). ....	27
Figure 1-19: The two enantiomeric forms of Thalidomide (reproduced from ref. <sup>213</sup> ). .....	28

Figure 1-20 Number of citations for publications about chiral nanomaterials by year. .....	29
Figure 1-21 Left and right-handed CdTe nanoribbons (reproduced from ref. <sup>221</sup> )....	30
Figure 1-22 Chiral (a) Cu(3,1,17) <sup>S</sup> and (b) Cu (3,1,17) <sup>R</sup> surfaces (reproduced from ref. <sup>234</sup> ) .....	32
Figure 1-23 Development of carbohydrate conjugated QDs from carbohydrates. .	34
Figure 1-24 The 3 stage (A-C) for cationic exchange in quantum dots. ....	35
Figure 2-1 Schematic describing the synthesis of ZnS:Mn QDs.....	50
Figure 2-2 Synthesis of CdS quantum dots with a 270°C hot injection. ....	56
Figure 2-3 Basic principles of a UV-Vis spectrometer.....	63
Figure 2-4 Diagram describing singlet and triplet electronic spin states. ....	64
Figure 2-5 Internal structure of a spectrofluorimeter .....	64
Figure 2-6 Diagram describing constructive interference in a crystal lattice.....	66
Figure 2-7 Basic operation of a transmission electron microscope (reproduced from ref. <sup>11</sup> ) .....	68
Figure 2-8 Diagram describing the general principles of EDX analysis.....	69
Figure 3-1 (A) Absorption (inset) and emission spectra for ZnS and ZnS:Mn QDs in chloroform: excitation $\lambda = 250$ nm. (B) Jablonski diagram showing effects of Mn doping.....	74
Figure 3-2 (A) TEM image of the Mn-doped ZnS, (B) a high-res close up of a single QD, (C) STEM image of ZnS:Mn QDs and (D) the area of the sample used for EDX analysis. ....	75
Figure 3-3 Size distribution for the ZnS:Mn QDs (n = 150). ....	76
Figure 3-4 EDX analysis of ZnS:Mn QDs. ....	77
Figure 3-5 XRD spectra for ZnS and ZnS:Mn QDs. ....	78
Figure 3-6 Scherrer analysis of ZnS and ZnS:Mn QD XRD patterns	<b>Error! Bookmark not defined.</b>
Figure 3-7 UV-Vis spectra of ZnS:Mn QDs before and after cysteine phase transfer. .....	80

Figure 3-8 PL spectra for organic oleylamine and aqueous D and L Cys stabilised ZnS:Mn QDs (Ex. $\lambda$ – 320 nm).	80
Figure 3-9 CD spectra for L and D cysteine stabilised ZnS:Mn QDs.	81
Figure 3-10 A) TEM and B) HRTEM of ZnS:Mn capped with L-cysteine.	82
Figure 3-11 Size distribution plot for ZnS:Mn QDs capped with L-cysteine (n=150).	82
Figure 3-12 Structure of A) cysteine and B) penicillamine.	83
Figure 3-13 UV-Vis spectra of D and L penicillamine stabilised ZnS:Mn QDs.	84
Figure 3-14 PL spectra for organic oleylamine and aqueous D and L pen stabilised ZnS:Mn QDs (Ex. $\lambda$ – 320 nm).	84
Figure 3-15 PL spectra comparing the organic ZnS:Mn QDs against the cysteine and penicillamine stabilised QDs (Ex. $\lambda$ – 320 nm).	85
Figure 3-16 CD spectra for pure D- and L- penicillamine (as free ligands).	85
Figure 3-17 CD spectra for D and L penicillamine capped ZnS:Mn QDs.	86
Figure 3-18 EDA assisted phase transfer scheme of ZnS:Mn QDs.	87
Figure 3-19 PL spectra for ZnS:Mn QDs following EDA assisted phase transfer for both L-Cys and D-Pen capped QDs.	88
Figure 3-20 CD spectra for cysteine capped ZnS:Mn QDs synthesised using the EDA phase transfer method.	89
Figure 3-21 CD spectra for penicillamine capped ZnS:Mn QDs using the EDA ligand exchange process.	89
Figure 3-22 Effect of chiral heat treatment on ZnS:Mn-penicillamine QDs.	90
Figure 3-23 Cell viability of A549 cells in the presence of cysteine capped ZnS:Mn QDs. <sup>26</sup>	92
Figure 3-24 Glutathione	93
Figure 3-25 Zn-GSH complexes at a) pH 6.5 – 8.3; b) pH 8.3 – 10.3; c) pH 10.3-11.5. <sup>29</sup>	93
Figure 3-26 UV-Vis spectra for ZnSe-Glutathione QDs.	94

Figure 3-27 A) TEM image of ZnSe QDs and B) Size distribution plot of ZnSe QDs (n=130). .....	94
Figure 3-28 CD spectra for Glutathione-ZnSe QDs. ....	95
Figure 3-29 PL spectra for ZnSe-Glutathione QDs (ex. $\lambda$ – 300 nm). ....	96
Figure 3-30 Effect on luminescence of ZnSe QDs by addition of penicillamine. ....	97
Figure 4-1 The UV-Vis spectra for the CdSe-CdS DiRs. Inset - the enlarged region from 525 to 700 nm in chloroform. ....	104
Figure 4-2 PL spectrum for the emission of CdSe-CdS DiRs in chloroform (Exc. $\lambda$ – 400 nm) .....	104
Figure 4-3 TEM image of (A) the CdSe-CdS DiRs from the organic phase with a (B) close up displaying crystallinity.....	105
Figure 4-4 (A) Length and (B) width size distributions histograms for the DiRs in the organic phase (N = 120 for length and 160 for width). ....	106
Figure 4-5 UV-Vis spectra for both aqueous (L-Pen) and DiRs in organic phase (chloroform). ....	106
Figure 4-6 PL Spectra for the DiRs in both the organic and aqueous phase (Exc. $\lambda$ – 400 nm). ....	107
Figure 4-7 CD spectra for D and L Penicillamine stabilised DiRs. ....	108
Figure 4-8 CD spectra of CdSe-CdS DiR stabilised with L- penicillamine (exciton region). ....	109
Figure 4-9 (A) TEM and (B) HRTEM images of CdSe-CdS DiRs stabilised with L- Penicillamine. ....	109
Figure 4-10 (A) Length and (B) Width distributions histograms for the L-Pen stabilised DiRs (N = 150 for length and 140 for width).....	110
Figure 4-11 UV-Vis spectra of (A) Cys-DiRs and (B) a close of up the CdSe exciton region. ....	111
Figure 4-12 PL spectra for Cys stabilised DiRs in DMSO (exc. $\lambda$ – 400 nm). ....	111
Figure 4-13 CD spectra for D and L Cys stabilised DiRs in DMSO. ....	112
Figure 4-14 CD spectra for L-Cys DiR in DMSO. ....	112

Figure 4-15 (A) TEM and (B) HRTEM of DiRs stabilised with L-Cysteine from H <sub>2</sub> O. .....	113
Figure 4-16 (A) Length and (B) width distribution histograms for L-Cys CdSe-CdS DiRs (N = 130 for length and 130 for width). .....	114
Figure 4-17 1-Thio-β-D-Glucose. ....	114
Figure 4-18 UV-Vis spectra for thioglucose stabilised CdSe-CdS DiRs. ....	115
Figure 4-19 PL spectra for thioglucose stabilised DiRs (Ex. λ– 500 nm). ....	116
Figure 4-20 CD Spectra for thioglucose stabilised DiRs in water. ....	117
Figure 4-21 (A) TEM and (B) HRTEM for CdSe-CdS DiR stabilised with D-Thioglucose. .....	118
Figure 4-22 (A) Length and (B) width distributions histograms for the DiR stabilised with thioglucose (N = 140 for length and 120 for width). ....	118
Figure 4-23 Effect of S-Naproxen on the PL of L/D-Cys DiRs (Version 1). ....	121
Figure 4-24 Effect of S-Naproxen on the PL of L/D-Cys DiRs (Version 2). ....	122
Figure 4-25 Effect of S and R-Naproxen on the PL of Thioglucose DiRs. (Version 1). .....	123
Figure 4-26 Effect of S and R-Naproxen on the PL of Thioglucose DiRs. (Version 2) .....	124
Figure 4-27 UV-Vis spectrum of CdSe-CdS TPs in chloroform (B) zoom in on 500 – 700 nm region .....	125
Figure 4-28 PL spectrum for CdSe-CdS TPs (Ex λ – 450 nm). ....	126
Figure 4-29 Schematic describing relationship between observed arm length and actual arm length for CdSe-CdS TP. ....	127
Figure 4-30 TEM image (left) and size distribution histogram (right) for CdSe-CdS tetrapods (organic phase) (N = 120). ....	127
Figure 4-31 UV-Vis spectra for CdSe-CdS TPs capped with cysteine .....	128
Figure 4-32 PL spectra for CdSe-CdS TPs capped with cysteine (Ex. λ – 450 nm). ....	129
Figure 4-33 TEM image (left) and size distribution histogram (right) for L-Cys-CdSe- CdS tetrapods (N = 120). ....	129



Figure 4-34 CD spectra for D and L cysteine stabilised CdSe-CdS tetrapods.....	130
Figure 5-1 – Absorption and emission spectra of CdS quantum dots synthesized with a 275°C hot injection (Ex. $\lambda$ – 393 nm).....	136
Figure 5-2 – (A) Absorption spectra of quantum dots synthesized with different injection temperatures (in degrees) and (B) their size as determined by the equation above.....	138
Figure 5-3 Absorbance spectra of CdS quantum dots before and after the phase transfer with penicillamine (inset: absorbance spectrum of penicillamine).....	140
Figure 5-4 – Emission spectra before and after the penicillamine phase transfer of CdS QDs. ....	141
Figure 5-5 – (A) CD spectra of L-pen and D-pen capped CdS in the nanoparticles absorption region (B) CD spectra of L-pen and D-pen capped CdS in the ligand absorption region, with the ligand own CD spectrum as inset. ....	142
Figure 5-6 – Comparison of the CD spectra of D-pen-capped CdS QDs made at different injection temperatures. ....	143
Figure 5-7 UV-Vis spectra of CdS QDs (Sample <b>A</b> ). ....	145
Figure 5-8 CD spectra for CdS QDs (Sample <b>A</b> ). ....	146
Figure 5-9 PL spectra of CdS QDs (Sample <b>A</b> ) (Ex. $\lambda$ – 325 nm). ....	147
Figure 5-10 UV-Vis spectra of CdS QDs (sample <b>B</b> ).....	148
Figure 5-11 CD spectra of sample <b>B</b> .....	148
Figure 5-12 Comparison of CD spectra for Sample <b>A</b> and Sample <b>B</b> . ....	149
Figure 5-13 PL spectra for D/L Pen CdS QDs (sample <b>B</b> ) (Ex. $\lambda$ – 325 nm).....	150
Figure 5-14 TEM image (left) and size distribution histogram (right) for D-Pen CdS Sample <b>A</b> (n = 150). ....	151
Figure 5-15 TEM image (left) and size distribution histogram (right) for D-Pen CdS Sample. <b>B</b> (n = 150). ....	151
Figure 5-16 UV-Vis spectra during reflux for sample <b>B</b> D-Pen.....	152
Figure 5-17 PL spectra during reflux for sample <b>B</b> (D-Pen) ( $\lambda$ ex. – 325 nm). ....	153
Figure 5-18 CD spectra over time for CdS QDs sample <b>B</b> (D-Pen). ....	153

Figure 5-19 CD spectra over time for CdS QDs sample <b>A</b> (D-Pen). .....	154
Figure 5-20 CD spectra at t = 2 hr and t = 4 hr of reflux for CdS QDs. ....	155
Figure 5-21 CD spectra for DDT stabilised CdS QDs. ....	156
Figure 5-22 UV-Vis for DDT stabilised CdS QDs. ....	157
Figure 5-23 UV-Vis data for cysteine stabilised CdS QDs (2 hr reflux). ....	158
Figure 5-24 PL spectra for luminescence ( $\lambda$ ex. – 325 nm). ....	158
Figure 5-25 CD spectra for D and L cys stabilised CdS QDs. ....	159
Figure 5-26 UV-Vis and PL spectra for D-Pen stabilised CdSe QDs ( $\lambda$ ex. – 400 nm). .....	160
Figure 5-27 CD spectra for D and L pen stabilised CdSe QDs in H <sub>2</sub> O. ....	161
Figure 5-28 (A) TEM and (B) Size distribution for D-Pen CdSe QDs. ....	162
Figure 5-29 Scheme for the synthesis of CdSe nanoplatelets. ....	163
Figure 5-30 Table of reaction conditions for synthesis of CdSe nanoplatelets for reference .....	164
Figure 5-31 UV-Vis and PL spectra for CdSe QPs with myristic acid, sample <b>1</b> ( $\lambda$ ex. – 420 nm). ....	164
Figure 5-32 UV-Vis and PL spectra for CdSe QPs with decanoic acid, sample <b>2</b> ( $\lambda$ ex. – 420 nm). ....	165
Figure 5-33 TEM images of CdSe NPs with myristic acid as the ligand (Sample <b>1</b> )	166
Figure 5-34 (A) CdSe QPs with myristic acid scroll thickness (n = 40), (B) CdSe QPs with myristic acid tube width (n = 100), (C) CdSe QPs with myristic acid scroll lengths (n = 100), (D) TEM of size 1.5nm CdSe QPs with myristic acid. ....	167
Figure 5-35 TEM images of CdSe NPs with decanoic acid as the ligand (Sample <b>2</b> ). .....	167
Figure 5-36 (A) Platelet thickness (n = 120), (B) Scroll width (n = 60), (C) Scroll length (n = 100), (D) TEM of twisted CdSe nanoplatelets 1.5 nm (sample <b>2</b> ). ....	168
Figure 5-37 UV-Vis spectrum for CdSe:Mn nanoplatelets. ....	169
Figure 5-38 PL spectrum of CdSe:Mn nanoplatelets (Ex. $\lambda$ – 380 nm) .....	170

Figure 5-39 UV-Vis spectra for sample <b>4.1</b> and <b>4.2</b> (before and after storage for 8 weeks). .....	171
Figure 5-40 Photoluminescence spectra for sample <b>4.1</b> and <b>4.2</b> (before and after 8 weeks storage) ( $\lambda$ ex. – 350 nm). .....	171
Figure 5-41 UV-Vis and PL spectra of CdSe Sample 5 with 1.2 nm thickness ( $\lambda$ ex. – 350 nm). .....	172
Figure 5-42 UV-Vis spectra before and after sample 2 had been transferred to water using penicillamine.....	174
Figure 5-43 PL spectra for before and after the phase transfer (Ex. $\lambda$ – 380 nm)..	174
Figure 5-44 CD spectra for size 1.5nm CdSe QPs capped with D-Pen and L-Pen ...	175
Figure 5-45 TEM image of sample 2 after the phase transfer with D-Pen. ....	175
Figure 5-46 UV-Vis spectra of sample <b>4.2</b> before and after phase transfer.....	176
Figure 5-47 CD spectra of sample <b>4.2</b> after phase transfer.....	177
Figure 5-48 UV-Vis spectra of sample <b>5</b> before and after phase transfer.....	177
Figure 5-49 CD spectra of sample <b>5</b> after phase transfer with D/L pen. ....	178
Figure 5-50 UV-Vis spectra of (A) sample <b>5-D</b> and (B) sample <b>5-L</b> 0 72 and 120 hours after synthesis. ....	179
Figure 5-51 CD spectra of sample 5 after penicillamine phase transfer at 0 and 72 hours.....	179
Figure 5-52 UV-Vis spectra for sample 2 before and after phase transfer with thiolactose.....	180
Figure 5-53 CD spectrum for sample 2 CdSe conjugated to thiolactose.....	181
Figure 6-1 Absorbance spectra of Pen-capped CdS before cation exchange and after (as Cu <sub>2</sub> S).....	188
Figure 6-2 CD spectra of L-pen and D-pen Cu <sub>2</sub> S quantum dots obtained from cation exchange from Pen-capped CdS synthesized at 300°C.....	189
Figure 6-3 Comparison of CD spectra before and after cation exchange. ....	189
Figure 6-4 UV-Vis spectral changes for Mn-doped CdSe QPs in chloroform before and after cation exchange and phase transfer. ....	191

Figure 6-5 CD spectra of resulting D/L penicillamine Cu <sub>2-x</sub> Se:Mn QPs in water. ....	192
Figure 6-6 Schematic for 50:50 penicillamine/thiolactose capped QD. ....	194
Figure 6-7 UV-Vis data for CdSe@ZnS/ZnS QDs capped with a combination of penicillamine and thiolactose. ....	195
Figure 6-8 PL spectra for CdSe/ZnS@ZnS QDs stabilised with penicillamine and thiolactose. ....	195
Figure 6-9 TEM image of CdSe/ZnS@ZnS QDs stabilised with lactose. ....	196
Figure 6-10 Size distribution histogram for QDs stabilised by lactose (n = 120)...	196
Figure 6-11 HRTEM image of CdSe/ZnS@ZnS QDs stabilised by penicillamine. ...	197
Figure 6-12 Size distribution histogram for CdSe/ZnS@ZnS QDs stabilised by penicillamine (n = 140). ....	197
Figure 6-13 TEM image of 50/50 lactose/penicillamine capped QDs. ....	198
Figure 6-14 HRTEM image of 50/50 lactose/penicillamine capped QDs. ....	198
Figure 6-15 Size distribution histogram for CdSe/ZnS@ZnS QDs stabilised by 50/50 lactose/penicillamine (n = 140). ....	199
Figure 6-16 Cell viability study at high concentration as a function of capping ligand (L = lactose, D = D-Pen). ....	200
Figure 6-17 Confocal microscopy results for samples analysed at a high concentration. ....	201
Figure 6-18 Confocal microscopy results for samples analysed at a lower concentration. Complexes were subjected to live confocal imaging, excitation 405nm, emission 500-600nm (Leica, 63X oil immersion lens). Images are representative of three experiment performed on independent days.) ....	202
Figure 6-19 Emission spectra of the complexes under cell culture conditions (Cell medium, pH7.4, 5% CO <sub>2</sub> ). HeLa cells were treated for 24h with 10µl of the indicated complexes and subjected to live confocal imaging, excitation 405nm, emission 410-760nm (Leica, 63X oil immersion lens). <b>A.</b> 50:50, <b>B.</b> 100D, <b>C.</b> 100L. ....	203
Figure 7-1 UV-Vis spectrum for D-Pen stabilised gold nanoparticles. ....	211
Figure 7-2 CD spectra for D- and L- pen stabilised gold nanoparticles. ....	211

Figure 7-3 TEM images of D-Pen stabilised QDs.....	212
Figure 7-4 Results of gold sensing using cysteine.....	213
Figure 7-5 Schematic describing the sensing of $\beta$ -galactosidase .....	214
Figure 7-6 CD spectra for lactose and glucose stabilised CdSe QDs.....	214
Figure 8-1 XRD patterns for both wurtzite and zinc blende ZnS (reproduced from reference <sup>1</sup> ) .....	i
Figure 8-2 UV-Vis and CD spectra for D and L cysteine .....	i
Figure 8-3 D-Pen in H <sub>2</sub> O after 48 hours at 50 °C.....	ii
Figure 8-4 PL spectra for ZnSe quenching experiment with L-Pen.....	ii
Figure 8-5 PL spectra for ZnSe quenching experiment with D-Pen.....	iii
Figure 8-6 Calculations for concentration of CdSe-CdS DiRs used for sensing .....	iv
Figure 8-7 PL spectra for L-Cys CdSe-CdS DiRs vs. Naproxen .....	iv
Figure 8-8 PL spectra for D-Cys CdSe-CdS DiRs vs. Naproxen.....	iv
Figure 8-9 2 sample t-test to test for significant difference in QD means .....	v
Figure 8-10 TEM image of CdSe@ZnS/ZnS QDs in the organic phase.....	v
Figure 8-11 TGA for CdSe@ZnS/ZnS .....	vi

# List of Abbreviations

ODE – Octadecene

1-D – 1- Dimensional

2-D – 2 – Dimensional

BSA – Bovine serum albumen

CD – Circular dichroism

Cys -Cysteine

DBA – Dibenzylamine

DDT - Dodecanethiol

DiR – Dot in Rod

DMSO – Dimethylsulfoxide

GSH – Glutathione

LED – Light emitting diode

MEH - poly(2-methoxy-5-(2'-ethyl-hexyloxy)-1,4-phenylene vinylene)

MPA – mercaptopropionic acid

NIR- Near Infra-red

NP – nanoplatelet

ODE- Octadecene

Pen – Penicillamine

PL- Photoluminescence

PLQY – Photoluminescence Quantum Yield

QD – Quantum Dot

SEM – Scanning electron microscope

TEM – Transmission electron microscope

TGA – Thermogravimetric analysis

TOP – Trioctylphosphine

TOPO – Trioctylphosphine oxide

TP – Tetrapod

UV-Vis – Ultraviolet-Visible

XRD – X ray diffraction

# Chapter 1: Introduction

## 1.1 Introduction to band structure and semiconductors

The electrons in an atom may occupy discrete energy levels known as atomic orbitals, a representation of the electron density around a nucleus. When atoms are bound in molecules, their individual atomic orbitals combine to lower the overall energy of the system, generating molecular orbitals which govern the electronic properties of that molecule. This approach is known as the linear combination of atomic orbitals. As more atoms are included in the system more molecular orbitals are generated, and once you extend the system to a quasi-infinite solid each molecular orbital is replaced with a band which will vary in energy as a function of the phase of the orbitals in the solid as seen in Figure 1-1 below, where bonding and anti-bonding represent the positive and negative overlap of orbitals respectively.

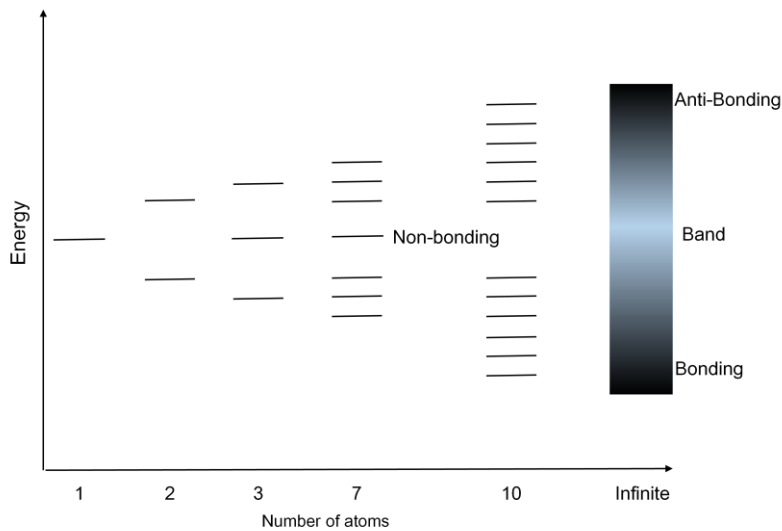


*Figure 1-1: The conversion of orbitals into bands for bulk materials.*

A material may be defined as a metal if the lowest unoccupied band (conduction band) overlaps with the highest energy occupied band (valence band) allowing free electron transport through the material. The difference in energy between the valence band and the conduction band is known as the band gap of the materials. A



semiconductor has a small band gap which can be overcome by thermal excitation, and an insulator has a very large band gap as demonstrated in Figure 1-2 below:

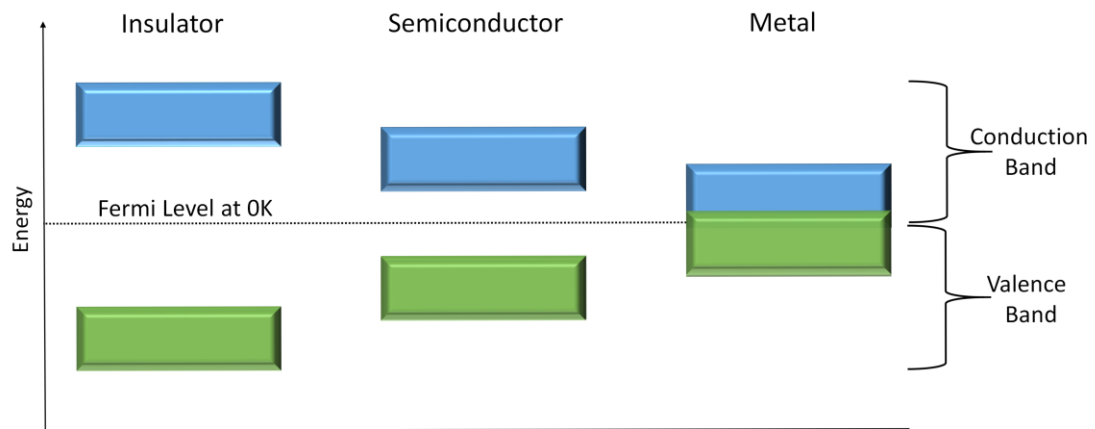


*Figure 1-2: Band structure of an insulator, semiconductor and metal.*

## 1.2 Quantum Dots

When materials have 1 or more of their dimensions limited to the nanoscale (1 -100 nm) these materials can be considered as nanomaterials. As technology and theory have advanced over the years the ability to create and analyse these materials has vastly increased and today, they can find applications in nearly every aspect of science. One of the greatest discoveries in the world of nanoscience is quantum dots (QDs). When semiconductor crystals are of a small enough size so that they exhibit quantum confinement effects (described below), they are known as quantum dots.

In semiconductors, when an electron is excited, it creates a positive hole in its absence. The electron and hole are bound by Coulombic interaction and collectively are known as an exciton. The distance between an excited electron and the positive hole it generates is known as the Bohr excitonic radius of the semiconductor,  $r_B$ . The exciton Bohr radius of a material is given below in Equation 1-1:

$$r_B = \frac{\hbar^2 \epsilon}{e^2} \left( \frac{1}{m_e^*} + \frac{1}{m_h^*} \right)$$

*Equation 1-1: Determination of Bohr excitonic radius*

Where  $e$  is the charge of the particle,  $m_e$  and  $m_h$  are the effective masses of the electron and hole respectively, and  $\epsilon$  is the dielectric constant of the material. The effective mass of an electron and hole change with different materials as does the dielectric constant and so the Bohr exciton radius varies with different materials. For example, indium phosphide<sup>1</sup> has an  $r_B$  of 15 nm whereas CdSe<sup>2</sup> has an  $r_B$  of 5.6 nm. When the size of the semiconductor crystal is smaller than the Bohr excitonic radius of the material, the exciton is said to be confined within a potential well, similar to the particle in a box thought experiment. This excitonic confinement leads to a number of size-dependent optoelectronic properties<sup>3,4</sup>. These include the changing of the energy levels near the band edge from continuous to discrete, and a band gap dependent on nanocrystal diameter (Figure 1-3).

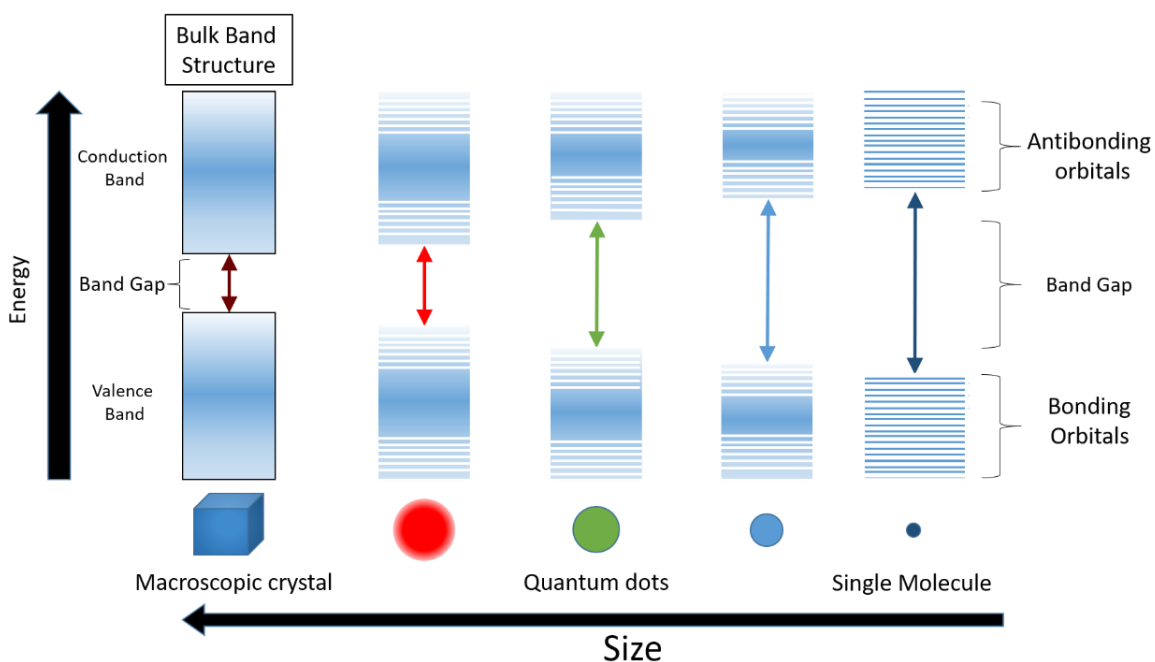


Figure 1-3 Effects of nanocrystal size on band gap properties.

The size dependant band-gap is one of the key features driving research in quantum dots and was popularised by Brus *et al*<sup>5</sup> in 1984 with his famous Brus equation seen below (Equation 1-2):

$$\Delta E(r) = E_{gap} + \frac{h^2}{8R^2} \left( \frac{1}{m_e^*} + \frac{1}{m_h^*} \right)$$

*Equation 1-2: The Brus Equation*

Where  $\Delta E(r)$  is the observed exciton energy,  $E_{\text{gap}}$  is the band gap energy of the bulk material,  $R$  is the QDs radius and  $m_e^*$  and  $m_h^*$  are the effective masses of the electron and hole respectively. Once a semiconductor undergoes confinement, the probability of radiative exciton recombination is much higher than in the bulk. This is due to a greater overlap between the electron and hole wavefunctions in the confined regime<sup>6</sup>. Whereas in the bulk, the charge carriers are not confined and may diffuse quickly increasing the likelihood of non-radiative decay. Therefore, QDs are primarily used as nano-sized light emitting materials in photonics, optical sensing and imaging.

As a result of quantum confinement, the size-dependent bandgap allows the tuning of the optical properties of the QD by controlling the size, as seen in the theoretical photoluminescence (PL) spectrum Figure 1-4:

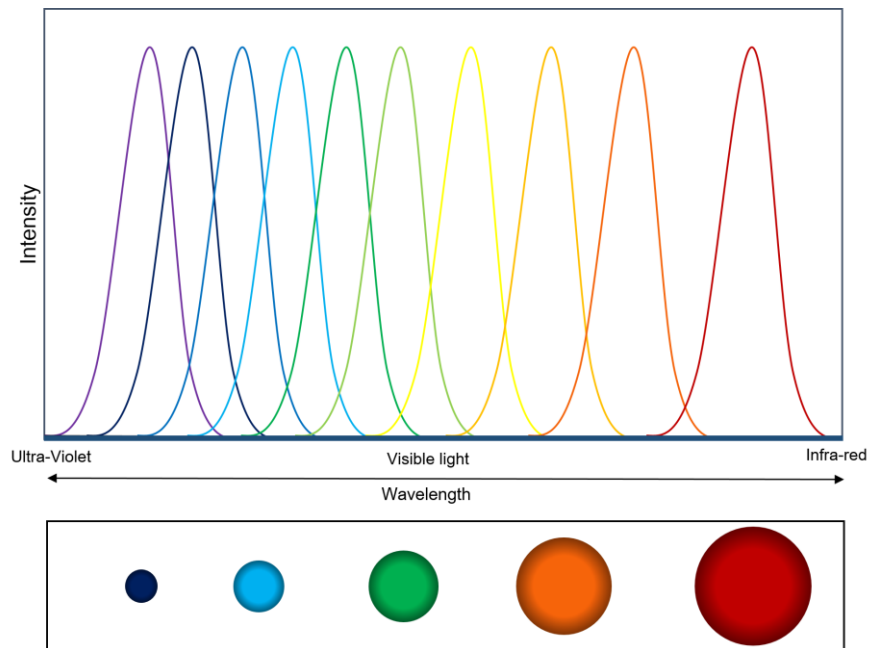


*Figure 1-4: Theoretical PL spectra demonstrating size-dependent band gap of QDs.*

Alternative methods for tuning the properties of quantum dots include doping<sup>7-9</sup> and alloying<sup>10,11</sup>. Doping is of particular interest as adding very small amounts of a dopant (around 1%) can drastically affect the properties of the QDs. Doping can be used for various effects such as improved lifetimes<sup>12</sup> and increased Stokes shifts<sup>13</sup>.

For example, Yu *et al.* demonstrated that doping zinc sulfide QDs with manganese (II) provides an alternative phosphorescent decay pathway through the manganese ( ${}^4T_1 \rightarrow {}^6A_1$ ) which is red-shifted when compared to the undoped ZnS QDs<sup>13</sup> emission. This Stokes shift of nearly 300 nm eliminates the possibility of self-absorption commonly seen in fluorophores. While excitation in the UV region is generally damaging to cells, this can be avoided with the use of three-photon excitation via a pulse laser combining three lower energy photons instead of one high energy photon. The phosphorescent nature of the resultant luminescence is another interesting property of the doped QDs, as detecting on a phosphorescent timescale eliminates noise associated with background biological fluorescence<sup>14</sup>. Figure 1-5 below presents a simplified Jablonski diagram which shows the effects of doping ZnS quantum dots with manganese.

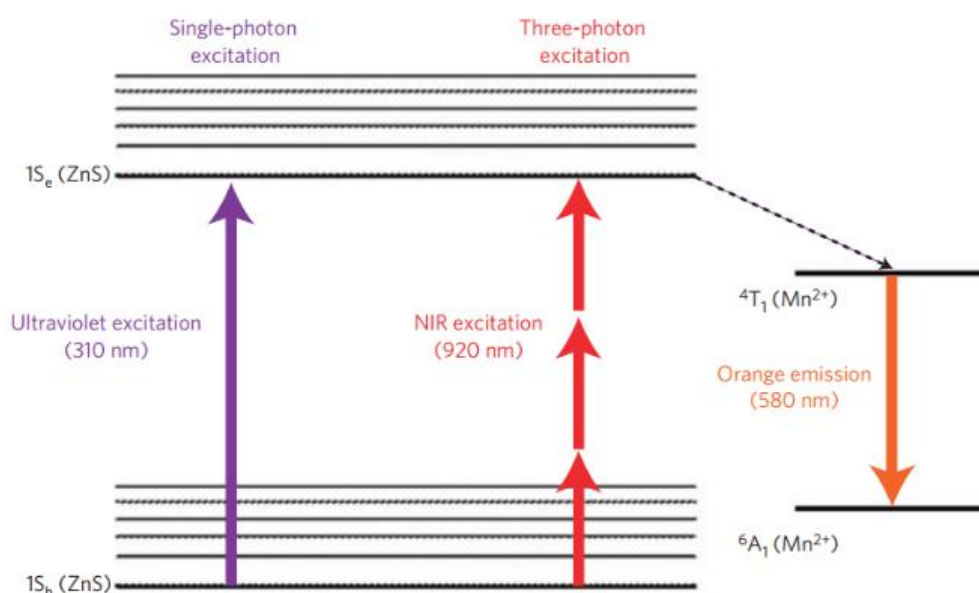


Figure 1-5: Diagram explaining Mn(II) doping effect on ZnS quantum dots

### 1.3 Synthesis of quantum dots

Quantum dots may be synthesised using a variety of methods such as chemical vapour deposition<sup>15,16</sup>, spray pyrolysis<sup>17</sup> and molecular beam epitaxy<sup>18</sup>, however, wet chemical techniques appear to feature most prominently in the literature. Wet-

chemical approaches produce colloidal quantum dots (CQDs) and will be discussed below.

### 1.3.1 The development of colloidal quantum dot synthesis

Scientists such as Brus and Heinglein were the first to develop colloidal quantum dot synthesis in the mid to late 80's following Brus' ground-breaking publication detailing the quantum confinement effect in semiconductor nanocrystals<sup>19-24</sup>. Early syntheses of QDs were performed in the aqueous phase involving the solvation of ions. While the authors of these papers pioneered the field, understanding of the synthetic mechanisms was limited. These initial protocols involved precipitation reactions in homogenous solutions with stabilising polymers or surfactants. Concurrently, an arrested precipitation technique was developed growing the nanocrystals in reverse micelles using amphiphilic stabilisers. This 2-phase method improved colloidal stability and minimised aggregation, however quantum yields remained low. These methods presented several advantages including simple experimental preparation, common reagents, and low temperature synthesis, however several drawbacks existed also. The low temperature approach led to poor size control and weak photoluminescence quantum yields (PLQY). The poor PLQY was attributed to a high degree of defect states present in the QDs due to the presence of oxygen moieties and poor QD crystallinity. The lack of size control caused a broadening of the absorption and emission characteristics limiting potential applications also. It was clear by the early 90's that the ability to synthesise a highly crystalline, monodisperse QD had to be discovered in order to truly exploit Brus' discovery.

### 1.3.2 Organometallic synthesis of colloidal quantum dots

This paradigm shift in QD synthesis appeared in 1993 when Murray *et al.* published their radical synthetic approach to producing highly crystalline CQDs with a narrow size distribution (<5%)<sup>25</sup>. This was the first reported organometallic protocol for CQD synthesis and involved the high-temperature pyrolysis of precursors in the presence

of co-ordinating capping agents in an organic solvent. To prepare CdS, CdSe, and CdTe CQDs, dimethyl cadmium was used as a cadmium precursor while the chalcogenide sources were phosphine bistrimethylsilyl sulphide, phosphine selenide and phosphine telluride respectively.

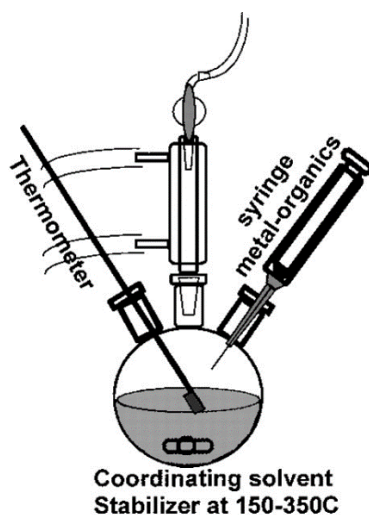


*Figure 1-6 Hot injection technique for CQD synthesis (reproduced from ref<sup>26</sup>).*

The solvent used in Murray's reaction was a mixture of trioctylphosphine oxide (TOPO) and trioctylphosphine (TOP), whose high boiling points facilitated the high temperature synthesis. This synthesis was so ground breaking as not only did it produce highly crystalline CQDs, but it allowed size control not previously recorded. Using the above method, CQDs ranging from 1 to 12 nm were produced.

This method of injecting organometallic precursors into high temperature organic solvents became known as hot injection and has largely shaped the CQD synthetic landscape ever since (Figure 1-6). This rapid injection of the organometallic precursor is the key to a narrow size distribution and monodispersity. This is due to the temporal separation of the nucleation and growth phase of the QDs achieved by creating a high monomer concentration in the hot solvent very quickly. Quenching of the reaction rapidly before significant Ostwald ripening could take place was deemed crucial to retaining a narrow size distribution. The theory underlying this growth mechanism predates QD's by several decades as Dinegar and La Mer initially discussed the growth of nanocrystals from a supersaturated solution

in 1950<sup>27</sup>. While previous QD synthesis required size selective fractioning in order to explore Brus' original findings, it was now possible to produce size-tuneable, crystalline QD size with a narrow size distribution without requiring post-synthetic processing.

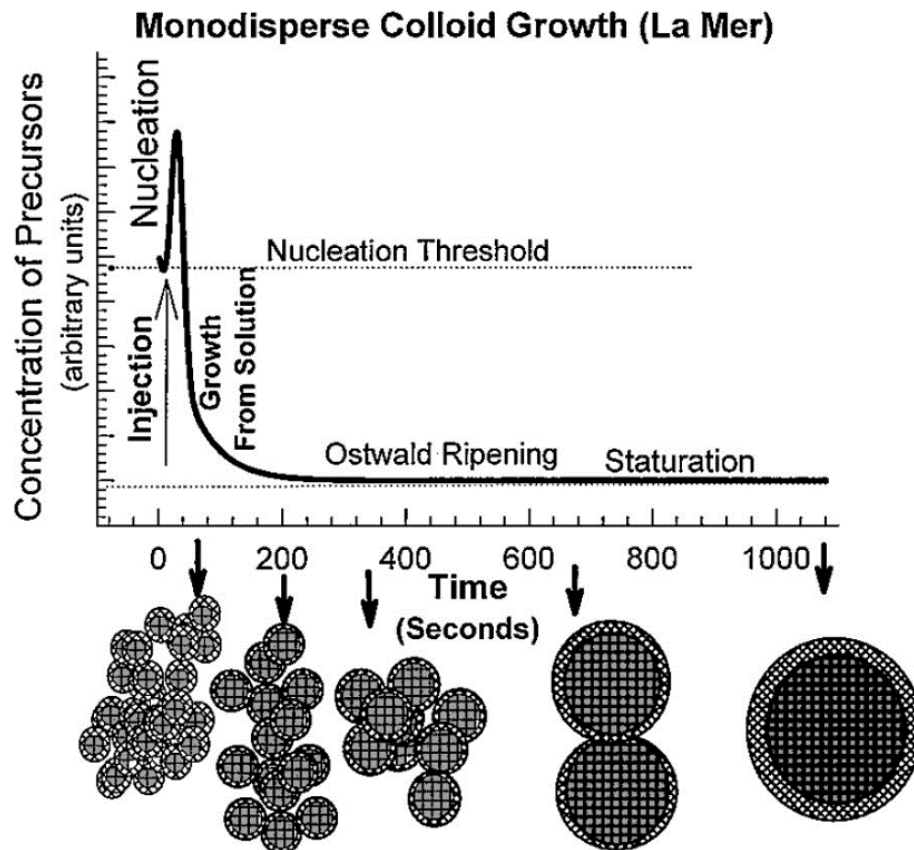


Figure 1-7 La Mer model for colloidal growth in solution (Reproduced from ref.<sup>26</sup>).

Further advancements in the understanding of size control were developed by Alivisatos *et al.* in their research on the focussing (narrowing) and defocussing (broadening) of size distributions<sup>28</sup>. In this research he identified the factors controlling the growth of II-VI (CdS, CdSe) and III-V (InAs, InP) QDs. Alivisatos reported that, assuming the growth rate is a diffusion limited process, the size dependant growth of QDs can be described by the equation below, considering the Gibbs-Thomson equation<sup>29</sup> on crystal solvation.

$$S_r = S_b \exp\left(\frac{2\sigma V_m}{rRT}\right)$$

Equation 1-3 Solubility of nanocrystal as a function of the crystal size where  $S_r$  = nanocrystal solubility;  $S_b$  = bulk crystal solubility;  $\sigma$  = surface energy;  $V_m$  = molar volume;  $R$  = gas constant;  $T$  = temperature;  $r$  = nanocrystal radius

$$\text{if } \frac{2\sigma V_m}{rRT} \ll 1 \text{ then } \frac{dr}{dt} = K\left(\frac{1}{r} + \frac{1}{\delta}\right)\left(\frac{1}{r^*} - \frac{1}{r}\right)$$

Equation 1-4 Nanocrystal growth rate as a function of time (constant described below)

In the above equation,  $K$  is a constant related to the diffusion constant of the monomer.  $\delta$  is the diffusion layer thickness.  $r^*$  is the zero-growth rate nanocrystal size (radius) for a given monomer concentration, otherwise known as the critical size. Sugimoto *et al.* plot the growth rate of nanocrystals as a function  $r/r^*$  and describes how crystals above or below this critical size behave (Figure 1-8).

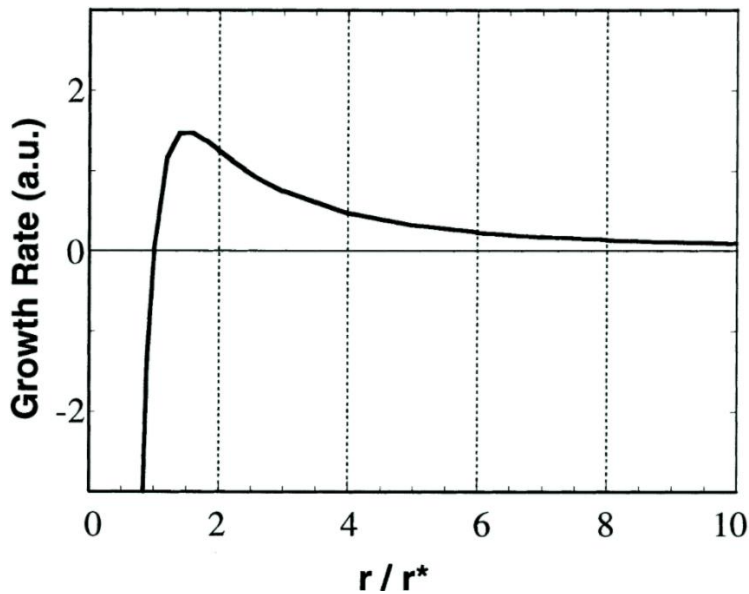


Figure 1-8 Effect of nanocrystal size on growth rate (reproduced from ref.<sup>29</sup>).

From the above it becomes clear that there is distinct difference in the growth rate of QDs larger than the critical size and smaller than the critical size. QDs smaller than the critical size ( $r/r^* < 1$ ) display a negative growth and therefore dissolve. Whereas QDs larger than the critical size grow at a rate which is largely dependent on their size, with a maximum growth rate occurring when  $r/r^* \approx 1.5$ . The size distribution undergoes focussing when the QDs in solution are all slightly larger than



$r^*$ . In this regime, the larger QDs grow more slowly than the smaller ones and a narrowing of the distribution takes place. As a consequence of this process, the monomer concentration is decreased and the critical size increases. Now QDs smaller than the increased  $r^*$  start to decrease in size while the larger ones continue to grow, this process is known as Ostwald ripening (defocussing). In order to refocus the size distribution additional monomer must be added in order to decrease the critical size  $r^*$  once again<sup>28</sup>.

### 1.3.3 Core-shell quantum dots

Due to the small size of QDs, a large proportion of the atoms are on the surface and so surface science become incredibly important when compared to bulk materials. Due to the lower co-ordination number of surface atoms compare to bulk, dangling bonds may be present on the surface. If the energy of the states in these dangling bonds overlaps with the bands of the bulk, electron and hole trapping can take place decreasing PLQY. For example, in CdSe, the dangling bonds in surface cadmium atoms behave as electron traps and the dangling bonds in the surface selenium atoms act as hole traps. In addition, distortion of the crystal lattice at the QD surface can introduce added trap states. This was one of the reasons that early CdSe QDs capped with organic ligands reported PLQYs primarily in the 5 to 15% range<sup>25,30</sup>. Due to the bulky nature of the organic ligands, it was proving difficult to achieve complete surface passivation and dangling bonds where somewhat unavoidable. The solution required passivation of both cationic and anionic surface atoms in order to limit both electron and hole traps simultaneously.

The major breakthrough in achieving higher PLQYs occurred when Guyot-Sionnest and Hines overcoated CdSe QDs with a wider band gap semiconductor, ZnS, to achieve a PLQY of 50%<sup>25</sup>. This was the first reported case of a core-shell QD and the large increase in PLQY is attributed to several factors. Firstly, by growing ZnS epitaxially on the surface simultaneous passivation of both the cation and anion surface atoms was achieved, limiting trap states. Secondly, by overcoating the

surface photooxidation of the emissive core is prevented, further limiting the potential for trap states. As the number of trap states decreases, the probability of radiative recombination increases and so the PLQY increases too. Finally, by using a wider band gap semiconductor as the shell, greater confinement of the exciton is achieved. When a wider bandgap semiconductor is used as the shell the core-shell QD is known as type I although type II and reverse type I also exist (Figure 1-9).

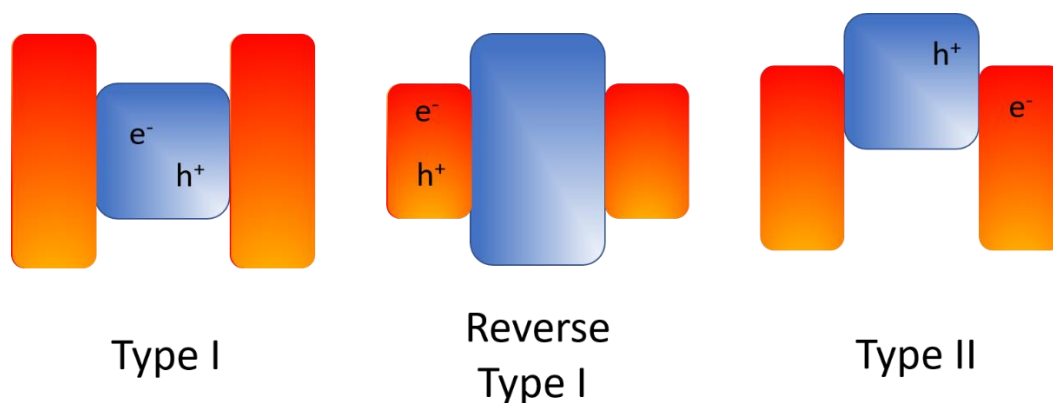


*Figure 1-9 Band gap alignment in type I, reverse type I and type II core shell QDs.*

Type I core shell structures confine the exciton to the core and are primarily used in the synthesis of high PLQY QDs where more recent synthetic protocols have produced CdSe/CdS QDs with PLQYs in excess of 95%<sup>31,32</sup>. Similar PLQYs have been reported for CdSe/ZnS core shell structures<sup>33</sup>. Reverse type I QDs use a smaller band gap material as the shell and therefore confine the exciton in the shell such as ZnSe/CdSe QDs and type II QDs are composed of 2 materials where there is band mismatch between the core and shell. In type II QDs, the hole and the electron reside in separate layer of the QD (either core or shell) depending on the materials used. In the case of type II QDs, the emitted photon energy is equal to the energy offset between the core and the shell.

Initial core-shell structures were prepared using a multi-stage process where the core seeds are synthesised and purified, followed by the growth of a shell in a separate reaction. Subsequently, newer core-shell preparations using a single step synthesis have been developed for a wide array of materials including CdSe/ZnSe<sup>34</sup>,

InP/ZnS<sup>35</sup> and CdSe/CdS<sup>36-38</sup>. As demands for precise shell thickness increased, a method known as successive ion layer adsorption and reaction (SILAR) was used for the synthesis of core-shell heterostructures<sup>39</sup>. Although this technique was developed to deposit thin films it has been successfully adopted for the preparation of a wide range of QD heterostructures<sup>40-43</sup>.

#### 1.3.4 Aqueous synthesis of Quantum dots

While organometallic approaches to producing quantum dots offer several advantages, development in the aqueous synthesis of QDs has continued ever since the initial research of Brus and Heinglein. A lot of this research was carried out by Heinglein's colleagues such as Weller<sup>44-46</sup>, Rogach<sup>47-51</sup>, Gao<sup>52-55</sup> and Eychmüller<sup>56-58</sup>. Hot injection techniques offer exceptional size and morphological control, yet aqueous synthesis offers significant advantages in terms of scalability, greener synthesis and cost-effectiveness. Furthermore, aqueous syntheses offer a far greater range of surface modification without including an extra ligand exchange step. The aqueous compatibility of a wide variety of biomolecules such as nucleotides, amino acids and proteins allow them to be used directly as ligands producing bio-functional nanoparticles in a one step process. To take this one step further, aqueous techniques have even expanded to the biosynthesis of QDs within biological media<sup>59-61</sup>.

The aqueous synthesis of QDs is generally governed by 4 thermodynamic process: the binding affinity for particle stabilising ligands; the binding affinity of hydroxyl ions and water to the metals; the solubility product of the QD in solution; and finally, the pH of the solution. These processes are largely governed by the theory of hard and soft Lewis acids and bases (HSAB theory)<sup>62</sup> as aqueous QD synthesis primarily involves Lewis acid and Lewis base reactions. The added complexity of aqueous synthesis, compared to organic synthesis, is the introduction of OH<sup>-</sup>, H<sup>+</sup>, and H<sub>2</sub>O species into these reactions. A full discussion on the effects of these 4 processes and

their effect on synthesis is beyond the remit of this thesis however the example of pH will be discussed as it is a highly important factor in aqueous synthesis<sup>63-66</sup>. OH<sup>-</sup> is a hard base according to HSAB theory and can form soluble and insoluble metal-hydroxide complexes in solution. This process competes with the formation of the intended metal chalcogenide semiconductor. As the hydroxide ion is considered a “hard” ion, it prefers to bind to “hard” cations such as Zn<sup>2+</sup>. Therefore, precise pH control is necessary to avoid the formation of Zn(OH)<sub>2</sub> when synthesising Zinc containing QDs<sup>67,68</sup>. By comparison, Cd<sup>2+</sup> is considered a “softer” cation and so there is less concern for the formation of Cd(OH)<sub>2</sub>. Therefore, the synthesis of cadmium containing QDs will tolerate a higher concentration of OH<sup>-</sup> ions. Despite being more tolerant than zinc based synthesis, there is still a limit. Exemplified in the synthesis of CdTe QDs where it was shown that exceeding a pH of 10.5 led to the undesirable formation of insoluble Cd(OH)<sub>3</sub><sup>-</sup> and Cd(OH)<sub>4</sub><sup>2-</sup> complexes<sup>57</sup>.

From a synthetic point of view, the synthesis of QDs in the aqueous phase is primarily based on simple precipitation reactions where the use of an appropriate capping ligand controls the growth to the correct size. Among ligands, thiol containing ligands such as mercaptopropionic acid (MPA) and thioglycolic acid (TGA) have found widespread use due to their proven applicability in the synthesis of a wide range of QDs. In the case of cadmium sulphide QDs, thiol ligands have even been successful in producing ultra-small clusters<sup>69,70</sup>, highlighting the control afforded by thiol ligands. Due to its comparable success compared to the preparation of CdS and CdSe, the aqueous synthesis of CdTe has received significant attention.

Initial CdTe aqueous synthesis was carried out by reacting Cd<sup>2+</sup> with Na<sub>2</sub>Te directly using a polyphosphate ligand,<sup>71</sup> however the resultant QDs did not exhibit fluorescence. Rogach *et al.* used mercapto-ethanol as the ligand leading to significantly better results, reporting a PLQY of 3%<sup>48</sup>. While still low, it demonstrated the strong Cd-S bond formed between cadmium-containing QDs and thiolated

capping agents could be used to control QD growth. Gao *et al.* used thioacids such as MPA<sup>54</sup> and TGA<sup>52</sup> to drastically improve the PLQYs, reporting PLQYs of 38% and 18% respectively. Using TGA and its derivatives, a wide range of interesting shapes could be synthesised including rods<sup>72</sup>, wires<sup>73</sup>, twisted ribbons<sup>74</sup>, and nanosheets<sup>75</sup>. Hydrothermal<sup>76,77</sup> and microwave assisted<sup>78,79</sup> techniques for the synthesis of CdTe QDs have also been developed based on previously optimised reactant concentrations. The mercapto acid approach for the synthesis of CdTe QDs has been applied to a wide range of other materials including: PbS and PbSe<sup>80,81</sup>; AgS<sup>82</sup>, AgSe<sup>83</sup>, and Ag<sub>2</sub>Te<sup>84</sup>; ZnS<sup>85</sup>, ZnSe<sup>86,87</sup>, and ZnTe<sup>67</sup>.

## 1.4 Anisotropic Nanostructures

Quantum dots are so named because they demonstrate quantum confinement effects in all three dimensions, due to their spherical shape. However, it is possible to synthesise a variety of other quantum confined nanostructures which demonstrate confinement in either 1 or 2 dimensions. When particles are confined in 2 dimensions, they are known as either rods or wires, and if they are confined in only one dimension, they are known as platelets or sheets, confined within a quantum well. Figure 1-10 below schematically presents the density of states for these three different confinement regimes<sup>88,89</sup>. One special case of the quantum rod is the dot-in-tetrapod<sup>90</sup>, which, from a confinement perspective may be seen as an assembly of quantum rods.

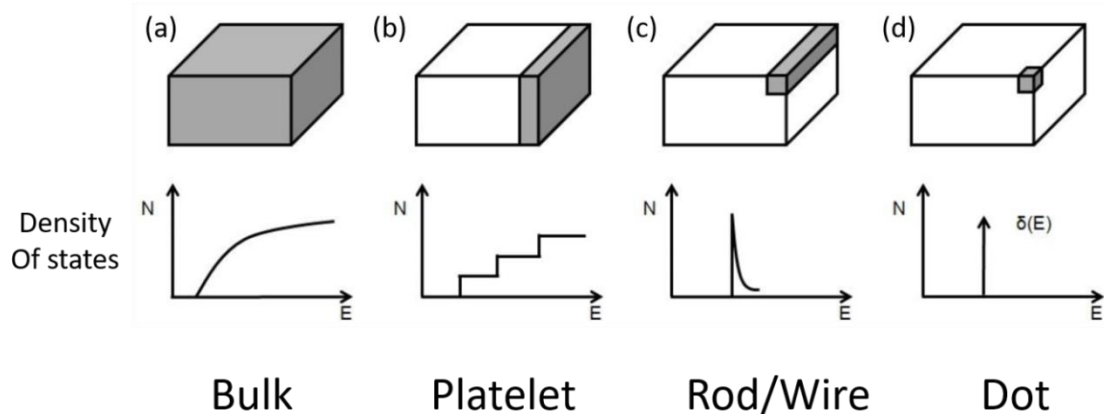


Figure 1-10: Density of states for materials either not confined (A) or confined in (B) 1, (C) 2 or (D) 3 dimensions (reproduced from ref<sup>91</sup>).

## 1.5 Quantum Rods and Dot-in-Tetrapods

Quantum rods were first controllably prepared by Peng *et al.* in 2000 when this group synthesised anisotropic wurtzite CdSe quantum rods. In this report, it was suggested that anisotropic growth could be driven by highly binding hexylphosphonic acid as a ligand<sup>92</sup>. Scher and Alivisatos suggest that the phosphonic acid binds more strongly to certain crystal faces limiting growth in those directions which directs anisotropic rod growth<sup>93</sup>. It was subsequently proposed that high monomer concentrations would preferentially drive growth along the c-axis of the wurtzite crystal structure<sup>94</sup>. This is because as anisotropy increases so do the surface energy and chemical potential, therefore to promote anisotropic growth an environment with a high chemical potential such as a high monomer concentration is required<sup>95</sup>. Later on new heterogenous core-shell dot-in-rod structures with very high quantum yields were developed. Talapin *et al.* proposed the mechanism for anisotropic CdS shell growth over CdSe seeds leading to the formation of CdSe-CdS dot in rods<sup>96</sup>. Several factors seem to promote anisotropic shell growth. Firstly, the lattice constant mismatch for hexagonal CdSe and CdS is larger along the (100) direction. This means that the growth of CdS upon the (100) surface of CdSe is slower due to greater interfacial strain than on the (001) or (00 $\bar{1}$ ) surface. Secondly, the cadmium atoms on the (00 $\bar{1}$ ) surface are more reactive due to an increased number of dangling bonds compared to either the (100) or (001) surface. Thirdly, the use of hexadecylamine in the shell growth promotes growth along the C axis, which also occurs in the synthesis of pure CdS rods<sup>97</sup>. Finally, temperature has a significant impact on the shape control in the synthesis. The shell growth is performed at lower temperatures as the kinetic driving force of the reaction (preferential growth along the c-axis) is overcome thermodynamically at higher temperatures leading to isotropic core/shell quantum dot growth. These dot-in-rod nanostructures

demonstrate far higher quantum yields than their homogenous CdSe analogues and have subsequently found applications in a variety of fields.

Similar techniques have been developed for the synthesis of CdSe-CdS dot-in-tetrapods. To synthesise tetrapods in this way, it is required to produce a zinc blende cubic CdSe core before growing four CdS wurtzite nanorods from the cores (111), (11 $\bar{1}$ ), ( $\bar{1}\bar{1}$ 1) and ( $\bar{1}\bar{1}\bar{1}$ ) surfaces<sup>98</sup>. A schematic of the dot-in-rod and dot-in-tetrapod is presented below in Figure 1-11.

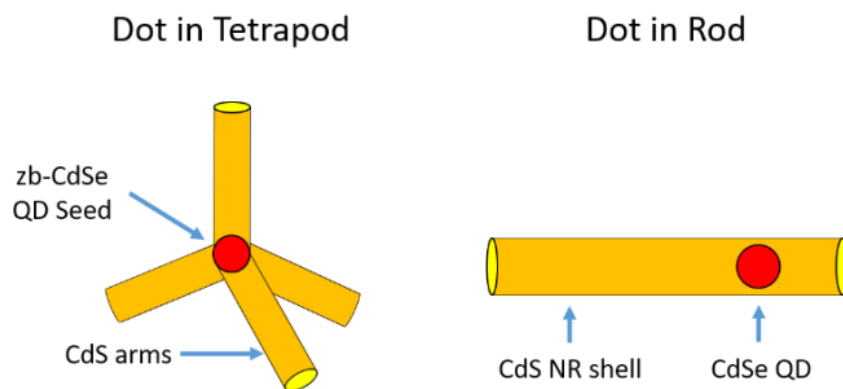


Figure 1-11 Diagram describing CdSe-CdS dot-in-rod and dot-in-tetrapod.

## 1.6 Applications of QDs in optoelectronics

Due to the unique optical and electronic properties of QDs, they are finding applications in a wide range of fields. The field of QD based optoelectronic devices has expanded rapidly in recent decades especially (Figure 1-12). Colvin *et al.* reported the first QD-LED prepared with CdSe QDs and p-paraphenylene vinylene contained within a layer of indium tin oxide (ITO) and a magnesium electrode however they exhibited a very low quantum efficiency of 0.01%. Since then, improvements in QD synthesis, device fabrications, and charge transport materials have all contributed to huge advancements in the field and recent QD-LED report external efficiencies as high as 18%<sup>99</sup>. Since the initial development of QD-LEDs, quantum dots have been proven effective in the development of solar cells<sup>100-104</sup>, solar concentrators<sup>105-109</sup>, lasers<sup>110-113</sup> and photodetectors<sup>114-118</sup>. In all of these

applications it is the versatile tuneability of the absorption and emission that lends itself to successful QD technology.

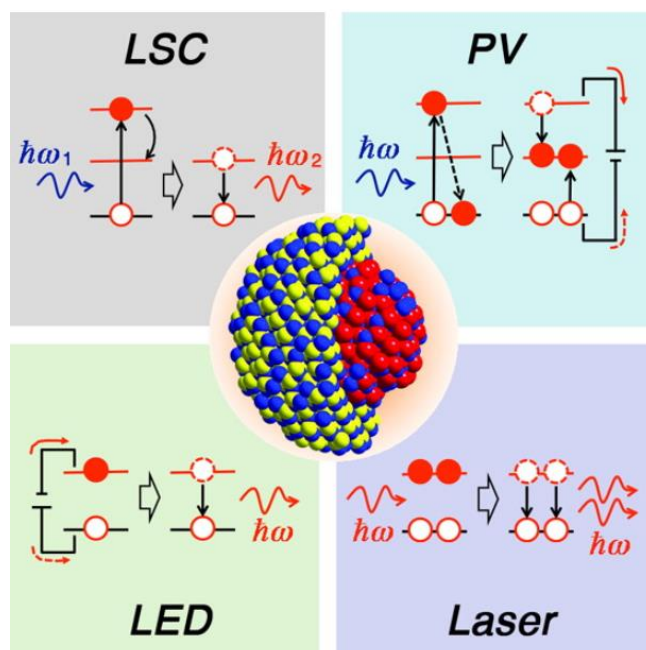


Figure 1-12 Optoelectronic applications of quantum dots (reproduced from ref.<sup>119</sup>).

By narrowing the QD emission as much as possible, QD-LEDs have been implemented in a variety of display technologies including modern televisions<sup>120,121</sup>. Contrasting this, by broadening the emission as much as possible QD-LEDs have found applications as efficient light sources<sup>120</sup>. As high photoluminescence quantum yields (PLQY) are required for either of these QD-LED applications to succeed, it becomes evident that effective preparation of high PLQY QDs is essential. Consequently, a huge array of high PLQY core-shell QD structures have been implemented in QD-LED technology. Furthermore, it has been demonstrated that alloyed QDs exhibit a softened confinement regime when compared to unalloyed QDs<sup>122</sup>. This smoothing of the confinement regime decreases Auger recombination by up to three orders of magnitude which is beneficial for LED technology. From the above one can conclude that an alloyed core coupled with an effective shelling regime produces QDs with optimal properties for LEDs.

While defective trap states would limit the efficiency of QD-LEDs, they become desirable in certain photodetectors, where the trap states perform as sensitizing



sites. Lead sulphide QDs have been largely adopted for photodetection due to absorbing over a broad range while being rich in intra-bandgap trap states. In the case of PbS, these states are largely due to a combination of oxide species and non-stoichiometric variance<sup>122,123</sup>.

In all of these applications it is evident that the large spectral range QDs absorb in and the ability to “tune” the absorption is significant for their application. By varying the chemical configuration and size of the QD, significant amounts of the electromagnetic spectrum, from NIR to UV, can be utilised (Figure 1-13). Concerns over the toxicity of heavy metal containing QDs have been alleviated to some extent in recent years resulting in the development of heavy metal free QDs such as InP and CuInS<sub>2</sub><sup>119</sup>.

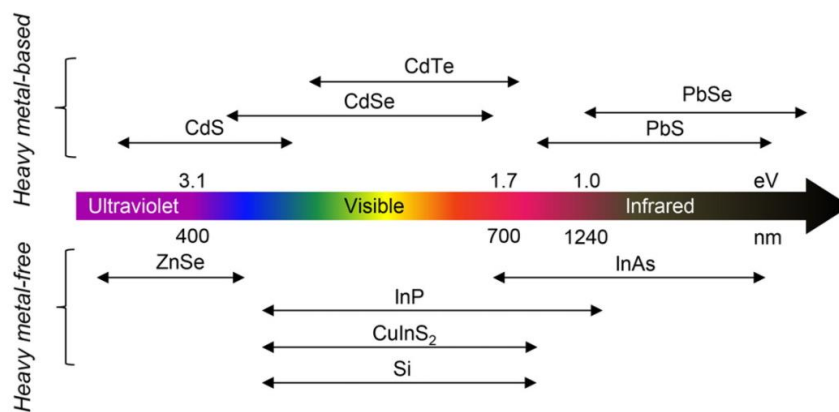


Figure 1-13 Spectral range of heavy metal and heavy metal free QDs varying from UV to IR (reproduced from ref.<sup>119</sup>).

Finally, colloidal QDs demonstrate advantageous solution state processing potential when compared with the alternatives allowing for the large-scale, affordable preparation of optoelectronic devices. Recent advancements of QD surface modifications pre-fabrication further expand the manufacturing potential. For example, by replacing organic surface ligands with halide inorganic ligands increased stability and charge carrier transport were achieved<sup>124,125</sup>. While most work up until recently has focused on small scale fabrication techniques including spin and dip-coating, more recent efforts have focused on the production of large QD films for optoelectronic devices<sup>126</sup>. Inkjet printing has also shown promise for large-scale QD

film technology for solar cells<sup>127</sup>, photodetectors<sup>128</sup> and LEDs<sup>129</sup>. Doctor blading is another viable technique for the production of QD based thin film devices. This technique uses a blade to deposit and spread a solution over a film with precise thickness control. Importantly it easily scalable as it can be applied in a process called roll-to-roll knife coating<sup>130,131</sup> for cheap large scale film production. Recently, large (2700 cm<sup>2</sup>) CdSe/Cd<sub>1-x</sub>Zn<sub>x</sub>S QD/PVK luminescent solar concentrators were produced by Li *et al.* using this doctor blade approach<sup>132</sup>.

### 1.6.1 Quantum dot light emitting diodes

Quantum dot LEDs operate on the principles of electroluminescence, a phenomenon first reported by Round *et al* in 1907<sup>133</sup>, where electron/hole generation is achieved using an applied voltage, followed by radiative recombination. In LEDs, a voltage is applied across a p-n junction and radiative recombination of separated electrons and holes takes place. QD-LEDs operate by using an applied voltage to inject electrons and holes into a quantum dot layer through charge transport layers (CTLs), allowing for radiative recombination within the QD. A typical QD-LED is presented below in Figure 1-14.

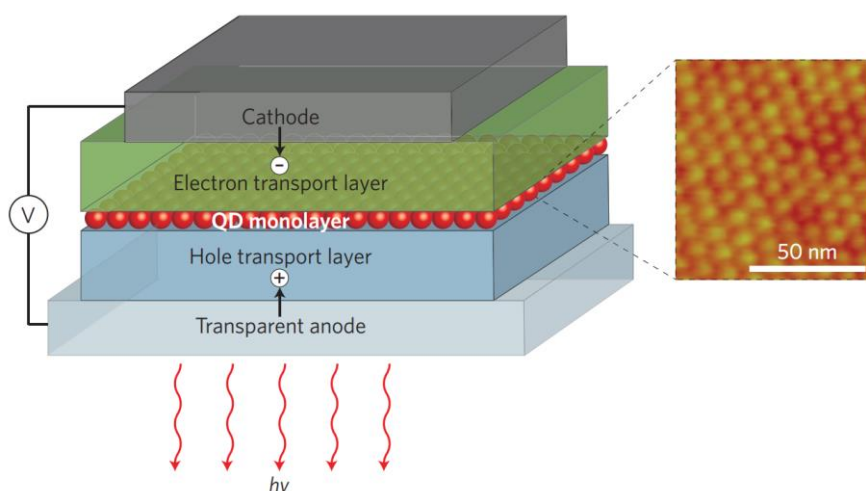


Figure 1-14 Typical QD LED (reproduced from ref.<sup>134</sup>).

The original QD-LED produced by Colvin *et al*<sup>135</sup> reported a very low external quantum efficiency (EQE) of 0.01% primarily because QD synthesis was in its infancy and the CdSe QDs used had a low PLQY. Therefore, once core-shell QDs with

improved PLQYs were developed, their inclusion in QD-LEDs shortly followed<sup>136,137</sup>. However, as reported by Mattoussi *et al*<sup>137</sup>, the increased efficiency in PLQY did not translate to a proportional increase in LED external efficiency as the charge transport layers (CTLs) became the limiting component in the device. The use of high PLQY QDs allowed for very thin QD emitting monolayers, which in turn led to improvements in electron and hole transport<sup>138</sup>. With this new method, the conducting polymer layer was replaced by small organic molecules as charge transport layers<sup>139</sup>. By eliminating the polymer electroluminescence, greater colour purity was achieved and devices exhibiting an EQE as high as 2.7% was reported by Anikeeva *et al*<sup>140</sup>.

The next development in QD-LED technology was facilitated by the removal of organic molecules entirely when novel electron transporting layers (ETL) and hole transporting layers (HTL) were developed entirely from inorganic systems. Examples include the use of CuO as a HTL<sup>141</sup>, ZrO<sub>2</sub><sup>142</sup> or ZnO nanoparticles for an ETL<sup>143</sup>, or a combination of MoO<sub>3</sub> and TiO<sub>2</sub> for an effecting CTL<sup>144</sup>. As the use of sequential inorganic layers led to interfacial defects, surface ligand modification was, again, implemented to reduce this issue. A tripling in EQE efficiency was reported when 7,7,8,8-tetracyanoquinodimethane was incorporated between the ZnO ETL and the emissive QD layer<sup>145</sup>. Subsequent generations of QD-LEDs employed a combination of inorganic and organic layers for CTLs as the sputtering process for depositing the oxide layer on top of the QDs was damaging the QDs. In this generation of QD-LEDs the HTL was built from a combination of PEDOT:PSS and either poly-TPD or TFD<sup>146-149</sup>. Further advancements on this design were carried out by Chen *et al* where the proposed that incorporating graphene oxide into the PEDOT:PSS layer improves band alignment between the HTL and the QD layer<sup>150</sup>. This was due to the an increased hole injection rate into the QDs as the HOMO level of the GO/PEDOT:PSS had greater overlap with the VB of the QDs.

While continued advancements in cadmium based QD-LEDs have led to highly efficient QD-LEDs there is still an underlying question of their safety due to the presence of heavy metals. More recently, efforts have been made to use cadmium free QDs for QD-LED devices. For example, InP QDs have been implemented in a number of QD-LED devices<sup>151,152</sup>. By using InP/ZnS core-shell QDs, not only have improvements in quantum yields been demonstrated, but the ability to tune the emission across the whole visible spectrum has been shown<sup>153</sup>. Other examples of cadmium free QD-LEDs include more complicated ternary systems such as I-III-VI QDs. Initially reported by Malik *et al.* these QDs demonstrated interesting optical properties such as a large Stokes shift and extended PL lifetimes<sup>154</sup>. While these QDs have been used in a number of QD-LEDs<sup>155,156</sup>, more recently Yang *et al* prepared highly effective CuInS/ZnS core-shell QD-LEDs<sup>157</sup>. These QDs were prepared by the sequential growth of 3 shells creating a thick outer shell and an alloyed core providing less lattice strain at the core-shell interface. Due to this structure, Auger recombination was minimised and an EQE of 7.3% was achieved, which is impressive for cadmium free systems. As is reported for these ternary QDs, the emission can be tuned over the whole visible spectrum by varying the ratio of copper to indium in the core. Alternative cadmium free QD-LEDs have been prepared using quaternary QD systems including CuZnInS<sup>158</sup> and CuInGaS<sup>159</sup>. Similar to the tertiary systems, the optical properties of these quaternary systems can be tuned by varying the stoichiometric ratio in the core, in doing this, the entire visible spectrum can be emitted. For example, green, red, and yellow emitting CuInZnS/ZnS core shell QDs were used to produce QD-LEDs by varying the copper content in the cores<sup>160</sup>. The QD-LEDs exhibited an EQE of 2.42%, significantly lower than the best cadmium containing QD-LEDs.

### 1.6.2 Quantum dot based solar cells

Solar energy involves the harvesting of sun light to generate an electric current, and QDs have been extensively explored for their potential in solar cell technology. This is primarily due to their relatively high efficiencies and low-cost manufacturing and

processing<sup>161-163</sup>. By utilising solution processing in colloidal quantum dot solar cell fabrication, costs can be hugely reduced through the use of roll-to-roll and spray coating techniques. Solar cell efficiency is generally quoted as power conversion efficiency (PCE), the ability for a PV cell to convert sunlight into current. It is described below in Equation 1-5 and facilitates the standardised comparison of different PV cell efficiencies.

$$PCE = \frac{I_{SC}V_{OC}FF}{P_{light}}$$

*Equation 1-5 Determination of the power conversion efficiency of a photovoltaic device.  $I_{sc}$  is the short circuit current,  $V_{oc}$  is the open circuit voltage,  $FF$  is the fill factor, and  $P_{light}$  is the power of the incident radiation.*

All QD solar cells operate under the same general principle: incident sunlight is absorbed by the QD layer generating an exciton, the hole and excited electron are separated and diffuse through conducting layers and subsequently recombine generating electricity. Initial QD PV cells were based upon a simple Schottky junction between a semiconductor and a metal. Primarily these cells include low work function metals such as aluminium combined with p-type QDs, on the opposite side of the QDs is a transparent conducting electrode (CTE) such as indium tin oxide (ITO) which acts as the hole conducting layer. When the device is irradiated, the QD generates an exciton after which the electrons diffuse to the metal and the holes travel to the CTE (Figure 1-15 (A)).

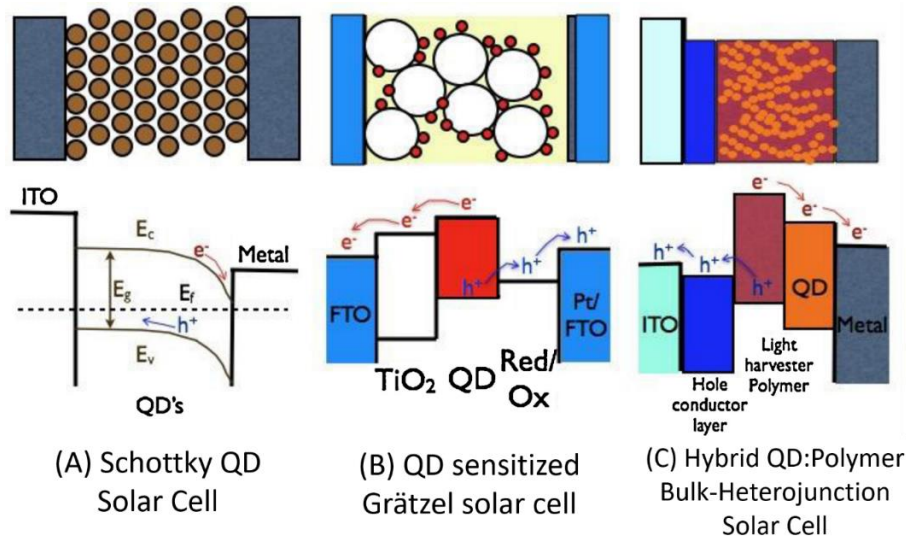


Figure 1-15 Graphical description of 3 types of QD solar cells as well as the associated energy diagrams (reproduced from ref.<sup>164</sup>)

Sargent *et al.* first demonstrated a QD Schottky photovoltaic device in 2008 with a PCE of 1.8%<sup>165</sup> producing a device made with PbS QDs, aluminium, and ITO. It should be noted that PbS and PbSe QDs appear to dominate the Schottky junction QD PV sector due to their p-type characteristics. Despite numerous attempts to improve the cathode material<sup>166,167</sup>, and introduce intermediate organic<sup>167,168</sup> and inorganic<sup>167</sup> layers, Schottky based QD PV devices struggled to exceed a PCE of 5%<sup>169</sup>. The highest efficiency in a Schottky device was produced using 3.7 nm PbS QDs with ITO as the CTE and LiF/Al as the cathode<sup>170</sup>.

Dye sensitised solar cells (DSSCs), or Grätzel cells, have also been designed with the implementation of QDs. DSSCs were originally developed using expensive ruthenium BIPY complexes as the sensitising dye<sup>171</sup>, therefore, quantum dots offered several advantages including increased photo-stability, broader absorption and cheaper manufacturing costs. The operation of a QD Grätzel cell is described in Figure 1-15 (B) above. When the QD layer absorbs light of sufficient energy, an exciton is formed. Due to band alignment the excited electron is injected into the CB of the TiO<sub>2</sub> and diffuse to the TCE such as fluorine-doped tin oxide (FTO). The electrolyte in contact with the QD reduces the QD and the hole “travels” through the redox electrolyte closing the circuit at the opposite electrode. A wide variety of

QDs have been examined as possible sensitizers in these cells such as PbS<sup>172,173</sup>, CdSe<sup>41,101,174-177</sup>, CdS<sup>178-181</sup>, CdTe<sup>174,182,183</sup> amongst many others. As QD properties alter with the QD size, the effect of QD size on the PCE of CdSe QD sensitised solar cells was investigated for CdSe QDs ranging from 2.5 to 7.8 nm<sup>184</sup>. They reported that larger QDs were more efficient at harvesting light over a broader spectrum, however the smaller QDs demonstrated more effective electron injection due to the higher energy conduction band of the smaller QD. The use of novel TiO<sub>2</sub> topologies has also been investigated for increased charge transport between the TiO<sub>2</sub> and the QD layers. For example, by vertically aligning TiO<sub>2</sub> nanowires and growing ZnO nanorods or nanosheets on the surface, a unique hybrid array photoanode was produced. It was shown to have improved fill factor and short circuit current when compared to the TiO<sub>2</sub> array without the ZnO<sup>185</sup>. The same scientists produced similar arrays using SnO<sub>2</sub> or Zn<sub>2</sub>SnO<sub>4</sub> on TiO<sub>2</sub><sup>186</sup>.

Figure 1-15 (C) above presents one final form of QD solar cell to be discussed, the QD-polymer hybrid solar cell. Initially, it was discovered that the inclusion of C<sub>60</sub> fullerenes in the polymer layer of a MEH-PPV photovoltaic device led to significantly higher efficiencies<sup>187</sup>. This is largely due to the increased charge separation and mobility introduced by the fullerenes. Quantum dots have since been found to be successful substitutes in these hybrid polymer solar cells. The use of QDs allow for precise bandgap engineering, increased light adsorption capabilities (including IR), and surface modification. In addition, the direct absorption of light by both the polymer and the QD present unique light harvesting opportunities. Alivisatos *et al* were the first to design QD/polymer hybrid solar cells however the reported efficiency was only 0.1%<sup>188</sup>. Since then polymer QD hybrid solar cells have been produced from a wide range of materials including CdS<sup>189-192</sup>, CdSe<sup>193-197</sup>, PbS<sup>198-201</sup>, PbSe<sup>199,202-204</sup> to name a few. More recent devices have reached efficiencies as high as 5.23% and 5.31% using PbS and PbSe based polymer devices<sup>205,206</sup>.

## 1.7 Biological applications of QDs

QDs offer several advantages for biological applications when compared with organic alternatives. For example, QDs are resistant to photo-bleaching when compared to traditional dyes<sup>207</sup>, this makes them attractive candidates for biological imaging. For example, in a side by side study, Rhodamine B was tested against cadmium selenide (CdSe) QDs in an experiment where the Rhodamine underwent photo-degradation after 10 minutes, whereas the CdSe QD sample was stable for 4 hours under irradiation<sup>207</sup>.

Traditionally, quantum dots are synthesised with heavy metals such as cadmium, tellurium, and selenium, as their Bohr exciton radius allows confinement within the visible part of the electromagnetic spectrum. However, due to toxicity concerns with these heavy metals, there has been a drive to develop less toxic quantum dots for biological applications. Cd based quantum dots are known to dissociate to Cd<sup>2+</sup> in physiological media under prolonged exposure to UV light in a process known as photolysis. This is due to the UV light being of similar energy to the bond energy and dissociating the particles<sup>208</sup>. In an attempt to reduce the toxicity of QDs, great efforts have been taken to produce so-called core-shell QDs. Although core-shell QDs are synthesised for a variety of reasons, for biocompatibility purposes, core-shell QDs attempt to encapsulate the toxic, fluorescent core of the QD within a layer of biologically inert material such as selected organic polymers<sup>209</sup>, silica or zinc based semiconductors<sup>210</sup>. While this method generally decreases the cytotoxicity of the QDs, it is axiomatic that removing toxic heavy metals entirely from the QDs would ensure safer opportunities going forward. As a consequence, research into cadmium-free quantum dots such as zinc sulfide or indium phosphide has recently attracted more attention.

Additionally, QDs must be water-soluble if they are to be biocompatible. QDs are primarily synthesised in organic solvents using oily ligands, such as trioctylphosphine oxide and oleylamine, which create a highly mono-disperse, crystalline product as previously discussed. However, as prepared, these particles



are not water-soluble and cannot be used for biological studies. To create water-soluble QDs, it is necessary either use an aqueous synthesis or to replace the hydrophobic surfactants with hydrophilic stabilisers using a method known as a phase transfer or ligand exchange. In a typical phase transfer, an organic QD solution is combined with an aqueous solution of the water-soluble ligand and the mixture is stirred. UV-Vis spectroscopy can be used to monitor the process as the fluorescent QDs are extracted from the organic layer and are then stabilised in the aqueous layer. The most common water stabilising ligand is mercaptopropionic acid (MPA), although subsequently, amino acids such as cysteine and penicillamine are being used more frequently due to increased functionality and optical activity. Figure 1-16 shows examples of some commonly used water-soluble ligands:

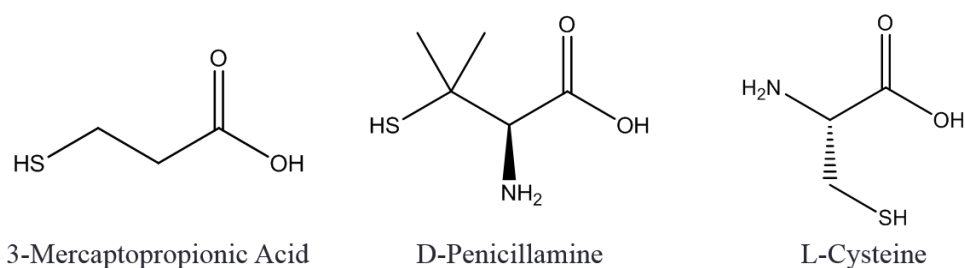


*Figure 1-16: Common water solubilising ligands for QD phase transfers.*

All of these ligands primarily bind to the quantum dots through the thiol group, although there is evidence to suggest that there is a secondary binding effect through the carboxylate group<sup>211</sup>. The carboxylate group is responsible for making the particles water stable, and deprotonation of this stabilising ligand generates a negative charge on the surface of the QD, increasing colloidal stability (Figure 1-17).

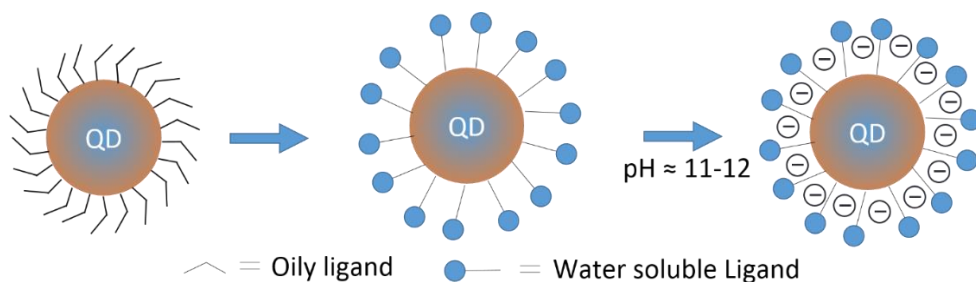


*Figure 1-17: General process for phase transfer and stabilising of quantum dots.*

In overall, there are many applications for biocompatible quantum dots including biosensing, cell imaging, fluorescent assays, photodynamic therapy and many others (Figure 1-18).

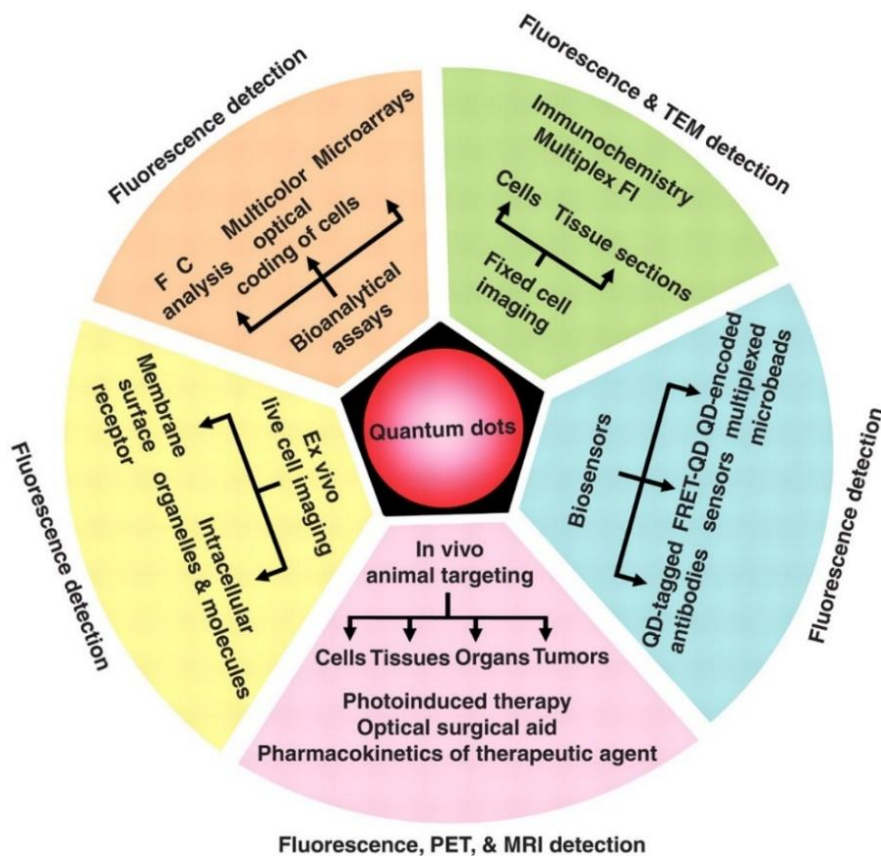
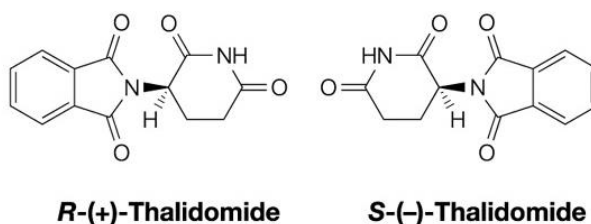


Figure 1-18: The numerous uses for quantum dots in biomedical applications. Reproduced from ref. <sup>212</sup>).

## 1.8 Chirality in nanoscience

A chiral molecule is one that has two mirror-image forms which are not superimposable in three dimensions. These mirror image forms of a molecule are known as enantiomers. Chirality is an integral property of the natural world as the majority of biological materials in this world, from proteins to DNA, are chiral. Therefore, the ability to analyse, interpret and apply the properties of chirality is highly important in the fields of chemistry, pharmacology, biology and medicine. One of the most famous examples of when chirality played a vital role is

Thalidomide, a morning sickness drug which existed in two enantiomeric forms as seen in Figure 1-19:



*Figure 1-19: The two enantiomeric forms of Thalidomide (reproduced from ref.<sup>213</sup>).*

Following its approval and large-scale distribution, it was found that one of the enantiomers led to irreparable birth defects. This example shows us that an in-depth understanding of chirality and its biological significance is necessary to develop solutions to the medical problems of the present and future. If a molecule is chiral, it possesses the ability to rotate plane polarised light or to absorb circularly polarised light of one direction or another preferentially. Circular dichroism is the technique used to monitor this preferential absorption and is discussed below in 2.6.3 of the experimental section.

A chiral center within a molecule may be described as either R (rectus, right) or S (sinister, left) according to the Cahn-Ingold system. Using the Cahn-Ingold system, the substituents surrounding a stereocenter are examined and an order of priority is assigned based on increasing molecular weight. If the priority of substituents increases in a clockwise direction, the stereocenter is assigned an **R**. Conversely if the substituents increase in priority in a counter clockwise direction, the stereocenter is assigned an **S**.

Furthermore, if a molecule rotates plane polarised light clockwise it is labelled **D** (dextrorotatory) and if a molecule rotates plane polarised light counter clockwise it is labelled **L** (laevorotatory).

Although chirality was originally the domain of molecular and biological research, as the field of nanomaterials has expanded so too has the emerging area of chirality in

nanomaterials. Figure 1-20 demonstrates the near exponential growth in interest in chirality in nanoscience over the past 15 years.

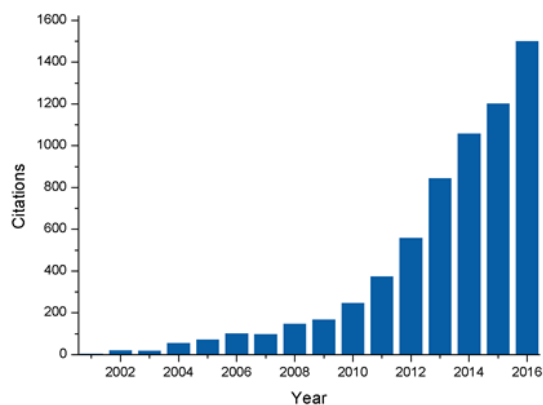


*Figure 1-20 Number of citations for publications about chiral nanomaterials by year.*

### 1.8.1 Chirality of nanomaterial macro-assemblies

Chiral nanomaterials can be produced through a variety of different techniques and approaches. One of the most prominent areas is the synthesis of chiral macrostructured nanomaterials. Nano-helices have been synthesised as single helices made out of silica and titania for example<sup>214-218</sup>, while silica double helices have also been synthesised<sup>219</sup>. Beyond this, helical chirality has been reported in macro-assemblies of achiral CuO into chiral flower structures<sup>219,220</sup>. Optically active CdTe nanoribbons have been synthesised by the self-assembly of achiral CdTe QDs capped with mercaptopropionic acid when interacted with circularly polarised light resulting in either left or right handed twisted ribbons demonstrating high degrees of optical activity (Figure 1-21)<sup>221</sup>.

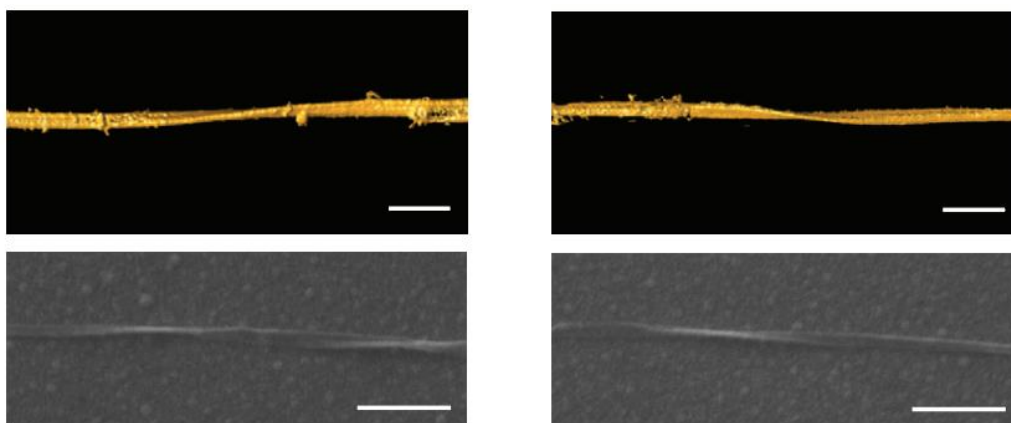


Figure 1-21 Left and right-handed CdTe nanoribbons (reproduced from ref.<sup>221</sup>)

It is understood the optical activity in these assemblies was due to the long-range order of molecules in a chiral arrangement collectively responding to circularly polarised light (CPL). The magnitude of the chiroptical response is proportional to the size of the assembly, and so these materials exhibit much stronger chiral signals compared to single chiral nanoparticles.

### 1.8.2 Ligand-induced chirality

Chirality in nanoparticles can often be attained through an interaction between an achiral nanoparticle and a chiral organic capping ligand. This was originally demonstrated for metallic nanoparticles such as gold and silver nanoparticles although it has subsequently been reported in a wide array of nanoparticle systems.

Originally reported by Schaff *et al.* in 2000, L-glutathione capped gold nanoparticles presented strong optical activity<sup>222</sup>. Similar experiments were then carried out using D and L penicillamine by Yao *et al.* in 2005 producing mirror image CD spectra<sup>223</sup>. Since then much research has involved chirality in gold nanoparticles<sup>224-226</sup>. Theoretical research by Govorov *et al.* has made attempts to model and identify the various chiral interactions that take place in these gold nanoparticles. Firstly, the chiral CD signal of the surface ligand is enhanced by Coulombic coupling with the plasmonic resonance of the metal nanoparticle. Secondly, the plasmonic absorption of the nanoparticle was influenced due to the dipole-dipole interaction with the chiral surface ligand. This second effect is primarily responsible for interesting

optical activity being present in the plasmonic absorption region where there is no direct absorption from the ligand<sup>227,228</sup>. Production of optically active silver<sup>229-231</sup> has also been achieved using a variety of techniques from traditional coprecipitation to irradiation methods.

Ligand-induced chirality has featured prominently in the field of optically active quantum dots, although the proposed mechanism by which induced chirality appears is different as the QDs are not plasmonic. As chiral quantum dots are the primary focus of this research, they will be discussed further in section 1.9.

### 1.8.3 Intrinsic chirality

One area of chirality in nanomaterials involves the concept of intrinsic chirality, where the nanoparticle surface or structure demonstrates chirality in the absence of any external influences by chiral ligands. For example, tellurium has a crystal structure which allows for two enantiomeric forms to exist. Markovich *et al.* have developed a synthetic approach to produce an enantiopure sample using thiolated chiral biomolecules<sup>232</sup> which produce huge CD signals.

Alternatively, certain faces of crystals present chiral surfaces such as copper. It has been shown that kinked-stepped, high miller index surfaces on copper, such as copper (643) are chiral and therefore display enantioselective properties<sup>233</sup>. Based on this it was shown that the kinetic separation of racemic 3-methylcyclohexanone using the Cu(643)<sup>R&S</sup> surfaces was possible. Molecular dynamic calculations on Cu(3,1,17)<sup>R&S</sup> demonstrated the enantioselective binding energies of R and S-propranolol. It was shown that the difference in binding energies on the Cu(3,1,17) surface are six times greater than the difference on the Cu(111) surface<sup>234</sup>.

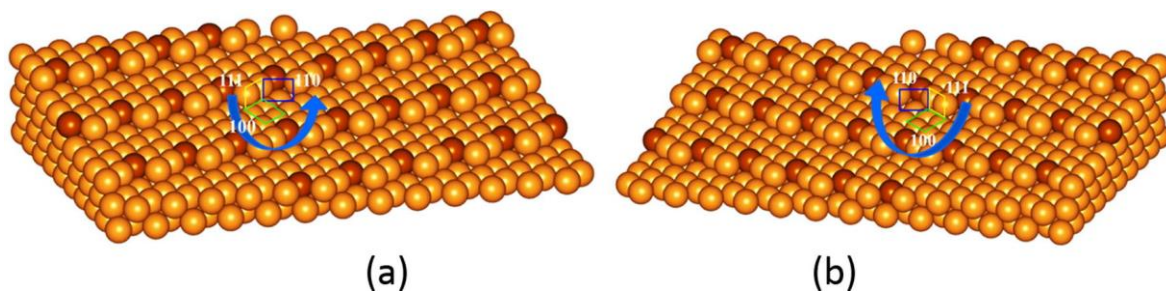


Figure 1-22 Chiral (a)  $\text{Cu}(3,1,17)^S$  and (b)  $\text{Cu}(3,1,17)^R$  surfaces (reproduced from ref.<sup>234</sup>)

## 1.9 Chiral Quantum Dots

Most of quantum dots can demonstrate optical activity due to ligand-induced chirality, as previously mentioned. However, some exceptions exist such as chiral imprinting<sup>235</sup>. To induce chirality in quantum dots chiral ligands must be bound directly to the surface and this can be done in one of two ways. In both instances, the mechanism by which chirality is induced primarily relates to the overlap of electronic states in the chiral molecule with the electronic states in the QD<sup>236,237</sup>, although there is some evidence enabling to suggest that physical distortions of the crystal lattice at the surface may contribute<sup>238,239</sup>. The two main methods for producing chiral quantum dots are discussed below.

Firstly, QDs may be synthesised in the aqueous phase in the presence of a chiral stabiliser such as cysteine or penicillamine. Nearly all available ligands which include a chiral centre are water soluble so creating chiral QDs in the aqueous phase allows for a more facile, 1-step synthesis. Moloney *et al.*<sup>240</sup> have synthesised chiral CdS using an aqueous microwave synthesis in the presence of D-penicillamine and L-penicillamine separately. It was found that these QDs demonstrated optical activity in the band edge absorption of the QDs. Similarly, Gallagher *et al.* used comparable microwave synthesis techniques to produce optically active CdSe QDs stabilised with D- and L- penicillamine. The aqueous approach to synthesising chiral QDs is not limited to microwave synthesis as traditional heating under reflux methods in the presence of chiral stabilisers have also been used. Reflux methods have been used

to produce optically active CdTe QDs<sup>241</sup> while Govan *et al.*<sup>242</sup> synthesised optically active CdS tetrapods using a similar approach.

The second approach to produce chiral quantum dots involves the initial synthesis of QDs in the organic phase using techniques such as hot-injection, followed by a ligand exchange to replace the achiral organic ligands with chiral aqueous ligands. This method offers a variety of advantages over the direct aqueous synthesis as there is far more literature and knowledge available about the organic synthesis of QDs. Consequently, there is a larger variety of materials available including core-shell structures, anisotropic structures and tertiary and quaternary quantum dots with which to perform ligand exchanges. This field of performing ligand exchanges to induce chirality in quantum dots was pioneered by M. Balaz *et al.* when they found that a phase transfer of trioctylphosphine oxide or oleic acid capped CdSe QDs from toluene into the aqueous phase using chiral ligands can induce chiroptical properties in originally achiral cadmium selenide QDs<sup>243</sup>. In this case, the authors have explained the origin of the induced CD in QDs by the hybridisation of the chiral ligand's HOMOs with the CdSe molecular orbitals. However, since then a number of publications on the topic have been published<sup>244-247</sup>.

While the field of chiral QDs is relatively new, initial results have indicated the promise of these nanomaterials for future biomedical applications. For example, Delgado-Pérez *et al.* synthesised chiral CdSe-ZnS core-shell QDs which were used to sense chiral drugs such as naproxen and ibuprofen. It was found that the chiral drug molecules quenched the QD emission in a concentration-dependent mode. The spectral differences in the behaviour of R- and S- enantiomers of these drugs enabled the quantitative determination of both chiral forms in mixtures and pharmaceutical samples<sup>248</sup>. Similar experiments were carried out by Wawrzyńczyk *et al.* showing the selective quenching of chiral CdSe of different sizes by R- and S-Naproxen<sup>249</sup>. In one experiment CdSe/ZnS QDs functionalised with a thiolated  $\beta$ -cyclodextrin demonstrated enantio-recognition of D- and L- penicillamine<sup>250</sup>. It is



clear from the above experiments that chiral quantum dots are finding uses in a variety of enantiospecific sensing experiments and as this field is relatively new, it is expected that more specific and useful applications will be found over time.

### 1.10 Thiosugars as ligands for QDs

II-VI type QDs can normally be capped and stabilised by ligands which contain a thiol group such as cysteine or dodecanethiol. As advancements in organic synthetic chemistry have taken place, a new class of thiolated carbohydrates has been developed and utilised for conjugation<sup>251-254</sup>. As this new class of compounds has emerged, research has begun to use thio-carbohydrates as ligands for biochemical applications<sup>255</sup>. The basic design of glucose conjugated QDs can be seen below although theoretically any carbohydrate can be used if the anomeric alcohol is replaced with a thiol group.

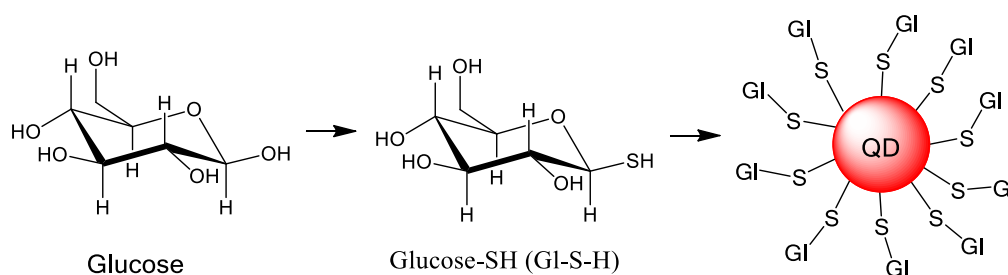


*Figure 1-23 Development of carbohydrate conjugated QDs from carbohydrates.*

For example, Coulon *et al*<sup>256</sup> conjugated CdTe QDs to glucose and used them to selectively label certain yeast strains for imaging. Similarly, Yang *et al*<sup>257</sup> conjugated various lactose derivatives to CdSe/ZnS QDs and used them to study carbohydrate-protein interactions. More recently, it has been shown that glycosylated copper doped CdS QDs could be used for the swift detection and discrimination of bacteria<sup>258</sup>. Discrimination was performed by differentiating the binding strengths between the bacterial cell walls and the glycol-QD conjugates.

In addition, these compounds are finding uses in probing protein-glycan interactions. It has been demonstrated that glycan conjugated QDs offer potential

probing applications for analysing protein-glycan binding modes using Forster resonance energy transfer (FRET) analysis<sup>258</sup>. From the above, we can see that QD-carbohydrate conjugates provide exciting opportunities for imaging and diagnostics in the field of biomedicine.

### 1.11 Cation exchange in quantum nanostructures

Cation exchange (CE) is a process of replacing the cation in an ionic solid for a different cation and is primarily performed in solution. It is a technique which has existed for quite some time however the applications have been limited until the development of the nanomaterial sector, as cationic exchanges in the bulk are very slow to proceed<sup>259</sup>. The rate of cationic exchange increases substantially when dealing with the nanoscale and the process has become viable for common use in synthesis. A schematic of how cation exchanges in quantum dots occurs may be seen below in Figure 1-24.

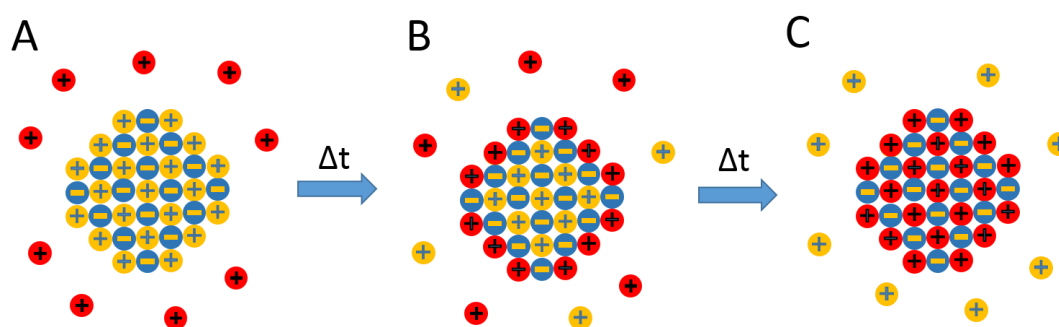


*Figure 1-24 The 3 stage (A-C) for cationic exchange in quantum dots.*

In Figure 1-24 (A) we see the QD before CE surrounded by the target cation in solution. Stage B indicates the initiation of the CE process as the surface cations are exchanged initially and finally in stage (C) we see the final product where all the cations have been exchanged. It is evident from the above schematic that it is possible through careful control to only modify the surface cations creating a core-shell structure. The cation exchange process is dictated by slight differences in

thermodynamic properties such as solvation energies, lattice energies, bond enthalpies and surface energies and so careful consideration to the starting conditions are required to control the extent of the CE and whether it will undergo exchange at all. CE is very effective for the synthesis of anisotropic materials. For example, PbS nanorods have been synthesised from CdS nanorods<sup>260</sup>, CdS nanorods have been converted to binary CdS-Cu<sub>2</sub>S nanorods<sup>261</sup>, and CdTe nanotetrapods have been converted into Ag<sub>2</sub>Te tetrapods. It is clear from the above that it is possible to exchange cations of differing valency using this method also and therefore cation exchanges provide a promising method for synthesising interesting, anisotropic materials which are otherwise difficult to create. Similar CE techniques have been applied to the synthesis of complicated tertiary core/shell systems as demonstrated by Park *et al.* who produced strongly emitting CuInS<sub>2</sub>/ZnS core-shell quantum dots using cation exchange techniques<sup>262</sup>.

Additionally, cation exchanges become helpful when synthesis in the absence of heat is required. For example, infra-red emitting PbSe QDs have shown potential for applications including lasers<sup>263</sup> and solar cells<sup>264</sup>. These QDs are inherently unstable at ambient conditions leading to reduced quantum yields and blue shifting of emission within days of exposure to air<sup>265</sup>. Therefore attempts have been made to shell PbSe QDs, however the high tendency of PbSe QDs for Ostwald ripening at mild reaction conditions<sup>266</sup> makes it problematic. Consequently, Pietryga *et al.* developed a cation exchange process to shell PbSe with CdSe at ambient conditions eliminating the risk of further nanocrystal growth<sup>267</sup>.

While using cation exchanges for synthetic purposes is one field, Chan *et al.* have introduced cation exchange for sensing applications. In this research, CdSe QDs were used for high sensitivity detection of copper (II) through a cation exchange process where the exchange of copper for cadmium led to PL intensity and wavelength shifts<sup>268</sup>.

## 1.12 Aims and objectives of the project

The main goal of this project is to produce a variety of optically active fluorescent nanomaterials and test them in a range of potential applications.

Firstly, we aim to synthesise cadmium free quantum dots such as ZnS and dope the ZnS with manganese to produce phosphorescent ZnS:Mn QDs. Using these QDs, we plan to perform a series of ligand exchange reactions with several different chiral ligands to induce a chiroptical response in the band edge absorption region of the QDs. Upon successful preparation of chiral ZnS:Mn QDs we aim to test the cytotoxicity of the QDs and monitor any enantioselective toxicity. Also attempts are to be made to produce optically active ZnSe QDs stabilised with glutathione also and to examine any enantioselective quenching behaviour.

CdSe/CdS heterostructured quantum rods and quantum tetrapods will be synthesised and transferred to the aqueous phase to induce chirality. Chiral sensing experiments will be carried out using the drug Naproxen and it is expected an enantioselective quenching should be observed.

Following this a variety of optically active cadmium containing nanoparticles such as QDs and nanoplatelets are planned to be produced either directly through aqueous synthesis or through the traditional organic synthesis followed by a phase transfer.

Finally, we aim to demonstrate some applications of our materials and techniques. In an attempt to convert our cadmium containing nanostructures into cadmium free materials a series of cation exchange reactions are to be performed to replace  $\text{Cd}^{2+}$  with  $\text{Zn}^{2+}$ . To demonstrate the utility of our phase transfer techniques we plan to produce highly luminescent CdZnSeS/ZnS alloyed core-shell QDs and then exchange the organic ligands for a mixture penicillamine and thiolactose. By varying the degree of glycosylation on the surface we aim to demonstrate a difference in cellular uptake and *in vivo* behaviour under confocal microscopy.

We hope that this research will result in new synthetic strategies for the preparation and investigation of different chiroptically active nanostructures and demonstrate their utility in a variety of applications.

### 1.13 References

- (1) Paul Mushonga, M. O. O., Abram M. Madiehe, Mervin Meyer *Journal of Nanomaterials* **2012**, 2012.
- (2) Meulenberg, R. W.; Lee, J. R. I.; Wolcott, A.; Zhang, J. Z.; Terminello, L. J.; van Buuren, T. *ACS Nano* **2009**, 3, 325.
- (3) Alivisatos, A. P. *The Journal of Physical Chemistry* **1996**, 100, 13226.
- (4) M G Bawendi; M L Steigerwald, a.; Brus, L. E. *Annual Review of Physical Chemistry* **1990**, 41, 477.
- (5) Brus, L. E. *The Journal of Chemical Physics* **1984**, 80, 4403.
- (6) Smith, A. M.; Nie, S. *Accounts of Chemical Research* **2010**, 43, 190.
- (7) Zhang, J.; Chen, Q. H.; Zhang, W. L.; Mei, S. L.; He, L. J.; Zhu, J. T.; Chen, G. P.; Guo, R. Q. *Appl. Surf. Sci.* **2015**, 351, 655.
- (8) Wang, C. L.; Hu, Z. Y.; Xu, S. H.; Wang, Y. B.; Zhao, Z. X.; Wang, Z. Y.; Cui, Y. P. *Nanotechnology* **2015**, 26, 6.
- (9) Huy, B. T.; Seo, M. H.; Phong, P. T.; Lim, J. M.; Lee, Y. I. *Chem. Eng. J.* **2014**, 236, 75.
- (10) Mei, S. L.; Zhu, J. T.; Yang, W.; Wei, X.; Zhang, W. L.; Chen, Q. H.; He, L. J.; Jiang, Y.; Guo, R. Q. *Journal of Alloys and Compounds* **2017**, 729, 1.
- (11) Bailey, R. E.; Nie, S. M. *Journal of the American Chemical Society* **2003**, 125, 7100.

- (12) Saikia, K.; Deb, P.; Mondal, B.; Kalita, E. *Materials Research Express* **2014**, *1*, 015014.
- (13) Yu, J. H.; Kwon, S. H.; Petrasek, Z.; Park, O. K.; Jun, S. W.; Shin, K.; Choi, M.; Park, Y. I.; Park, K.; Na, H. B.; Lee, N.; Lee, D. W.; Kim, J. H.; Schwillie, P.; Hyeon, T. *Nature materials* **2013**, *12*, 359.
- (14) Marriott, G.; Clegg, R. M.; Arndt-Jovin, D. J.; Jovin, T. M. *Biophysical Journal* **1991**, *60*, 1374.
- (15) Dhawan, T.; Tyagi, R.; Bag, R.; Singh, M.; Mohan, P.; Haldar, T.; Murlidharan, R.; Tandon, R. P. *Nanoscale Research Letters* **2010**, *5*, 31.
- (16) Sun, Z. H.; Liu, Z. K.; Li, J. H.; Tai, G. A.; Lau, S. P.; Yan, F. *Adv. Mater.* **2012**, *24*, 5878.
- (17) Zhu, G.; Lv, T.; Pan, L.; Sun, Z.; Sun, C. *Journal of Alloys and Compounds* **2011**, *509*, 362.
- (18) Ploog, K. H.; Noetzel, R. 1992; Vol. 1676, p 74.
- (19) Brus, L. E. *The Journal of Chemical Physics* **1984**, *80*, 4403.
- (20) Brus, L. *The Journal of Physical Chemistry* **1986**, *90*, 2555.
- (21) Steigerwald, M. L.; Brus, L. E. *Accounts of Chemical Research* **1990**, *23*, 183.
- (22) Henglein, A. *Chemical Reviews* **1989**, *89*, 1861.
- (23) Spanhel, L.; Haase, M.; Weller, H.; Henglein, A. *Journal of the American Chemical Society* **1987**, *109*, 5649.
- (24) Weller, H.; Schmidt, H. M.; Koch, U.; Fojtik, A.; Baral, S.; Henglein, A.; Kunath, W.; Weiss, K.; Dieman, E. *Chemical Physics Letters* **1986**, *124*, 557.
- (25) Murray, C. B.; Norris, D. J.; Bawendi, M. G. *Journal of the American Chemical Society* **1993**, *115*, 8706.
- (26) Murray, C. B.; Kagan, C. R.; Bawendi, M. G. *Annual Review of Materials Science* **2000**, *30*, 545.
- (27) LaMer, V. K.; Dinegar, R. H. *Journal of the American Chemical Society* **1950**, *72*, 4847.
- (28) Peng, X.; Wickham, J.; Alivisatos, A. P. *Journal of the American Chemical Society* **1998**, *120*, 5343.
- (29) Sugimoto, T. *Advances in Colloid and Interface Science* **1987**, *28*, 65.
- (30) Norris, D. J.; Bawendi, M. G. *Physical Review B* **1996**, *53*, 16338.
- (31) Nasilowski, M.; Spinicelli, P.; Patriarche, G.; Dubertret, B. *Nano Letters* **2015**, *15*, 3953.
- (32) Chen, O.; Zhao, J.; Chauhan, V. P.; Cui, J.; Wong, C.; Harris, D. K.; Wei, H.; Han, H.-S.; Fukumura, D.; Jain, R. K.; Bawendi, M. G. *Nature materials* **2013**, *12*, 445.
- (33) Hao, J.-j.; Zhou, J.; Zhang, C.-y. *Chemical Communications* **2013**, *49*, 6346.
- (34) Reiss, P.; Bleuse, J.; Pron, A. *Nano Letters* **2002**, *2*, 781.
- (35) Li, L.; Reiss, P. *Journal of the American Chemical Society* **2008**, *130*, 11588.
- (36) Nan, W. N.; Niu, Y. A.; Qin, H. Y.; Cui, F.; Yang, Y.; Lai, R. C.; Lin, W. Z.; Peng, X. G. *Journal of the American Chemical Society* **2012**, *134*, 19685.
- (37) Mekis, I.; Talapin, D. V.; Kornowski, A.; Haase, M.; Weller, H. *J. Phys. Chem. B* **2003**, *107*, 7454.
- (38) Lim, J.; Jun, S.; Jang, E.; Baik, H.; Kim, H.; Cho, J. *Adv. Mater.* **2007**, *19*, 1927.
- (39) Li, J. J.; Wang, Y. A.; Guo, W.; Keay, J. C.; Mishima, T. D.; Johnson, M. B.; Peng, X. *Journal of the American Chemical Society* **2003**, *125*, 12567.
- (40) Li, T. L.; Lee, Y. L.; Teng, H. S. *Journal of Materials Chemistry* **2011**, *21*, 5089.

- (41) Lee, H.; Wang, M. K.; Chen, P.; Gamelin, D. R.; Zakeeruddin, S. M.; Gratzel, M.; Nazeeruddin, M. K. *Nano Letters* **2009**, *9*, 4221.
- (42) Guerguerian, G.; Elhordoy, F.; Pereyra, C. J.; Marotti, R. E.; Martin, F.; Leinen, D.; Ramos-Barrado, J. R.; Dalchiele, E. A. *Nanotechnology* **2011**, *22*.
- (43) Blackman, B.; Battaglia, D.; Peng, X. G. *Chemistry of Materials* **2008**, *20*, 4847.
- (44) Eychmüller, A.; Mews, A.; Weller, H. *Chemical Physics Letters* **1993**, *208*, 59.
- (45) Mews, A.; Eychmüller, A.; Giersig, M.; Schooss, D.; Weller, H. *The Journal of Physical Chemistry* **1994**, *98*, 934.
- (46) Vossmeier, T.; Reck, G.; Katsikas, L.; Haupt, E. T. K.; Schulz, B.; Weller, H. *Science (New York, N.Y.)* **1995**, *267*, 1476.
- (47) Rogach, A. L.; Katsikas, L.; Kornowski, A.; Su, D.; Eychmüller, A.; Weller, H. *Berichte der Bunsengesellschaft für physikalische Chemie* **1997**, *101*, 1668.
- (48) Rogach, A. L.; Katsikas, L.; Kornowski, A.; Su, D.; Eychmüller, A.; Weller, H. *Berichte der Bunsengesellschaft für physikalische Chemie* **1996**, *100*, 1772.
- (49) Rogach, A.; Kershaw, S. V.; Burt, M.; Harrison, M. T.; Kornowski, A.; Eychmüller, A.; Weller, H. *Adv. Mater.* **1999**, *11*, 552.
- (50) Rogach, A. L.; Kornowski, A.; Gao, M.; Eychmüller, A.; Weller, H. *The Journal of Physical Chemistry B* **1999**, *103*, 3065.
- (51) Rogach, A.; Susha, A.; Caruso, F.; Sukhorukov, G.; Kornowski, A.; Kershaw, S.; Möhwald, H.; Eychmüller, A.; Weller, H. *Adv. Mater.* **2000**, *12*, 333.
- (52) Gao, M.; Kirstein, S.; Möhwald, H.; Rogach, A. L.; Kornowski, A.; Eychmüller, A.; Weller, H. *The Journal of Physical Chemistry B* **1998**, *102*, 8360.
- (53) Gao, M.; Lesser, C.; Kirstein, S.; Möhwald, H.; Rogach, A. L.; Weller, H. *J. Appl. Phys.* **2000**, *87*, 2297.
- (54) Zhang, H.; Zhou, Z.; Yang, B.; Gao, M. *The Journal of Physical Chemistry B* **2003**, *107*, 8.
- (55) Bao, H.; Gong, Y.; Li, Z.; Gao, M. *Chemistry of Materials* **2004**, *16*, 3853.
- (56) Eychmüller, A.; Rogach, A. L. In *Pure and Applied Chemistry* 2000; Vol. 72, p 179.
- (57) Shavel, A.; Gaponik, N.; Eychmüller, A. *The Journal of Physical Chemistry B* **2006**, *110*, 19280.
- (58) Gaponik, N.; Hickey, S. G.; Dorfs, D.; Rogach, A. L.; Eychmüller, A. *Small* **2010**, *6*, 1364.
- (59) Zhou, J.; Yang, Y.; Zhang, C.-y. *Chemical Reviews* **2015**, *115*, 11669.
- (60) Cui, R.; Liu, H.-H.; Xie, H.-Y.; Zhang, Z.-L.; Yang, Y.-R.; Pang, D.-W.; Xie, Z.-X.; Chen, B.-B.; Hu, B.; Shen, P. *Advanced Functional Materials* **2009**, *19*, 2359.
- (61) Stürzenbaum, S. R.; Höckner, M.; Panneerselvam, A.; Levitt, J.; Bouillard, J. S.; Taniguchi, S.; Dailey, L. A.; Khanbeigi, R. A.; Rosca, E. V.; Thanou, M.; Suhling, K.; Zayats, A. V.; Green, M. *Nature Nanotechnology* **2012**, *8*, 57.
- (62) Pearson, R. G. *Journal of the American Chemical Society* **1963**, *85*, 3533.
- (63) Gaponik, N.; Talapin, D. V.; Rogach, A. L.; Hoppe, K.; Shevchenko, E. V.; Kornowski, A.; Eychmüller, A.; Weller, H. *The Journal of Physical Chemistry B* **2002**, *106*, 7177.
- (64) Li, L.; Qian, H.; Fang, N.; Ren, J. *Journal of Luminescence* **2006**, *116*, 59.
- (65) Tomasulo, M.; Yildiz, I.; Kaanumalle, S. L.; Raymo, F. M. *Langmuir* **2006**, *22*, 10284.

- (66) Jeong, S.; Achermann, M.; Nanda, J.; Ivanov, S.; Klimov, V. I.; Hollingsworth, J. A. *Journal of the American Chemical Society* **2005**, *127*, 10126.
- (67) Xu, S.; Wang, C.; Xu, Q.; Zhang, H.; Li, R.; Shao, H.; Lei, W.; Cui, Y. *Chemistry of Materials* **2010**, *22*, 5838.
- (68) Cheng, T.; Li, D.; Li, J.; Ren, B.; Wang, G.; Cheng, J. *Journal of Materials Science: Materials in Electronics* **2015**, *26*, 4062.
- (69) Vossmeier, T.; Katsikas, L.; Giersig, M.; Popovic, I. G.; Diesner, K.; Chemseddine, A.; Eychmueller, A.; Weller, H. *The Journal of Physical Chemistry* **1994**, *98*, 7665.
- (70) Zhu, X.; Chass, G. A.; Kwek, L.-C.; Rogach, A. L.; Su, H. *The Journal of Physical Chemistry C* **2015**, *119*, 29171.
- (71) Resch, U.; Weller, H.; Henglein, A. *Langmuir* **1989**, *5*, 1015.
- (72) Zhang, H.; Wang, D.; Yang, B.; Möhwald, H. *Journal of the American Chemical Society* **2006**, *128*, 10171.
- (73) Tang, Z.; Kotov, N. A.; Giersig, M. *Science (New York, N.Y.)* **2002**, *297*, 237.
- (74) Srivastava, S.; Santos, A.; Critchley, K.; Kim, K.-S.; Podsiadlo, P.; Sun, K.; Lee, J.; Xu, C.; Lilly, G. D.; Glotzer, S. C.; Kotov, N. A. *Science (New York, N.Y.)* **2010**, *327*, 1355.
- (75) Wu, K.; Li, Q.; Jia, Y.; McBride, J. R.; Xie, Z.-x.; Lian, T. *ACS Nano* **2015**, *9*, 961.
- (76) Guo, J.; Yang, W.; Wang, C. *The Journal of Physical Chemistry B* **2005**, *109*, 17467.
- (77) Zhang, H.; Wang, L.; Xiong, H.; Hu, L.; Yang, B.; Li, W. *Adv. Mater.* **2003**, *15*, 1712.
- (78) Li, L.; Qian, H.; Ren, J. *Chemical Communications* **2005**, 528.
- (79) He, Y.; Sai, L.-M.; Lu, H.-T.; Hu, M.; Lai, W.-Y.; Fan, Q.-L.; Wang, L.-H.; Huang, W. *Chemistry of Materials* **2007**, *19*, 359.
- (80) Yu, Y.; Zhang, K.; Sun, S. *Appl. Surf. Sci.* **2012**, *258*, 7181.
- (81) Primera-Pedrozo, O. M.; Arslan, Z.; Rasulev, B.; Leszczynski, J. *Nanoscale* **2012**, *4*, 1312.
- (82) Wang, C.; Wang, Y.; Xu, L.; Zhang, D.; Liu, M.; Li, X.; Sun, H.; Lin, Q.; Yang, B. *Small* **2012**, *8*, 3137.
- (83) Tan, L.; Wan, A.; Zhao, T.; Huang, R.; Li, H. *ACS Applied Materials & Interfaces* **2014**, *6*, 6217.
- (84) Yang, M.; Gui, R.; Jin, H.; Wang, Z.; Zhang, F.; Xia, J.; Bi, S.; Xia, Y. *Colloids and Surfaces B: Biointerfaces* **2015**, *126*, 115.
- (85) Koneswaran, M.; Narayanaswamy, R. *Sens. Actuator B-Chem.* **2009**, *139*, 104.
- (86) Zhang, J.; Li, J.; Zhang, J.; Xie, R.; Yang, W. *The Journal of Physical Chemistry C* **2010**, *114*, 11087.
- (87) Shavel, A.; Gaponik, N.; Eychmüller, A. *The Journal of Physical Chemistry B* **2004**, *108*, 5905.
- (88) Szczech, J. R.; Higgins, J. M.; Jin, S. *Journal of Materials Chemistry* **2011**, *21*, 4037.
- (89) Rajabi, H. R. *Photocatalytic Activity of Quantum Dots*, 2016.
- (90) Mishra, N.; Mukherjee, B.; Xing, G.; Chakraborty, S.; Guchhait, A.; Lim, J. Y. *Nanoscale* **2016**, *8*, 14203.
- (91) White, S.; Cataluna, M. *Photonics* **2015**, *2*, 719.



- (92) Peng, X.; Manna, L.; Yang, W.; Wickham, J.; Scher, E.; Kadavanich, A.; Alivisatos, A. P. *Nature* **2000**, *404*, 59.
- (93) Scher, E. C.; Manna, L.; Alivisatos, A. P. *Philosophical Transactions: Mathematical, Physical and Engineering Sciences* **2003**, *361*, 241.
- (94) Peng, Z. A.; Peng, X. *Journal of the American Chemical Society* **2001**, *123*, 1389.
- (95) Peng, X. *Adv. Mater.* **2003**, *15*, 459.
- (96) Talapin, D. V.; Koeppel, R.; Götzinger, S.; Kornowski, A.; Lupton, J. M.; Rogach, A. L.; Benson, O.; Feldmann, J.; Weller, H. *Nano Letters* **2003**, *3*, 1677.
- (97) Jun, Y.-w.; Lee, S.-M.; Kang, N.-J.; Cheon, J. *Journal of the American Chemical Society* **2001**, *123*, 5150.
- (98) Peng, P.; Milliron, D. J.; Hughes, S. M.; Johnson, J. C.; Alivisatos, A. P.; Saykally, R. J. *Nano Letters* **2005**, *5*, 1809.
- (99) Mashford, B. S.; Stevenson, M.; Popovic, Z.; Hamilton, C.; Zhou, Z.; Breen, C.; Steckel, J.; Bulovic, V.; Bawendi, M.; Coe-Sullivan, S.; Kazlas, P. T. *Nature Photonics* **2013**, *7*, 407.
- (100) Im, J. H.; Lee, C. R.; Lee, J. W.; Park, S. W.; Park, N. G. *Nanoscale* **2011**, *3*, 4088.
- (101) Lee, Y. L.; Lo, Y. S. *Advanced Functional Materials* **2009**, *19*, 604.
- (102) Nozik, A. J. *Physica E-Low-Dimensional Systems & Nanostructures* **2002**, *14*, 115.
- (103) Ruhle, S.; Shalom, M.; Zaban, A. *Chemphyschem* **2010**, *11*, 2290.
- (104) Semonin, O. E.; Luther, J. M.; Choi, S.; Chen, H. Y.; Gao, J. B.; Nozik, A. J.; Beard, M. C. *Science (New York, N.Y.)* **2011**, *334*, 1530.
- (105) Bomm, J.; Buchtemann, A.; Chatten, A. J.; Bose, R.; Farrell, D. J.; Chan, N. L. A.; Xiao, Y.; Slooff, L. H.; Meyer, T.; Meyer, A.; van Sark, W.; Koole, R. *Solar Energy Materials and Solar Cells* **2011**, *95*, 2087.
- (106) Chandra, S.; Doran, J.; McCormack, S. J.; Kennedy, M.; Chatten, A. J. *Solar Energy Materials and Solar Cells* **2012**, *98*, 385.
- (107) Hyldahl, M. G.; Bailey, S. T.; Wittmershaus, B. P. *Solar Energy* **2009**, *83*, 566.
- (108) Purcell-Milton, F.; Gun'ko, Y. K. *Journal of Materials Chemistry* **2012**, *22*, 16687.
- (109) Reda, S. M. *Acta Materialia* **2008**, *56*, 259.
- (110) Asryan, L. V.; Suris, R. A. *Semiconductor Science and Technology* **1996**, *11*, 554.
- (111) Bimberg, D.; Kirstaedter, N.; Ledentsov, N. N.; Alferov, Z. I.; Kopev, P. S.; Ustinov, V. M. *Ieee Journal of Selected Topics in Quantum Electronics* **1997**, *3*, 196.
- (112) Fafard, S.; Hinzer, K.; Raymond, S.; Dion, M.; McCaffrey, J.; Feng, Y.; Charbonneau, S. *Science (New York, N.Y.)* **1996**, *274*, 1350.
- (113) Heinrichsdorff, F.; Mao, M. H.; Kirstaedter, N.; Krost, A.; Bimberg, D.; Kosogov, A. O.; Werner, P. *Applied Physics Letters* **1997**, *71*, 22.
- (114) Chakrabarti, S.; Stiff-Roberts, A. D.; Su, X. H.; Bhattacharya, P.; Ariyawansa, G.; Perera, A. G. U. *Journal of Physics D-Applied Physics* **2005**, *38*, 2135.
- (115) Chang, C. C.; Sharma, Y. D.; Kim, Y. S.; Bur, J. A.; Shenoi, R. V.; Krishna, S.; Huang, D. H.; Lin, S. Y. *Nano Letters* **2010**, *10*, 1704.
- (116) Krishna, S. *Journal of Physics D-Applied Physics* **2005**, *38*, 2142.

- (117) Maimon, S.; Finkman, E.; Bahir, G.; Schacham, S. E.; Garcia, J. M.; Petroff, P. M. *Applied Physics Letters* **1998**, *73*, 2003.
- (118) Oertel, D. C.; Bawendi, M. G.; Arango, A. C.; Bulovic, V. *Applied Physics Letters* **2005**, *87*.
- (119) Pietryga, J. M.; Park, Y.-S.; Lim, J.; Fidler, A. F.; Bae, W. K.; Brovelli, S.; Klimov, V. I. *Chemical Reviews* **2016**, *116*, 10513.
- (120) Kang, Y. Y.; Song, Z. C.; Qiao, P. S.; Du, X. P.; Zhao, F. *Progress in Chemistry* **2017**, *29*, 467.
- (121) Jang, E.; Jun, S.; Jang, H.; Lim, J.; Kim, B.; Kim, Y. *Adv. Mater.* **2010**, *22*, 3076.
- (122) Cragg, G. E.; Efros, A. L. *Nano Letters* **2010**, *10*, 313.
- (123) Zhang, Y. J.; Zherebetsky, D.; Bronstein, N. D.; Barja, S.; Lichtenstein, L.; Alivisatos, A. P.; Wang, L. W.; Salmeron, M. *Acs Nano* **2015**, *9*, 10445.
- (124) Lan, X. Z.; Voznyy, O.; Kiani, A.; de Arquer, F. P. G.; Abbas, A. S.; Kim, G. H.; Liu, M. X.; Yang, Z. Y.; Walters, G.; Xu, J. X.; Yuan, M. J.; Ning, Z. J.; Fan, F. J.; Kanjanaboos, P.; Kramer, I.; Zhitomirsky, D.; Lee, P.; Perelgut, A.; Hoogland, S.; Sargent, E. H. *Adv. Mater.* **2016**, *28*, 299.
- (125) Wang, R. L.; Shang, Y. Q.; Kanjanaboos, P.; Zhou, W. J.; Ning, Z. J.; Sargent, E. H. *Energy & Environmental Science* **2016**, *9*, 1130.
- (126) Mutlugun, E.; Hernandez-Martinez, P. L.; Eroglu, C.; Coskun, Y.; Erdem, T.; Sharma, V. K.; Unal, E.; Panda, S. K.; Hickey, S. G.; Gaponik, N.; Eychmuller, A.; Demir, H. V. *Nano Letters* **2012**, *12*, 3986.
- (127) Pi, X. D.; Zhang, L.; Yang, D. R. *Journal of Physical Chemistry C* **2012**, *116*, 21240.
- (128) Boberl, M.; Kovalenko, M. V.; Gamerith, S.; List, E. J. W.; Heiss, W. *Adv. Mater.* **2007**, *19*, 3574.
- (129) Haverinen, H. M.; Myllyla, R. A.; Jabbour, G. E. *Journal of Display Technology* **2010**, *6*, 87.
- (130) Krebs, F. C. *Solar Energy Materials and Solar Cells* **2009**, *93*, 465.
- (131) Wengeler, L.; Schmidt-Hansberg, B.; Peters, K.; Scharfer, P.; Schabel, W. *Chemical Engineering and Processing* **2011**, *50*, 478.
- (132) Li, H. B.; Wu, K. F.; Lim, J.; Song, H. J.; Klimov, V. I. *Nature Energy* **2016**, *1*.
- (133) *Electrical World*; McGraw-Hill, 1907.
- (134) Shirasaki, Y.; Supran, G. J.; Bawendi, M. G.; Bulović, V. *Nature Photonics* **2012**, *7*, 13.
- (135) Colvin, V. L.; Schlamp, M. C.; Alivisatos, A. P. *Nature* **1994**, *370*, 354.
- (136) Schlamp, M. C.; Peng, X. G.; Alivisatos, A. P. *J. Appl. Phys.* **1997**, *82*, 5837.
- (137) Mattoussi, H.; Radzilowski, L. H.; Dabbousi, B. O.; Thomas, E. L.; Bawendi, M. G.; Rubner, M. F. *J. Appl. Phys.* **1998**, *83*, 7965.
- (138) Coe, S.; Woo, W. K.; Bawendi, M.; Bulovic, V. *Nature* **2002**, *420*, 800.
- (139) Anikeeva, P. O.; Halpert, J. E.; Bawendi, M. G.; Bulovic, V. *Nano Letters* **2009**, *9*, 2532.
- (140) Anikeeva, P. O.; Halpert, J. E.; Bawendi, M. G.; Bulovic, V. *Nano Letters* **2007**, *7*, 2196.
- (141) Ding, T.; Yang, X. Y.; Bai, L. Y.; Zhao, Y. B.; Fong, K. E.; Wang, N.; Demir, H. V.; Sun, X. W. *Organic Electronics* **2015**, *26*, 245.
- (142) Kim, H. Y.; Park, Y. J.; Kim, J.; Han, C. J.; Lee, J.; Kim, Y.; Greco, T.; Ippen, C.; Wedel, A.; Ju, B. K.; Oh, M. S. *Advanced Functional Materials* **2016**, *26*, 3454.

- (143) Ka, Y.; Jang, H. R.; Choi, W. S. *Science of Advanced Materials* **2016**, *8*, 382.
- (144) Kwack, Y. J.; Jang, H. R.; Ka, Y.; Choi, W. S. *Journal of Nanoelectronics and Optoelectronics* **2016**, *11*, 234.
- (145) Koh, W. K.; Shin, T.; Jung, C.; Cho, D. K. S. *Chemphyschem* **2016**, *17*, 1095.
- (146) Yang, Y. X.; Zheng, Y.; Cao, W. R.; Titov, A.; Hyvonen, J.; Manders, J. R.; Xue, J. G.; Holloway, P. H.; Qian, L. *Nature Photonics* **2015**, *9*, 259.
- (147) Cho, K. S.; Lee, E. K.; Joo, W. J.; Jang, E.; Kim, T. H.; Lee, S. J.; Kwon, S. J.; Han, J. Y.; Kim, B. K.; Choi, B. L.; Kim, J. M. *Nature Photonics* **2009**, *3*, 341.
- (148) Ho, M. D.; Kim, D.; Kim, N.; Cho, S. M.; Chae, H. *Acs Applied Materials & Interfaces* **2013**, *5*, 12369.
- (149) Yang, X. Y.; Divayana, Y.; Zhao, D. W.; Leck, K. S.; Lu, F.; Tan, S. T.; Abiyasa, A. P.; Zhao, Y. B.; Demir, H. V.; Sun, X. W. *Applied Physics Letters* **2012**, *101*.
- (150) Chen, J.; Pan, J. Y.; Huang, Q. Q.; Xu, F.; Zhang, Z. C.; Lei, W.; Nathan, A. *Physica Status Solidi a-Applications and Materials Science* **2015**, *212*, 2856.
- (151) Park, J. P.; Kim, T. H.; Kim, S. W. *Dyes and Pigments* **2016**, *127*, 142.
- (152) Lee, S. H.; Lee, K. H.; Jo, J. H.; Park, B.; Kwon, Y.; Jang, H. S.; Yang, H. *Opt. Mater. Express* **2014**, *4*, 1297.
- (153) Yang, X. Y.; Zhao, D. W.; Leck, K. S.; Tan, S. T.; Tang, Y. X.; Zhao, J. L.; Demir, H. V.; Sun, X. W. *Adv. Mater.* **2012**, *24*, 4180.
- (154) Malik, M. A.; O'Brien, P.; Revaprasadu, N. *Adv. Mater.* **1999**, *11*, 1441.
- (155) Song, W. S.; Yang, H. *Applied Physics Letters* **2012**, *100*.
- (156) Chen, B. K.; Zhong, H. Z.; Zhang, W. Q.; Tan, Z. A.; Li, Y. F.; Yu, C. R.; Zhai, T. Y.; Bando, Y. S.; Yang, S. Y.; Zou, B. S. *Advanced Functional Materials* **2012**, *22*, 2081.
- (157) Kim, J. H.; Yang, H. *Chemistry of Materials* **2016**, *28*, 6329.
- (158) Zhang, W. J.; Lou, Q.; Ji, W. Y.; Zhao, J. L.; Zhong, X. H. *Chemistry of Materials* **2014**, *26*, 1204.
- (159) Song, W. S.; Kim, J. H.; Lee, J. H.; Lee, H. S.; Do, Y. R.; Yang, H. *Journal of Materials Chemistry* **2012**, *22*, 21901.
- (160) Liu, Z. Y.; Zhao, K.; Tang, A. W.; Xie, Y. H.; Qian, L.; Cao, W. R.; Yang, Y. X.; Chen, Y.; Teng, F. *Organic Electronics* **2016**, *36*, 97.
- (161) Yuan, M. J.; Liu, M. X.; Sargent, E. H. *Nature Energy* **2016**, *1*.
- (162) Kramer, I. J.; Moreno-Bautista, G.; Minor, J. C.; Kopilovic, D.; Sargent, E. H. *Applied Physics Letters* **2014**, *105*.
- (163) Kramer, I. J.; Minor, J. C.; Moreno-Bautista, G.; Rollny, L.; Kanjanaboos, P.; Kopilovic, D.; Thon, S. M.; Carey, G. H.; Chou, K. W.; Zhitomirsky, D.; Amassian, A.; Sargent, E. H. *Adv. Mater.* **2015**, *27*, 116.
- (164) Alberio, J.; Clifford, J. N.; Palomares, E. *Coordination Chemistry Reviews* **2014**, *263-264*, 53.
- (165) Johnston, K. W.; Pattantyus-Abraham, A. G.; Clifford, J. P.; Myrskog, S. H.; MacNeil, D. D.; Levina, L.; Sargent, E. H. *Applied Physics Letters* **2008**, *92*.
- (166) Debnath, R.; Tang, J.; Barkhouse, D. A.; Wang, X. H.; Pattantyus-Abraham, A. G.; Brzozowski, L.; Levina, L.; Sargent, E. H. *Journal of the American Chemical Society* **2010**, *132*, 5952.
- (167) Tang, J.; Wang, X. H.; Brzozowski, L.; Barkhouse, D. A. R.; Debnath, R.; Levina, L.; Sargent, E. H. *Adv. Mater.* **2010**, *22*, 1398.
- (168) Kuo, C. Y.; Su, M. S.; Hsu, Y. C.; Lin, H. N.; Wei, K. H. *Advanced Functional Materials* **2010**, *20*, 3555.

- (169) Olson, J. D.; Rodriguez, Y. W.; Yang, L. D.; Alers, G. B.; Carter, S. A. *Applied Physics Letters* **2010**, *96*.
- (170) Piliago, C.; Protesescu, L.; Bisri, S. Z.; Kovalenko, M. V.; Loi, M. A. *Energy & Environmental Science* **2013**, *6*, 3054.
- (171) Oregan, B.; Gratzel, M. *Nature* **1991**, *353*, 737.
- (172) Lee, H.; Leventis, H. C.; Moon, S. J.; Chen, P.; Ito, S.; Haque, S. A.; Torres, T.; Nuesch, F.; Geiger, T.; Zakeeruddin, S. M.; Gratzel, M.; Nazeeruddin, M. K. *Advanced Functional Materials* **2009**, *19*, 2735.
- (173) Lee, H. J.; Chen, P.; Moon, S. J.; Sauvage, F.; Sivula, K.; Bessho, T.; Gamelin, D. R.; Comte, P.; Zakeeruddin, S. M.; Seok, S. I.; Gratzel, M.; Nazeeruddin, M. K. *Langmuir* **2009**, *25*, 7602.
- (174) Bang, J. H.; Kamat, P. V. *Acs Nano* **2009**, *3*, 1467.
- (175) Shen, Q.; Kobayashi, J.; Diguna, L. J.; Toyoda, T. *J. Appl. Phys.* **2008**, *103*.
- (176) Lee, H. J.; Yum, J. H.; Leventis, H. C.; Zakeeruddin, S. M.; Haque, S. A.; Chen, P.; Seok, S. I.; Gratzel, M.; Nazeeruddin, M. K. *Journal of Physical Chemistry C* **2008**, *112*, 11600.
- (177) Diguna, L. J.; Shen, Q.; Kobayashi, J.; Toyoda, T. *Applied Physics Letters* **2007**, *91*.
- (178) Santra, P. K.; Kamat, P. V. *Journal of the American Chemical Society* **2012**, *134*, 2508.
- (179) Sun, W. T.; Yu, Y.; Pan, H. Y.; Gao, X. F.; Chen, Q.; Peng, L. M. *Journal of the American Chemical Society* **2008**, *130*, 1124.
- (180) Lee, Y. L.; Chang, C. H. *Journal of Power Sources* **2008**, *185*, 584.
- (181) Chang, C. H.; Lee, Y. L. *Applied Physics Letters* **2007**, *91*.
- (182) Wang, J.; Mora-Sero, I.; Pan, Z. X.; Zhao, K.; Zhang, H.; Feng, Y. Y.; Yang, G.; Zhong, X. H.; Bisquert, J. *Journal of the American Chemical Society* **2013**, *135*, 15913.
- (183) Gao, X. F.; Li, H. B.; Sun, W. T.; Chen, Q.; Tang, F. Q.; Peng, L. M. *Journal of Physical Chemistry C* **2009**, *113*, 7531.
- (184) Yun, H. J.; Paik, T.; Diroll, B.; Edley, M. E.; Baxter, J. B.; Murray, C. B. *Acs Applied Materials & Interfaces* **2016**, *8*, 14692.
- (185) Feng, H. L.; Wu, W. Q.; Rao, H. S.; Wan, Q.; Li, L. B.; Kuang, D. B.; Su, C. Y. *Acs Applied Materials & Interfaces* **2015**, *7*, 5199.
- (186) Wu, W. Q.; Xu, Y. F.; Rao, H. S.; Feng, H. L.; Su, C. Y.; Kuang, D. B. *Angewandte Chemie-International Edition* **2014**, *53*, 4816.
- (187) Yu, G.; Gao, J.; Hummelen, J. C.; Wudl, F.; Heeger, A. J. *Science (New York, N.Y.)* **1995**, *270*, 1789.
- (188) Greenham, N. C.; Peng, X. G.; Alivisatos, A. P. *Physical Review B* **1996**, *54*, 17628.
- (189) Kang, Y.; Kim, D. *Solar Energy Materials and Solar Cells* **2006**, *90*, 166.
- (190) Leventis, H. C.; King, S. P.; Sudlow, A.; Hill, M. S.; Molloy, K. C.; Haque, S. A. *Nano Letters* **2010**, *10*, 1253.
- (191) Ren, S. Q.; Chang, L. Y.; Lim, S. K.; Zhao, J.; Smith, M.; Zhao, N.; Bulovic, V.; Bawendi, M.; Gradecak, S. *Nano Letters* **2011**, *11*, 3998.
- (192) Wang, L.; Liu, Y. S.; Jiang, X.; Qin, D. H.; Cao, Y. *Journal of Physical Chemistry C* **2007**, *111*, 9538.
- (193) Dayal, S.; Kopidakis, N.; Olson, D. C.; Ginley, D. S.; Rumbles, G. *Nano Letters* **2010**, *10*, 239.

- (194) Huynh, W. U.; Dittmer, J. J.; Alivisatos, A. P. *Science (New York, N.Y.)* **2002**, *295*, 2425.
- (195) Huynh, W. U.; Dittmer, J. J.; Libby, W. C.; Whiting, G. L.; Alivisatos, A. P. *Advanced Functional Materials* **2003**, *13*, 73.
- (196) Saunders, B. R.; Turner, M. L. *Advances in Colloid and Interface Science* **2008**, *138*, 1.
- (197) Sun, B. Q.; Marx, E.; Greenham, N. C. *Nano Letters* **2003**, *3*, 961.
- (198) Gunes, S.; Fritz, K. P.; Neugebauer, H.; Sariciftci, N. S.; Kumar, S.; Scholes, G. D. *Solar Energy Materials and Solar Cells* **2007**, *91*, 420.
- (199) Koleilat, G. I.; Levina, L.; Shukla, H.; Myrskog, S. H.; Hinds, S.; Pattantyus-Abraham, A. G.; Sargent, E. H. *Acs Nano* **2008**, *2*, 833.
- (200) McDonald, S. A.; Konstantatos, G.; Zhang, S. G.; Cyr, P. W.; Klem, E. J. D.; Levina, L.; Sargent, E. H. *Nature materials* **2005**, *4*, 138.
- (201) Watt, A. A. R.; Blake, D.; Warner, J. H.; Thomsen, E. A.; Tavenner, E. L.; Rubinsztein-Dunlop, H.; Meredith, P. *Journal of Physics D-Applied Physics* **2005**, *38*, 2006.
- (202) Cui, D. H.; Xu, J.; Zhu, T.; Paradee, G.; Ashok, S.; Gerhold, M. *Applied Physics Letters* **2006**, *88*.
- (203) Qi, D. F.; Fischbein, M.; Drndic, M.; Selmic, S. *Applied Physics Letters* **2005**, *86*.
- (204) Tang, J. A.; Sargent, E. H. *Adv. Mater.* **2011**, *23*, 12.
- (205) Yuan, J. Y.; Gallagher, A.; Liu, Z. K.; Sun, Y. X.; Ma, W. L. *Journal of Materials Chemistry A* **2015**, *3*, 2572.
- (206) Sun, Y. X.; Liu, Z. K.; Yuan, J. Y.; Chen, J. M.; Zhou, Y.; Huang, X. D.; Ma, W. L. *Organic Electronics* **2015**, *24*, 263.
- (207) Murphy, C. J. *Analytical Chemistry* **2002**, *74*, 520 A.
- (208) Mazumder, S.; Dey, R.; Mitra, M. K.; Mukherjee, S.; Das, G. C. *Journal of Nanomaterials* **2009**, 2009.
- (209) Hezinger, A. F. E.; Teßmar, J.; Göpferich, A. *European Journal of Pharmaceutics and Biopharmaceutics* **2008**, *68*, 138.
- (210) Law, W.-C.; Yong, K.-T.; Roy, I.; Ding, H.; Hu, R.; Zhao, W.; Prasad, P. N. *Small* **2009**, *5*, 1302.
- (211) Elliott, S. D.; Moloney, M. c. I. P.; Gun'ko, Y. K. *Nano Letters* **2008**, *8*, 2452.
- (212) Michalet, X.; Pinaud, F. F.; Bentolila, L. A.; Tsay, J. M.; Doose, S.; Li, J. J.; Sundaresan, G.; Wu, A. M.; Gambhir, S. S.; Weiss, S. *Science (New York, N.Y.)* **2005**, *307*, 538.
- (213) Bartlett, J. B.; Dredge, K.; Dalglish, A. G. *Nature Reviews Cancer* **2004**, *4*, 314.
- (214) Kim, J.; Lee, J.; Kim, W. Y.; Kim, H.; Lee, S.; Lee, H. C.; Lee, Y. S.; Seo, M.; Kim, S. Y. *Nature Communications* **2015**, *6*, 8.
- (215) Kawasaki, T.; Araki, Y.; Hatase, K.; Suzuki, K.; Matsumoto, A.; Yokoi, T.; Kubota, Y.; Tatsumi, T.; Soai, K. *Chemical Communications* **2015**, *51*, 8742.
- (216) Kobayashi, S.; Hamasaki, N.; Suzuki, M.; Kimura, M.; Shirai, H.; Hanabusa, K. *Journal of the American Chemical Society* **2002**, *124*, 6550.
- (217) Delclos, T.; Aimé, C.; Pouget, E.; Brizard, A.; Huc, I.; Delville, M.-H.; Oda, R. *Nano Letters* **2008**, *8*, 1929.

- (218) Liu, S.; Han, L.; Duan, Y.; Asahina, S.; Terasaki, O.; Cao, Y.; Liu, B.; Ma, L.; Zhang, J.; Che, S. *Nature Communications* **2012**, *3*, 1215.
- (219) Jin, R.-H.; Yao, D.-D.; Levi, R. *Chemistry – A European Journal* **2014**, *20*, 7196.
- (220) Qian, Y.; Duan, Y.; Che, S. *Advanced Optical Materials* **2017**, *5*, 1601013.
- (221) Yeom, J.; Yeom, B.; Chan, H.; Smith, K. W.; Dominguez-Medina, S.; Bahng, Joong H.; Zhao, G.; Chang, W.-S.; Chang, S.-J.; Chuvilin, A.; Melnikau, D.; Rogach, A. L.; Zhang, P.; Link, S.; Král, P.; Kotov, N. A. *Nature materials* **2014**, *14*, 66.
- (222) Schaaff, T. G.; Whetten, R. L. *The Journal of Physical Chemistry B* **2000**, *104*, 2630.
- (223) Yao, H.; Miki, K.; Nishida, N.; Sasaki, A.; Kimura, K. *Journal of the American Chemical Society* **2005**, *127*, 15536.
- (224) Gautier, C.; Burgi, T. *Chemphyschem* **2009**, *10*, 483.
- (225) Gautier, C.; Burgi, T. *Journal of the American Chemical Society* **2006**, *128*, 11079.
- (226) Xia, Y. H.; Zhou, Y. L.; Tang, Z. Y. *Nanoscale* **2011**, *3*, 1374.
- (227) Govorov, A. O.; Fan, Z. Y.; Hernandez, P.; Slocik, J. M.; Naik, R. R. *Nano Letters* **2010**, *10*, 1374.
- (228) Fan, Z. Y.; Govorov, A. O. *Nano Letters* **2010**, *10*, 2580.
- (229) Cathcart, N.; Mistry, P.; Makra, C.; Pietrobon, B.; Coombs, N.; Jelokhani-Niaraki, M.; Kitaev, V. *Langmuir* **2009**, *25*, 5840.
- (230) Nishida, N.; Yao, H.; Ueda, T.; Sasaki, A.; Kimura, K. *Chemistry of Materials* **2007**, *19*, 2831.
- (231) Choi, S. H.; Lee, S. H.; Hwang, Y. M.; Lee, K. P.; Kang, H. D. *Radiat. Phys. Chem.* **2003**, *67*, 517.
- (232) Ben-Moshe, A.; Wolf, S. G.; Sadan, M. B.; Houben, L.; Fan, Z.; Govorov, A. O.; Markovich, G. *Nature Communications* **2014**, *5*, 4302.
- (233) Horvath, J. D.; Koritnik, A.; Kamakoti, P.; Sholl, D. S.; Gellman, A. J. *Journal of the American Chemical Society* **2004**, *126*, 14988.
- (234) Sedghamiz, T.; Bahrami, M.; Ghatee, M. H. *Chemical Physics* **2017**, *487*, 48.
- (235) Bloom, B. P.; Graff, B. M.; Ghosh, S.; Beratan, D. N.; Waldeck, D. H. *Journal of the American Chemical Society* **2017**, *139*, 9038.
- (236) Ben-Moshe, A.; Maoz, B. M.; Govorov, A. O.; Markovich, G. *Chemical Society Reviews* **2013**, *42*, 7028.
- (237) Moshe, A. B.; Markovich, G. *Israel Journal of Chemistry* **2012**, *52*, 1104.
- (238) Nakashima, T.; Kobayashi, Y.; Kawai, T. *Journal of the American Chemical Society* **2009**, *131*, 10342.
- (239) Elliott, S. D.; Moloney, M. P.; Gun'ko, Y. K. *Nano Letters* **2008**, *8*, 2452.
- (240) Moloney, M. P.; Gun'ko, Y. K.; Kelly, J. M. *Chemical Communications* **2007**, 3900.
- (241) Moloney, M. P.; Gallagher, S. A.; Gun'ko, Y. K. *MRS Proceedings* **2011**, 1241.
- (242) Govan, J. E.; Jan, E.; Querejeta, A.; Kotov, N. A.; Gun'ko, Y. K. *Chemical Communications* **2010**, *46*, 6072.
- (243) Tohgha, U.; Deol, K. K.; Porter, A. G.; Bartko, S. G.; Choi, J. K.; Leonard, B. M.; Varga, K.; Kubelka, J.; Muller, G.; Balaz, M. *ACS Nano* **2013**, *7*, 11094.
- (244) Varga, K.; Tannir, S.; Haynie, B. E.; Leonard, B. M.; Dzyuba, S. V.; Kubelka, J.; Balaz, M. *Acs Nano* **2017**, *11*, 9846.

- (245) Purcell-Milton, F.; Visheratina, A. K.; Kuznetsova, V. A.; Ryan, A.; Orlova, A. O.; Gun'ko, Y. K. *ACS Nano* **2017**, *11*, 9207.
- (246) Tamang, S.; Beaune, G.; Poillot, C.; Waard, M.; Texier, I.; Reiss, P. *Compact and highly stable quantum dots through optimized aqueous phase transfer*, 2011; Vol. 7909.
- (247) Mukhina, M. V.; Korsakov, I. V.; Maslov, V. G.; Purcell-Milton, F.; Govan, J.; Baranov, A. V.; Fedorov, A. V.; Gun'ko, Y. K. *Scientific Reports* **2016**, *6*, 24177.
- (248) Delgado-Pérez, T.; Bouchet, L. M.; de la Guardia, M.; Galian, R. E.; Pérez-Prieto, J. *Chemistry – A European Journal* **2013**, *19*, 11068.
- (249) Wawrzyńczyk, D.; Szeremeta, J.; Samoć, M.; Nyk, M. *Sensors and Actuators B: Chemical* **2017**, *252*, 483.
- (250) Duran, G. M.; Abellan, C.; Contento, A. M.; Rios, A. *Microchim. Acta* **2017**, *184*, 815.
- (251) Hjuler, C. T.; Maolanon, N. N.; Sauer, J.; Stougaard, J.; Thygesen, M. B.; Jensen, K. J. *Nat. Protoc.* **2017**, *12*, 2411.
- (252) Smith, E. A.; Thomas, W. D.; Kiessling, L. L.; Corn, R. M. *Journal of the American Chemical Society* **2003**, *125*, 6140.
- (253) Cagnoni, A. J.; Varela, O.; Kovensky, J.; Uhrig, M. L. *Org. Biomol. Chem.* **2013**, *11*, 5500.
- (254) Reed, L. A.; Goodman, L. *Carbohydr. Res.* **1981**, *94*, 91.
- (255) Yu, M.; Yang, Y.; Han, R.; Zheng, Q.; Wang, L.; Hong, Y.; Li, Z.; Sha, Y. *Langmuir* **2010**, *26*, 8534.
- (256) Coulon, J.; Thouvenin, I.; Aldeek, F.; Balan, L.; Schneider, R. *Journal of fluorescence* **2010**, *20*, 591.
- (257) Yang, Y.; Yu, M.; Yan, T. T.; Zhao, Z. H.; Sha, Y. L.; Li, Z. J. *Bioorganic & medicinal chemistry* **2010**, *18*, 5234.
- (258) Qi, P.; Chen, X. T.; Sun, Y.; Zhang, D. *Sens. Actuator B-Chem.* **2018**, *254*, 431.
- (259) Camargo, P. H.; Lee, Y. H.; Jeong, U.; Zou, Z.; Xia, Y. *Langmuir* **2007**, *23*, 2985.
- (260) Luther, J. M.; Zheng, H.; Sadtler, B.; Alivisatos, A. P. *Journal of the American Chemical Society* **2009**, *131*, 16851.
- (261) Sadtler, B.; Demchenko, D. O.; Zheng, H.; Hughes, S. M.; Merkle, M. G.; Dahmen, U.; Wang, L.-W.; Alivisatos, A. P. *Journal of the American Chemical Society* **2009**, *131*, 5285.
- (262) Park, J.; Kim, S. W. *Journal of Materials Chemistry* **2011**, *21*, 3745.
- (263) Schaller, R. D.; Petruska, M. A.; Klimov, V. I. *J. Phys. Chem. B* **2003**, *107*, 13765.
- (264) Schaller, R. D.; Klimov, V. I. *Physical Review Letters* **2004**, *92*, 186601.
- (265) Schaller, R. D.; Sykora, M.; Pietryga, J. M.; Jeong, S.; Klimov, V. I. *Abstr. Pap. Am. Chem. Soc.* **2007**, *234*, 1.
- (266) Pietryga, J. M.; Schaller, R. D.; Werder, D.; Stewart, M. H.; Klimov, V. I.; Hollingsworth, J. A. *Journal of the American Chemical Society* **2004**, *126*, 11752.
- (267) Pietryga, J. M.; Werder, D. J.; Williams, D. J.; Casson, J. L.; Schaller, R. D.; Klimov, V. I.; Hollingsworth, J. A. *Journal of the American Chemical Society* **2008**, *130*, 4879.
- (268) Chan, Y. H.; Chen, J. X.; Liu, Q. S.; Wark, S. E.; Son, D. H.; Batteas, J. D. *Analytical Chemistry* **2010**, *82*, 3671.

## Chapter 2 Experimental

### 2.1 Starting materials and general equipment

All starting materials were supplied by Fischer Scientific and Sigma Aldrich unless stated otherwise. For cleaning of nanomaterials, solvents (HPLC grade) obtained from the solvents stores in Trinity College were used unless stated otherwise. Millipore water was obtained by filtering water through a MilliQ 18M $\Omega$  system.

Materials for biological experiments were purchased from Invitrogen. Glass-bottomed Petri dishes and  $\mu$ -slides were supplied by Ibidi.

A Hettich Zentrifugen Universal 32 centrifuge was used for large volumes, namely for fractioning QDs and gelatin nanoparticles. For small volumes and higher speed required to wash metal nanoparticles, a Hermle Z233 M-2 centrifuge was used.

For ultrasonic agitation, a Grant XB6 ultrasonic bath was operated at 5-60 Hz. A Model GEX-750 ultrasonic processor fitted with a Model CV33 tip with  $\frac{1}{4}$  in. tapered tip was also used. It was operated at 20 % of maximum power.

UV-Vis was carried out using a Varian/Cary 50 single beam spectrophotometer. All samples were analysed using a 1 cm quartz fluorescence cuvette. If the solvent was volatile, a capped cuvette was used.

PL spectroscopy was performed using a Cary Eclipse spectrometer and 1 cm quartz fluorescence cuvettes.

CD spectroscopy was carried out using a Jasco J-810 operating under a N<sub>2</sub> flow of 5-8 L/min. Samples were analysed in 1 cm quartz fluorescence cuvettes. Samples were analysed with a 100 nm / minute scan rate and a 1 second response time (9 accumulations).

Our samples were imaged using a FEI Titan electron microscope operating at a beam voltage of 200 kV. Samples were diluted to approximately 1mg/10mL, deposited on



lacey or holey carbon on copper grids and then allowed to dry under vacuum for 12-24 hours depending on the solvent.

EDX analysis was performed using the FEI Titan in STEM mode using the EDAX detector.

X-Ray powder diffraction was performed using a Bruker D2 Phaser diffractometer. Patterns were recorded with a 2.5 hour scan time. X-Ray diffractometer. Diffractograms were then compared to the JCPDS database. A wavelength of 1.5406 was selected for our measurements. A range of  $2\theta = 10^\circ - 90^\circ$  was used with a step size of  $0.01^\circ$ .

## 2.2 Experimental details for chapter 3

### 2.2.1 Synthesis of ZnS and ZnS:Mn quantum dots

ZnS and ZnS:Mn quantum dots have been prepared by previously reported procedure<sup>1</sup>. A schematic of the reaction is described below in Figure 2-1.

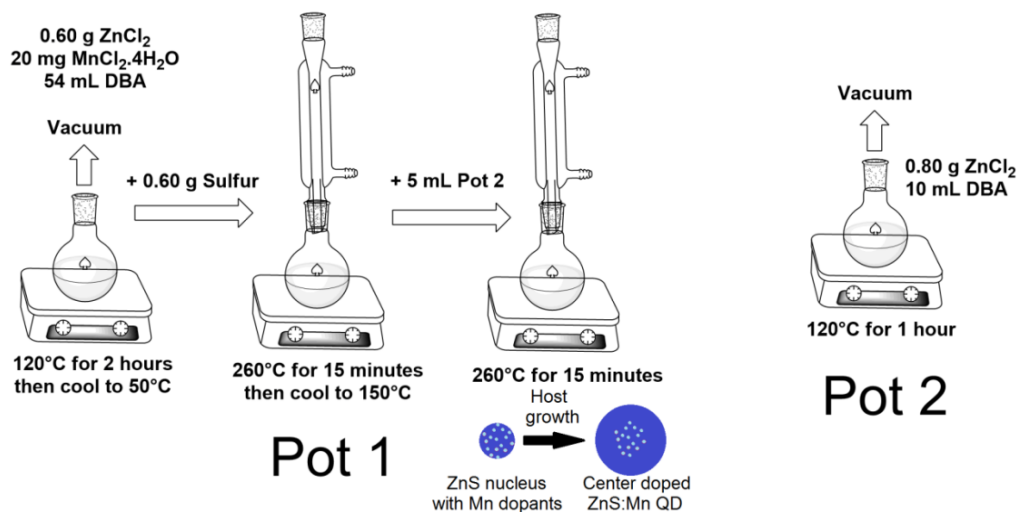


Figure 2-1 Schematic describing the synthesis of ZnS:Mn QDs

0.6 g (2.9 mmol) of ZnCl<sub>2</sub> and 0.02 g (0.1 mmol) of MnCl<sub>2</sub>·4H<sub>2</sub>O were dissolved in 54 mL of dibenzylamine and heated under vacuum at 120°C for 2 hours (named pot 1). A separate solution must be made up of 0.8 g (5.8 mmol) of ZnCl<sub>2</sub> in dibenzylamine and heated under vacuum at 120°C for 1 hour (named pot 2). The pot 1 solution was then cooled down to 50°C and removed from vacuum and 0.6 g

(18.7 mmol) of sulphur powder was added. After that the solution was heated to 260°C under argon and held at this temperature for 15 minutes. The solution was then cooled to 160°. 5 mL of the pot 2 solution and heated again to 260°C and held at that temperature for a further 15 minutes. The solution was then cooled to around 160°C and ethanol was added to precipitate out the quantum dots. The quantum dots were then washed and centrifuged several times with ethanol in order to remove excess of sulphur until the supernatant was no longer yellow. Once cleaned, the quantum dots were stored in chloroform (20 mL) and 100 µL of oleylamine was added for improved colloidal stability. For comparison, undoped ZnS QDs were synthesised using the same method but without the addition of manganese chloride.

### 2.2.2 Phase transfer of ZnS:Mn doped QDs by precipitation technique

1 mL of concentrated ZnS:Mn QD solution in chloroform was treated with 1-3 mL of methanol. The resulting mixture was then centrifuged at 4000 RPM for 10 minutes to separate the QDs from the methanol/ chloroform solution. The QDs were then re-dissolved in 1 mL of chloroform. At the same time 10 mg of L-Cysteine hydrochloride was dissolved in 300 µL of methanol. 100 µL of this solution was then mixed with the quantum dots and shaken for 20 minutes after which it became cloudy. The solution was then centrifuged for a further 10 minutes at 4000 RPM to separate the precipitated QDs. The QDs were then washed with methanol and centrifuged twice. The resulting QDs were then dissolved in water and the solution was adjusted to pH 12 using 1M NaOH to increase colloidal stability.

### 2.2.3 Phase transfer of Mn Doped ZnS QDs using ethylenediamine (EDA)

ZnS:Mn QDs in 1 mL of chloroform were precipitated out by methanol (1 mL) flocculation and centrifugation. The supernatant was decanted, and the pellet was re-dispersed in 2 mL of chloroform and loaded in a glass vial. A 1 mL portion of EDA was added to the solution under vigorous stirring. Because of the considerable solubility of EDA in chloroform, no phase separation was observed. After 30 min, 2

mL of aqueous solution containing D-penicillamine (45 mg, 0.15M in Millipore water) as the substitute ligand was added to the mixture, and it was left to stay for another 1 h. An aqueous phase (water and EDA) and an organic phase (chloroform) were evidently separated. Absence of luminescence under UV in the organic phase indicated the complete transferring of QDs to the aqueous phase. The pH of the aqueous phase was made neutral by adding a drop of hydrochloric acid and QDs were precipitated using methanol and centrifuged. Following this, the QDs were dissolved in millipore water (10 mL).

#### 2.2.4 Synthesis of L-glutathione capped ZnSe QDs

Firstly a 0.2 M (10mL) solution of sodium hydroselenide (NaHSe) was prepared by mixing 0.16 g (2 mmol) of selenium with 0.2 g (6 mmol) of NaBH<sub>4</sub> in 10 mL of millipore water and allowed to react until all of the selenium was reduced and the solution was clear.

2 mL of this solution was added to 98 mL of millipore water containing 18 mg of Zn(Ac)<sub>2</sub> and 37 mg of glutathione. The amount of Zn / Se / GSH in solution were 1 / 0.4 / 1.2 mM respectively. The pH of the solution was adjusted to 11.5 using a 2 M NaOH aqueous solutions. Following this the reaction mixture was refluxed for 1 hour. The QDs were then precipitated and washed with 2-propanol several times and finally dissolved in water.

#### 2.2.5 Chiral recognition of penicillamine by ZnSe-GSH QDs

In order to perform the chiral recognition of penicillamine experiments solutions were prepared of both D- and L- penicillamine. These were made by dissolving 20 mg of each enantiomer in 10 mL of water (13 mM). This concentration was chosen as any higher led to the quenching occurred over too narrow a range and any lower gave the quenching effect wasn't larger enough to accurately measure.

2.5 mL of the ZnSe QD solution ( $5 \times 10^{-6}$  mol) was placed in a fluorescence cuvette ready for testing. A PL spectrum was recorded before the addition of penicillamine and the maximum intensity of the excitonic emission was recorded. Then 25  $\mu$ L of

the L-pen solution was added, the solution was left to stay for 5 minutes and then another PL spectrum was recorded. This process was repeated multiple times until 600  $\mu\text{L}$  of L-pen was added. The experiment was repeated with a new solution of ZnSe QDs and D-penicillamine instead of L-pen. Using this data, graphs were constructed to demonstrate the loss of excitonic luminescence as a function of penicillamine added.

## 2.3 Experimental details for chapter 4

The dot in rod and tetrapods used in this chapter were synthesised by first preparing either wurtzite (for DiRs) or zinc blende CdSe (for TPs) nanocrystals. These TPs and DiRs were produced by hot injection of either wurtzite or zinc blende seeds into a solution of cadmium, octadecylphosphonic acid, propylphosphonic acid, trioctylphosphine and trioctylphosphine oxide according to published procedure<sup>2</sup>. The preparation of the seed solutions, the Cd/ODPA/PPA/TOP/TOPO solution, and the subsequent DiR and TP synthesis are described below.

### 2.3.1 Synthesis of wurtzite CdSe QDs

CdSe QDs have been prepared using previously reported procedure<sup>2</sup>.

A solution of 25.9 mmol (10.g) of TOPO and 20.7 mmol (5.00 g) of hexadecylamine were mixed in a 50 mL three-neck flask and held at 110 °C for 50 minutes under vacuum. In an inert atmosphere under argon, 1.68 mmol (0.3 g) of octadecylphosphonic acid was added and the reaction mixture was degassed for 5 minutes under vacuum. The solution was then heated to 300 °C under argon, and a solution of 1 mmol of TOPSe and 1.64 mmol of CdMe<sub>2</sub> in 5 mL of TOP was rapidly injected into the mixture with constant stirring. The reaction was held at 300 °C under argon overnight. The reaction was then cooled to room temperature at which point the reaction mixture becomes solid. The mixture is then dissolved in toluene (anhydrous). Any remaining solids were centrifuged out and the resultant mixture was then precipitated using ethanol (anhydrous) and redissolved in toluene.

### 2.3.2 Synthesis of zinc blende CdSe QDs

CdSe QDs with zinc blende structure have been prepared using previously reported procedure<sup>2</sup>.

0.6 mmol (0.34 g) of cadmium myristate was dissolved in 1-octadecene in a 100 mL 3-neck flask. The mixture was then degassed by heating to 90 °C and holding it for 40 minutes under vacuum. The resultant solution was cooled to room temperature, at which point 0.3 mmol (0.024 g) of selenium powder (99.999%) is added. The solution was then degassed for 10 mins at 50 °C. After that the solution was heated to 240 °C at a rate of 20 degrees per minute and held at this temperature for 3 minutes. At this point a solution of 0.1 mL of oleic acid and 1 mL of oleylamine in ODE (4 mL) was added dropwise. The reaction was then cooled to room temperature and the resultant QDs were precipitated with ethanol and redispersed in hexane.

### 2.3.3 Preparation of solutions for synthesis of CdSe/CdS DiRs and TPs

CdSe/CdS DiRs have been prepared according to previously published procedure<sup>2</sup>.

A 25 mL three neck round bottomed was loaded with CdO (0.207 g, 1.61 mmol), n-octadecylphosphonic acid (1.08 g, 3.23 mmol), n-propylphosphonic acid (0.015 g, 0.12 mmol) and TOPO (3.35g, 9.18 mmol) and the mixture was degassed under vacuum at 120 °C for 30 minutes. The mixture was then heated to 320 °C under argon until a clear solution was obtained. Once the CdO had dissolved completely the solutions was cooled to 120 °C and once again placed under vacuum for a further 2 hours. It was then heated to 340 °C (for dot in rods) or 300 °C (for tetrapods) under argon. TOP (1.5 g, 4.05 mmol) was then injected and the solution was allowed to come back up to either 340 °C or 300 °C for either rods or tetrapods respectively. For subsequent sections this solution will be known as solution **1**.

Separately, for a source of sulfur, TOPS was prepared by reacting equimolar amounts of TOP and elemental sulphur at 50 °C under inert atmosphere.

#### 2.3.4 Synthesis of CdSe/CdS dot in rods

CdSe/CdS tetrapods have been prepared according to previously published procedure<sup>2</sup>.

TOPS (0.3 g, 1.61 mmol) was injected into solution **1** at 340 °C. After twenty seconds,  $\sim 10^{-8}$  mol of wurtzite CdSe seeds dissolved in TOP (0.5 g, 1.35 mmol) was injected. The wurtzite CdSe QD solution was prepared by taking 1 mL of the lower concentration stock solution and reducing it to approximately 50  $\mu$ L and adding TOP (0.5 g). The temperature of the reaction was adjusted to 320 °C and was kept at that temperature for 10 minutes. Anhydrous toluene was then used to quench the reaction and it was removed from the heat. The room temperature crude solution was combined with toluene and the dot-in-rods were precipitated using ethanol. After centrifugation the pellet was redispersed in 8:1 hexane/octylamine and precipitated again using ethanol. The DiRs were then stored in toluene.

#### 2.3.5 Synthesis of CdSe/CdS tetrapods

CdSe/CdS tetrapods have been prepared according to previously published procedure<sup>2</sup>.

TOPS (0.65 g) was injected into solution **1** at 300 °C. After forty seconds,  $\sim 10^{-8}$  mol of zinc blende CdSe seeds dissolved in TOP (0.5 g, 1.35 mmol) was injected. The temperature of the reaction was increased to 315 °C and was kept at that temperature for 20 minutes. The solution was then cooled to room temperature. The room temperature crude solution was combined with toluene and the tetrapods were precipitated using acetone. After centrifugation the pellet was redispersed in 8:1 hexane/octylamine and precipitated again using acetone. The tetrapods were then stored in toluene.

### 2.3.6 Phase Transfer of CdSe-CdS DiR using thioglucose

The phase transfer used for these DiRs is the same that is highlighted in section 2.2.2, which was used to perform ligand exchanges on ZnS:Mn QDs. In this case the 10 mg of cysteine is replaced with 22 mg of 1-thio- $\beta$ -D-glucose. In the case of preparing these DiRs in DMSO instead of water, following the precipitation and washing steps the final product is dissolved in DMSO instead of H<sub>2</sub>O.

## 2.4 Experimental details for chapter 5

### 2.4.1 Synthesis of CdS quantum dots

CdS QDs have been prepared according to previously published procedure<sup>3</sup>.

A schematic of the synthetic procedure is shown in Figure 2-2.

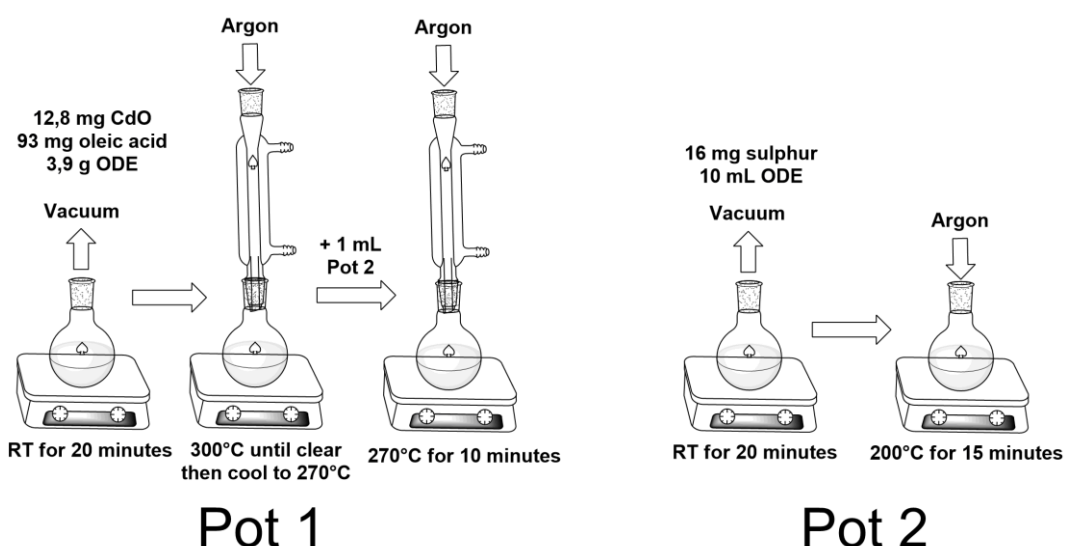


Figure 2-2 Synthesis of CdS quantum dots with a 270°C hot injection.

A flask containing 12,8 mg (0.1 mmol) of CdO, 93 mg (0.33 mmol) of oleic acid and 3.9 g of ODE (1-octadecene) was put under vacuum to degas the solution for 20 minutes. The reaction was then heated to 300°C to allow formation of Cd(oleate) and then cooled to the desired temperature. In another flask, 16 mg of sulphur was dissolved in 10 mL of degassed ODE by heating the solution under argon to 200°C for 15 minutes. 1 mL of this solution was injected into the first one and growth was allowed to proceed for 10 minutes. The reaction was removed from the heat and

the reaction was quenched using 20 mL of degassed acetone. The QD were then washed and centrifuged several times (3500 RPM, 10 minutes) with acetone, and the pellet was redissolved in either 20 mL of chloroform or toluene.

#### 2.4.2 Phase transfer for CdS QDs with penicillamine

30 mg (0.2 mmol) of penicillamine was dissolved in 150  $\mu$ L of Millipore water and 0.5 mL of methanol. The solution was then adjusted to pH 10 with 0.5 M NaOH. This solution was added into 2.5 mL of CdS QDs in chloroform or toluene and stirred for 3 hours to allow transfer of the QDs to the small methanol layer. 5.0 mL of water was added into the mixture and the stirring went on for another 20 minutes. The aqueous phase containing the QDs was collected and precipitated with addition of acetone. The pellet was redissolved in 5 mL of water and the pH adjusted to 10. By replacing penicillamine with cysteine in this reaction the corresponding cysteine stabilised CdS QDs were prepared.

#### 2.4.3 Synthesis of small CdSe QDs

Small CdSe QDs have been prepared according to a synthesis developed by Dr. Finn Purcel Milton of our group.

For the preparation of cadmium oleate ( $\text{Cd}(\text{OA})_2$ ) solution, 10 mmol of CdO (1.284 g), 7.8 mL of OA (6.981 g, 26 mmol), 6.2 mL of ODE (4.89 g, 19.5 mmol), and 1 mL of TOP were placed in an 100 mL 3-neck round flask with a reflux condenser. The mixture was heated to 280  $^{\circ}\text{C}$  under argon flow for 20 min. After the mixture was optically clear, it was cooled down to 50  $^{\circ}\text{C}$  and 0.14 mmol of dissolved CTAB (0.051 g) under argon flow was added. Separately, 12 mmol of Se and 6 mL of TOP were mixed in a 50 mL 2-neck round flask with a condenser and sonicated until the mixture became a transparent solution. After the TOPSe was cooled down to room temperature, 5 mL of TOPSe solution was added to the  $\text{Cd}(\text{OA})_2$  solution at 50  $^{\circ}\text{C}$ , and the mixed solution was stirred for 5 min.



#### 2.4.4 Aqueous synthesis of L- and D- penicillamine stabilised QDs

Aqueous solutions of D/L penicillamine (10 mL, 0.01 M) and  $\text{CdCl}_2$  (8 mL, 0.01 M) were mixed with 40 mL of Millipore water. The pH of this solution was adjusted to pH 12 using a 1 M NaOH solution. Thioacetamide (2 mL, 0.01 M) was then added to the solution before heating up to 100 ° C and allowed to reflux for 4 hours. The resultant QDs were precipitated using acetone and redispersed in Millipore water (20 mL).

#### 2.4.5 Reverse phase transfer using dodecanethiol (DDT) on aqueous CdS QDs

3 mL of the as prepared CdS aqueous solution (either D or L pen stabilised) was combined with a solution of dodecanethiol (DDT) (1 mL) in chloroform (3 mL) and shaken vigorously for 2 minutes. The 2 layers were allowed to separate completely followed by extraction of the organic layer now containing the DDT-CdS QDs. The QDs were precipitated with ethanol and then redispersed in chloroform (3 mL).

#### 2.4.6 Synthesis of 1.5 nm size CdSe nanoplatelets capped with myristic acid

CdSe nanoplatelets have been prepared according to previously published procedure<sup>4,5</sup>.

$\text{Cd}(\text{Ac})_2 \cdot 2\text{H}_2\text{O}$  (0.8 mmol) 0.213 g, Se (0.2 mmol) 0.0158 g, and Myristic Acid(MA) (0.2 mmol) 0.0457 g, were added to 25.35mL of ODE in a three-neck round bottom flask, with a condenser, a septum and a mercury thermometer (range to 300°C). The mixture was then put under vacuum and heated to 220 °C, and kept at this temperature for 3 hours. Following this, the atmosphere was switched to argon and the reaction was then allowed to cool to room temperature.

The sample of QDs was washed by adding 50 ml of ethanol. The sample was then placed in a centrifuge and spun at 4,000 for 10 minutes. Following this the precipitate was dissolved in 15 ml of hexane, spun at 2,000 in a centrifuge for 10 minutes to remove non-reacted Se and Cd. The sample was precipitated once more

by the addition of ethanol, and then redispersed in chloroform. 0.0115 g of MA was added to the sample in chloroform.

#### 2.4.7 Synthesis of 1.5 nm size CdSe nanoplatelets capped with decanoic acid

Cd(Ac)<sub>2</sub>·2H<sub>2</sub>O (0.8 mmol) 0.213 g, Se (0.2 mmol) 0.0158 g, and Decanoic Acid(DA) (0.2 mmol) 0.0345 g, were added to 25.35mL of ODE in a three-neck round bottom flask, with a condenser, a septum and a mercury thermometer (range to 300°C). The reaction was put under vacuum and heated to 130 °C, and kept at this temperature for 2 hours. Following this, the atmosphere was changed to argon, and the reaction was heated to 220 °C and kept at this temperature for 30 minutes. The mixture was then allowed to cool to room temperature and the QPs were washed as before.

#### 2.4.8 Synthesis of both 1.5 nm and 1.2 nm size CdSe nanoplatelets capped with Myristic Acid

Cd(Ac)<sub>2</sub>·2H<sub>2</sub>O (0.8 mmol) 0.213 g, Se (0.2 mmol) 0.0158 g, and Myristic Acid(MA) (0.2 mmol) 0.0457 g, were added to 25.35mL of ODE in a three-neck round bottom flask, with a condenser, a septum and a mercury thermometer (range to 300°C). The reaction was then put under vacuum and heated to 120 °C, and kept at this temperature for 3 hours. The atmosphere was switched to argon, the mixture was then allowed to cool to room temperature and the QPs were washed.

#### 2.4.9 Synthesis of 1.2 nm size CdSe nanoplatelets capped with decanoic acid

Cd(Ac)<sub>2</sub>·2H<sub>2</sub>O (0.8 mmol) 0.213 g, Se (0.2 mmol) 0.0158 g, and Decanoic Acid(DA) (0.2 mmol) 0.0345 g, were added to 25.35mL of ODE in a three-neck round bottom flask, with a condenser, a septum and a mercury thermometer (range to 300°C). The reaction mixture was put under vacuum and heated to 120 °C. The atmosphere was changed to argon after 1 hour and the reaction was kept at 120°C for 7 days. The reaction mixture was then allowed to cool to room temperature and the QPs were washed as before.

#### 2.4.10 Synthesis of Mn doped CdSe nanoplatelets of size 1.5 nm

Cd(Ac)<sub>2</sub>·2H<sub>2</sub>O (0.8 mmol) 0.213 g, Se (0.2 mmol) 0.0158 g, Mn(OAc)<sub>2</sub>·4H<sub>2</sub>O (0.05mmol) 0.0123g and Myristic Acid(MA) (0.2 mmol) 0.0457 g, were added to 25.35mL of ODE in a three-neck round bottom flask, with a condenser, a septum and a mercury thermometer (range to 300°C). The reaction mixture was then put under vacuum and heated to 140 °C, and kept at this temperature for 2 hours 45 minutes. Following this, the atmosphere was switched to argon and the mixture was heated to 220°C for 1 hour. The sample was then allowed to cool to room temperature and washed.

#### 2.4.11 Phase transfer of 1.5 nm size CdSe QPs

30 mg (0.2 mmol) L-Pen was dissolved in 150 µL of millipore water and 0.5 mL of methanol. The solution was adjusted to pH 10 using 2 M NaOH. This solution was added to 1 mL CdSe QPs in chloroform and stirred for 10 minutes. 5 mL water was added into the mixture and the mixture was stirred for another 10 minutes. The aqueous phase was collected and precipitated with acetone, the pellet was redissolved in 5 mL of water and the pH was adjusted to 10.

#### 2.4.12 Phase transfer of 1.2 nm size CdSe QPs

30 mg (0.2 mmol) L-Pen was dissolved in 150 µL of millipore water and 0.5 mL of methanol. The solution was adjusted to pH 10 using 2 M NaOH. This solution was added to 2.5 mL CdSe QPs in chloroform and stirred for 3 hours. 5 mL water was added into the mixture and the mixture was stirred for another 20 minutes. The aqueous phase was collected and precipitated with acetone, the pellet was redissolved in 5 mL of water and the pH was adjusted to 10.

### 2.5 Experimental details for chapter 6

#### 2.5.1 Cation exchange from pen capped CdS to pen capped Cu<sub>2</sub>S

The cation exchange reaction was adapted from previously reported procedure<sup>6</sup>.

1 mL of Pen-capped CdS (10  $\mu\text{mol}$ ) stock solution was added to a solution of 15 mg (0.1 mmol) L-pen or D-pen in 1 mL water. A solution of 11 mg of  $\text{Cu}(\text{CH}_3\text{CN})_4\text{PF}_6$  (30  $\mu\text{mol}$ ) in 500  $\mu\text{L}$  of methanol was added. The reaction was allowed to proceed for 5 minutes, before crashing out the QDs with ethanol and centrifuging them for 15 minutes. The pellet was then redissolved in 5 mL of water.

### 2.5.2 Cation exchange from CdSe:Mn platelets to $\text{Cu}_2\text{Se}$ :Mn platelets

The cation exchange reaction was adapted from previously reported procedure<sup>6</sup>.

11 mg of  $\text{Cu}(\text{CH}_3\text{CN})_4\text{PF}_6$  (30  $\mu\text{mol}$ ) in 1 mL methanol was rapidly added to a vigorously stirred solution of 2 ml CdSe platelets. The exchange was allowed to proceed for a few minutes after which 1mL of methanol was added and the solution was centrifuged at 4000 for 10 minutes. The  $\text{Cu}_2\text{Se}$  QPs were redispersed in 3mL of toluene and 10mg of myristic acid was added to help stabilization.

### 2.5.3 Synthesis of CdSe@ZnS/ZnS QDs

CdSe@ZnS/ZnS QDs have been prepared according to previously reported procedure<sup>7</sup>.

Cd(II)acetate (0.14 mmol) and ZnO (3.41 mmol) were mixed with oleic acid (7 mL) in a 50 mL three neck flask. It was then heated to 150  $^\circ\text{C}$  under nitrogen followed by the addition of ODE (15 mL) and further heating to 310  $^\circ\text{C}$ . In a separate flask TOP(S/Se) was prepared by dissolving 5 mmol of both selenium and sulfur in TOP (5 mL). 2 mL of this solution was then injected into the hot Cd(acetate)/OA/ODE solution. The reaction was held at 310  $^\circ\text{C}$  for 10 minutes. Sulfur (1.6 mmol) dissolved in ODE (2.4 mL) was then injected and the mixture was held at 310  $^\circ\text{C}$  for a further 12 minutes. Zinc acetate (2.86 mmol, anhydrous) dissolved in OA (1 mL) and ODE (4 mL) was swiftly injected at 310  $^\circ\text{C}$ , at which point the reaction temperature was lowered to 270  $^\circ\text{C}$ . Finally, a solution of sulphur (9.65 mmol) dissolved in TOP (5 mL) was added dropwise at a rate of 0.5 mL per minute and the reaction was held at 270  $^\circ\text{C}$  for 20 minutes. The resultant QDs precipitated using ethanol and washed with a

ethanol/hexane (4:1 volume ratio) mixture multiple times before being finally dispersed in chloroform.

#### 2.5.4 Phase transfer of the above QDs using thiolactose and penicillamine

The above CdSe@ZnS/ZnS QDs were subsequently used for ligand exchange reactions using penicillamine and thiolactose. The procedure for the exchange is the exact method used for the ZnS:Mn QDs detailed in section 2.2.2. In order to vary the ratio of penicillamine to thiolactose on the surface, equimolar solutions of penicillamine in methanol and thiolactose in methanol were prepared. By combining the correct ratio of these solutions before combining with the QDs, the final ratio of penicillamine to thiolactose on the surface of the QD could be approximately controlled.

## 2.6 Characterisation techniques

### 2.6.1 UV-Vis spectroscopy

The Beer-Lambert law describes the relationship between absorbance and concentration and is seen in Equation 2-1 where  $A$  is absorbance,  $\epsilon$  is the extinction coefficient, and  $l$  is the path length of the sample.

$$A = \epsilon cl$$

*Equation 2-1 The Beer-Lambert Law*

By passing light through a sample of various wavelengths and monitoring the loss in intensity as a function of incident wavelength an absorbance spectrum is created. While commonly used to analyse the electronic transitions in organic molecules, UV-Vis spectroscopy is a powerful tool for analysing quantum dots as the absorbance spectra will yield information about the band gap energy as well as approximate sizes, distributions and concentrations.

Although dual beam UV-Vis spectrometers exist our measurements were all carried out using a single beam photometer as described below in Figure 2-3.

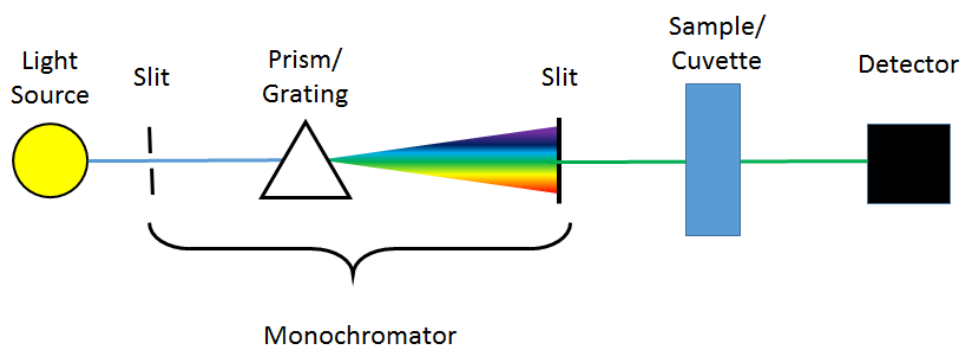


*Figure 2-3 Basic principles of a UV-Vis spectrometer.*

## 2.6.2 Photoluminescence Spectroscopy

Photoluminescence can be divided into two different forms, fluorescence and phosphorescence, both of which feature in this research. When an electron is excited by a photon of suitable energy, it exists in an excited and unstable state. When the excited electron loses energy and emission takes place it is known as photoluminescence. To differentiate between fluorescence and phosphorescence the spin state of the ground state and excited state electrons must be examined below in Figure 2-4. When observing a pair of electrons occupying the same ground energy state their spins must be opposite due to the Pauli Exclusion principle. If the multiplicity of this state is equal to 1, then the state is said to be a singlet state. Multiplicity is calculated using the  $2S + 1$  formula where  $S$  is the total spin angular momentum. In case (a) the electrons have opposite spins, and so  $S = 0$  and the overall multiplicity is 1. In case (b) when one of the electrons is excited to a higher energy level the spins are still opposite, and so the multiplicity remains 1 and is said to be the excited singlet state of the system. If, however, the spin of the excited state is reversed so that the spins of the ground state electron and excited state electron are in parallel the total spin angular momentum is now 1 and so the multiplicity is 3, known as the triplet state<sup>8</sup>. With regards to photoluminescence, if no change in multiplicity takes place the transition is described as fluorescence, however, if a change in multiplicity takes place the transition is described as phosphorescence.

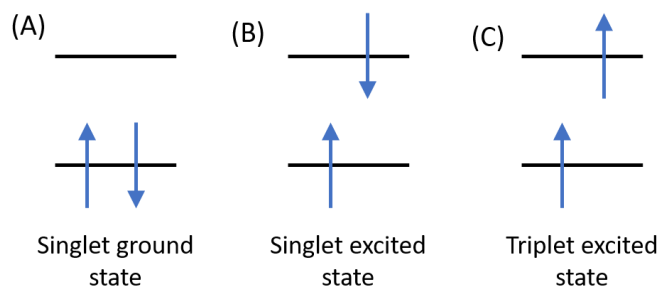


Figure 2-4 Diagram describing singlet and triplet electronic spin states.

For fluorescence measurements, a xenon arc lamp is often used as a continuous emission spectrum light source. By using a monochromator, an excitation wavelength is chosen which passes through the sample in the cuvette. The emission then passes through a second monochromator before it reaches the detector. By adjusting the emission monochromator, an emission intensity spectrum as a function of wavelength may be obtained. The process is described below in Figure 2-5.

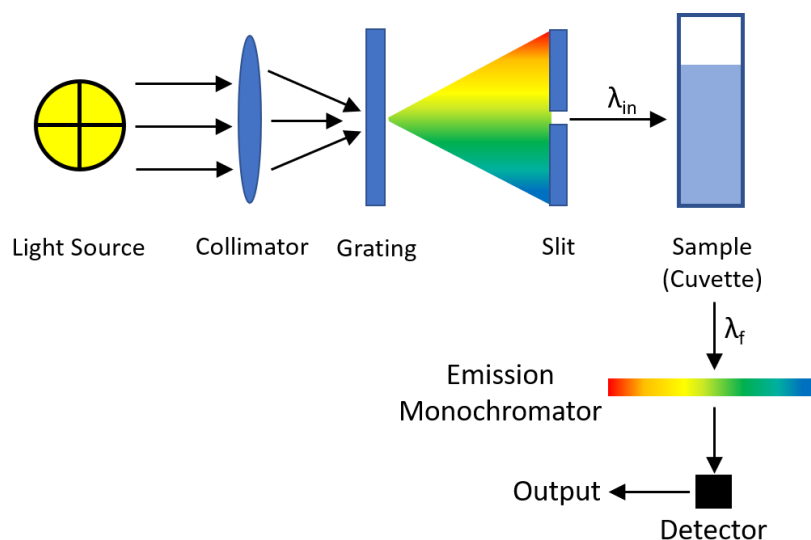


Figure 2-5 Internal structure of a spectrofluorimeter

The instrumentation for phosphorescence is very similar to fluorescence detection however it is necessary to discriminate between the two radiative processes. As the two processes operate on very different timescales, it is possible to introduce a delay between the excitation of the sample and the measuring of the luminescence. One possible method to achieve this is to use two choppers which are running out

of phase which would prevent the emission from reaching the detector at the same time that the sample is being excited.

In our work PL spectroscopy was performed using a Cary Eclipse spectrometer and 1 cm quartz fluorescence cuvettes.

### 2.6.3 Circular Dichroism Spectroscopy

Molecules with a chiral structure preferentially absorb circularly polarised light (CPL) of one handedness over the other due to a greater overlap between the electric field of the light and the dipole in the molecule. By alternatively passing left and right-handed circularly polarised light through a sample circular dichroism signals may be measured as the difference in absorbance of left and right-handed CPL according to the following equation:

$$CD(\Delta A) = A^L - A^R$$

*Equation 2-2 Equation for circular dichroism*

Circular dichroism results are more commonly recorded as a function of ellipticity,  $\theta$ . Ellipticity, in this case, refers to the extent of distortion of the CPL to an elliptical shape as the sample absorbs either left or right-handed light more and is measured in millidegrees (mDeg). In order to convert from  $\Delta A$  to mDeg, the following equation is used.

$$\theta(mDeg) = CD(\Delta A) \times 32980$$

*Equation 2-3 Conversion of CD( $\Delta A$ ) to CD(mDeg)*

Circular dichroism is absorbance dependent, so it is important to ensure all of your samples are of equal concentration in order to quantitatively compare results. Alternatively, it is possible to convert CD results to a unitless factor by dividing by absorbance in order to eliminate the effects of varying concentration. This factor is known as the g-factor, or Kuhn's anisotropy factor<sup>10</sup> and is described below where  $A^L$  and  $A^R$  are the absorbances of left and right-handed CPL respectively, and  $A$  is the total absorbance.



$$g - factor = \frac{A^L - A^R}{A}$$

*Equation 2-4 G-factor conversion for CD measurements.*

#### 2.6.4 X-Ray Diffraction

X-ray diffraction (XRD) is a method by which the crystal structure of crystalline solids may be determined by analysing the diffraction patterns of incident X-rays. This characterisation technique is based upon Braggs law for describing the conditions required for diffraction. It is outlined in Equation 2-5 below where  $\lambda$  is the wavelength,  $d$  is the lattice spacing, and  $\theta$  represents the incident angle of the x-ray beam.

$$n\lambda = 2d\sin\theta$$

*Equation 2-5 Braggs Law*

By using Braggs Law, it can be seen that for certain incident angles constructive interference will take place (Figure 2-6). By exposing a crystalline sample to x-rays over a range of different angles and recording the subsequent pattern formation, the crystal structure of the material may be determined.

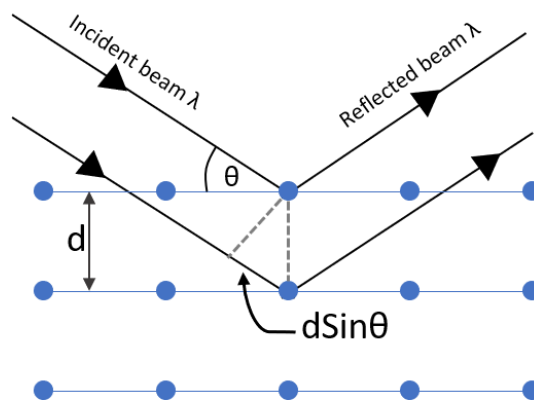


*Figure 2-6 Diagram describing constructive interference in a crystal lattice.*

The most informative form of X-Ray diffraction is single crystal XRD where a single crystal is placed in a holder and rotated on its axis to produce a series of spots corresponding to the different lattice planes. However, for materials and quantum dot research it is more practical to use x-ray powder diffraction. This technique

analyses a homogenous, powdered sample and allows the average crystal structure to be resolved.

Powder XRD is carried out by first producing electrons from a heated filament; these electrons are then bombarded at a metal target using a high voltage. The X-rays are then monochromated using either foils or a monochromator before passing through a collimator. The monochromatic x-rays are aimed at the sample, and as the source and detector are rotated, the detector records the reflected x-ray intensity as a function of the incident angle. In quantum dot research this technique is particularly helpful in determining the crystal structure of your product as you can compare your result against a library of recorded XRD patterns for known materials.

#### 2.6.5 Transmission Electron Microscopy

Traditionally optical microscopes were limited in their resolution by the wavelength of light being used to image a sample. Using the visible light spectrum as a photon source limits the resolution of the microscopes to sub-micron resolution. However, this is not sufficient for modern day nanomaterial requirements, and so a new form of microscopy was developed, transmission electron microscopy (TEM).

Transmission electron microscopy uses a beam of electrons as the wave source for imaging. This was possible due to De Broglie's wave-particle duality theory which explains how a beam of electrons possesses wave-like properties such as diffraction and interference. The associated wavelength of these electron beams is proportional to the energy of the electron beam and is far shorter than the wavelength of visible light, leading to a much higher resolution than optical microscopes. TEM is a powerful tool to elucidate a wide variety of information about a sample. This information includes but is not limited to morphology, crystallinity, composition, topography and size distribution. Figure 2-7 below describes the basic operation of the transmission electron microscope.

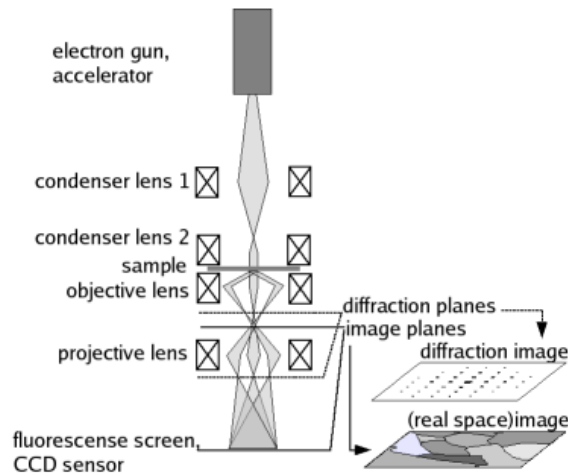


*Figure 2-7 Basic operation of a transmission electron microscope (reproduced from ref.<sup>11</sup>)*

By combining an electron gun and a series of condenser lenses, a monochromatic beam of parallel electrons can be produced and passed through the sample of interest. The subsequent scattered electrons are focused using the objective lens into a primary image. This image is then magnified as it passes through successive lenses before it reaches the CCD detector where the image signal is converted into an electronic signal for analysis. By adjusting the lens configuration, it is possible to use the microscope for scanning transmission electron microscopy. This is done by changing the parallel beam of electrons which is normally projected onto the sample into a single point which is then rastered over the sample instead. This method is useful for nanomaterials as Z-contrast annular dark field microscopy is possible. Dark field microscopy works very well for size distribution analysis as the contrast in the images between the quantum dot and the substrate is large due to the large difference in atomic weight. Furthermore, STEM mode allows elemental analysis (EDX) to be performed which is discussed in the following section.

By adjusting the sample and aperture positions it is possible to analyse just the diffracted electrons instead of the incident electrons. This is commonly known as dark field TEM analysis and allows significant structural information to be determined.

### 2.6.6 Energy-dispersive X-Ray Spectroscopy

Energy-dispersive x-ray spectroscopy (EDX) is a technique which allows the elemental composition of samples to be determined. It may be incorporated as an extra feature in transmission electron microscopes facilitating elemental analysis while visually seeing the area being analysed using the TEM. A diagram presented below in Figure 2-8 explains the basic theory of EDX analysis. In principle it operates by ejecting inner shell electrons from a sample using a high energy electron beam or x-rays (A), creating an inner shell hole (B). When an electron from an outer shell relaxes to fill this inner shell hole the difference in energy is given off in the form of x-rays (C). The number of x-rays and their corresponding energies may be analysed using the energy-dispersive photometer. As the difference in shell energies is unique to each element, this technique allows a determination of the elements in the sample to occur.

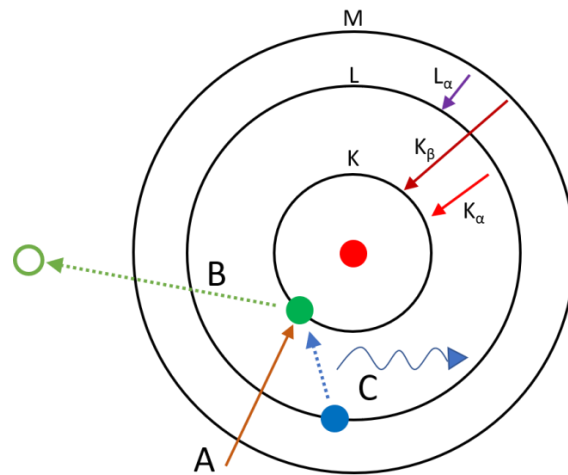
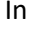


Figure 2-8 Diagram describing the general principles of EDX analysis.

## 2.7 References

- (1) Yu, J. H.; Kwon, S. H.; Petrasek, Z.; Park, O. K.; Jun, S. W.; Shin, K.; Choi, M.; Park, Y. I.; Park, K.; Na, H. B.; Lee, N.; Lee, D. W.; Kim, J. H.; Schwille, P.; Hyeon, T. *Nature materials* **2013**, *12*, 359.
- (2) Talapin, D. V.; Nelson, J. H.; Shevchenko, E. V.; Aloni, S.; Sadtler, B.; Alivisatos, A. P. *Nano Letters* **2007**, *7*, 2951.
- (3) Yu, W. W.; Peng, X. *Angewandte Chemie International Edition* **2002**, *41*, 2368.
- (4) Ouyang, J.; Zaman, M. B.; Yan, F. J.; Johnston, D.; Li, G.; Wu, X.; Leek, D.; Ratcliffe, C. I.; Ripmeester, J. A.; Yu, K. *The Journal of Physical Chemistry C* **2008**, *112*, 13805.
- (5) Ithurria, S.; Tessier, M. D.; Mahler, B.; Lobo, R. P. S. M.; Dubertret, B.; Efros, A. L. *Nature materials* **2011**, *10*, 936.
- (6) Li, H.; Zanella, M.; Genovese, A.; Povia, M.; Falqui, A.; Giannini, C.; Manna, L. *Nano Letters* **2011**, *11*, 4964.
- (7) Lee, K.-H.; Lee, J.-H.; Kang, H.-D.; Park, B.; Kwon, Y.; Ko, H.; Lee, C.; Lee, J.; Yang, H. *ACS Nano* **2014**, *8*, 4893.
- (8) McClure, D. S. *J. Chem. Phys.* **1949**, *17*, 905.
- (9) Balzani, V.; Bergamini, G.; Campagna, S.; Puntoriero, F. In *Photochemistry and Photophysics of Coordination Compounds I*; Balzani, V., Campagna, S., Eds.; Springer-Verlag Berlin: Berlin, 2007; Vol. 280, p 1.
- (10) Zsila, F. In *Pharmaceutical Sciences Encyclopedia*; John Wiley & Sons, Inc.: 2010.
- (11) Falke, W. In  In [https://upload.wikimedia.org/wikipedia/commons/f/f6/TEM\\_ray\\_diag2.basic.en.png](https://upload.wikimedia.org/wikipedia/commons/f/f6/TEM_ray_diag2.basic.en.png); Wikipedia: [www.wikipedia.org](http://www.wikipedia.org), 2011.

## Chapter 3: Synthesis of non-toxic, optically active ZnS, ZnS:Mn and ZnSe QDs

### 3.1 Introduction

As the field of nanoscience continues to expand at an ever-increasing rate, there is a growing demand for research pertaining to non-toxic fluorescent nanomaterials, including quantum dots. II-VI quantum dots have traditionally been synthesised using cadmium as a component. However, these type of QDs have demonstrable toxicity *in vitro* and *in vivo*<sup>1</sup>, and consequently, the field of non-toxic quantum dots is emerging. Some examples of non-toxic (or at least less toxic) quantum dots include the following.

Thomas *et al.* have synthesised InP/ZnS core/shell quantum dots which demonstrated effective Förster resonance energy transfer (FRET) properties<sup>2</sup>. Due to the environmental friendliness and relatively low toxicity of the QDs, they would be appropriate for a variety of applications including photodynamic therapy.

Li *et al.* have developed a range of CuInS<sub>2</sub>/ZnS core/shell quantum dots which were successfully shown to work for *in vivo* imaging of mice<sup>3</sup>, while whole animal imaging of an oral vaccine containing CuInSeS/ZnS core/shell QDs was achieved by Panthani *et al.*<sup>4</sup>.

By combining blue emitting carbon dots with red and green emitting copper indium zinc sulphide core/shell QDs Sun *et al.* have developed new QDs for white light emitting diodes<sup>5</sup>. Indium based, low toxicity QDs are now being used in a variety of applications including televisions and other visual displays.

While indium-based QDs have found widespread applications in optoelectronic devices, a lot of research is being invested in transition-metal doping of zinc-based quantum dots for biomedical purposes<sup>6-10</sup>. For example, size tuneable manganese doped zinc sulphide quantum rods have been synthesised by Deng *et al.*<sup>10</sup> using a

phosphine free organic synthesis. Green emitting copper-doped zinc sulphide quantum dots have been synthesised for use in cancer cell labelling by Ang *et al.*<sup>11</sup> Using selenourea as an alternative selenium source, manganese doped zinc selenide QDs have been synthesised according to research by Acharya *et al.*<sup>12</sup>

Thus, due to the ongoing interest in the field, we believe that it is appropriate to use doped and undoped zinc based quantum dots for our non-toxic chiral quantum dot research.

As biological systems are heavily dependent on chirality it is also important to assess the role of chirality in quantum dot interactions, most generally caused by the presence of chiral ligands on the surface of the QDs. The investigation of chirality and its potential applications in quantum dots is relatively new, however preliminary results are promising. Therefore, the primary focus of our research on non-toxic QDs is the induction of optical activity in QDs and the subsequent interaction of our chiral QDs with other chiral systems. Investigations into chirality and quantum dots have emerged in recent years and have drawn some interesting conclusions. For example, Balaz *et al.* demonstrated that CdSe QDs stabilised by D- or L- cysteine displayed optical activity in the band edge region of the QDs. Interestingly, these QDs stabilised by chiral ligands demonstrated circularly polarised emission<sup>13</sup>. CdTe QDs capped with N-acetyl-L-cysteine were used for the chiral recognition of the enantiomers of phenylglycinol by Guo *et al.*<sup>14</sup>. Optically active CdSe/CdS core/shell QDs were used for the chiral recognition of cysteine stabilised magnetic CoFe<sub>2</sub>O<sub>4</sub> nanoparticles by Visheratina *et al.*<sup>15</sup>. While manganese-doped ZnS QDs stabilised with a thiolated form of  $\beta$ -cyclodextrin have been shown to successfully discriminate tryptophan enantiomers *via* quenching processes<sup>16</sup> by Wei. *et al.*

### 3.2 Aims of this chapter

The main aims of this chapter are two-fold. Firstly, the aim of this chapter was to produce both chiral ZnS and ZnSe based quantum dots and secondly, our objective

is to investigate the potential of these materials for biological applications and chiral recognition of selected species. It was then planned to synthesise ZnS and ZnS:Mn quantum dots in the organic phase and transfer the particles from the organic phase to the aqueous phase using chiral ligands such as cysteine and penicillamine. It is expected that the use of an organic synthesis followed by a phase transfer would produce higher quality optically active quantum dots as opposed to performing an aqueous synthesis in the presence of chiral ligands.

As this project involved chirality and biological applications, one of the aims was to test anti-bacterial properties and cytotoxicity of both L-Cys-ZnS:Mn and D-Cys-ZnS:Mn QDs. It is expected that the difference in chiral ligand stereochemistry should affect both the toxicity and antibacterial properties of the two enantiomeric forms of QDs.

The final aim of the chapter was to synthesise chiral ZnSe QDs in the presence of a larger chiral ligand, such as glutathione. Glutathione is a larger ligand containing more chiral centres than small cysteine or penicillamine ligands, and therefore any chiral recognition effects might be more pronounced due to stronger chiral interactions. Using these ZnSe-glutathione QDs, the demonstration of chiral discrimination through the quenching of the luminescence was planned.



### 3.3 Synthesis and characterisation of ZnS and ZnS:Mn quantum dots in chloroform

The ZnS and ZnS:Mn quantum dots were synthesised according to the published procedure described in the previous section<sup>17</sup>. The synthesis involves heating up zinc chloride and elemental sulfur to high temperatures in the presence of the coordinating solvent dibenzylamine. The majority of the characterisation was carried out on the manganese doped QDs as these QDs were used for most of our research. In order to study the effect of the dopant manganese ions on the optical properties of ZnS QDs the UV-Vis and photoluminescence spectra for both the doped and undoped QDs have been recorded (Figure 3-1.)

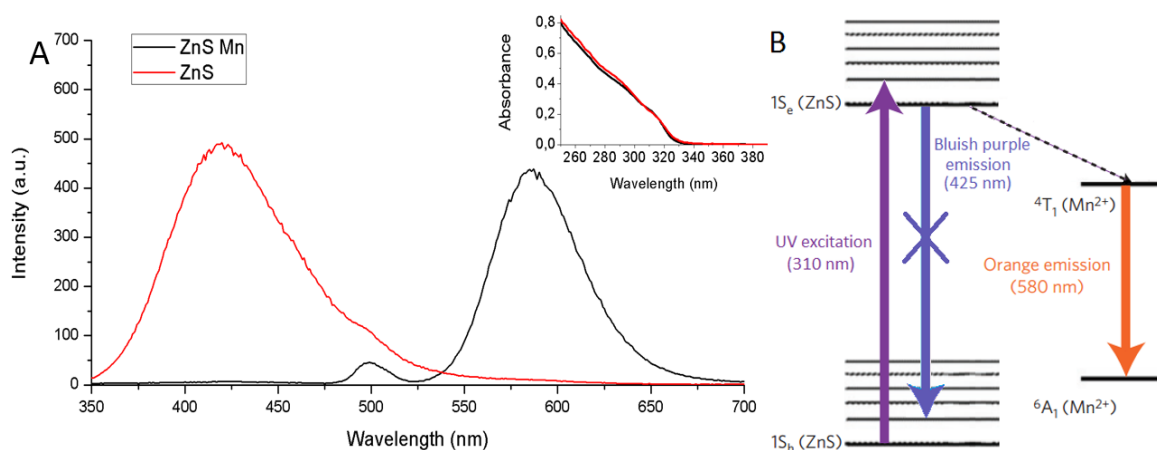


*Figure 3-1 (A) Absorption (inset) and emission spectra for ZnS and ZnS:Mn QDs in chloroform: excitation  $\lambda = 250$  nm. (B) Jablonski diagram showing effects of Mn doping.*

The UV-Vis spectra in the inset of Figure 3-1 (A) show a characteristic absorbance profile for ZnS quantum dots with the first exciton located at around 300 nm; this wavelength corresponds to a band gap energy of 4.1 eV. This demonstrates a widening of the bandgap due to confinement when compared with the bandgap for bulk cubic ZnS which is 3.50 eV<sup>18</sup>. The PL spectra in Figure 3-1 (A) show the luminescence properties of both the doped and undoped QDs. The undoped ZnS QDs show a broad emission with a peak located at 420 nm which correlates well with literature values<sup>20</sup>. As can be seen in Figure 3-1 (B) the addition of the

manganese into the nanocrystal lattice creates an alternative phosphorescent radiative decay pathway corresponding to an emission of wavelength 580 nm<sup>17</sup> which is clearly present in our emission spectra for the doped sample. It should be noted that nearly all of the original ZnS emission has disappeared once the QDs have been doped with manganese suggesting a highly efficient electron transfer from the ZnS conduction band to the manganese ions. The small peak located at 500 nm in the doped PL spectra is a consequence of choosing 250 nm as our excitation wavelength, as any multiple of the excitation wavelength according to Bragg's equation where  $n\lambda = d\sin(\theta)$  will also pass through the diffraction grating.

The quantum yield of these QDs in chloroform was determined using the integrating sphere method and was determined to be 35%.

TEM and high-resolution transmission electron microscopy (HR-TEM), scanning tunnelling electron microscopy (STEM) and energy dispersive X-Ray spectroscopy (EDX) were all used to study the ZnS:Mn QD samples. The results of the HR-TEM and STEM are presented in Figure 3-2 below.

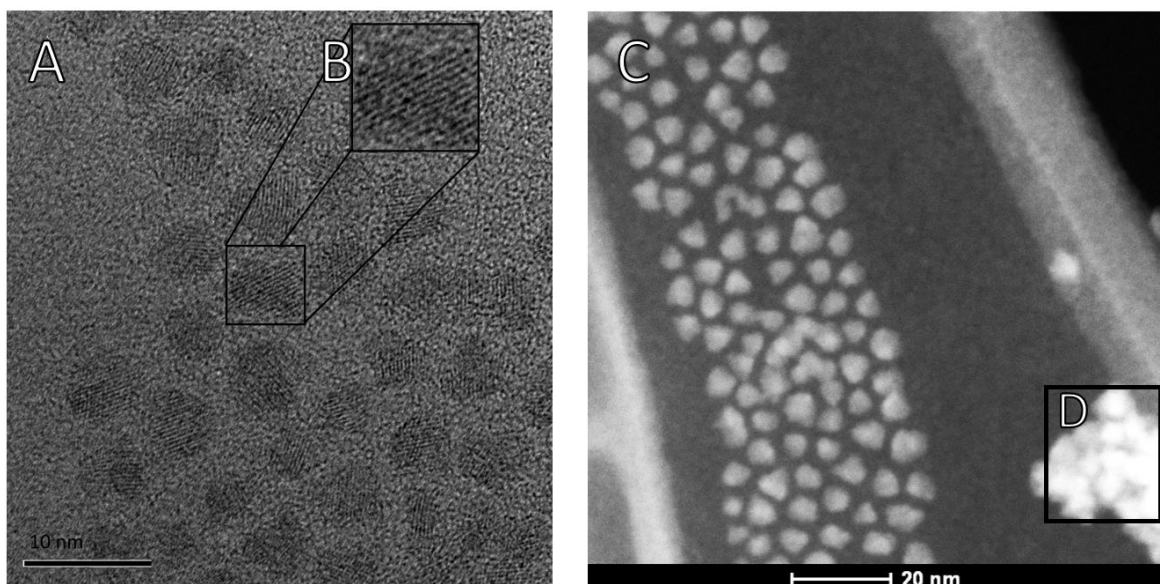


*Figure 3-2 (A) TEM image of the Mn-doped ZnS, (B) a high-res close up of a single QD, (C) STEM image of ZnS:Mn QDs and (D) the area of the sample used for EDX analysis.*

Figure 3-2 (A) demonstrates that ZnS nanoparticles are roughly spherical and monodisperse. Figure 3-2(B) shows a single QD where a high degree of crystallinity

was observed. HR-TEM is very useful for determining crystallinity. However, the contrast was very poor, and therefore STEM was used for high contrast imaging. Figure 3-2 (C) is a STEM image with high contrast and allows accurate size distributions to be determined. The STEM image also showed that, while most of the QDs are roughly round, there are a few anisotropic triangular shaped particles formed.

Figure 3-2 (D) was used to calculate the size distribution of the QDs, and the results can be seen in Figure 3-3 below. The particles have an average size of  $5.3 \text{ nm} \pm 0.7 \text{ nm}$ ; these results correlate well with what was expected from the literature<sup>17</sup>.

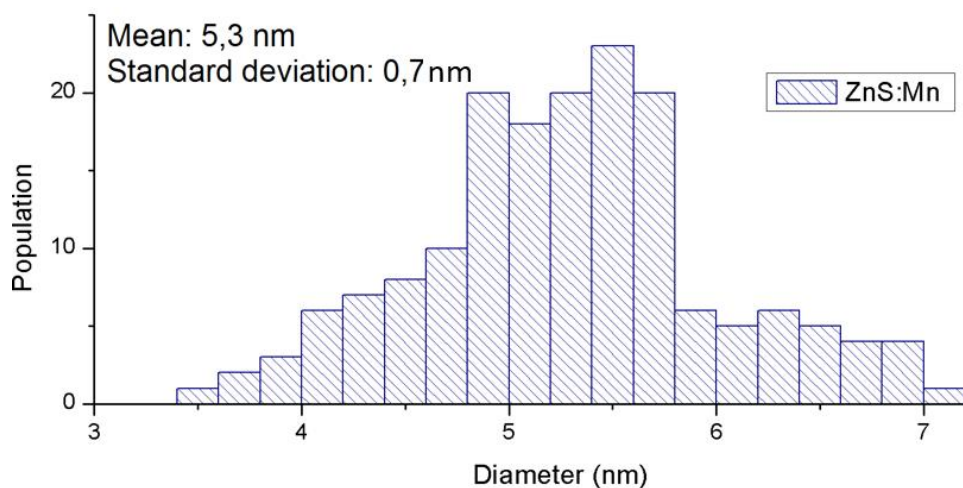


*Figure 3-3 Size distribution for the ZnS:Mn QDs (n = 150).*

Energy-dispersive X-ray spectroscopy (EDX) analysis was used to confirm the presence of manganese ions in the quantum dots; the results are presented in Figure 3-4 below. EDX uses electrons or X-rays to excite and eject inner shell electrons. When electrons from higher energy levels relax to fill the hole created x-rays are released. The energy of these X-rays allows us to identify different elements based on their unique emission spectra.

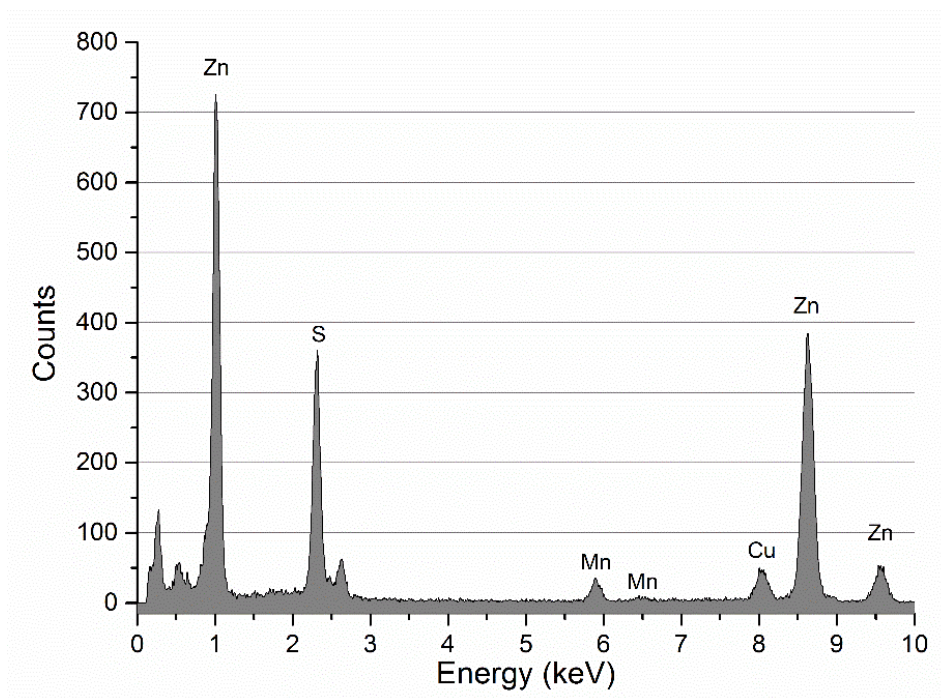


Figure 3-4 EDX analysis of ZnS:Mn QDs.

From our EDX spectra for the ZnS:Mn QDs we can see strong peaks for both zinc and sulphur which would indicate the formation of ZnS. The smaller peak for manganese is further evidence of successful doping of the QDs. While quantitative analysis of the peaks to determine the manganese concentration is difficult, Yu *et al.* used inductively coupled plasma-atomic emission spectroscopy to confirm a manganese concentration of 1.1% for particles produced using the same synthesis<sup>17</sup>. A peak for copper is also visible however this is a consequence of analysing our samples using copper grids.

X-ray diffraction was also performed on both the doped and undoped QDs to determine their crystal structure and to ascertain if there is any noticeable difference between the doped and undoped QDs. Upon analysis of the resultant data (Figure 3-5) there appears to be little difference in the XRD patterns produced for both the ZnS and ZnS:Mn QDs suggesting that the addition of manganese at this concentration has not impacted the crystallinity of the QDs. By comparing the XRD patterns presented below with the accepted patterns for wurtzite and zinc blende ZnS (appendix Figure 8-1) it is clear that our products contain a combination of both

crystal structures. By comparing the size of the relative peaks it is evident that the QDs are primarily zinc blende in structure with a smaller proportion of wurtzite present.

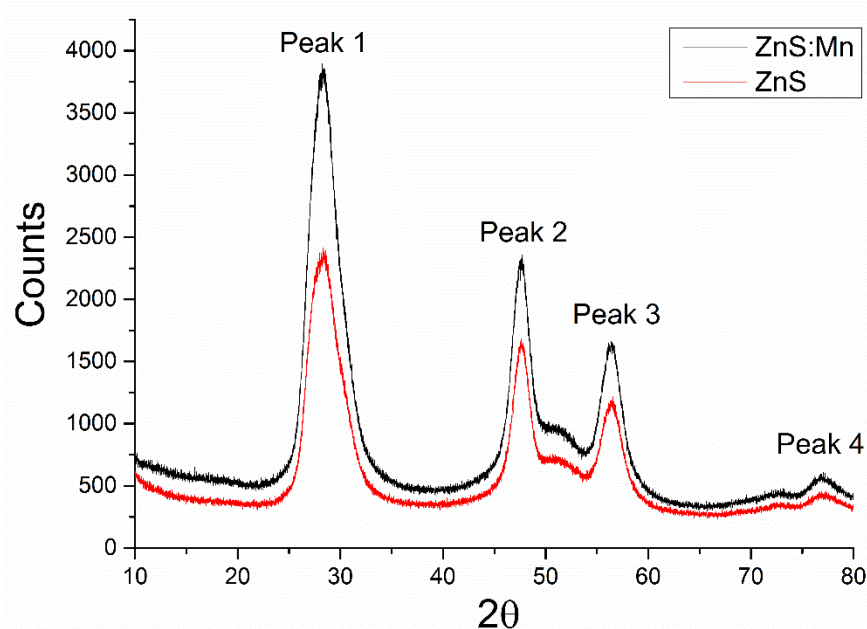


Figure 3-5 XRD spectra for ZnS and ZnS:Mn QDs.

Scherrer analysis was carried out on 4 peaks for both the doped and undoped QDs (**Error! Reference source not found.**) to determine the average crystallite size for the particles. While peaks 2-4 are in relative agreement, peak 1 is significantly different and this is due to the zinc blende contribution broadening the peak and significantly decreasing the calculated crystallite size. By omitting peak 1 and taking an average of peaks 2-4 for both ZnS and ZnS:Mn QDs we get an average crystallite size of 5.4 nm and 5.8 nm respectively. This correlates well with the size distributions determined from the TEM images.

Peak Number	ZnS		ZnS:Mn	
	Peak position ( $^{\circ}2\theta$ )	Crystallite Size ( $\text{\AA}$ )	Peak position ( $^{\circ}2\theta$ )	Crystallite Size ( $\text{\AA}$ )
1	28.375	27.4	28.412	26.3
2	47.539	51.4	47.635	56.8
3	56.43	46.8	56.454	49.5
4	77.096	64.5	77.097	66.9

Table 3-1 Scherrer analysis of ZnS and ZnS:Mn QD XRD patterns

### 3.4 Ligand Exchange on ZnS:Mn quantum dots to produce chiral quantum dots

As these ZnS:Mn QDs were intended for biomedical applications they first had to be transferred into the aqueous phase. In order to do this, a ligand exchange was performed where the organic oleylamine and any residual dibenzylamine was replaced with a chiral, water-soluble ligand such as cysteine or penicillamine. This process was carried out primarily using the method outlined in section 2.2.2 of chapter 2. Once the excess organic ligand was washed off, the QDs were mixed with an acidified solution of the ligand of choice. Once the ligand exchange had taken place, the QDs were no longer soluble in chloroform and so precipitated from solution. The QDs were centrifuged, washed with methanol several times and then re-dispersed in alkaline (pH $\approx$ 11) water. The resulting aqueous particles were characterised using various instrumental techniques: UV-Vis spectroscopy, PL spectroscopy, circular dichroism spectroscopy and transmission electron microscopy. While it was interesting to prepare both doped and undoped QDs, for biological purposes, it was advantageous only to continue using the manganese-doped quantum dots. This is due to the undoped ZnS QDs emitting in the ultraviolet range which is damaging to biological media. The absorbance is also in the UV however it has been shown that 3 photon excitation circumvents this issue<sup>17</sup>.

#### 3.4.1 Preparation of L- and D- cysteine stabilised ZnS:Mn QDs

As cysteine has traditionally been used as a ligand for quantum dot biomedical applications<sup>21-23</sup>, it was decided to use L- and D- cysteine as the initial ligands to perform our phase transfer experiments with. The results of the UV-Vis spectroscopy may be seen in Figure 3-6. From the UV-Vis, it is evident that no spectral change occurred, indicating no morphological change has taken place in the QDs as a consequence of the ligand exchange. The QDs still exhibit a shoulder at 300 nm, while the onset of absorption begins at 340 nm.

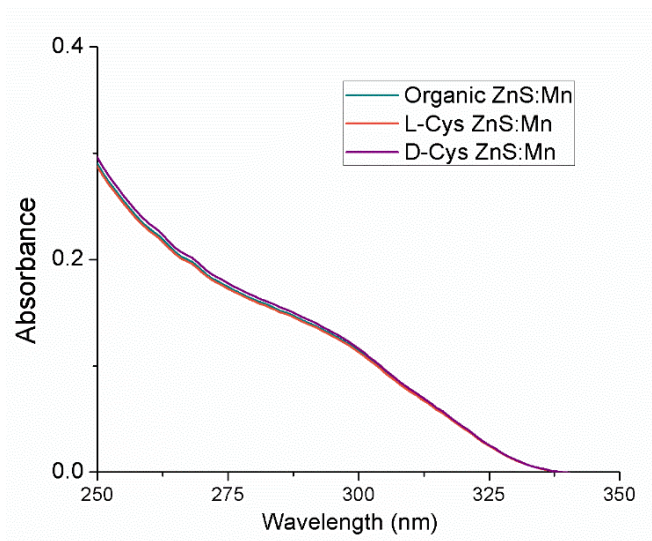


*Figure 3-6 UV-Vis spectra of ZnS:Mn QDs before and after cysteine phase transfer.*

Following this, photoluminescence spectra were recorded to monitor the effect of the ligand exchange on the emission properties of the QDs (Figure 3-7). From the spectra it is clear that there is a slight loss of luminescence. However, D- and L- Cys ZnS:Mn have retained 88 and 89% of their luminescence intensity respectively. There is also no observable shift in the emission wavelength before and after the ligand exchange which can occur during phase transfers either due to etching or aggregation of the sample.

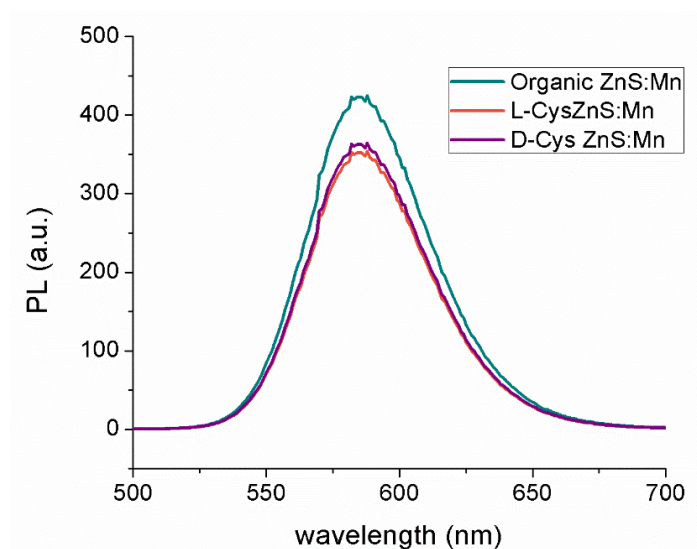


*Figure 3-7 PL spectra for organic oleylamine and aqueous D and L Cys stabilised ZnS:Mn QDs (Ex.  $\lambda$  – 320 nm).*

Finally, the sample was analysed using circular dichroism spectroscopy to see if the samples demonstrated any optical activity. Optical activity in chiral quantum dots is a relatively recent phenomenon, and Prof. Gun'ko's group was the first to report on it<sup>24</sup>. However, as far as we are aware, this is the first time that optical activity in cadmium-free QDs has been reported (Figure 3-8)

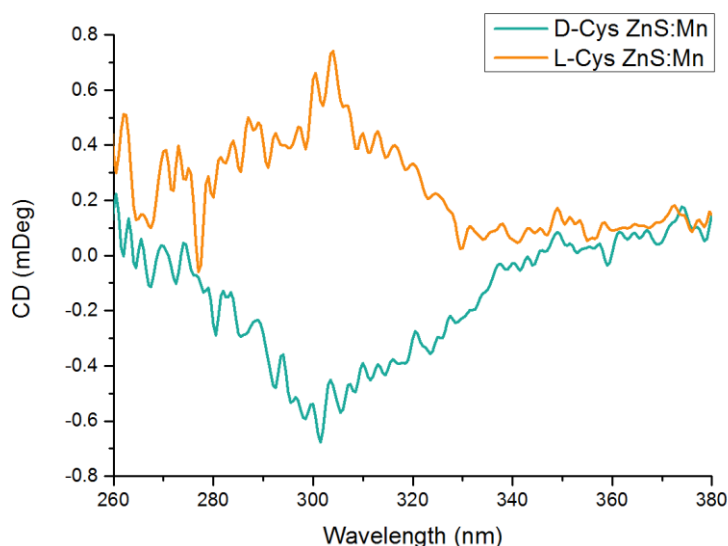


*Figure 3-8 CD spectra for L and D cysteine stabilised ZnS:Mn QDs.*

According to CD spectra ZnS:Mn particles clearly demonstrate optical activity in the exciton absorption region of the ZnS:Mn QDs. It may be noted that the ligand on its own does not display any optical activity at wavelengths longer than 240 nm (Appendix Figure 8-2) so this signal clearly originates from an interaction between the ligand and the quantum dot. Furthermore, the CD signals are equal mirror images for L- and D- Cys stabilised QDs, proving that these signals are not some artefacts. Due to present optical activity located at the onset of the QD absorption, it is theorised that an interaction with both defect states and the exciton is taking place in these materials.

TEM analysis was carried out on the samples and the results for the L-Cys-ZnS:Mn QDs are shown in Figure 3-9. From the TEM it is clear that the particles are still spherical and crystalline indicating that little to no morphological change has taken place throughout the phase transfer process.



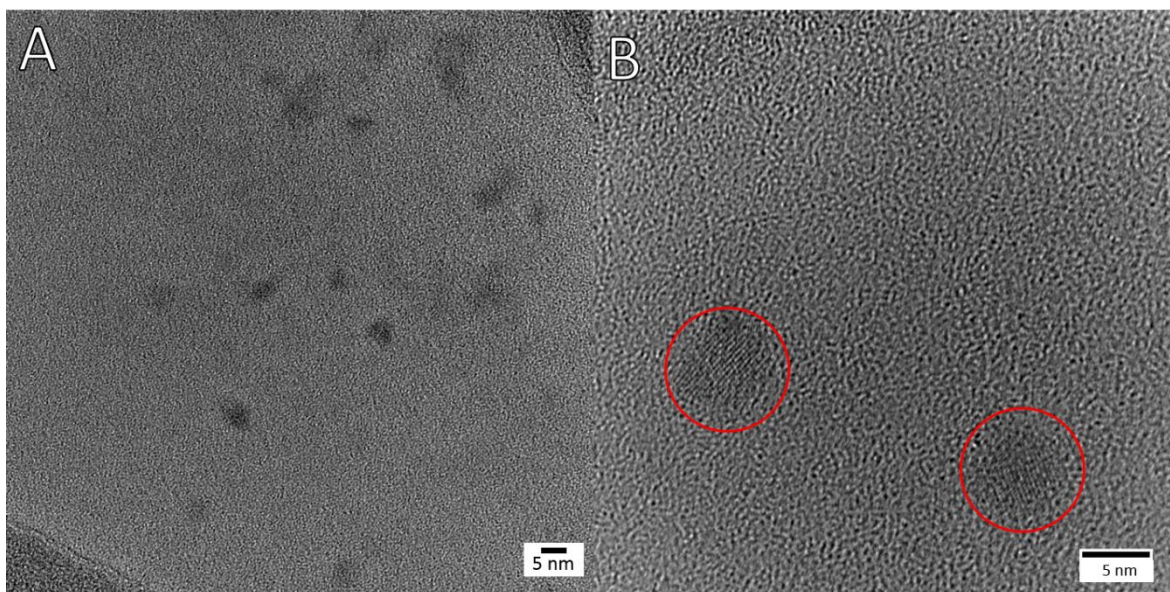


Figure 3-9 A) TEM and B) HRTEM of ZnS:Mn capped with L-cysteine.

Using the TEM images, a size distribution analysis was carried out, and results are presented in Figure 3-10. The ZnS:Mn QDs have an average size of  $5.46 \pm 0.53$  nm. This is in good agreement with the results for the size of the QDs in the organic phase,  $5.3 \pm 0.7$  nm. While there may be a slight increase in size, statistically speaking it is insignificant. One reason that the average size might increase slightly is due to the method used for the ligand exchange. Because the particles are separated by precipitation, the smaller particles are more stable in solution preventing them from easy precipitation and separation. Therefore, it is quite possible that the average size of QDs measured in the aqueous phase is slightly higher.

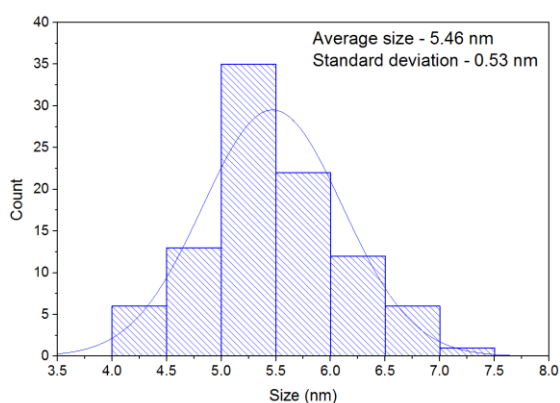
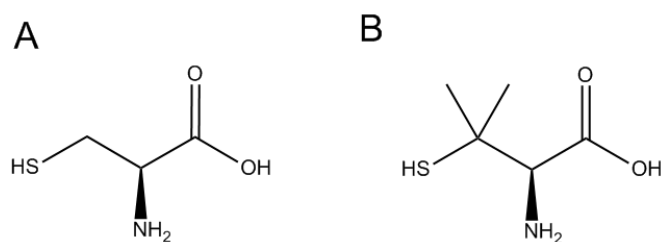


Figure 3-10 Size distribution plot for ZnS:Mn QDs capped with L-cysteine ( $n=150$ ).

### 3.4.2 Penicillamine capped ZnS:Mn quantum dots

Following the preparation of cysteine capped QDs, we also decided to produce D- and L-penicillamine capped QDs. Penicillamine, like cysteine, contains a thiol group and an adjacent chiral centre making it a great candidate for chiral ligand-exchange research. Therefore, we repeated the same procedures used for the cysteine ligand exchange but with penicillamine. Unfortunately, the same method was not successful, so another modified ligand exchange technique was applied. We believe the 2 ligands, cysteine and penicillamine, cannot be used interchangeably due to the differences in stereochemistry and solubility. As we see in Figure 3-11 penicillamine contains 2 methyl groups adjacent to the anchoring thiol group which alters the phase transfer process. By sterically hindering the availability of the thiol group the overall kinetics of the ligand exchange was different.



*Figure 3-11 Structure of A) cysteine and B) penicillamine.*

Therefore, another modified phase transfer technique was used in this case which is outlined in section 2.4.2 of the methods section. Instead of precipitation occurring, this phase transfer works by interacting two liquids, one containing the QDs in toluene and the other containing the penicillamine in solution. Over time the QDs transfer from the organic to the aqueous phase which is monitored by UV-Vis spectroscopy. The subsequent penicillamine capped quantum dots were analysed using UV-Vis, PL, CD spectroscopy. From the UV-Vis spectra in Figure 3-12, it is evident that the D- and L- penicillamine stabilised QDs both have identical spectra and are similar to the spectra obtained from the QDs in the organic phase before the ligand exchange (Figure 3-1). This would indicate that no structural change has occurred during the phase transfer processing.

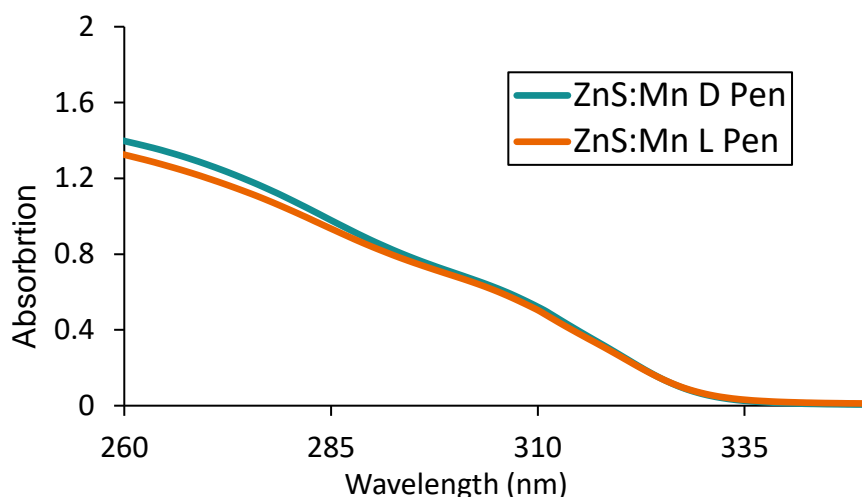


Figure 3-12 UV-Vis spectra of D and L penicillamine stabilised ZnS:Mn QDs.

Following UV-Vis spectroscopy, the QDs were tested for photoluminescence, and the results are presented in Figure 3-13. A loss in luminescence is observed as the penicillamine stabilised samples retain 60% of their luminescence when compared to the original organic sample. It may also be observed that no shift in emission wavelength occurred.

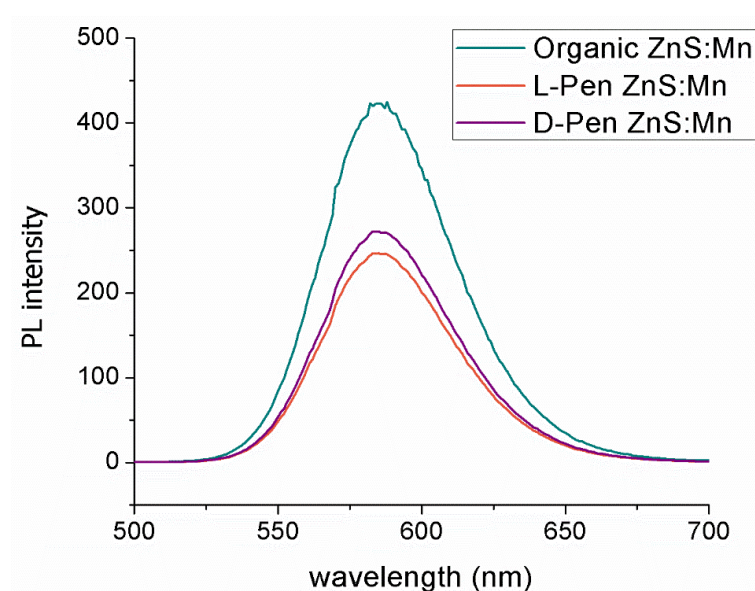


Figure 3-13 PL spectra for organic oleylamine and aqueous D and L pen stabilised ZnS:Mn QDs (Ex.  $\lambda$  – 320 nm).

It is interesting to note that when comparing the emission intensities of both the cysteine and penicillamine samples against the organic sample, the penicillamine

stabilised sample is the least luminescent. This is possible due to the more sterically hindered providing less passivation on the surface of the QD (Figure 3-14).

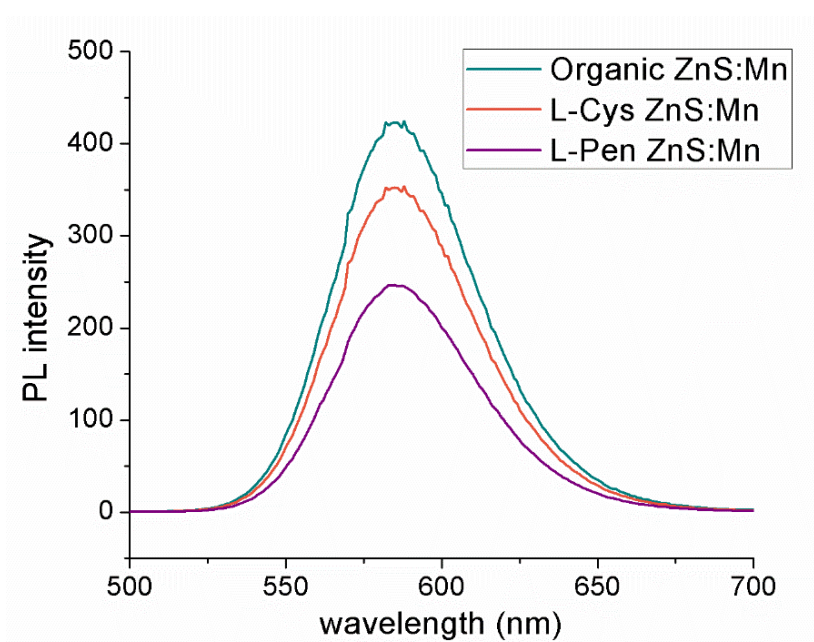


Figure 3-14 PL spectra comparing the organic ZnS:Mn QDs against the cysteine and penicillamine stabilised QDs (Ex.  $\lambda$  – 320 nm).

Following this, the QDs were analysed using CD spectroscopy to identify any optical activity. Similar to the cysteine capped ZnS:Mn QDs, the penicillamine capped QDs also demonstrate optical activity. The CD spectra of D- and L- penicillamine was also included for comparison and is shown in Figure 3-15.

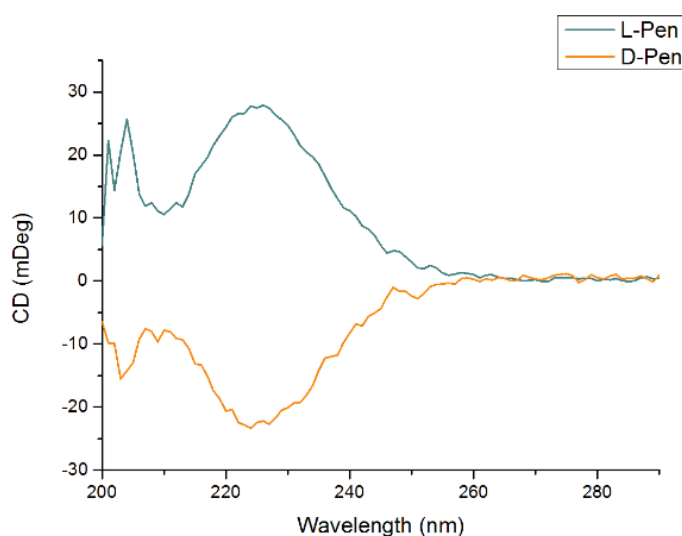


Figure 3-15 CD spectra for pure D- and L- penicillamine (as free ligands).

The D- and the L- pen stabilised QDs show optical activity beginning at 340 nm which corresponds with the onset of the QD absorption (Figure 3-16). Similar to the cysteine ZnS:Mn samples, the optical activity present between 340 – 300 nm would suggest an interaction between the defect states present in the QDs also. From comparing the CD spectra in the ligand region for the conjugated ligand and the free ligand, it's evident that the optical activity of the ligand itself has also been affected by the binding to the QD.

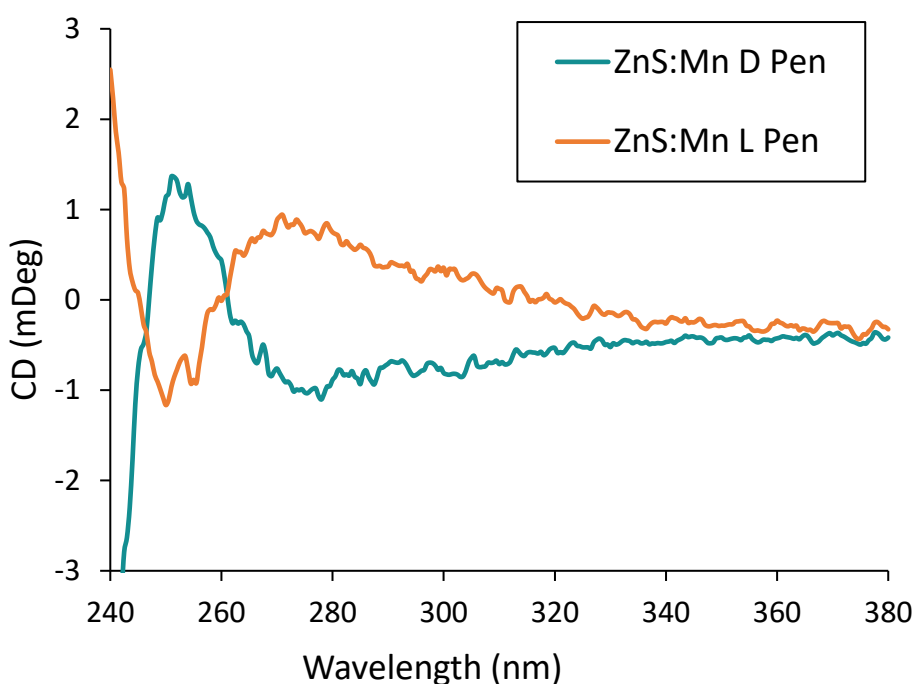
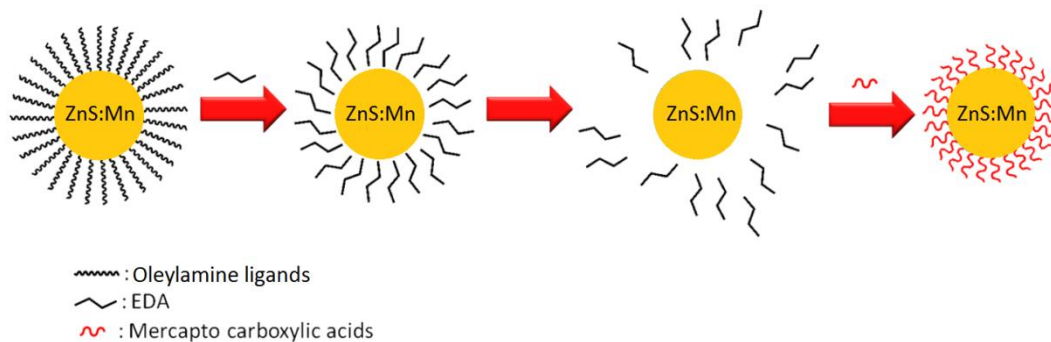


Figure 3-16 CD spectra for D and L penicillamine capped ZnS:Mn QDs.

### 3.4.3 Preparation of cysteine and penicillamine capped ZnS:Mn using ethylenediamine as transfer agent

To further understand phase transfer processes and their influence on the chirality of QDs, it was decided to use a different ligand exchange method to see if a higher degree of optical activity could be observed. To do this, we used a phase transfer method which uses ethylenediamine (EDA) as an intermediate ligand reported by Dai *et al*<sup>25</sup>; the synthesis is detailed in section 2.2.3 of the Experimental chapter. The organic QD solution is first reacted with EDA before being combined with the

aqueous ligand solution (Figure 3-17). The EDA provides a lower energy intermediate for exchanging the oleylamine to the cysteine or penicillamine when compared with the direct phase transfer.



*Figure 3-17 EDA assisted phase transfer scheme of ZnS:Mn QDs.*

The samples were analysed using photoluminescence and CD spectroscopy. Figure 3-18 below shows the relative intensity of the ZnS:Mn QDs capped with D-penicillamine and L-cysteine compared to the original organic QDs in chloroform. According to the spectra below, the QDs still remain luminescent following the phase transfer. The results show that the cysteine sample retains 65% of its luminescence and the penicillamine sample retains 50% of its peak luminescence intensity while no shift in emission wavelength is observed either. The decrease in luminescence compared to the previous QDs may be due to the relative harsh reaction conditions used here by adding a significant amount of EDA to the QDs.

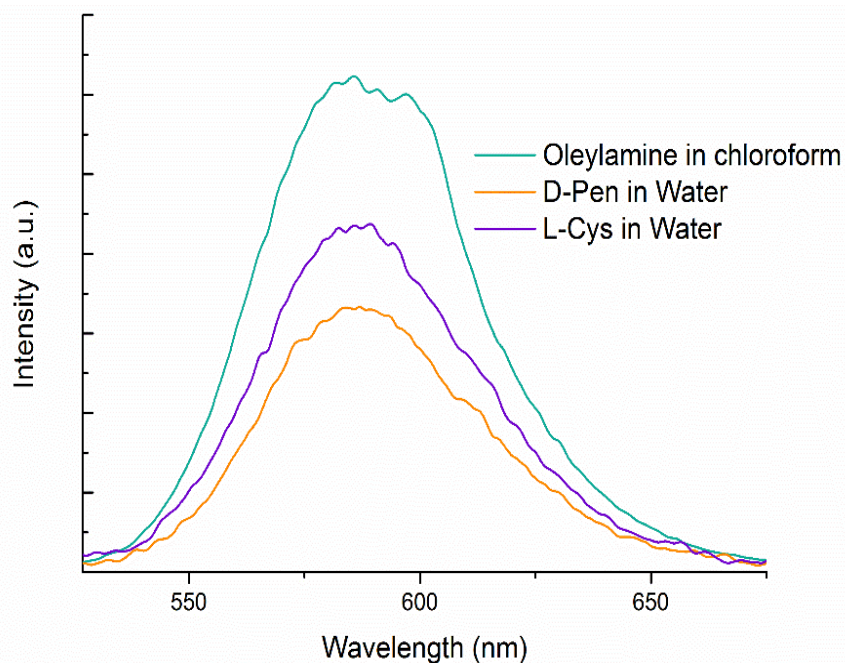


*Figure 3-18 PL spectra for ZnS:Mn QDs following EDA assisted phase transfer for both L-Cys and D-Pen capped QDs.*

Once the QDs were confirmed to be luminescent, we tested them for optical activity using circular dichroism and the results can be seen in Figure 3-19 and Figure 3-20. Figure 3-19 shows the CD spectra for the cysteine capped ZnS:Mn QDs prepared using EDA. According to spectra, there was little to no optical activity present in the sample when compared with the cysteine capped QDs prepared using the previously outlined method, therefore no more experiments were carried out with cysteine capped QDs synthesised using the EDA method. We believe the lack of optical activity may be due to the achiral EDA not being fully displaced by the cysteine, causing less of a chiral interaction at the surface of the QDs.

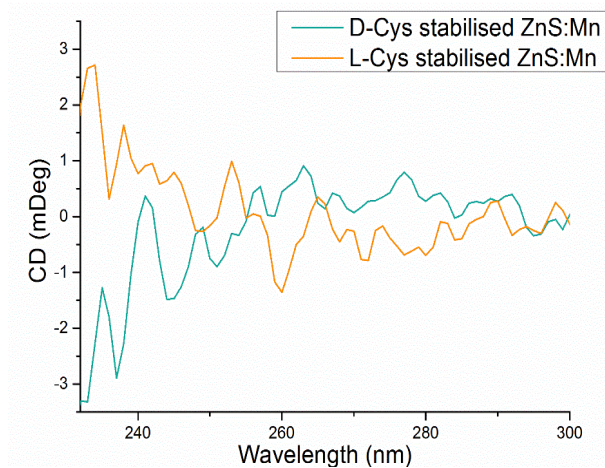


*Figure 3-19 CD spectra for cysteine capped ZnS:Mn QDs synthesised using the EDA phase transfer method.*

The CD spectra for the penicillamine capped QDs synthesised using the same method can be seen below, along with the racemic product. No optical activity was observed in the exciton absorption region of the QDs indicating little to no electronic interaction between the ligand and the QDs. When investigating the CD spectra, it may be noted that the spectrum is very similar to the spectrum for free penicillamine in solution (Figure 3-15). The only difference is that in the spectra of the QDs conjugated with penicillamine the optical activity is reversed in the region between 200 and 210 nm. Again, no optical activity was observed in the QD exciton region, whereas there was optical activity in the sample prepared using previously outlined methods.

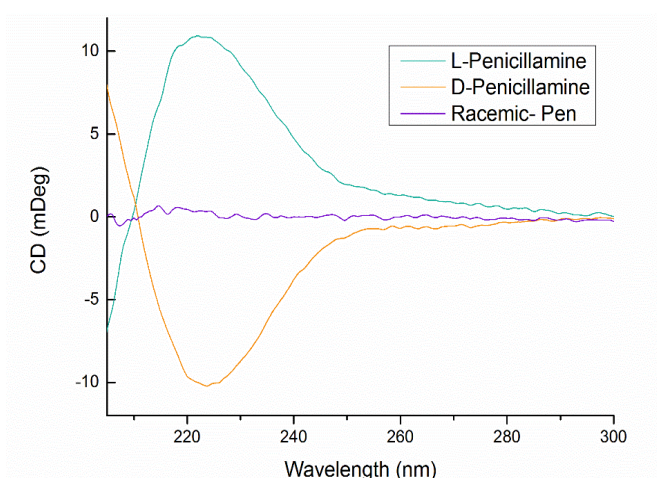


*Figure 3-20 CD spectra for penicillamine capped ZnS:Mn QDs using the EDA ligand exchange process.*



In an attempt to induce a greater degree of interaction between the ligand and the QDs we performed an experiment to enhance the optical activity of the QDs. It was theorised that if the penicillamine stabilised QDs were combined with a solution containing an excess of penicillamine at an elevated temperature we could induce a CD signal with optical activity present in the exciton absorption region of the QD. In order to test this hypothesis a simple experiment was carried out. 5 mL of our D-Pen ZnS:Mn QD solution was dissolved in 45 mL of Millipore water and 50 mg of D-penicillamine was added followed by stirring for 72 hours at 50°C. The same experiment was carried out with L-Pen ZnS:Mn and excess L-penicillamine.

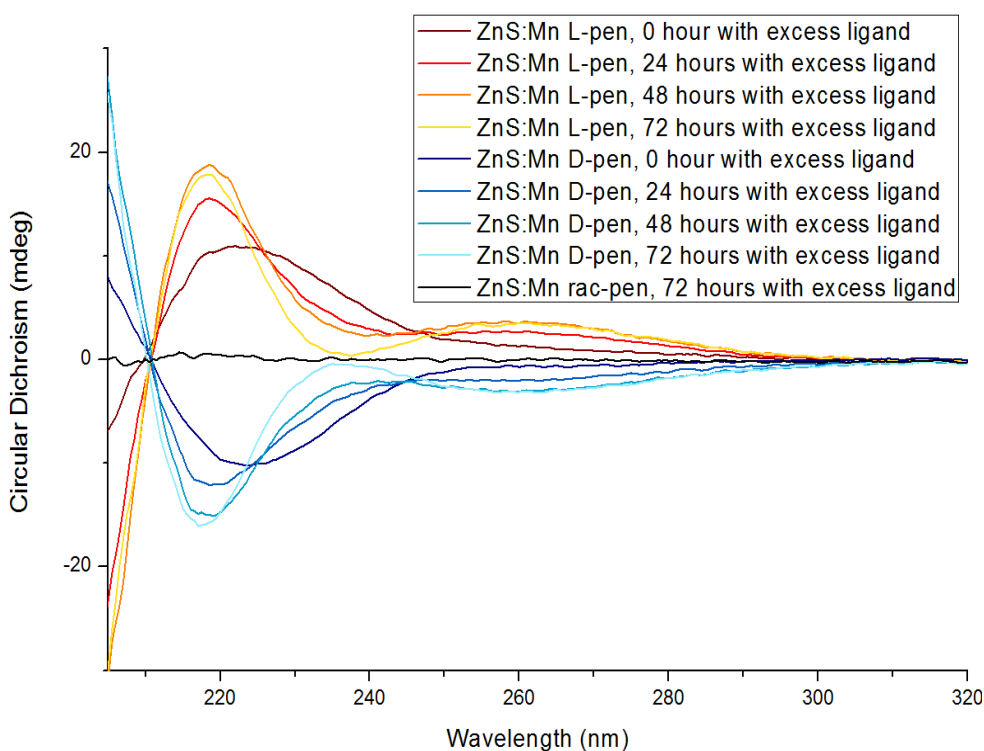


*Figure 3-21 Effect of chiral heat treatment on ZnS:Mn-penicillamine QDs.*

According to the CD spectra (Figure 3-21), a noticeable change occurs over time as the QDs interact with the excess penicillamine in solution. Initially, we thought we had been successful in introducing a greater degree of chiral interaction, and the CD spectra are mirror images for the D- and L- penicillamine samples which would rule out any artefacts being generated. However, upon further inspection, it was discovered that something different was happening. What was observed was the

conversion of the penicillamine into its disulphide derivative which was confirmed when we compare our results to the CD spectra of the disulphide analogue of penicillamine<sup>25</sup>. A control experiment was carried to see if the conversion would occur under similar conditions in the absence of the QDs and the thiol oxidation and dimerization occurred in the absence of the ZnS:Mn QDs. (appendix Figure 8-3). Therefore, we can conclude that the ZnS:Mn QDs did not catalyse the reaction.

### 3.5 Toxicity studies for L and D cysteine capped ZnS:Mn QDs

As these optically active QDs were designed for potential biological applications, it was important to test the toxicity of these nanoparticles. These studies were performed using the particles that were synthesised in collaboration with another member of the Gun'ko group, Vera Kutznetsova. The cells chosen for the study were A549 cancer cells, and cytotoxicity was measured as a function of QD concentration. The QDs were first mixed with bovine serum albumin as it helped to prevent aggregation for subsequent toxicity studies. Aggregation was monitored using dynamic light scattering, and the results clearly showed that the presence of BSA prevented aggregation in the cytotoxicity studies. The results of this study found that the D-cysteine stabilised QDs displayed higher levels of toxicity for all concentrations of QDs<sup>26</sup> (Figure 3-25). This is an interesting result as it clearly shows discrimination of chiral quantum dots within a biological species. It is not surprising that the D-cysteine sample is more toxic as L-cysteine occurs naturally whereas D-cysteine is not. This is the first example of toxicity studies when cadmium-free QDs demonstrated a chiral dependency. The implications of this are significant for the field of quantum dots in biomedicine as future applications may incorporate chirality into material design for increased activity or control.

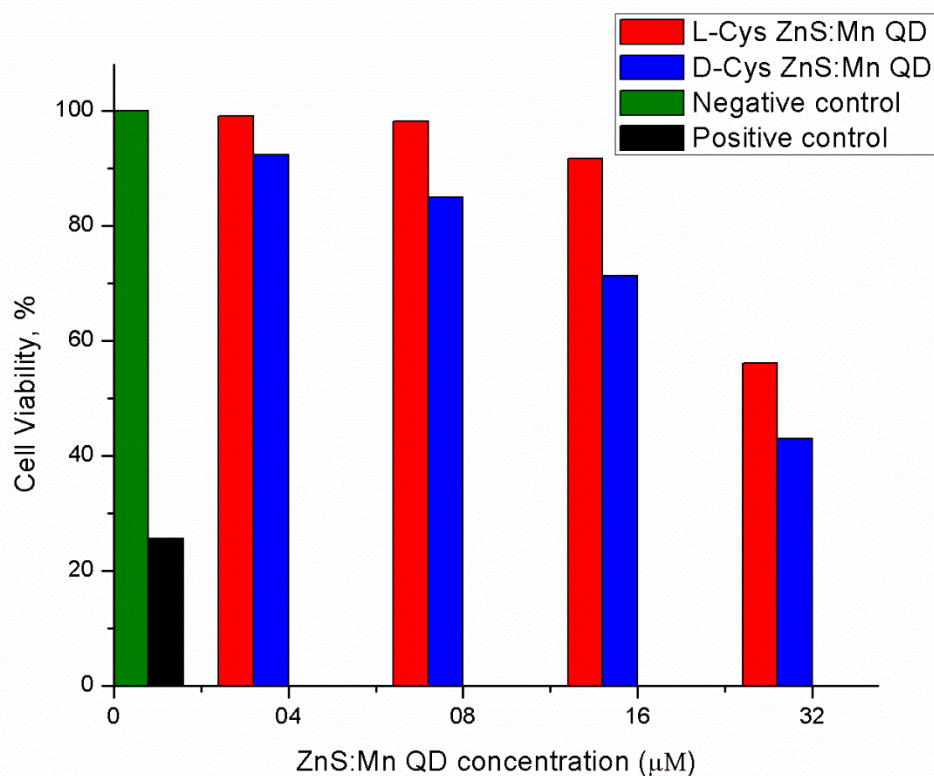


Figure 3-22 Cell viability of A549 cells in the presence of cysteine capped ZnS:Mn QDs.<sup>26</sup>

In the above diagram, the negative control represents when nothing is added to the cells, and the positive control is when the drug Validamycin is added. It is believed that two separate effects are responsible for the difference in cytotoxicity in the samples. Firstly, the different enantiomers present on the surface of the QDs may influence cellular uptake and secondly, the opposite enantiomers may lead to a difference of cellular activity within the cells.

### 3.6 Preparation of ZnSe quantum dots capped with glutathione

In an effort to prepare chiral ZnSe QDs, an aqueous procedure using glutathione as a ligand was carried out according to the report by Zhang *et al*<sup>29</sup>. The synthesis involves the reflux of a zinc precursor with NaHSe in degassed water under basic conditions. Glutathione contains multiple chiral centres, and so it was expected that corresponding glutathione-capped QDs would demonstrate optical activity (Figure 3-23 ).

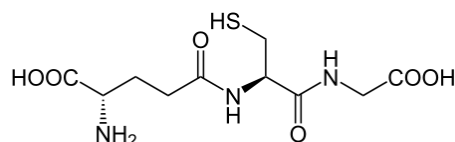


Figure 3-23 Glutathione

These QDs were subsequently used for chiral sensing experiments, and while the results were positive, these studies are only preliminary, and we believe there is great potential for future development. In this synthesis, the pH of the solution is very important as it affects the binding mode of the ligand to the metal ions, therefore, impacting nanoparticles growth. The effect of pH on  $Zn^{2+}$  complex formation is shown in Figure 3-24. According to Zhang *et al.* keeping the reaction mixture within the 10.3-11.5 pH range led to the highest luminescence and so we used their suggested parameters for our synthesis. The QDs were characterised using UV-Vis, PL, circular dichroism and transmission electron microscopy.

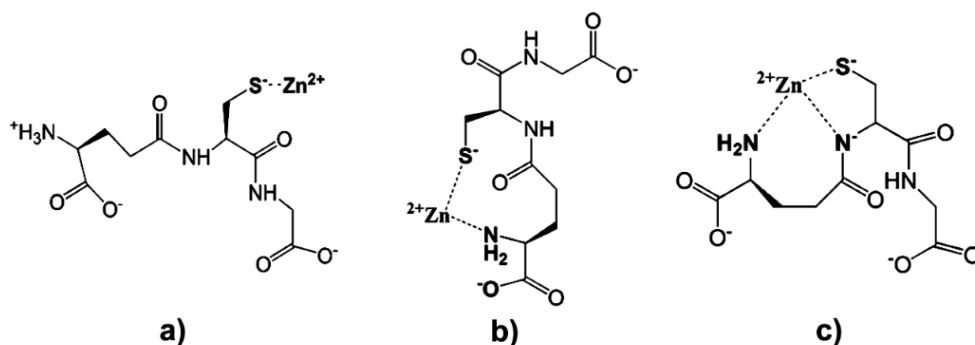
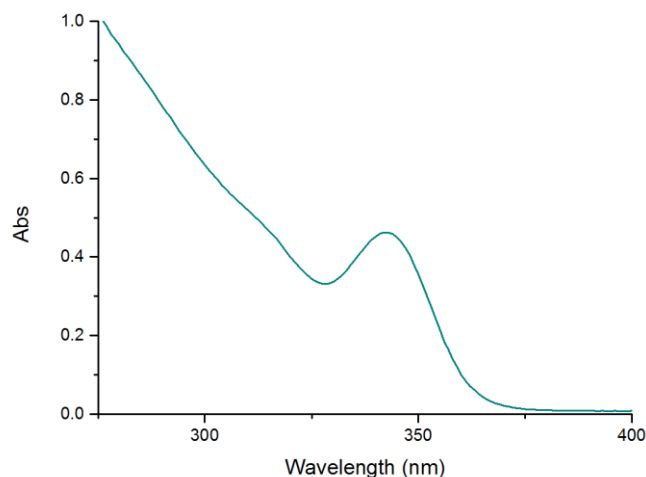


Figure 3-24 Zn-GSH complexes at a) pH 6.5 – 8.3; b) pH 8.3 – 10.3; c) pH 10.3-11.5.<sup>29</sup>

Upon inspection of the UV-Vis spectra in Figure 3-25, it is clear that the ZnSe QDs demonstrated a typical absorption spectrum. The first exciton has a maximum at 340 nm which corresponds to a band gap energy of 3.65 eV. When we compare that to the band gap energy of bulk ZnSe, 2.70 eV<sup>30</sup>, it is evident that confinement of the exciton is occurring. The relatively narrow exciton peak would indicate a narrow size distribution which was further confirmed by TEM.



*Figure 3-25 UV-Vis spectra for ZnSe-Glutathione QDs.*

The QDs were characterised using TEM analysis (Figure 3-26). From the TEM it is evident that the QDs are spherical and monodisperse and from the size distribution with an average size of 4.2 nm and a standard deviation of 0.6 nm. This lies somewhere between what was reported for the 1 hr reflux (3.2 nm) and the 9 hr reflux (5 nm) reported by Zhang. As the reactant concentrations are identical to those reported we conclude that our larger QDs are due to unintended variations in heating regimes.

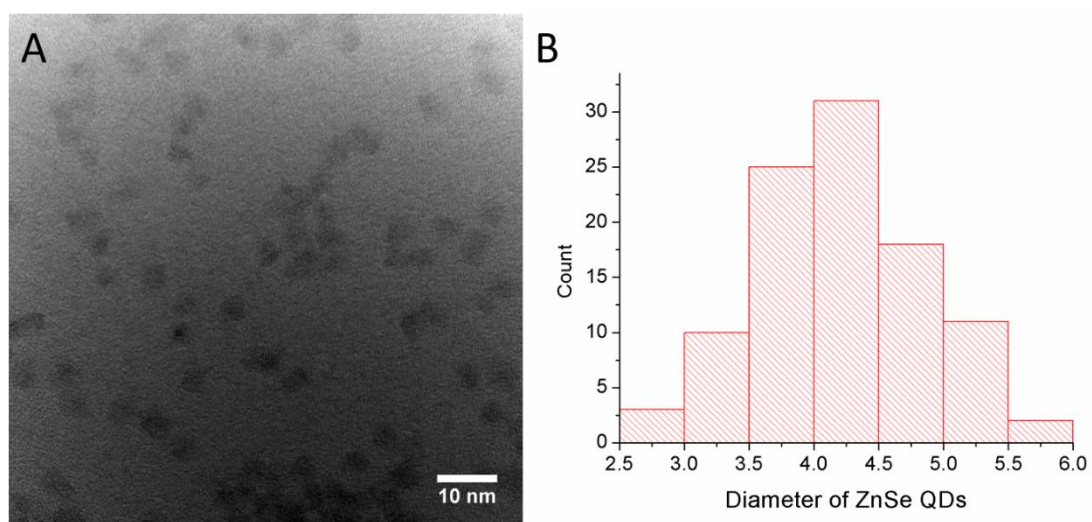


*Figure 3-26 A) TEM image of ZnSe QDs and B) Size distribution plot of ZnSe QDs (n=130).*

These ZnSe QDs were subsequently characterised using CD spectroscopy as it was expected that they would demonstrate optical activity due to the chiral nature of

glutathione. The results of the CD spectroscopy are presented in Figure 3-27. They are clearly chiroptically active with a CD signal beginning to emerge around 340 nm. As the onset of optical activity does not correlate exactly with the exciton absorption we believe that an interaction with the defect surface states of the QD is responsible for optical activity in this case. All of these experiments were carried out using only L-glutathione as it is naturally occurring. In order to repeat the same synthesis using D-glutathione, we would need to synthesise it ourselves which was not possible, unfortunately, however it is expected that a mirror image CD spectrum would occur.

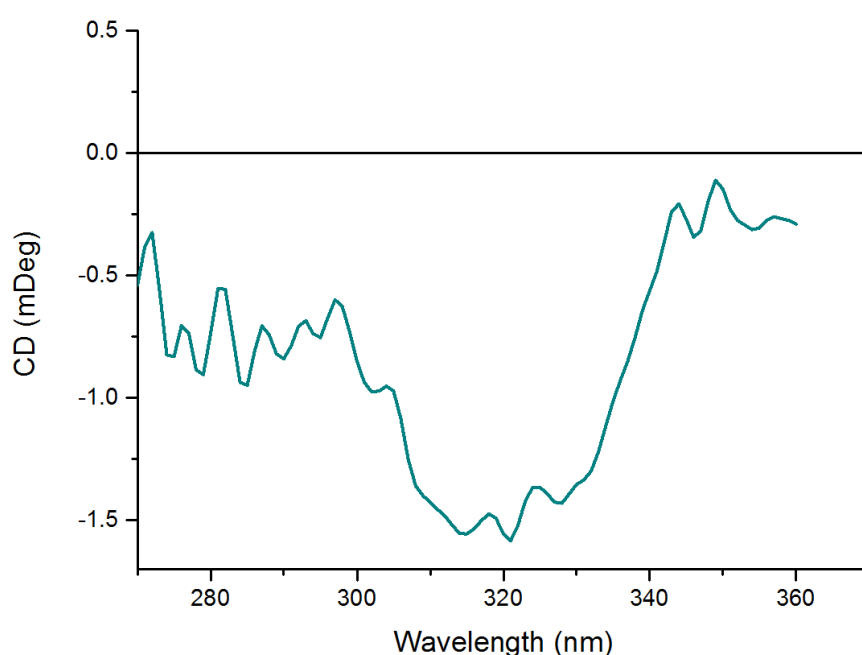


*Figure 3-27 CD spectra for Glutathione-ZnSe QDs.*

The glutathione capped ZnSe QDs were then characterised using photoluminescence spectroscopy, and the results are presented in Figure 3-28. From the PL spectra, it is evident that these ZnSe QDs demonstrate a combination of defect and excitonic luminescence. The broad peak beginning at 600 nm can be attributed to defect luminescence. Defect luminescence often occurs in QDs synthesised by aqueous methods due to the various distortions and oxygen moieties in the nanoparticle crystal structure. These defects provide non-radiative deactivation pathways for excited electrons thereby reducing the number of

electrons emitting light of the full band gap energy. The excitonic emission has a maximum intensity at 370 nm, corresponding to a Stokes shift of 30 nm.

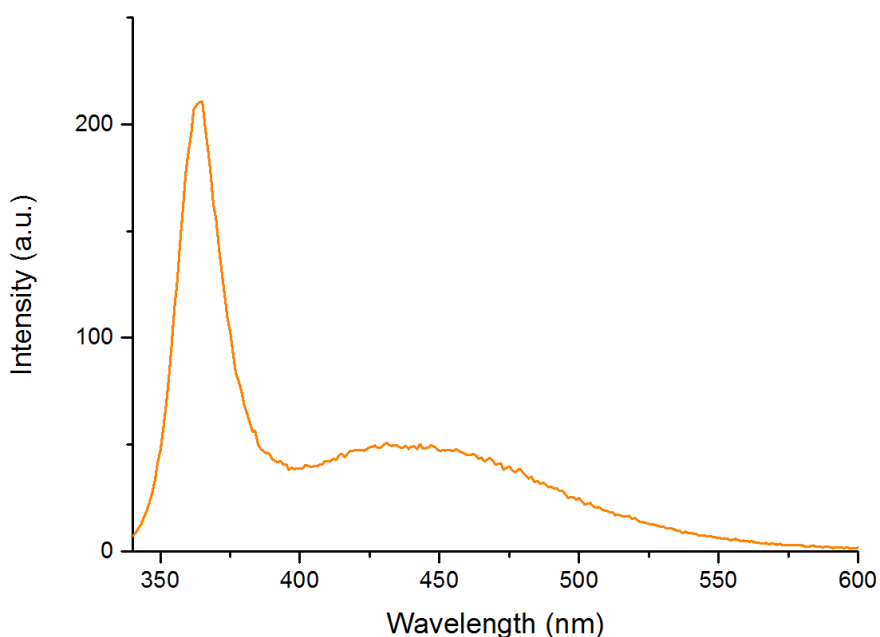


*Figure 3-28 PL spectra for ZnSe-Glutathione QDs (ex.  $\lambda$  – 300 nm).*

After characterisation, we performed quenching experiments to examine the potential of this system for future chiral sensing applications. This work involved the titration of chiral glutathione- stabilised QD solution against solutions of both L- and D- penicillamine ligands and monitoring of luminescence changes. The details of the quenching experiment can be found in experimental section 2.2.5. Appropriate concentrations of the GSH-ZnSe QDs and the quenching penicillamine were chosen. The ZnSe QD solution was then titrated against a solution of either D- or -L penicillamine, and the resultant PL maximum intensity was recorded. The PL results (appendix Figure 8-4 and Figure 8-5) were used to create the graph (Figure 3-32) showing the effect of penicillamine addition on the ZnSe luminescence.

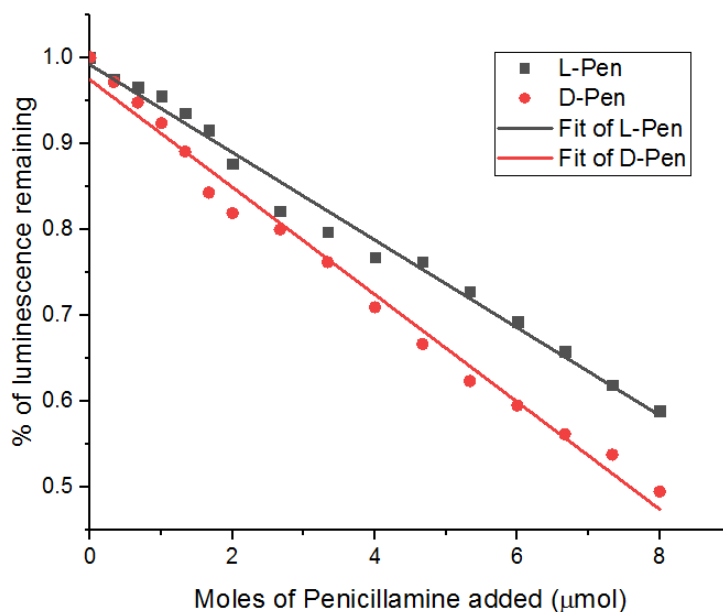


*Figure 3-29 Effect on luminescence of ZnSe QDs by addition of penicillamine.*

From the above graph (Figure 3-32) it is clear that there is a noticeable difference in excitonic luminescence following the addition of 8  $\mu\text{mol}$  of either D- or L - penicillamine. The titration with D-penicillamine has a more pronounced effect in quenching of chiral glutathione stabilised ZnSe QDs. The mechanism by which quenching is occurring here is not fully understood so far, and we plan to explore this system further in the future. One theory we have proposed is based on the fact that the highly chelating glutathione ligand provides greater surface passivation than penicillamine. Therefore, when penicillamine is added, it displaces some of the glutathione and decreases the luminescence of the QDs. Due to the chirality present in both penicillamine and glutathione, a difference in displacement effects may be taking place leading to a difference in quenching during the addition of either D- or L- penicillamine. These experiments clearly demonstrate the chiral recognition and enantioselective nature of quenching of chiral QDs by enantiomeric D- or L – penicillamine ligands.

### 3.7 Conclusions

In this chapter, we have successfully produced a variety of optically active, cadmium-free quantum dots. Zinc sulphide QDs were prepared and doped with



manganese to provide beneficial optical properties for biological applications. These QDs were subsequently subjected to a range of phase transfer processes in order to induce optical activity in the band edge region. For the first time, cadmium free optically active QDs have been reported by performing ligand exchanges using cysteine and penicillamine. The aqueous QDs exhibited optical activity in the band edge region where the chiral ligands do not absorb directly suggesting ligand-induced chirality is taking place. Following the successful preparation of chiral cadmium-free ZnS:Mn QDs cytotoxicity studies were performed. The results of the tests demonstrated a clear difference in toxicity between the D and L Cys stabilised QDs where D Cys stabilised ZnS:Mn QDs presented higher toxicity for all concentrations.

Following the preparation of chiral ZnS:Mn QDs, optically active ZnSe QDs were synthesised. By capping the ZnSe QDs with glutathione ligand, optical activity was demonstrated in the band edge absorption region of the QDs. These QDs were used in chiral discrimination experiments to demonstrate a difference in quenching upon the addition of either D or L penicillamine to a solution of the QDs. This experiment was successful as D- penicillamine had a greater quenching effect on the glutathione capped QDs than L- penicillamine. Further research is necessary to scale up the synthesis of chiral Cd-free QDs and to performed their detailed biological testing including their *in vitro* behaviour and antibacterial activity studies.

## 3.8 References

- (1) Oh, E.; Liu, R.; Nel, A.; Gemill, K. B.; Bilal, M.; Cohen, Y.; Medintz, I. L. *Nature Nanotechnology* **2016**, *11*, 479.
- (2) Thomas, A.; Nair, P. V.; George Thomas, K. *The Journal of Physical Chemistry C* **2014**, *118*, 3838.
- (3) Li, L.; Daou, T. J.; Texier, I.; Kim Chi, T. T.; Liem, N. Q.; Reiss, P. *Chemistry of Materials* **2009**, *21*, 2422.
- (4) Panthani, M. G.; Khan, T. A.; Reid, D. K.; Hellebusch, D. J.; Rasch, M. R.; Maynard, J. A.; Korgel, B. A. *Nano letters* **2013**, *13*, 4294.
- (5) Sun, C.; Zhang, Y.; Wang, Y.; Liu, W.; Kalytchuk, S.; Kershaw, S. V.; Zhang, T.; Zhang, X.; Zhao, J.; Yu, W. W.; Rogach, A. L. *Applied Physics Letters* **2014**, *104*, 261106.
- (6) Chunlei, W.; Zhiyang, H.; Shuhong, X.; Yanbin, W.; Zengxia, Z.; Zhuyuan, W.; Yiping, C. *Nanotechnology* **2015**, *26*, 305601.
- (7) Cooper, J. K.; Gul, S.; Lindley, S. A.; Yano, J.; Zhang, J. Z. *ACS Applied Materials & Interfaces* **2015**, *7*, 10055.
- (8) Xue, G.; Chao, W.; Lu, N.; Xingguang, S. *Journal of Luminescence* **2011**, *131*, 1300.
- (9) Kumar, P.; Singh, K. *Journal of Nanoparticle Research* **2011**, *13*, 1613.
- (10) Deng, Z.; Tong, L.; Flores, M.; Lin, S.; Cheng, J.-X.; Yan, H.; Liu, Y. *Journal of the American Chemical Society* **2011**, *133*, 5389.
- (11) Ang, H.; Bosman, M.; Thamankar, R.; Zulkifli, M. F. B.; Yen, S. K.; Hariharan, A.; Sudhakaran, T.; Selvan, S. T. *ChemPhysChem* **2016**, *17*, 2489.
- (12) Acharya, S.; Sarma, D. D.; Jana, N. R.; Pradhan, N. *The Journal of Physical Chemistry Letters* **2010**, *1*, 485.
- (13) Tohgha, U.; Deol, K. K.; Porter, A. G.; Bartko, S. G.; Choi, J. K.; Leonard, B. M.; Varga, K.; Kubelka, J.; Muller, G.; Balaz, M. *ACS Nano* **2013**, *7*, 11094.
- (14) Guo, Y.; Zeng, X.; Yuan, H.; Huang, Y.; Zhao, Y.; Wu, H.; Yang, J. *Spectrochimica Acta Part A: Molecular and Biomolecular Spectroscopy* **2017**, *183*, 23.
- (15) Visheratina, A. K.; Purcell-Milton, F.; Serrano-Garcia, R.; Kuznetsova, V. A.; Orlova, A. O.; Fedorov, A. V.; Baranov, A. V.; Gun'ko, Y. K. *Journal of Materials Chemistry C* **2017**, *5*, 1692.
- (16) Wei, Y.; Li, H.; Hao, H.; Chen, Y.; Dong, C.; Wang, G. *Polymer Chemistry* **2015**, *6*, 591.
- (17) Yu, J. H.; Kwon, S. H.; Petrusek, Z.; Park, O. K.; Jun, S. W.; Shin, K.; Choi, M.; Park, Y. I.; Park, K.; Na, H. B.; Lee, N.; Lee, D. W.; Kim, J. H.; Schwille, P.; Hyeon, T. *Nature materials* **2013**, *12*, 359.
- (18) Khenata, R.; Bouhemadou, A.; Sahnoun, M.; Reshak, A. H.; Baltache, H.; Rabah, M. *Computational Materials Science* **2006**, *38*, 29.
- (19) Sooklal, K.; Cullum, B. S.; Angel, S. M.; Murphy, C. J. *The Journal of Physical Chemistry* **1996**, *100*, 4551.
- (20) Becker, W. G.; Bard, A. J. *The Journal of Physical Chemistry* **1983**, *87*, 4888.
- (21) Zhao, W.; Fung, Y.; O, W.; Cheung, M. P. *Analytical sciences : the international journal of the Japan Society for Analytical Chemistry* **2010**, *26*, 879.
- (22) Zhang, Y.-h.; Zhang, H.-s.; Guo, X.-f.; Wang, H. *Microchemical Journal* **2008**, *89*, 142.
- (23) Liu, W.; Choi, H. S.; Zimmer, J. P.; Tanaka, E.; Frangioni, J. V.; Bawendi, M. *Journal of the American Chemical Society* **2007**, *129*, 14530.
- (24) Moloney, M. P.; Gun'ko, Y. K.; Kelly, J. M. *Chemical Communications* **2007**, 3900.
- (25) Dai, M.-Q.; Yung, L.-Y. L. *Chemistry of Materials* **2013**, *25*, 2193.
- (26) Kuznetsova, V. A.; Visheratina, A. K.; Ryan, A.; Martynenko, I. V.; Loudon, A.; Maguire, C. M.; Purcell-Milton, F.; Orlova, A. O.; Baranov, A. V.; Fedorov, A. V.; Prina-Mello, A.; Volkov, Y.; Gun'ko, Y. K. *Chirality* **2017**.
- (27) Parvin, N.; Amiri, G.; Karbasizadeh, V. *Nanomedicine Journal* **2016**, *3*, 191.

- (28) Chaliha, C.; Nath, B. K.; Verma, P. K.; Kalita, E. *Arabian Journal of Chemistry* **2016**.
- (29) Zhang, J.; Li, J.; Zhang, J.; Xie, R.; Yang, W. *The Journal of Physical Chemistry C* **2010**, *114*, 11087.
- (30) Al-Kuhaili, M. F.; Kayani, A.; Durrani, S. M. A.; Bakhtiari, I. A.; Haider, M. B. *ACS Applied Materials & Interfaces* **2013**, *5*, 5366.

## Chapter 4: Synthesis and characterisation of CdSe-CdS dot in rod and tetrapods for sensing applications.

### 4.1 Introduction

Chirality in quantum dots is an emerging area of research, so unsurprisingly interest in the optical activity of 1-D quantum rods is also increasing rapidly, although very few studies have been published to date. Due to the anisotropy of quantum rods and dot-in-rods unique chiral features can emerge. For example, Gao. *et al* have investigated the relationship between the aspect ratio of CdSe quantum rods and the intensity of the excitonic optical activity<sup>1</sup>. The researchers have found that an aspect ratio of 3 led to the highest optical activity for the band edge exciton CD signal. More importantly they demonstrated that all levels of anisotropy, from 1.7 to 7.3, demonstrated increased optical activity compared to the isotropic quantum dots.

Originally Baimuratov *et al.* have proposed a theory suggesting that quantum rods may demonstrate intrinsic chirality due to the presence of screw dislocations in the crystal<sup>2</sup>. This theory was subsequently proved in practice by Mukhina *et al*<sup>3</sup>. using CdSe-ZnS dot in rods. In this research it was shown that DiR solutions may actually be a racemic combination of intrinsically chiral “L” and “D” rods with left and right handed screw dislocations respectively. The researchers have also developed an enantioselective phase transfer technique to separate chiral nanocrystals using an appropriate chiral ligand and isolate optically active CdSe/ZnS QDs and QRs. The same group has also subsequently published an investigation on both the linear and circular dichroism properties in CdSe-CdS dot-in-rods oriented under the influence of an electric field<sup>4</sup>. While there are several reports of ligand exchange reaction on quantum rods<sup>5-7</sup>, none of them are related to the chiroptical properties of the extracted nanomaterials. Chiral recognition experiments using quantum dots have been explored by several researchers<sup>8-11</sup> however to the best of our knowledge no

examples of using optically active dot in rods for chiral recognition have been reported to date.

Some work has also been done on chiral tetrapods synthesised in the aqueous phase. For example, Govan *et al.* developed the preparation of optically active chiral CdS tetrapods<sup>12</sup> which involves the aqueous reflux of cadmium chloride and thioacetamide in the presence of D/L penicillamine and Wawrzynczyk *et al.* demonstrated these particles use in 2 photon excitation experiments subsequently<sup>13</sup>. However, no research has been performed on the preparation of CdSe-CdS tetrapods by the phase transfer using chiral ligands.

## 4.2 Aims of this chapter

As the field of optically active anisotropic nanostructures is relatively new, we aimed to contribute to this area by developing a variety of different chiroptically active anisotropic nanostructures. We plan to explore the possibility to induce chirality in anisotropic quantum structures through ligand exchange approaches. Initial CdSe-CdS dot in rods are to be synthesised by hot injection technique in organic solvents. Then we plan to develop a phase transfer protocol which could be used to exchange the organic ligands on the DiR with a variety of different chiral water-soluble ligands. Using UV-Vis, PL, CD and TEM we aimed to investigate the optical properties of DiR capped with D- and L- cysteine, D- and L- penicillamine and thioglucose.

Our next objective is to use these optically active materials to perform a series of chiral recognition experiments to evaluate their efficacy in optical discrimination of selected chiral molecules. Previous successful research in this field has been carried out discriminating<sup>14</sup> Naproxen and Ketoprofen enantiomers using CdSe-ZnS QDs so it was hoped our DiR system would yield similar results for Naproxen sensing.

Finally, our goal is to produce tetrapod samples in organic solvents and induce optical activity through ligand exchanges. We plan to focus on the initial synthesis of CdSe-CdS tetrapods in the organic phase and then we aim to induce chirality in them using L- and D- cysteine via ligand exchange. The new chiroptically active

anisotropic nanomaterials are to be investigated using UV-Vis, CD, PL spectroscopies and TEM.

### 4.3 Synthesis and characterisation of CdSe-CdS DiRs

The synthesis of CdSe-CdS DiRs nanostructures was performed according to published procedure<sup>15</sup> outlined in section 2.3.4 of the experimental chapter. The growth of the DiRs can be directed by the use of specific ligands which have different binding energies to the different crystal facets. This allows for preferential growth along certain axes, causing the anisotropic growth. These DiRs were initially synthesised in house by Dr. Finn Purcel-Milton in the organic phase by the hot injection technique. Then, these nanomaterials were subsequently transferred to the aqueous phase using a variety of different chiral ligands including cysteine, penicillamine and thioglucose. The DiRs in the organic phase before a ligand exchange were analysed using UV-Vis, PL spectroscopy and TEM. The absorbance spectra have shown a large band with a maximum at 490 nm. This band is attributed to the large CdS shell (rod) around a rather small CdSe core. The enlarged view (Figure 4-1 B) of the spectra between 700 nm and 525 nm reveals a very small peak located at 610 nm. This peak corresponds to the first exciton absorption peak for the CdSe core. The difference in absorption between the CdSe core and the CdS shell is a consequence of the both the larger amount of CdS present and the much larger absorption cross section of CdS<sup>15</sup>.

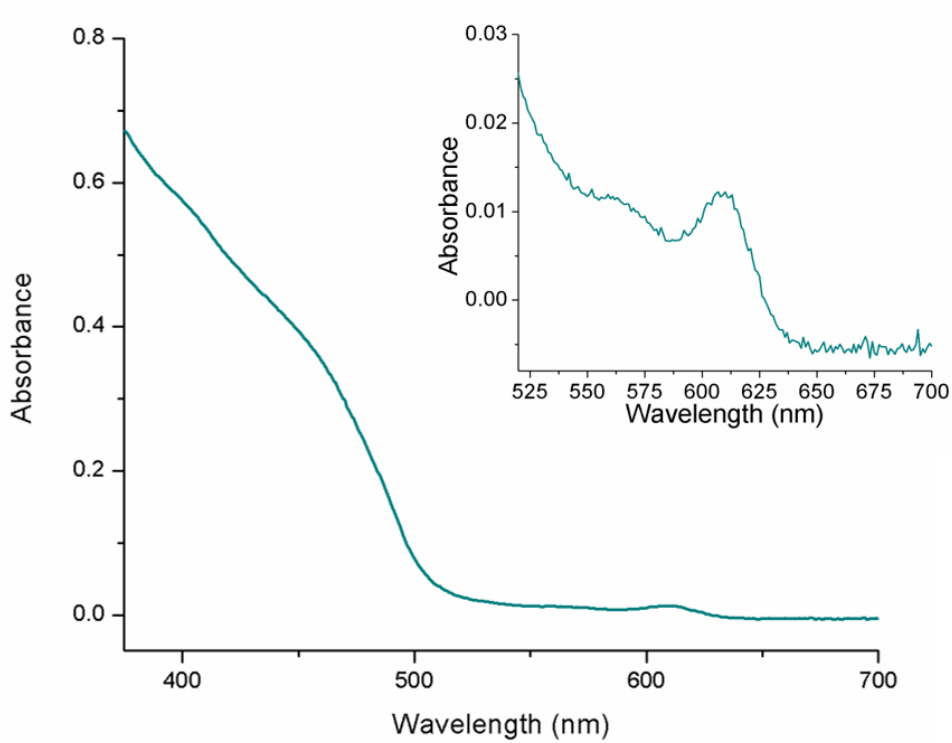


Figure 4-1 The UV-Vis spectra for the CdSe-CdS DiRs. Inset - the enlarged region from 525 to 700 nm in chloroform.

The PL spectrum below in Figure 4-2 shows emission centred around 622 nm.

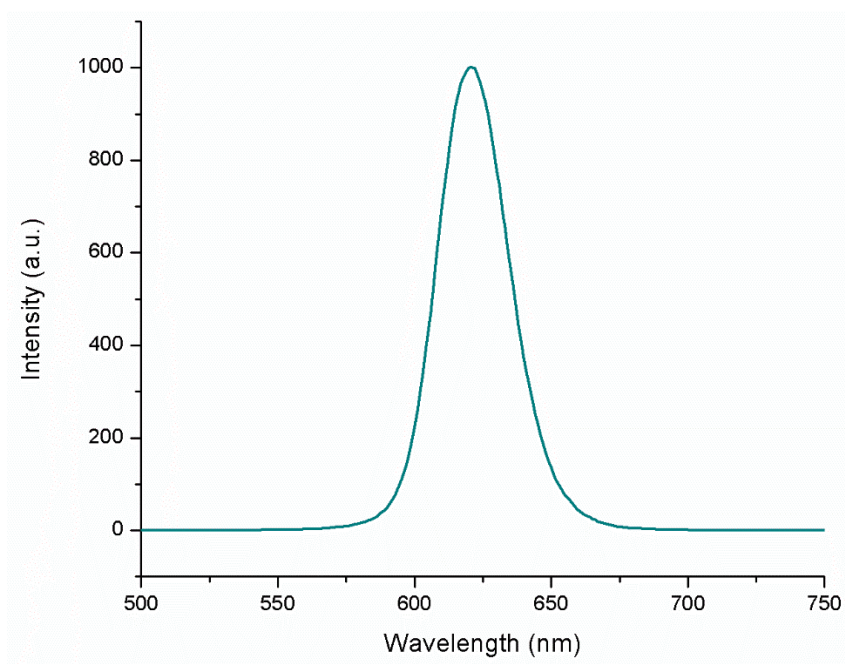
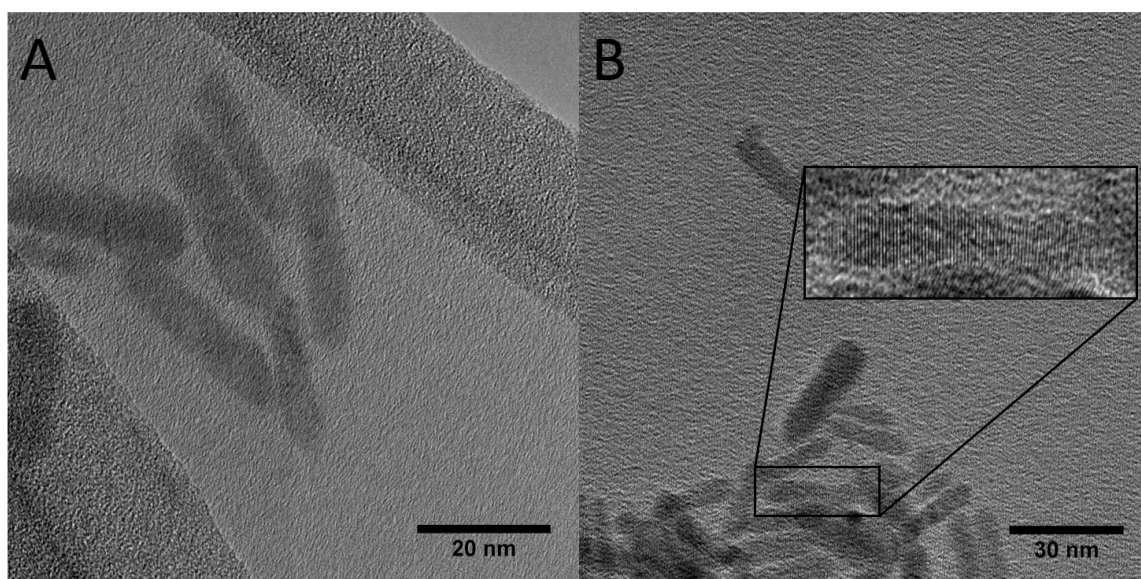


Figure 4-2 PL spectrum for the emission of CdSe-CdS DiRs in chloroform (Exc.  $\lambda$  – 400 nm)

The full width half maximum for the spectra is 30 nm which would indicate a relatively narrow size distribution of the light emitting CdSe cores.

The quantum yields of the CdSe-CdS DiRs in the organic phase was determined using an integrating sphere and was  $\approx 65\%$

TEM images are presented in Figure 4-3. The images show DiRs with a high degree of monodispersity and crystallinity.



*Figure 4-3 TEM image of (A) the CdSe-CdS DiRs from the organic phase with a (B) close up displaying crystallinity*

Using the TEM images above it was possible to create size (length and width) distribution histograms for the DiRs (Figure 4-4). According to these histograms and analysis of TEM images it is evident that the DiRs have an average width of  $6.5 \pm 0.9$  nm and an average length of  $27.3 \pm 2.6$  nm. This correlates to an aspect ratio of approximately 4.



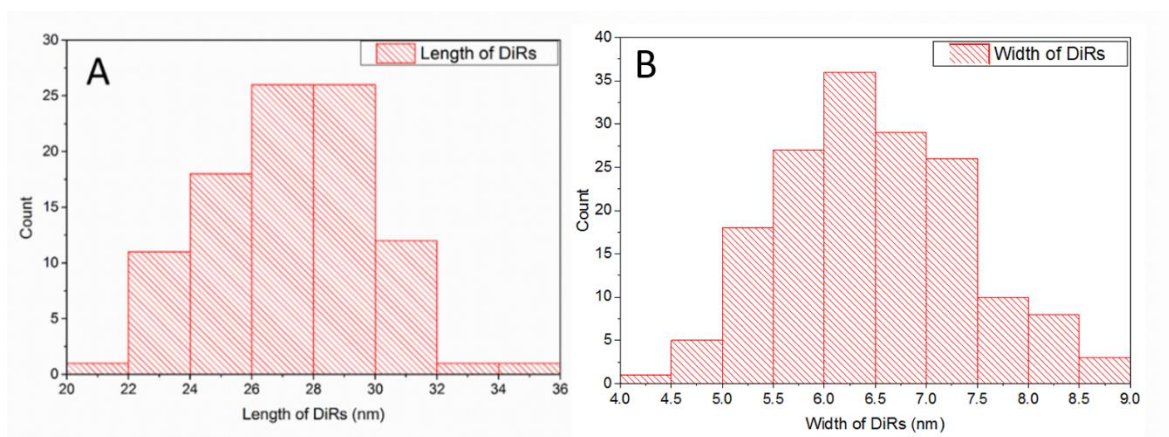


Figure 4-4 (A) Length and (B) width size distributions histograms for the DiRs in the organic phase ( $N = 120$  for length and  $160$  for width).

Following the characterisation of the DiRs in the organic phase, a ligand exchange to transfer the DiRs from the organic to the aqueous phase was performed. Firstly, penicillamine was used as the chiral ligand and the resulting DiRs were characterised by UV-Vis, PL spectroscopy, TEM and circular dichroism spectroscopy. The UV-Vis spectra in Figure 4-5 demonstrate that no observable change has occurred during the ligand exchange process. The UV-Vis spectra for the D- and L- Pen samples look identical and so one was omitted from the subsequent spectra for clarity.

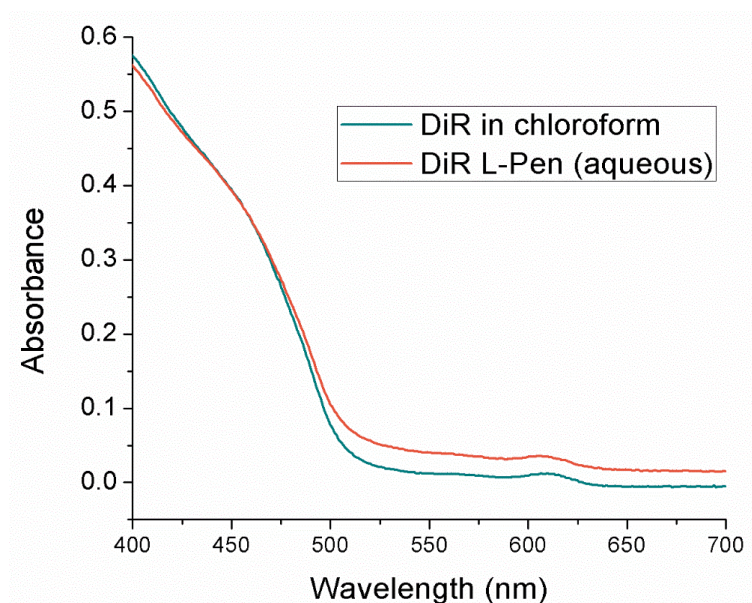
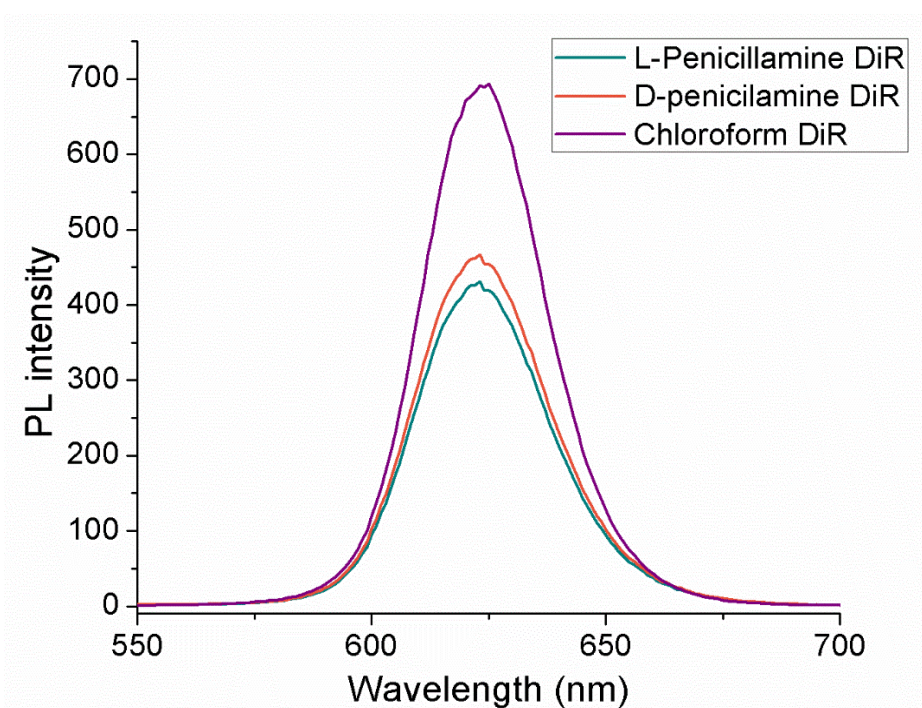


Figure 4-5 UV-Vis spectra for both aqueous (L-Pen) and DiRs in organic phase (chloroform).

The photoluminescence spectra below in Figure 4-6 confirm that the penicillamine capped DiRs retain 60% of their luminescence, however the DiRs are still highly luminescent. No observable shift in peak position is recorded relative to the DiRs in chloroform. In order to compare PL spectra the concentrations of the sample were normalised by observing the UV-Vis and diluting accordingly.



*Figure 4-6 PL Spectra for the DiRs in both the organic and aqueous phase (Exc.  $\lambda$  – 400 nm).*

As the DiRs are now capped by a chiral ligand it was expected that they would demonstrate optical activity, therefore the samples have been studied by CD spectroscopy (Figure 4-7). The above PL spectra was normalised by UV-Vis analysis

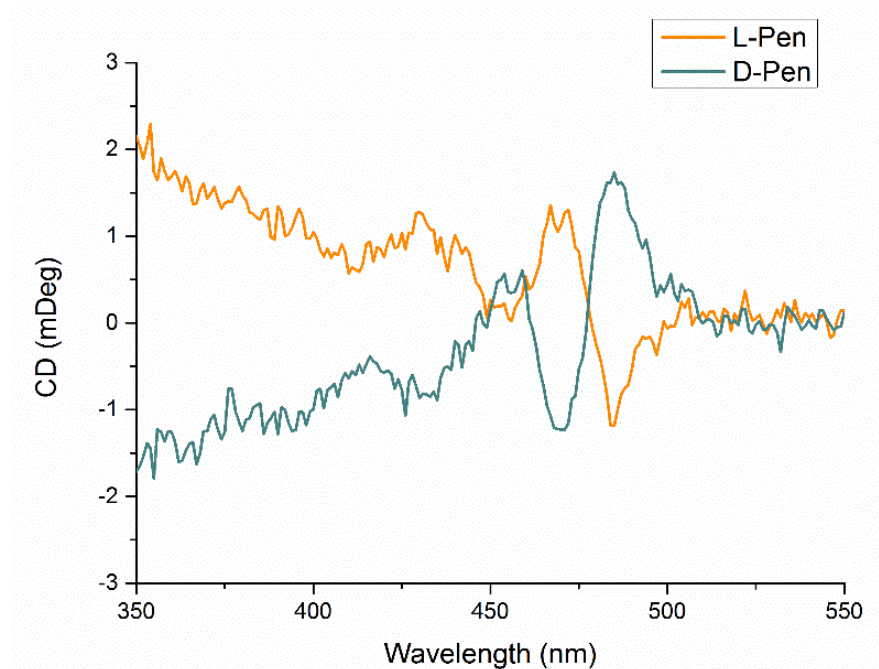


*Figure 4-7 CD spectra for D and L Penicillamine stabilised DiRs.*

As expected, opposite DiR enantiomers have shown mirror image circular dichroism spectra. It is also interesting to note that the onset of the CD spectra begins at approximately 500 nm, which corresponds to the onset of the shell absorption. It was expected that there would be optical activity in the first exciton region of the CdSe core of the DiRs, however it would be very small compared to the larger signal generated from the interaction between the ligand and the shell. Furthermore, the ligand was in direct contact with the shell, however there was a distance separating the core from the chiral ligand, decreasing the probability of their interaction. In order to investigate this system in more details, the concentration of the sample was increased significantly. According to the spectra in Figure 4-8 there is a very small CD signal corresponding to the optical activity of the CdSe core, visible between 500 and 600 nm.

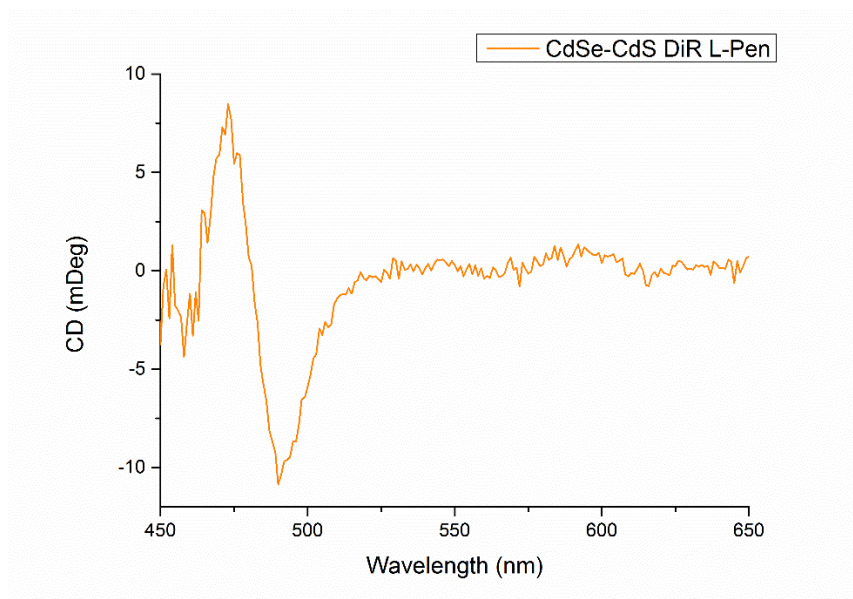


*Figure 4-8 CD spectra of CdSe-CdS DiR stabilised with L- penicillamine (exciton region).*

The TEM images below in Figure 4-9 show that the DiRs have remained relatively unchanged throughout the phase transfer process. The DiRs remain monodisperse and, as is visible in Figure 4-9 (B), crystalline. From the TEM images it was possible to create size distribution data which allows the investigation of any morphological changes taking place during the ligand exchange. There were no significant changes observed in nanostructures sizes and morphology as expected.

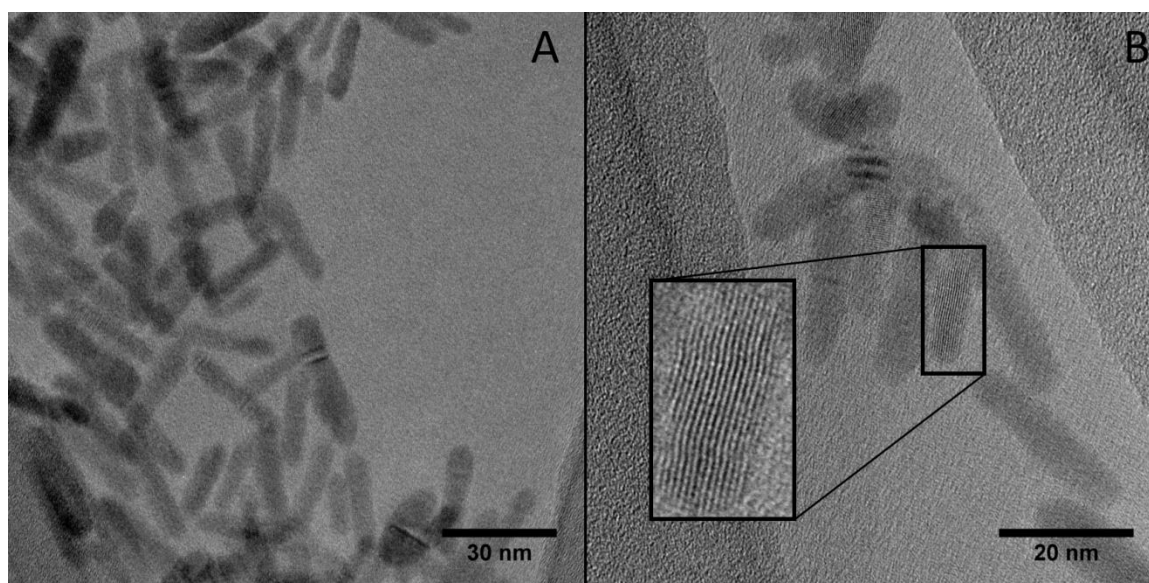


*Figure 4-9 (A) TEM and (B) HRTEM images of CdSe-CdS DiRs stabilised with L- Penicillamine.*

According to the size distribution data below in Figure 4-10, the DiR conjugated to penicillamine have an average width of  $6.2 \pm 1.1$  nm and an average length of  $25.9 \pm 2.4$  nm. This again, corresponds to an approximate aspect ratio of 4. It may be noted that the average length and width of the DiRs has decreased slightly, but the results are well within the margin of error, so it is hard to be certain if anything noticeable difference has actually occurred.

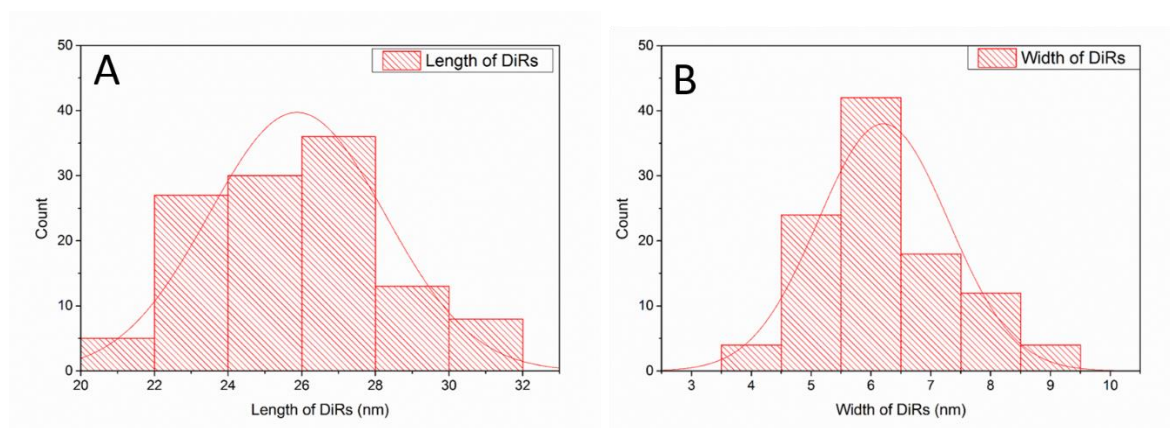


*Figure 4-10 (A) Length and (B) Width distributions histograms for the L-Pen stabilised DiRs ( $N = 150$  for length and  $140$  for width).*

Once the above ligand exchange was shown to work using penicillamine we carried out the same experiment using chiral cysteine stabiliser instead of penicillamine, presented in the following section. It may be noted at this stage that we used DMSO as a solvent for the DiRs instead of water after the phase transfer. This was done to perform further subsequent biological sensing experiments. The chiral drugs we selected to investigate were not soluble in water and therefore DMSO was used as it dissolved both the Cys-DiRs and the drugs, this will be covered in more detail in the next section. The UV-Vis spectra below in Figure 4-11 confirmed that the DiRs remain unchanged when they are transferred from hexane to water using the ligand exchange. Figure 4-11 (B) shows a close up of the exciton region to demonstrate that no observable change in this region has taken place either. The spectra still demonstrate the characteristic large increase in absorption around 500 nm related to the large CdS shell surrounding the CdSe core.

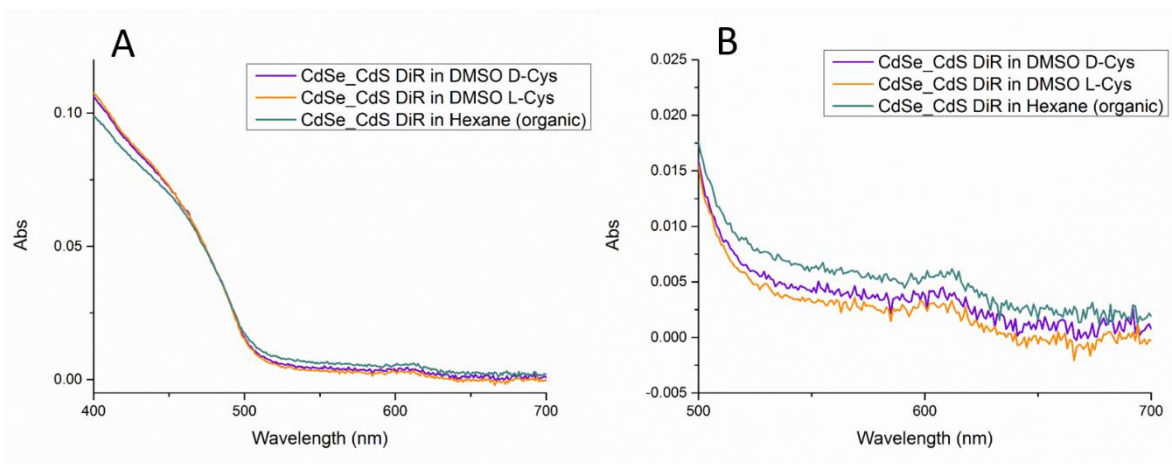


Figure 4-11 UV-Vis spectra of (A) Cys-DiRs and (B) a close of up the CdSe exciton region.

As these DiRs were going to be used for sensing purposes, a high degree of luminescence was important. Therefore, we had to ensure that the DiRs retained their luminescence after being transferred into DMSO. The PL spectra in Figure 4-12 below proved that the DiRs retain most of their luminescence following the phase transfer. The cysteine capped DiR retain  $\approx 75\%$  of their luminescence and no observable shift in peak position is evident. It is interesting to note that the cysteine capped DiRs retain more of their luminescence (75%) compared to the penicillamine capped DiRs (60%). A similar trend was observed for our previously discussed ZnS:Mn QDs and may be due to less effective surface passivation, or greater lattice strain, from the sterically bulkier penicillamine molecule.

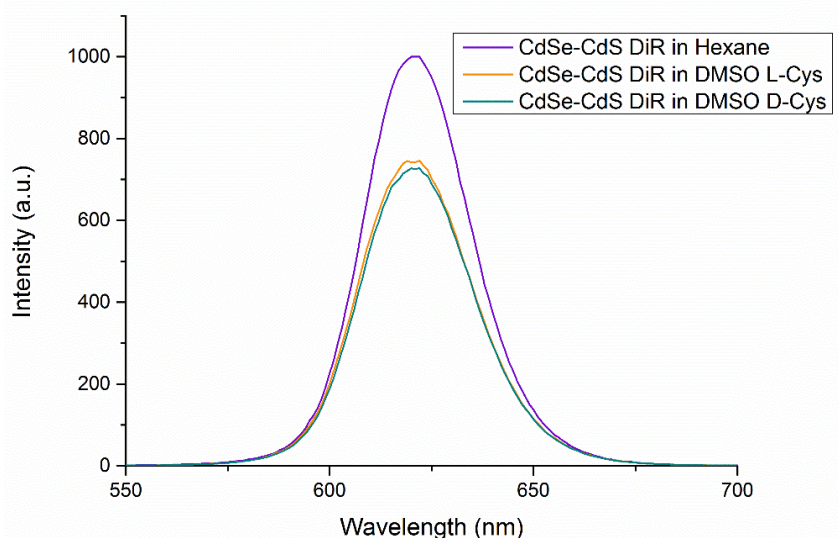
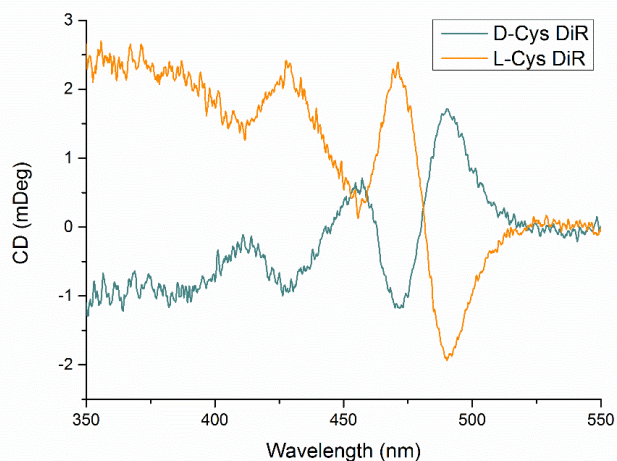


Figure 4-12 PL spectra for Cys stabilised DiRs in DMSO (exc.  $\lambda$  – 400 nm).

As cysteine is also a chiral ligand, circular dichroism spectroscopy was carried out on the sample. It was expected that optical activity would be present despite the change of solvent from water to DMSO. The results are shown in Figure 4-13 below.



*Figure 4-13 CD spectra for D and L Cys stabilised DiRs in DMSO.*

Similar to the penicillamine stabilised sample, the D- and L- cys stabilised DiR samples exhibit opposite optical activity with CD signals of an equal intensity. The CD spectra were quite similar to that for the penicillamine sample in Figure 4-8. To see if optical activity could be observed in the exciton region of the CdSe core, the concentration of the sample was, again, increased significantly and CD spectra were recorded again (Figure 4-14).

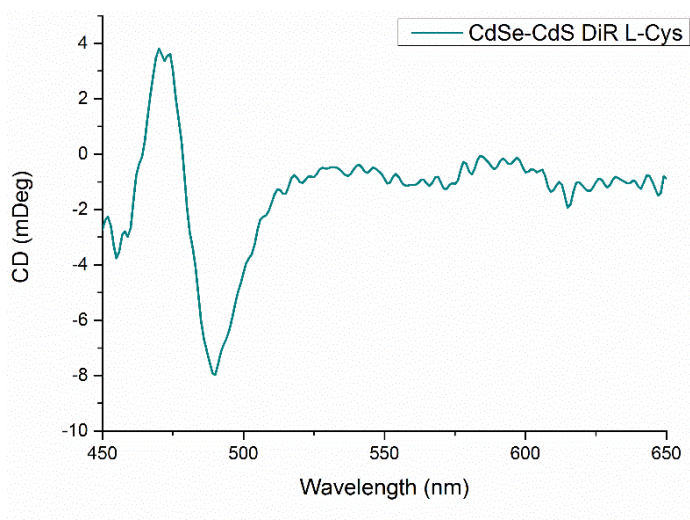


*Figure 4-14 CD spectra for L-Cys DiR in DMSO.*

As before, a signal is clearly visible between 600 and 500 nm. As there is no CdS absorption in this region we can attribute this section of optical activity to the interaction with the CdSe core. The signal is very small compared to the signal originated from the interaction with the CdS shell, due to above mentioned reasons.

As DMSO has a high boiling point (189 °C), it was deemed impractical to prepare samples for TEM from DMSO as the preparation involves evaporation. Instead, we performed the same cysteine phase transfer using water instead which allowed us to prepare samples for TEM analysis.

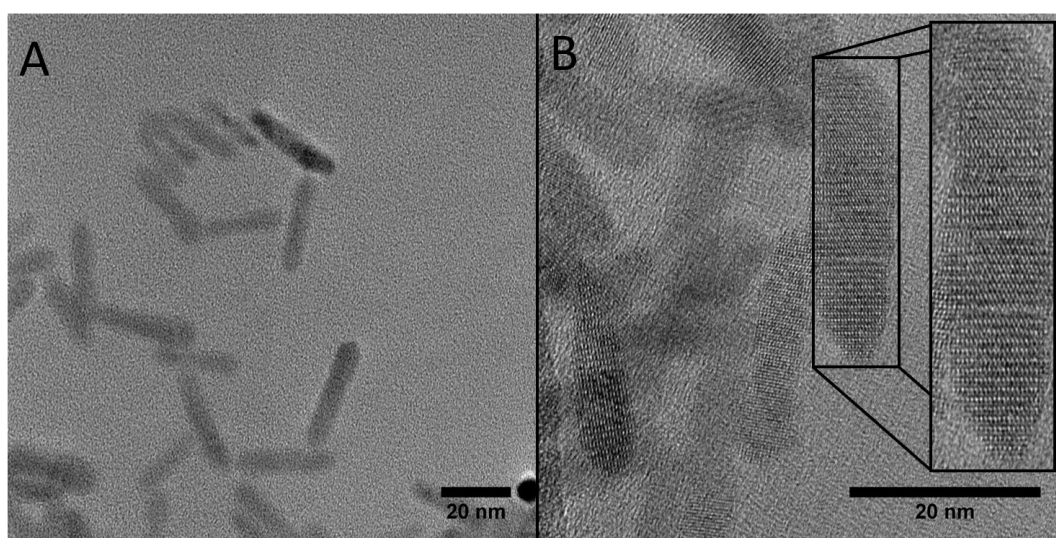


*Figure 4-15 (A) TEM and (B) HRTEM of DiRs stabilised with L-Cysteine from H<sub>2</sub>O.*

According to TEM images in Figure 4-15 above the DiRs are approximately uniform in shape and length. In the HRTEM in Figure 4-15 (B) multiple lattice fringes are observed, confirming high crystallinity of the rods. The TEM images were analysed to create the size distributions shown below in Figure 4-16.



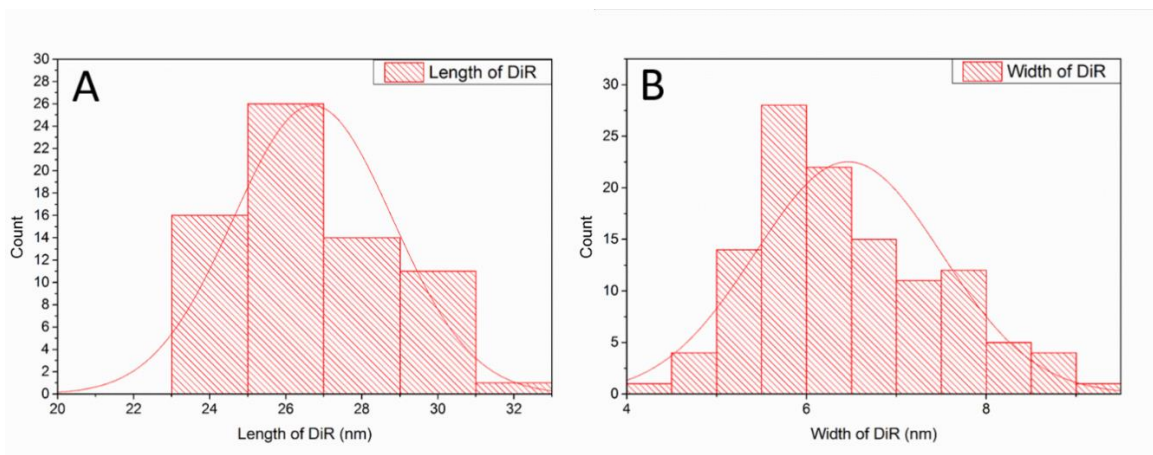


Figure 4-16 (A) Length and (B) width distribution histograms for L-Cys CdSe-CdS DiRs ( $N = 130$  for length and 130 for width).

From the above distributions we can calculate the average size of the DiRs after the phase transfer. They have an average length and width of  $26.7 \pm 2.1$  nm and  $6.45 \pm 1.0$  nm, respectively. This correlates well with the results for both the DiRs in hexane and the DiRs stabilised with penicillamine. These results still indicate that the aspect ratio for the DiRs is approximately 4.

The final ligand used for these DiR experiments was 1-Thio- $\beta$ -D-Glucose (Figure 4-17). As previously discussed, chiral quantum dots are starting to find a range of potential applications in the fields of chiral recognition or chiral sensing. This normally involves the titration or assaying of the chiral QDs against a chiral drug and looking for a selective luminescent response depending on both the chirality of the QD and the molecule being investigated. Previous studies have used Ibuprofen, Naproxen and several other drugs.

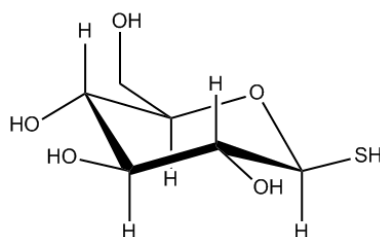
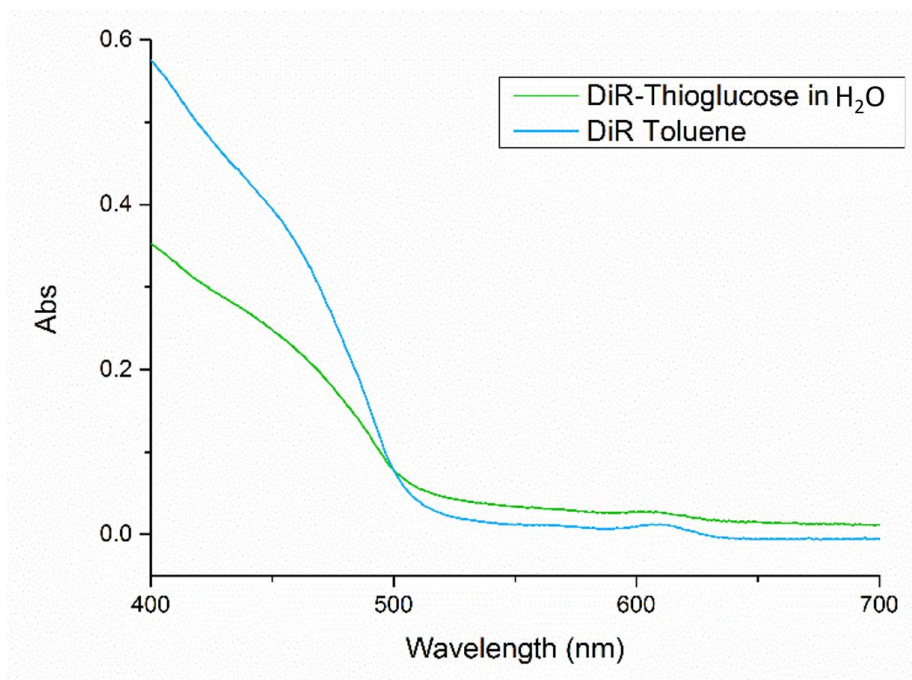


Figure 4-17 1-Thio- $\beta$ -D-Glucose.

The use of oligosaccharides in chiral chromatography is well documented<sup>16-18</sup> therefore it was decided to produce monosaccharide stabilised DiRs and employ them for chiral recognition purposes. The UV-Vis spectra in Figure 4-18 show the results of the phase transfer using D-thioglucoase as the ligand.



*Figure 4-18 UV-Vis spectra for thioglucoase stabilised CdSe-CdS DiRs.*

The UV-Vis spectra above showed some minimal changes. The slightly higher absorbance from 700 to 500 nm in the thioglucoase sample can possibly be attributed to scattering. Thioglucoase is a larger ligand than penicillamine or cysteine and so might contribute to a higher degree of scattering. The clear difference between the large shell absorption and the smaller core absorption is still present. The PL spectra are shown in Figure 4-19.

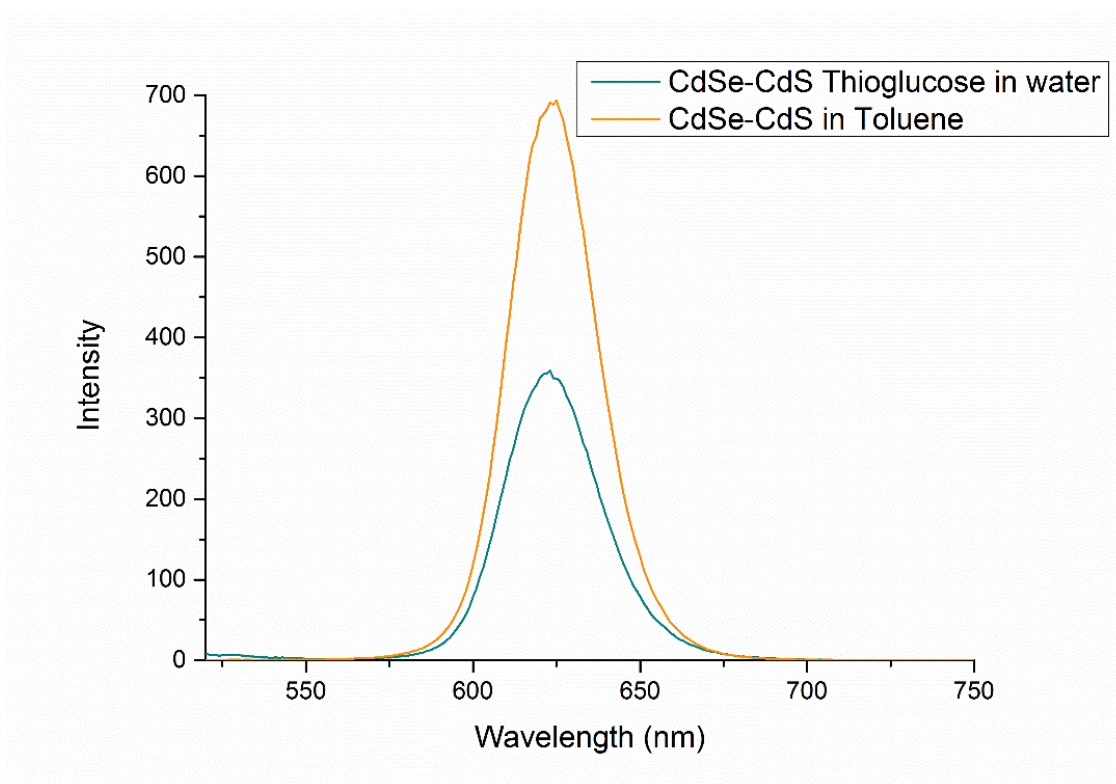


*Figure 4-19 PL spectra for thioglucose stabilised DiRs (Ex.  $\lambda$ – 500 nm).*

From the above spectra we can see that the luminescence has decreased by a factor of 2 approximately, however the DiRs were very luminescent to begin with and so they were still appropriate candidates for further chiral sensing purposes. There was also no observable shift in the position of the luminescence. The peak position was still a maximum at around 625 nm.

CD spectroscopy was carried out, as thioglucose has multiple chiral centres and so we expected that the sample would once again demonstrate optical activity in the DiR absorption region of the spectrum. The results are presented in Figure 4-20 below. Unlike cysteine, where we have both enantiomers, we only have one enantiomer of the thioglucose to analyse this time.

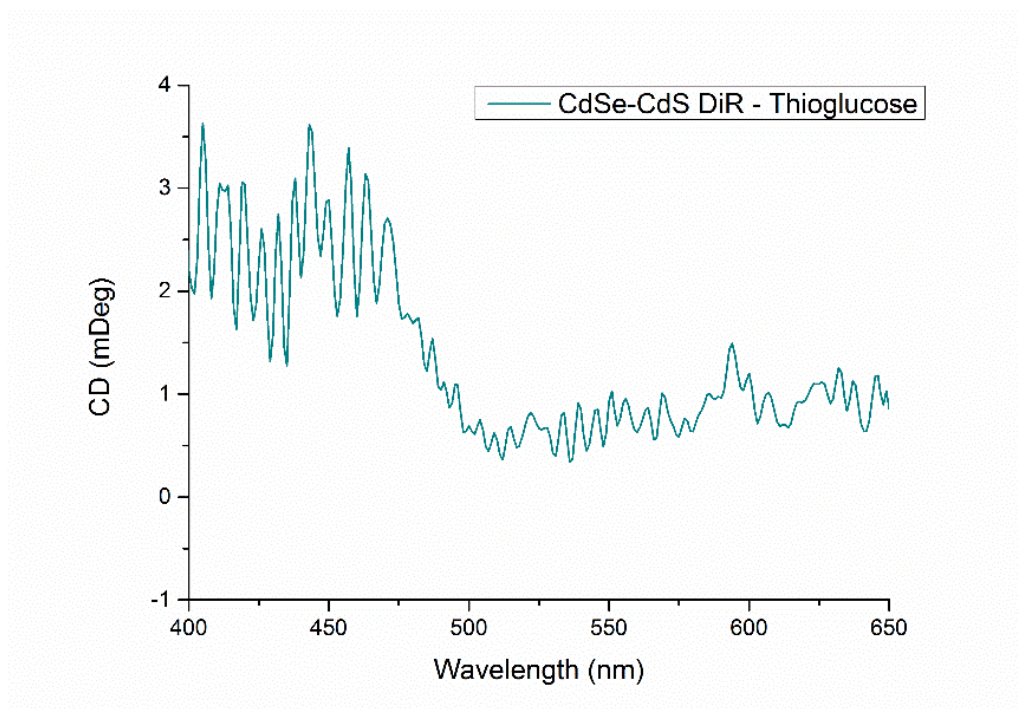


*Figure 4-20 CD Spectra for thioglucose stabilised DiRs in water.*

The CD spectrum is a lot noisier than some of the other DiR samples however optical activity is still clearly visible. Some previous research has been carried out linking optical activity in quantum dots with the interaction of multiple binding groups on ligands (carboxyl and amine groups) with the surface<sup>19</sup>. Thioglucose does not contain these functional groups and so this may be the reason optical activity is not stronger in this sample. Like the other samples, the activity increases dramatically around 500 nm, where the CdS shell starts absorbing. However, slight activity is still visible in the 500 to 600 nm range.

TEM analysis was again used to confirm that no morphological changes had taken place throughout the phase transfer. The images in Figure 4-21 proved that the DiRs are still monodisperse and uniform in size.

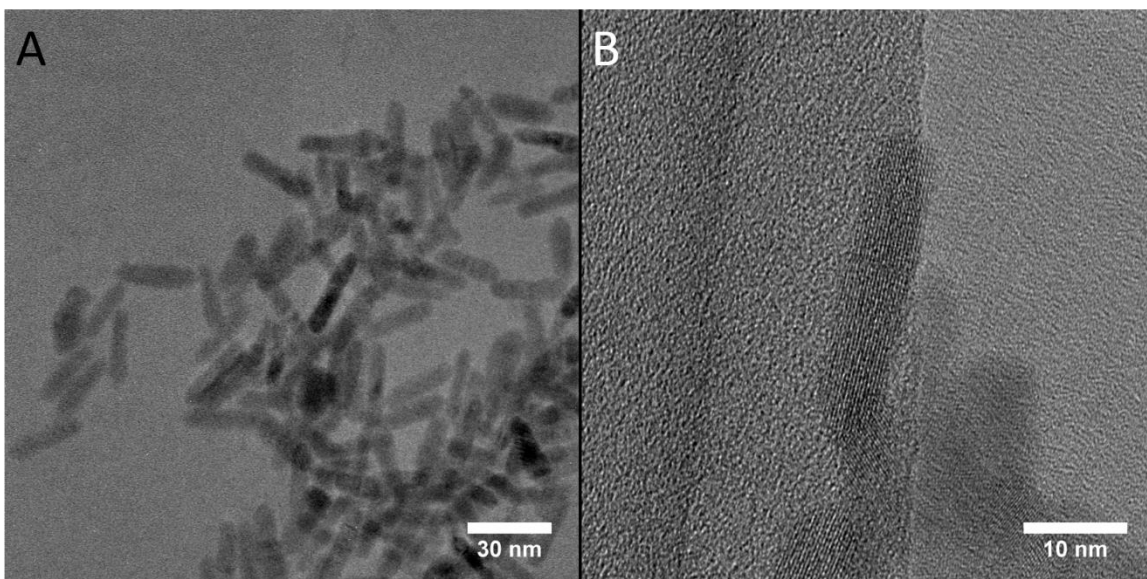


Figure 4-21 (A) TEM and (B) HRTEM for CdSe-CdS DiR stabilised with D-Thiogluucose.

The size distribution data below in Figure 4-22 shows that the rods have an average length of  $26.1 \pm 2.6$  nm and an average width of  $6.6 \pm 1.0$  nm. This data once again correlates well with the sizes of the DiRs in the organic phase and so we can be confident that no change has taken place.

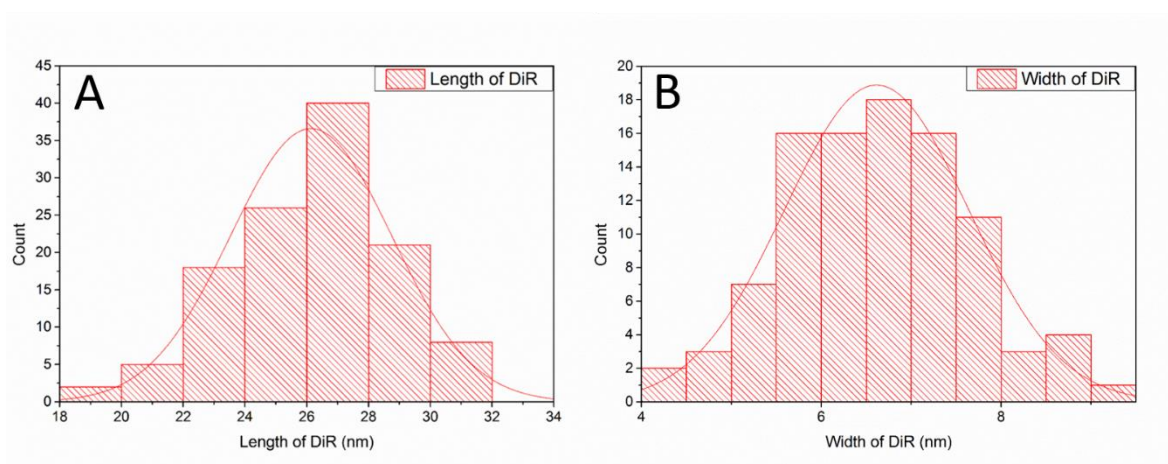


Figure 4-22 (A) Length and (B) width distributions histograms for the DiR stabilised with thiogluucose ( $N = 140$  for length and  $120$  for width).

#### 4.4 Use of CdSe-CdS DiRs for chiral recognition

Once the DiRs were fully characterised, solutions were prepared for chiral recognition studies. Some previous research has been carried out using chiral quantum dots for enantiomeric recognition so it was decided to perform similar

experiments. Delgado-Pérez *et al.* have used chiral CdSe-ZnS QDs for the enantiomeric discrimination of drugs such as Naproxen and Ibuprofen<sup>14</sup>. Recently, Visheratina *et al* demonstrated chiral quenching effects when interacting cysteine stabilised CdSe-CdS QDs with L- and D- cysteine stabilised magnetic CoFe<sub>2</sub>O<sub>4</sub> nanoparticles<sup>10</sup>.

Since enantiomeric separation of molecules, such as drugs or amino acids, has been carried out using cyclodextrin<sup>20-22</sup>, a monosaccharide, it was decided to use a sugar (1-thio-β-D-glucose) as a ligand for our DiR sensing experiments as well as the cysteine. Therefore, we used 3 samples (D-Cys DiR, L-Cys DiR and β-thioglucose stabilised DiR) to interact with the chiral drugs in these experiments.

For the sensing experiments, two types of non-steroidal anti-inflammatory drugs (NSAIDs) were selected, naproxen and ibuprofen. Since naproxen and ibuprofen are poorly soluble in water, but soluble in DMSO, the sensing experiments were performed in DMSO. Unfortunately, the preliminary results from the ibuprofen sensing were very inconsistent so naproxen was chosen the primary focus of this research.

The aim of these experiments was to mix NSAIDs with chiral nanomaterials and see if there was a difference in the quenching of the DiRs due to the chirality of the NSAID and nanomaterial used. The first experiments were conducted using L- and D-Cys DiRs and S-Naproxen. The naproxen solution was prepared by dissolving 100 mg of naproxen in 1 mL of DMSO (0.43 M).

For our experiments a constant concentration of DiRs was necessary, we have chosen a concentration of DiRs which corresponded to an absorbance of 0.1 at 400 nm, which was called as concentration  $C_{\lambda}$ . Using reported values for the extinction coefficient<sup>15</sup>, the molar concentration of DiR at this concentration was determined to be 7 nM (appendix Figure 8-6). In order to prepare this solution, 100 μL of the DiRs was diluted in 8 mL of DMSO. This was carried out for both D- and L- Cys stabilised dot in rods, after which the concentration was verified using UV-Vis

spectroscopy. Table 4-1 presents the volumes of solutions used in the sensing experiments.

Sample #	1	2	3	4	5	6
Volume of DiRs (mL)	1.000	1.000	1.000	1.000	1.000	1.000
Volume of Naproxen added ( $\mu\text{L}$ )	0.000	6.667	13.333	20.000	26.667	33.333
Total volume (mL)	1.000	1.007	1.013	1.020	1.027	1.033

*Table 4-1 Adjusted volumes of DiRs and naproxen for the sensing experiments.*

To carry out the experiment, six cuvettes with 1.5 mL of the DiR solution (concentration =  $C_\lambda$ ) were prepared and mixed with a certain amount of S-Naproxen. In order to reduce error, the solutions were allowed to stay for 1 hour before any measurements were taken. This allowed sufficient time for homogeneity within the samples to be achieved. The samples were then analysed using PL spectroscopy to monitor the effect of the amount of Naproxen added to the excitonic emission of the CdSe-CdS dot in rods. The resulting graphs demonstrate the effect of the naproxen on the DiR emission as a percentage change in luminescence relative to the control sample which does not contain Naproxen (Figure 4-23).

The PL spectra used to create these graphs are shown in appendix Figure 8-7 and Figure 8-8.

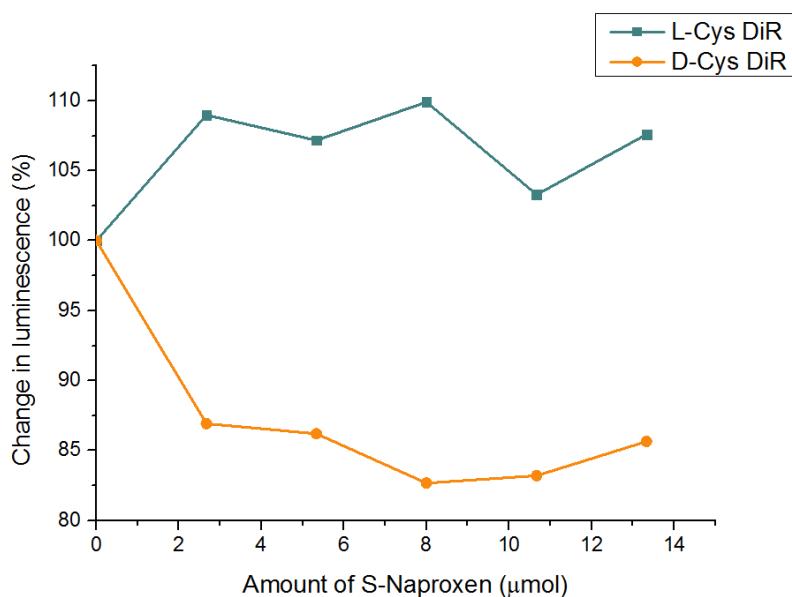


*Figure 4-23 Effect of S-Naproxen on the PL of L/D-Cys DiRs (Version 1).*

The results shown above clearly demonstrate a difference in quenching for D- and L-cys capped DiRs. For the largest Naproxen addition there was nearly a 22 % difference in the luminescence of the samples relative to the control. The quenching of the D-cysteine capped dot in rods appears to follow a roughly exponential decay in the luminescence as a function of S-Naproxen addition. The greatest loss in luminescence occurred following the smallest addition and in the case of the largest Naproxen addition, the D-Cys capped DiRs have lost 15% of their luminescence relative to the control. Interestingly, when adding S-Naproxen to the L-Cys dot in rods no loss in luminescence was observed. To ensure the results were accurate and reproducible the experiment was carried out a second time using the same conditions but a fresh sample of DiRs (Figure 4-24).



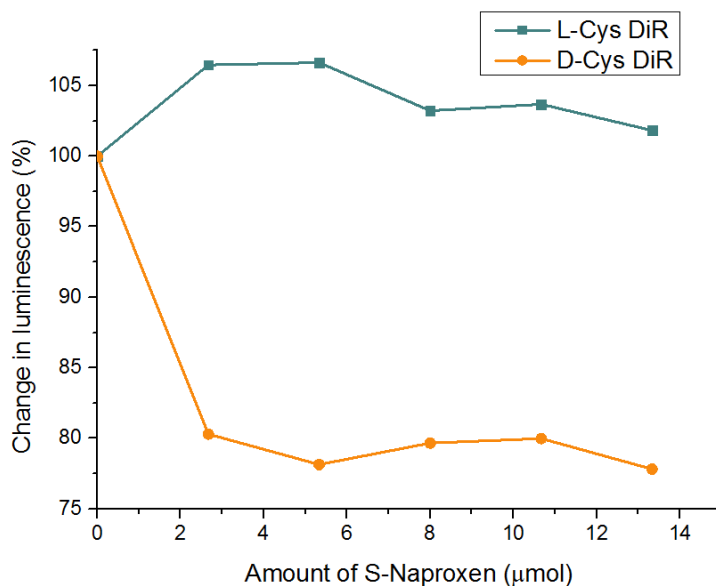


*Figure 4-24 Effect of S-Naproxen on the PL of L/D-Cys DiRs (Version 2).*

The results of the second experiment correlate well with the first experiment. Significant loss of luminescence for the D-cys capped dot in rods is present again while slight enhancement of the L-Cys stabilised DiRs also exists. The loss of the luminescence intensity in the case of D-Cys stabilised DiRs can be explained by preferential binding of carboxylic acid group from the naproxen molecule to the surface of DiRs resulting in their quenching. Due to the differences in stereochemistry between the cysteine enantiomers and naproxen a difference in interactions is not surprising.

The next set of experiments was conducted using thioglucose DiRs and R- and S-Naproxen. In this case, only one solution of DiRs was prepared. Details of the preparation of these thioglucose capped CdSe-CdS DiRs can be found in 2.3.6 of the methods chapter.

Similar to the previous experiment, the DiRs solution had a concentration which corresponded to an absorbance of 0.1 at a wavelength of 400 nm,  $C_{\lambda}$ . To prepare the solution 200  $\mu$ L of the DiRs were diluted in approximately 15 mL of DMSO. The concentration of Naproxen used in this experiment was kept the same as last time (0.43 M for both R- and S- naproxen). For this experiment the volumes and additions

were kept the same as previous time. So, for the R-Naproxen experiment seven 1 mL cuvettes of thioglucose capped DiRs were prepared to which varying amounts of R-Naproxen were added (between 0 and 40  $\mu$ L). The samples were allowed to come to rest for an hour and then PL spectra were recorded to observe the change in exciton emission intensity. The same experiment was repeated with S – Naproxen to compare the results for the 2 enantiomers.

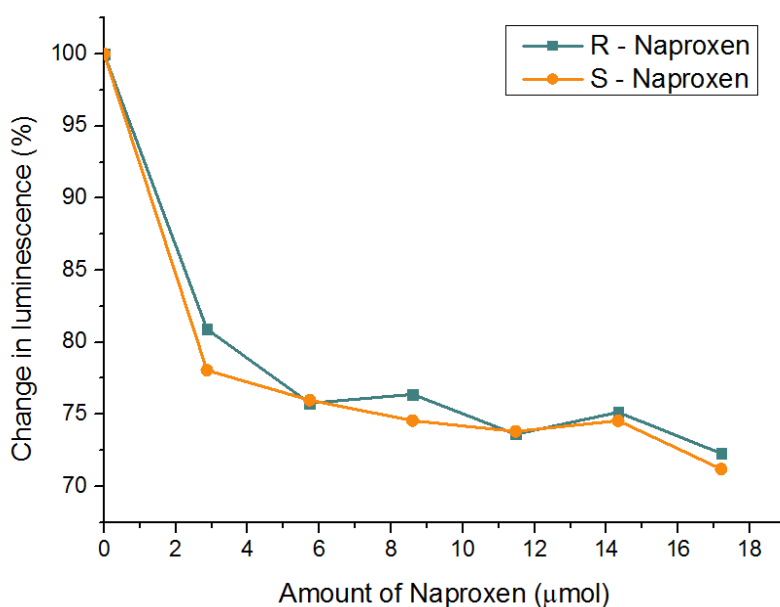


*Figure 4-25 Effect of S and R-Naproxen on the PL of Thioglucose DiRs. (Version 1).*

Both R and S-Naproxen seem to have almost the same effect on the thioglucose DiRs. This contrasts to the previous experiment where only 1 enantiomer was quenched by Naproxen. When using both enantiomers of Naproxen (R and S) with thioglucose capped DiRs a similar result is seen for both experiments. Significant quenching appears to be taking place for the thioglucose capped DiRs when interacted with either R or S naproxen. The quenching effect seems to be concentration dependant and follows an approximate exponential decay. The experiment was carried out a second time to ensure the results were accurate (Figure 4-26). Excluding experimental error, the results are the same showing the same quenching effect for both R- and S- naproxen. The quenching in this case may be due to the lower packing density of the thioglucose allowing greater interaction

with the naproxen molecules. However, it is obvious that thioglucose capped DiRs do not demonstrate any strong selective recognition of naproxen enantiomers by contrast to L/D-Cys stabilised DiRs above. This can be explained by the large size of the thioglucose ligand, which effectively covers all surface of DiRs preventing the interaction and binding of Naproxen molecules to the quantum nanostructures.

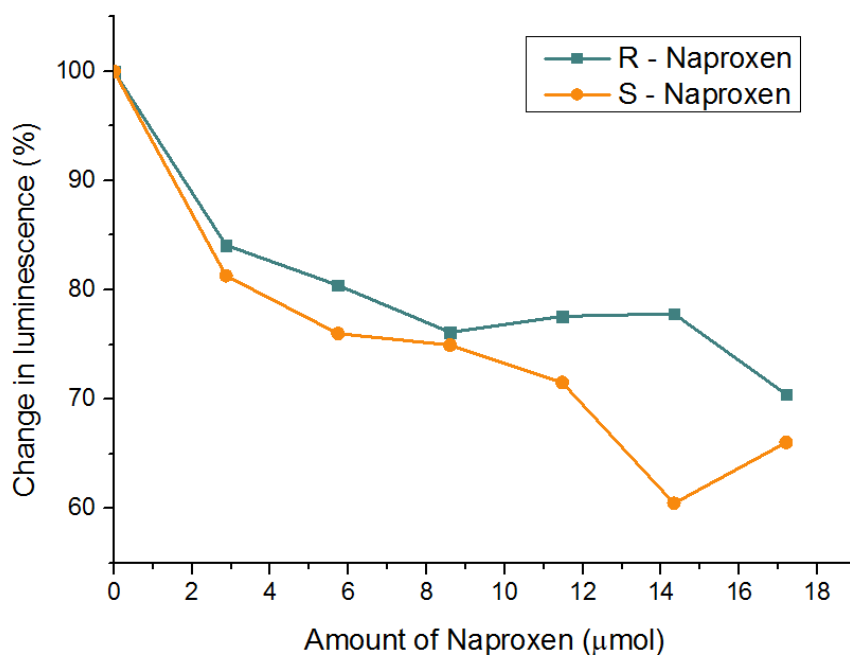


Figure 4-26 Effect of S and R-Naproxen on the PL of Thioglucose DiRs. (Version 2)

While the exact quenching mechanism for this reaction is not fully understood, it is believed to involve an interaction with the carboxylic acid group of naproxen. This leading to potential overlap of densities of states of the QDs with the  $\pi$  orbitals of the naphthalene ring in the naproxen, thereby introducing a non-radiative decay pathway and decreasing luminescence.

#### 4.5 Synthesis and characterisation of CdSe-CdS dot in tetrapods

While tetrapods are technically 3 dimensional in shape each of the arms of the tetrapod are governed by the same confinement regime (1D) as the dot in rods. Therefore, by studying the optical activity of tetrapods (TPs) it was expected that some interesting optical properties could be observed. CdSe-CdS tetrapods were synthesised according to procedure reported by Talapin *et al.*<sup>15</sup> and produced in

house by Dr. Finn Purcel-Milton. The synthesis starts from the preparation of the less common cubic zinc blende CdSe core using a combination of cadmium myristate and selenium in ODE. These seeds are subsequently reacted with a solution of sulfur and cadmium to selectively direct growth of wurtzite CdS along the tetrapod arms directions. These TPs were obtained in the organic phase (chloroform) and were characterised using UV-Vis, PL and TEM analysis.

The UV-Vis spectrum is presented in Figure 4-27 below. The spectrum has two primary features of interest. By examining the inset graph highlighting the spectral region between 500 and 700 nm it is clear that the excitonic absorption peak of the CdSe core is located at 635 nm.

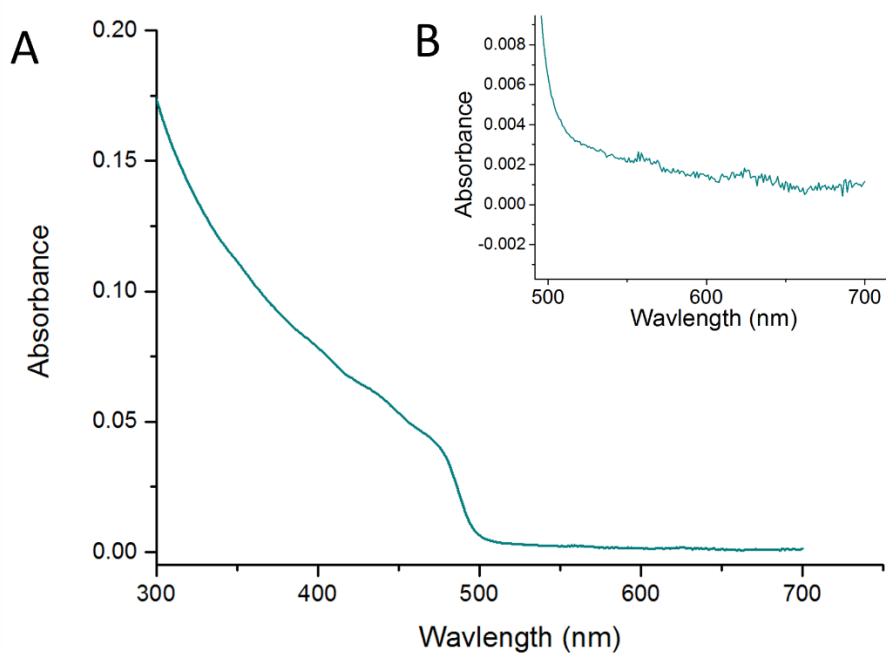


*Figure 4-27 UV-Vis spectrum of CdSe-CdS TPs in chloroform (B) zoom in on 500 – 700 nm region*

The characteristic increase in absorption due to the large CdS shell on these nanoparticles is also present. The large absorption begins at 500 nm and continues to increase as the wavelength increases in energy. The big difference in absorption between the CdSe core and CdS shell would indicate that the majority of these nanoparticles is composed of CdS material.

Photoluminescence spectroscopy was used to analyse the emission from the CdSe core of the TPs (Figure 4-28). Upon analysis of these TPs, it is clear that they remain emissive following the arm growth with an emission maximum located at 635 nm. However, it must be noted that these particles are very weakly emitting, with high concentrations required to produce a clear PL signal. Quantum yield measurements were carried out Dr. Purcel-Milton and found the TPs to have a QY of 4%.

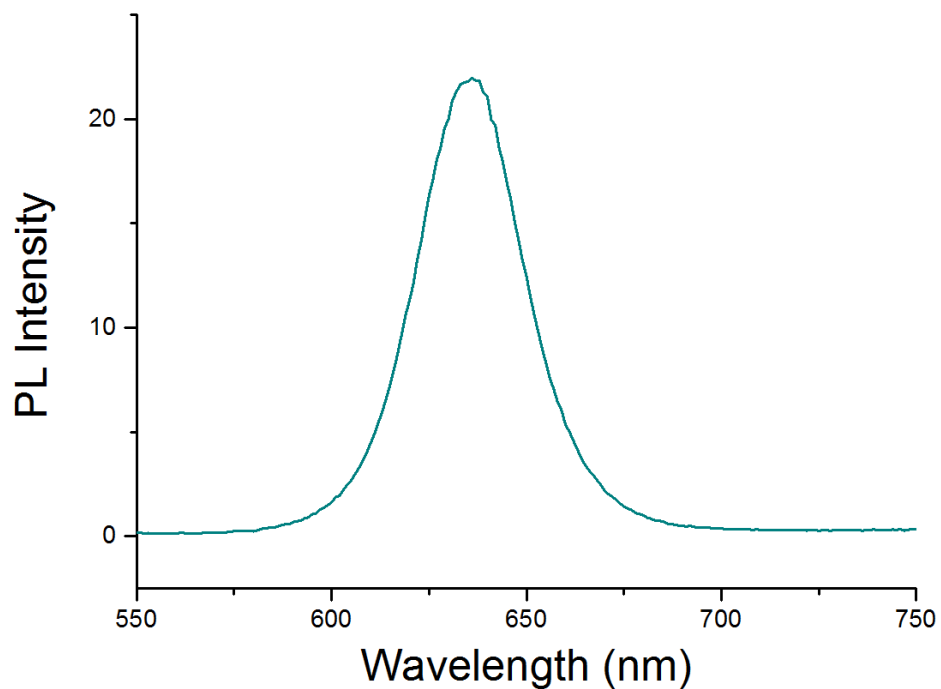


*Figure 4-28 PL spectrum for CdSe-CdS TPs (Ex  $\lambda$  – 450 nm).*

TEM analysis below confirms that the particles being investigated are in fact tetrapodal in shape. It is difficult to calculate an average arm length due to the tetrapods sitting in a variety of conformations. Therefore, it was decided to measure the length of the arms of the tetrapods sitting with 3 legs on the horizontal plane and one pointing directly out of the plane of the TEM grid. Using simple trigonometry (Figure 4-29) it is clear that by measuring the observed arm length of the TPs who are sitting with 3 arms on the ground and dividing the result by 0.86 we should get a reasonable estimation for the actual arm length. Arm thicknesses were calculated as usual.

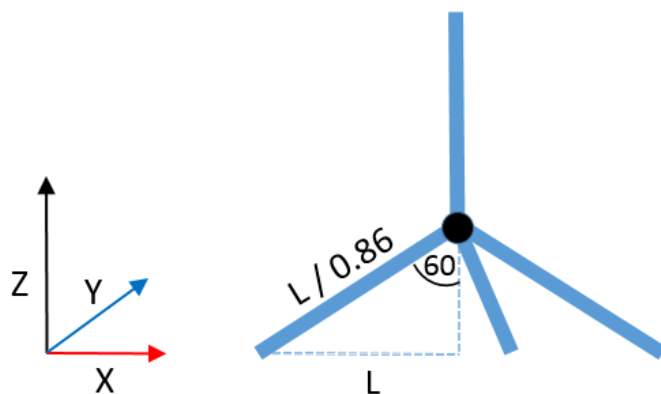


Figure 4-29 Schematic describing relationship between observed arm length and actual arm length for CdSe-CdS TP.

TEM analysis confirms the synthesis of monodisperse tetrapods (Figure 4-30). The tetrapods in the organic phase in the organic phase have an average size of 23.7 nm  $\pm$  2.8 nm which is consistent with literature values<sup>15</sup>.

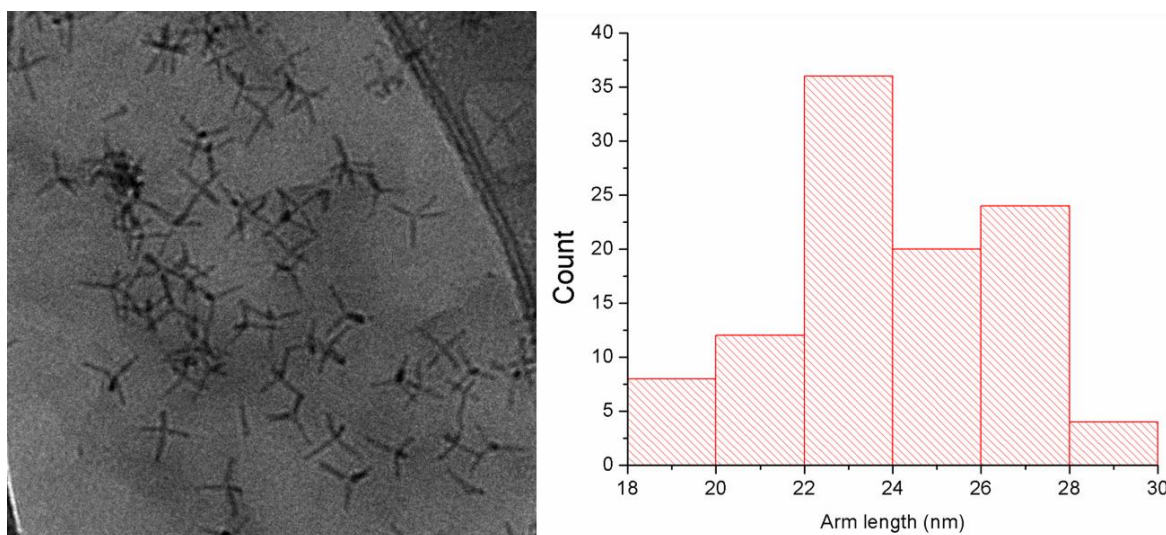
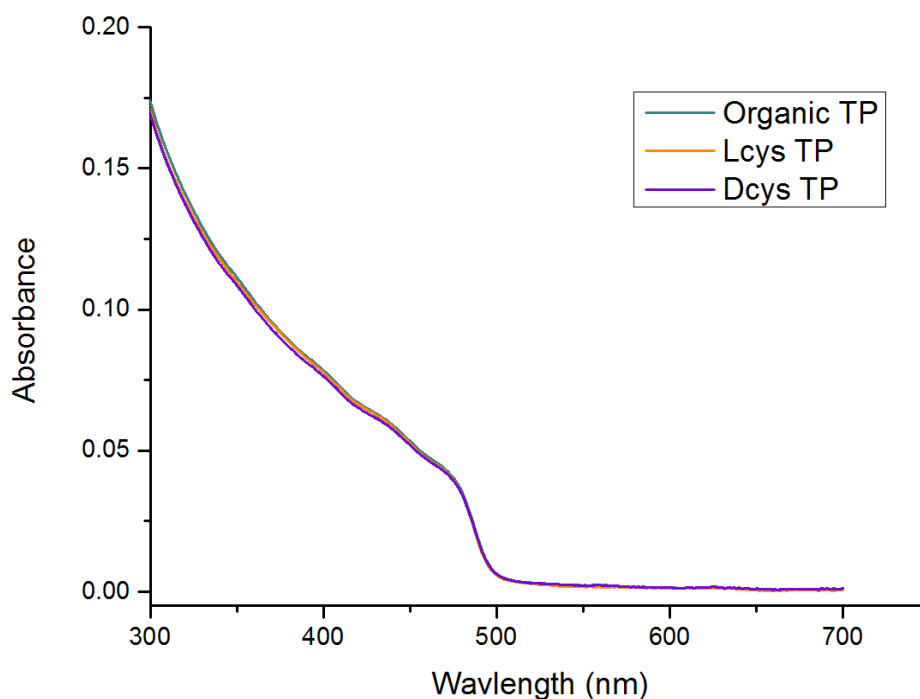


Figure 4-30 TEM image (left) and size distribution histogram (right) for CdSe-CdS tetrapods (organic phase) (N = 120).

Following TEM analysis confirming successful tetrapod formation, the same phase transfer that used to produce chiral DiRs (4.3) was used to produce the optically active tetrapods with details described in the experimental chapter section 2.3.5.

These samples were subsequently analysed using UV-Vis, PL, CD spectroscopies and TEM analysis. UV-Vis data presented below (Figure 4-31) suggests that no change in absorption has taken place. The UV-Vis spectrum has not changed shape when

comparing before and after the ligand exchange, presenting both the large CdS shell absorption and the much smaller CdSe core absorbance.



*Figure 4-31 UV-Vis spectra for CdSe-CdS TPs capped with cysteine*

PL spectra presented in Figure 4-32 below demonstrated that the TPs still retain their luminescence following the successful cysteine exchange. The TPs emission intensity is about 50% of its value in the organic phase and the emissive properties for both L- and D- cysteine samples are identical. It must be noted that these samples were not very luminescent in the organic phase and were even less so in the aqueous phase. The emission maximum was still located at 635 nm.

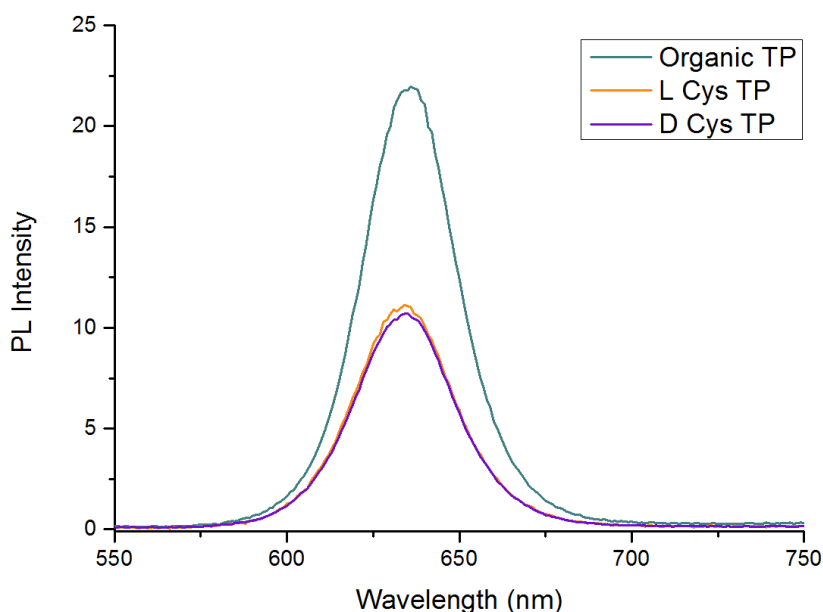


Figure 4-32 PL spectra for CdSe-CdS TPs capped with cysteine (Ex.  $\lambda$  – 450 nm).

TEM analysis confirmed no change in shape has occurred as the sample is still entirely composed of tetrapods (Figure 4-33). The average size was calculated to be  $23.9 \text{ nm} \pm 2.6 \text{ nm}$  which would indicate that no change in arm length has occurred as a consequence of the phase transfer.

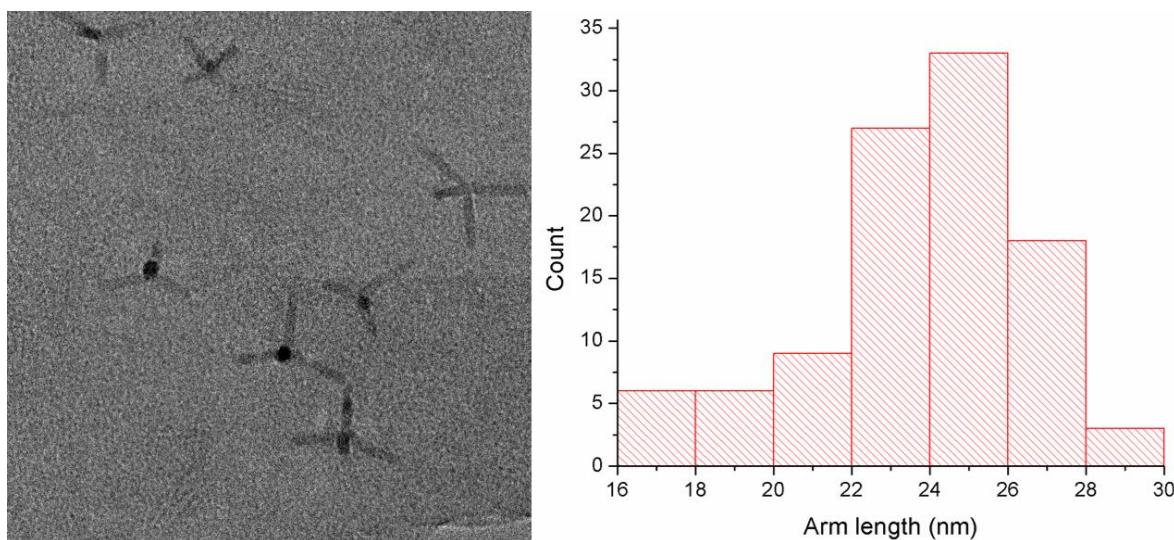
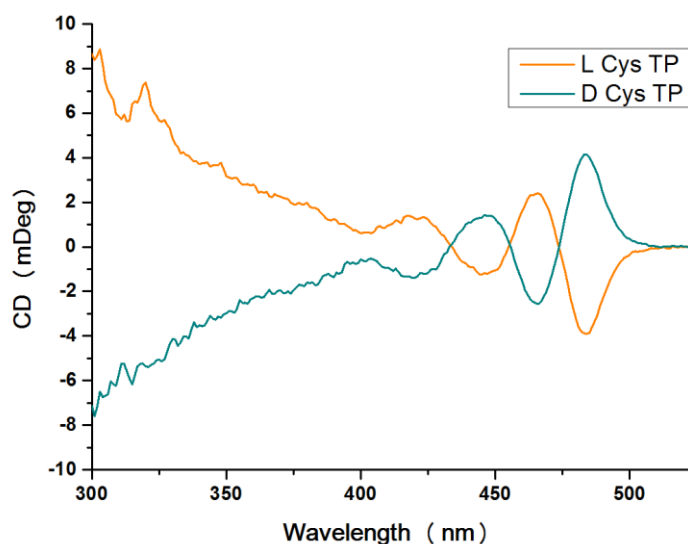


Figure 4-33 TEM image (left) and size distribution histogram (right) for L-Cys-CdSe-CdS tetrapods ( $N = 120$ ).

It was expected that the tetrapods would exhibit some degree of optical activity and therefore the samples have been studied using CD spectroscopy (Figure 4-34). The CD signal begins around 515 nm and crosses the axis several times. The resultant



spectra for D- and L- cysteine stabilised TPs are mirror images of each other as expected. Contrary to the DiR sample no optical activity was present in the exciton band edge region of the CdSe core. This is primarily due to the fact that there is far more CdS present in these samples compared to the DiRs. The CdS absorption in the UV-Vis corresponds to the optical activity bands present in the CD spectra.



*Figure 4-34 CD spectra for D and L cysteine stabilised CdSe-CdS tetrapods.*

It is interesting to note that the CD spectra for the CdSe-CdS DiR and the TPs are somehow similar to each other. This is to be expected as the rod-like morphology of the CdS occurs in both samples.

## 4.6 Conclusions

In this chapter an efficient phase transfer method for preparing optically active CdSe-CdS DiRs which worked for a variety of different ligands has been prepared. Using this approach, we were able to successfully prepare DiRs capped with cysteine and penicillamine. Both of these samples retained a significant luminescence in the aqueous phase and remained homogenous in size and aspect ratio. Interestingly, both the cysteine and penicillamine capped samples demonstrated optical activity in the band edge absorption region of the nanomaterials indicating an electronic interaction between the chiral ligand and the DiR. Furthermore, DiRs capped with 1-thio- $\beta$ -D-glucose were successfully produced. These DiRs also displayed optical

activity, however it was much less clear than the other samples potentially due to the lack of co-ordinating functional groups on the thioglucose molecule responsible for inducing chirality.

Using L- and D- cysteine stabilised DiRs we were able to show quenching effects when interacted with S-Naproxen. A 22% difference in luminescence between L- and D- cysteine stabilised DiRs clearly demonstrate a possibility of chiral recognition through luminescence. It was expected that some chiral discrimination could be achieved when examining the interactions between glycosidated dot in rods (thioglucose) and R and S Naproxen, however no such chiral recognition was observed. Potentially the mechanism for chiral recognition is inhibited by the much larger thiolactose molecule when compared to cysteine.

Finally, successful production of optically active luminescent CdSe-CdS tetrapods was achieved. By performing a ligand exchange on TPs synthesised in the organic phase to cap them with L and D cysteine optical activity was successfully induced. Interestingly, the optical activity of the TPs is similar to the DiRs which makes sense given the similarities in structure and morphology. We expect that these new chiral anisotropic nanomaterials will find potential applications in chiral sensing, biological imaging and photonics. However, further research is necessary in order to explore the properties and applications of these nanomaterials.

## 4.7 References

- (1) Gao, X.; Zhang, X.; Deng, K.; Han, B.; Zhao, L.; Wu, M.; Shi, L.; Lv, J.; Tang, Z. *Journal of the American Chemical Society* **2017**, *139*, 8734.
- (2) Baimuratov, A. S.; Rukhlenko, I. D.; Gun'ko, Y. K.; Baranov, A. V.; Fedorov, A. V. *Nano Letters* **2015**, *15*, 1710.
- (3) Mukhina, M. V.; Maslov, V. G.; Baranov, A. V.; Fedorov, A. V.; Orlova, A. O.; Purcell-Milton, F.; Govan, J.; Gun'ko, Y. K. *Nano Letters* **2015**, *15*, 2844.
- (4) Mukhina, M. V.; Baimuratov, A. S.; Rukhlenko, I. D.; Maslov, V. G.; Milton, F. P.; Gun'ko, Y. K.; Baranov, A. V.; Fedorov, A. V. *Acs Nano* **2016**, *10*, 8904.
- (5) Di Stasio, F.; Grim, J. Q.; Lesnyak, V.; Rastogi, P.; Manna, L.; Moreels, I.; Krahne, R. *Small* **2015**, *11*, 1328.
- (6) Kodanek, T.; Banbela, H. M.; Naskar, S.; Adel, P.; Bigall, N. C.; Dorfs, D. *Nanoscale* **2015**, *7*, 19300.
- (7) Wilkerson, R. J.; Elder, T.; Sowinski, O.; Fostvedt, J. I.; Hoefelmeyer, J. D. *Surface Science* **2016**, *648*, 333.
- (8) Mukhina, M. V.; Korsakov, I. V.; Maslov, V. G.; Purcell-Milton, F.; Govan, J.; Baranov, A. V.; Fedorov, A. V.; Gun'ko, Y. K. *Scientific Reports* **2016**, *6*, 24177.
- (9) Ngamdee, K.; Kulchat, S.; Tuntulani, T.; Ngeontae, W. *Journal of Luminescence* **2017**, *187*, 260.
- (10) Visheratina, A. K.; Purcell-Milton, F.; Serrano-Garcia, R.; Kuznetsova, V. A.; Orlova, A. O.; Fedorov, A. V.; Baranov, A. V.; Gun'ko, Y. K. *Journal of Materials Chemistry C* **2017**, *5*, 1692.
- (11) Zhang, Y.-h.; Zhang, H.-s.; Guo, X.-f.; Wang, H. *Microchemical Journal* **2008**, *89*, 142.
- (12) Govan, J. E.; Jan, E.; Querejeta, A.; Kotov, N. A.; Gun'ko, Y. K. *Chemical Communications* **2010**, *46*, 6072.
- (13) Wawrzynczyk, D. *Journal of Materials Chemistry C* **2017**, *5*, 1724.
- (14) Delgado-Pérez, T.; Bouchet, L. M.; de la Guardia, M.; Galian, R. E.; Pérez-Prieto, J. *Chemistry – A European Journal* **2013**, *19*, 11068.
- (15) Talapin, D. V.; Nelson, J. H.; Shevchenko, E. V.; Aloni, S.; Sadtler, B.; Alivisatos, A. P. *Nano Letters* **2007**, *7*, 2951.
- (16) Dzema, D.; Kartsova, L.; Kapizova, D.; Tripp, S.; Polikarpov, N.; Appelhans, D.; Voit, B. *Jpc-Journal of Planar Chromatography-Modern Tlc* **2016**, *29*, 108.
- (17) Hui, B. Y.; Raoov, M.; Zain, N. N. M.; Mohamad, S.; Osman, H. *Critical Reviews in Analytical Chemistry* **2017**, *47*, 454.
- (18) Kalikova, K.; Slechtova, T.; Tesarova, E. *Current Medicinal Chemistry* **2017**, *24*, 829.
- (19) Choi, J. K.; Haynie, B. E.; Tohgha, U.; Pap, L.; Elliott, K. W.; Leonard, B. M.; Dzyuba, S. V.; Varga, K.; Kubelka, J.; Balaz, M. *ACS Nano* **2016**, *10*, 3809.
- (20) Han, C.; Li, H. *Small* **2008**, *4*, 1344.
- (21) de Boer, T.; de Zeeuw, R. A.; de Jong, G. J.; Ensing, K. *Electrophoresis* **2000**, *21*, 3220.
- (22) Armstrong, D. W.; Ward, T. J.; Armstrong, R. D.; Beesley, T. E. *Science (New York, N.Y.)* **1986**, *232*, 1132.

## Chapter 5: Chiral cadmium containing 0D dots, and 2D Platelets

### 5.1 Introduction

While cadmium free nanomaterials have several advantages over toxic cadmium containing nanomaterials, traditional cadmium chalcogenide based QDs still present great interest. Primarily, the band gaps of cadmium chalcogenide nanomaterials allow for absorption and emission in the visible region of the electromagnetic spectrum<sup>1,2</sup>. This is significant when the primary focus of the research is optical activity as it allows a clear distinction between optical activity due to the ligands direct absorption and optical activity due to interactions between the chiral ligands and quantum dots. When investigating ZnS quantum dots for optical activity it was more challenging due to a partial overlap in ligand absorption and QD absorption.

Furthermore, as cadmium containing nanostructures have been studied more extensively there is a much larger variety of publications to date allowing for a broader scope for synthetic approaches to produce optically active nanomaterials. For example, a large part of this research involves the synthesis of CdSe nanoplatelets where a wide variety of synthetic approaches have been published<sup>3-8</sup>. For comparison there is very little literature available for the synthesis of ZnS nanoplatelets<sup>9,10</sup>.

The majority of chiral quantum dot research has revolved around optically active cadmium containing quantum dots and their potential applications in sensing. For example, Sianglam *et al.* have demonstrated the use of cysteamine/penicillamine stabilised CdS QDs as a CD based sensor of Cd<sup>2+</sup> ions<sup>11</sup>. In this research a common room temperature synthesis using sodium sulfide was implemented to prepare cysteamine and penicillamine stabilised QDs. Similarly, Ngamdee *et al.* recently published the synthesis of CdS QDs using sodium sulfide and penicillamine precursors and tested the chiral QDs as sensors for cysteamine<sup>12</sup>. CdTe has also

been investigated for chiral sensing applications, Guo *et al.* synthesised CdTe QDs stabilised with N-acetyl-L-cysteine. These particles were then used for the chiral recognition of phenylglycinol enantiomers<sup>13</sup>. Comparably, enantiomeric discrimination of tyrosine using chiral CdSe-CdS core shell quantum dots stabilised with N-acetyl-L-cysteine was developed by Gao *et al.* this year<sup>14</sup>.

Following the discovery of optically active quantum dots some research has been targeted towards assessing the relationships between the physical properties of the quantum dots and the CD signals they generate. Efforts have been made to investigate the effect of QD size on optical activity<sup>15</sup> using CdSe quantum dots stabilised by L- and D- cysteine, these cysteine capped QDs even demonstrated circularly polarised emission. Visheratina *et al.* very recently published research examining the relationship between shell thickness and CD intensity for a series of CdSe-CdS core shell quantum dots<sup>16</sup>. Furthermore, CdSe nanorods of varying aspect ratios were synthesised by Gao *et al.* to investigate the relationship between the aspect ratio of the nanorods and the excitonic CD intensity<sup>17</sup>.

While there is a variety of papers related to chiral quantum dots being published, there has been little development in the field of chiral anisotropic nanomaterials such as nanoplatelets. One reference to chiral CdSe nanoplatelets exists to date, briefly discussing the optical properties of cysteine stabilised CdSe nanoplatelets by Mukhina *et al.*<sup>18</sup>. Developing from this Tepliakov *et al.* have published theoretical research on chiral CdSe nanoscrolls and their potential applications for sensing of chiral molecules<sup>19</sup>. Thus this area of research is still unexplored.

## 5.2 Aims

The first aim of this research was to successfully synthesise excitonic emitting CdS quantum dots of various different sizes using traditional hot injection techniques and investigate properties of these QDs. Once the optical properties were studied, ligand exchanges were performed on these QD samples using chiral ligands to induce optical activity. By replacing the initial organic surfactants with penicillamine we aimed to produce a series of optically active QDs to investigate the effect of QD size on the resultant circular dichroism signals. The preparation of new chiral CdS QDs directly *via* aqueous synthesis was also planned; it was expected that the heating of appropriate cadmium and chalcogenide precursors under reflux in the presence of chiral ligands should result in new optically active QDs. It was predicted that monitoring of the development of circular dichroism signals as a function of reflux time would provide significant information about the origin of optical activity in these chiral QDs.

Subsequent production of both chiral quantum dots and chiral 2D nanoplatelets and the comparison of properties of these nanomaterials was planned. By synthesising very small CdSe QDs it was expected that an increased level of optical activity would be present when compared to research performed on larger CdSe QDs. As research into chiral CdSe nanosheets and nanoplatelets was virtually non-existent, this research was intended to produce a variety of different CdSe nanoplatelets and perform ligand exchanges on these platelets in order to induce chirality. It was hoped that the development and detailed comparative analysis of our CdSe samples would contribute to further understanding of chirality and optical activity in various nanomaterials.

## 5.3 Preparation and characterisation of chiral CdS

### 5.3.1 Hot injection synthesis and characterisation of CdS

Cadmium sulfide QDs were synthesised using traditional hot injection techniques<sup>20</sup>.

The hot injection synthesis uses cadmium oxide and oleic acid as precursors in 1-octadecene (ODE). Oleic acid acts as the surfactant in this reaction which stabilizes the nanocrystals and the cationic precursors, its concentration in the reaction highly affects the kinetics of the reaction. After degassing, the solution was heated to 300°C to allow formation of the Cd(oleate) precursor, during which the solution evolves from a red colour to colourless. Elemental sulphur dissolved in ODE was then added by hot injection at the 275°C and growth proceeds for 10 minutes, after which the flask was allowed to cool down. The initial amount of ODE, hot injection temperature and growth time have to be monitored to control the size of the final QDs. The particles were finally precipitated, washed with acetone and centrifuged several times and stocked in toluene or chloroform. The quantum dots were then characterised using UV-Vis and photoluminescence spectroscopy, the results of which are presented in Figure 5-1 below. The experiment was repeated with a variety of different injection temperatures in order to produce a range of CdS sizes.

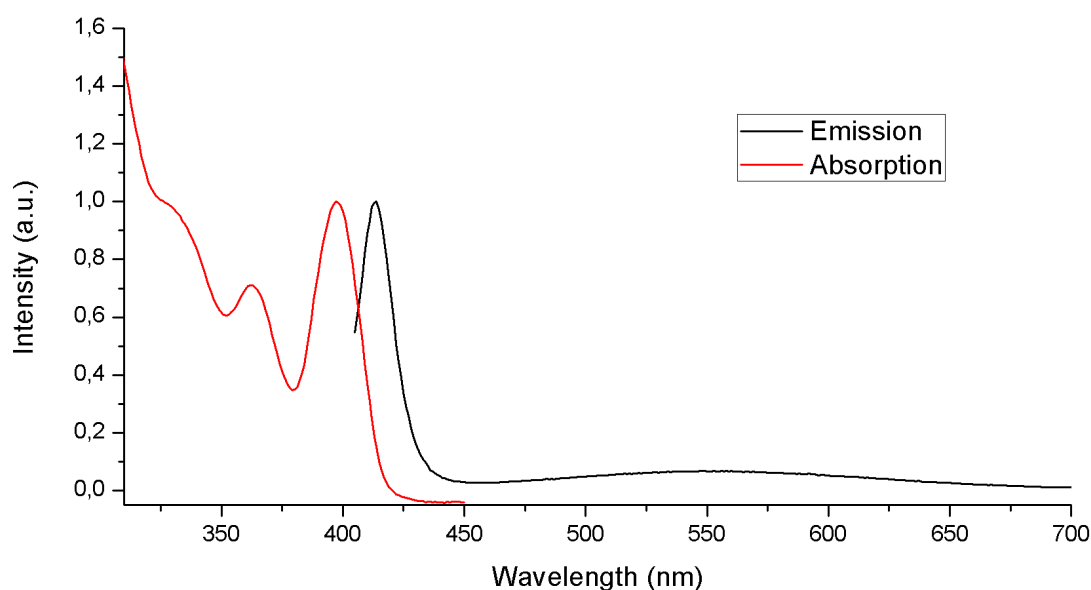


Figure 5-1 – Absorption and emission spectra of CdS quantum dots synthesized with a 275°C hot injection (Ex.  $\lambda$  – 393 nm).

According to the spectra above, these CdS QDs demonstrate typical for quantum dots absorption bands. The first exciton has a maximum intensity at 398 nm with an onset beginning at 425 nm. The full width half maximum of the QDs is 26 nm which would indicate a relatively narrow size distribution for the quantum dots. The narrow emission spectrum is further evidence of this. Upon inspection of the emission spectrum it becomes clear that there are 2 components. Firstly, the excitonic emission has its maximum intensity located at 413 nm, indicating a relatively small Stokes shift of 15 nm. Secondly, there is a very small broad luminescence band between 700 – 450 nm. This luminescence is the surface based defect emission caused by defect trap states decreasing the emissive wavelength energy compared to the excitonic emission.

The quantum yield of these QDs was determined using the integrating sphere technique and was 20%

### 5.3.2 Effect of injection temperature on the size of CdS nanoparticles

One of the advantages of quantum dots is that they have a size tuneable bandgap, and therefore tuneable emission. This property is important for potential applications of quantum dots. Furthermore, as circular dichroism signals in QDs often originate from an interaction between the surface of the QD and the ligand, it was proposed that changing the size would also alter the CD signal<sup>15,21</sup>. As the surface to volume ratio of QDs increases with decreasing size we also believed that by synthesising smaller sizes of CdS QDs we may induce higher intensity circular dichroism signals. There are a few ways to affect the final size of QDs made using hot injection methods. There are possibilities to alter the injection temperature, change the reaction time or alter reactant concentrations. We decided to vary the size by changing the initial injection temperature while keeping the reaction time and concentrations constant.

Several batches of QDs with different sizes were made using a range of different injection temperatures. As the injection temperature was increased, the absorption



spectra were more red-shifted (Figure 5-2 below). This red shifting of the first exciton absorption peak is indicative of an increase in the average size of the QDs being synthesised. As quantisation increases with decreasing QD size, the larger QDs have a smaller band gap and therefore lower energy exciton absorption. The size of the QDs may be approximated using an empirical formula developed by Yu *et al*<sup>22</sup> below in Equation 5-1:

$$D = (-6.65 \times 10^{-8})\lambda^3 + (1.9557 \times 10^{-2})\lambda + 13.29$$

*Equation 5-1 Empirical determination of CdS size using exciton wavelength, where*

*D = QD diameter in nm and  $\lambda$  = exciton wavelength in nm*

The effect of altering the injection temperature on the absorption spectra are clearly visible in Figure 2-2. The lowest injection temperature, 270°C, yielded QDs with an average diameter of 3.23 nm. Whereas the highest injection temperature, 315°C, led to a QD diameter of 4.33 nm.

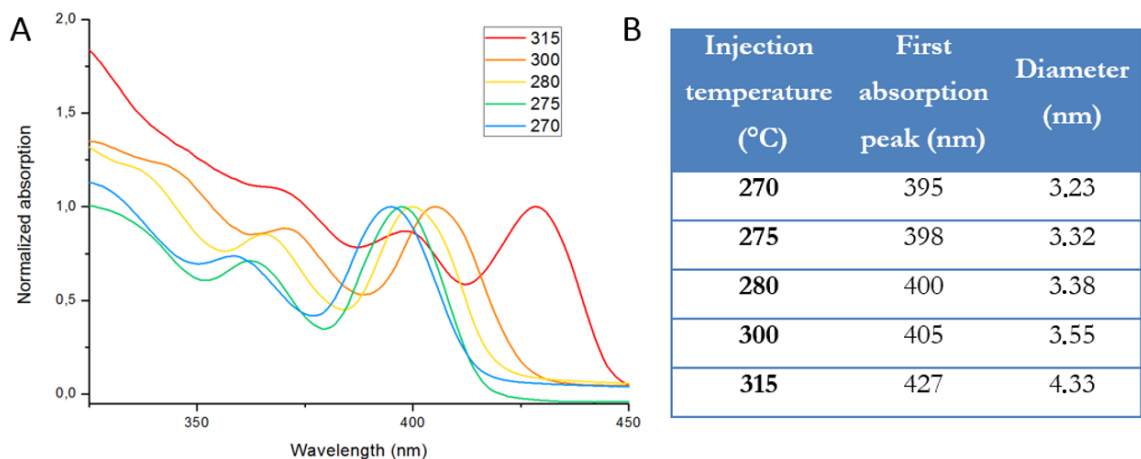
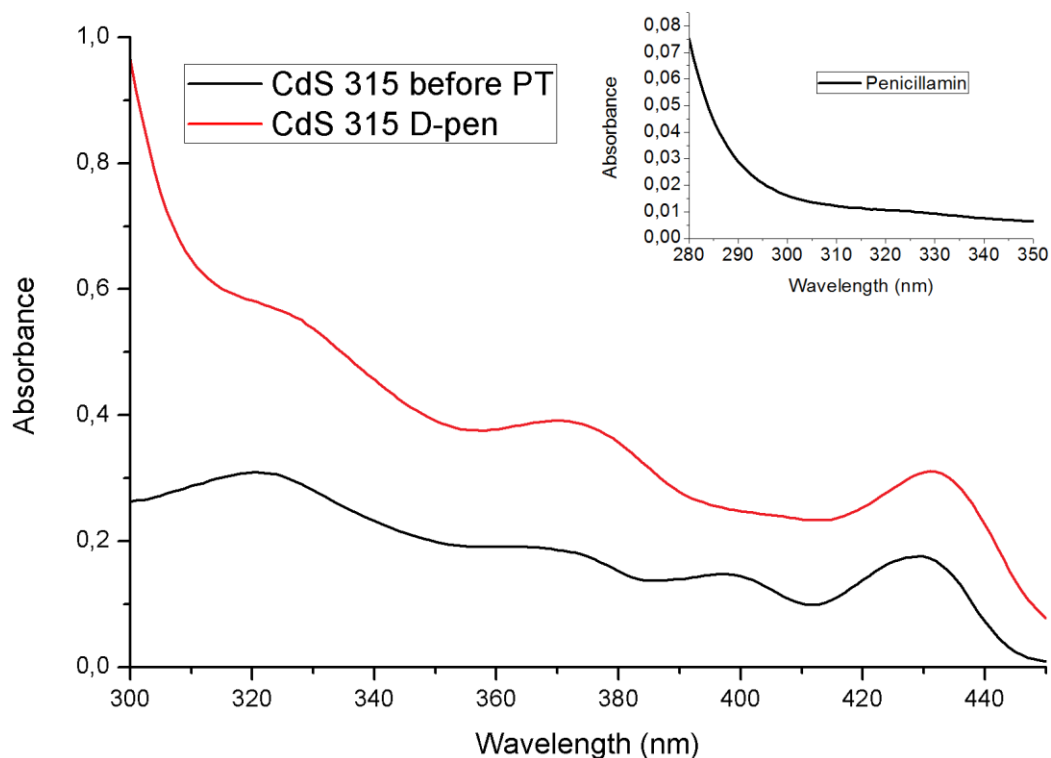


*Figure 5-2 – (A) Absorption spectra of quantum dots synthesized with different injection temperatures (in degrees) and (B) their size as determined by the equation above.*

### 5.3.3 Phase transfer of CdS QDs using penicillamine ligands

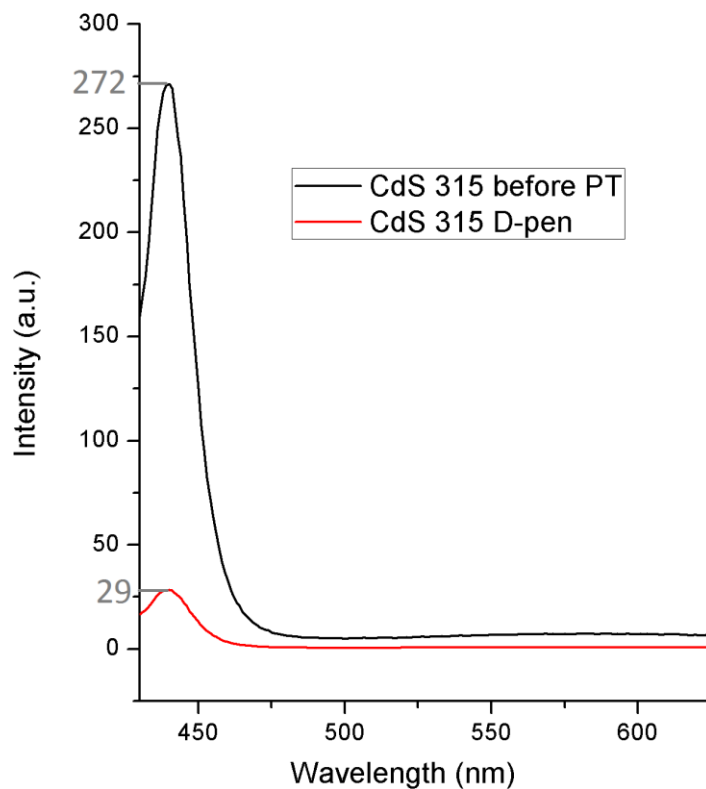
The phase transfer techniques that were successfully used for the ligand exchange of the ZnS:Mn QDs did not work for these QDs, therefore it was required to find an alternative method. Phase transfer techniques are successful when the thermodynamic and kinetic parameters drive the forward reaction. It is possible that the different binding energies of Cd-S compared to Zn-S, or the use of different organic ligands may play a role in why previous approaches did not work. The new synthesis is outlined in section 2.4.2 of the experimental section. In this procedure a basic penicillamine solution dissolved in methanol is combined with a solution of CdS QDs in toluene and allowed to stir for 3 hours. Following the transfer of the QDs from the organic to the aqueous phase a large excess of water is added and the QDs are stirred for a further 20 minutes. The QDs are then washed using acetone and finally stored in a basic aqueous solution. These QDs were analysed using UV-Vis, PL, CD spectroscopies and TEM analysis.

Figure 5-3 below presents the UV-Vis data for the CdS QDs which were synthesised using an injection temperature of 315 °C before and after the phase transfer took place. From the spectroscopic evidence provided in Figure 5-3 it is clear that the QDs have been successfully transferred into the aqueous phase. In the region from 450 nm – 320 nm very little difference in the spectra is observed. There seems to be a slight red shifting of the first exciton peak from 427 nm to 435 nm which may be due to partial aggregation following the phase transfer. There is a large increase in absorption below 320 nm when comparing the CdS QDs before and after phase transfer and this is due to the absorption of the penicillamine ligand directly, it is visible in the inset of Figure 5-3.



*Figure 5-3 Absorbance spectra of CdS quantum dots before and after the phase transfer with penicillamine (inset: absorbance spectrum of penicillamine).*

Following UV-Vis analysis photoluminescence measurements were recorded for the QDs before and after the phase transfer. According to Figure 5-4, the QDs are still luminescent following the phase transfer procedure however a drastic reduction in emission is observed, nearly a 90% reduction in luminescence is noticed. The large loss in luminescence may be explained by the lack of a protective ligand shell on these CdS QDs and quenching by water molecules. Core-shell QDs are more resistant to changes in environment when compared to unshelled QDs, in this case no shell is present so it is unsurprising that a large portion of the luminescence is lost during the phase transfer.



*Figure 5-4 – Emission spectra before and after the penicillamine phase transfer of CdS QDs.*

Figure 5-5 below presents the results for the CdS CD analysis. It is clear that these penicillamine capped CdS QDs demonstrate optical activity in the semiconductor band edge region of the absorption spectrum which indicates an interaction between the chiral ligand and the CdS QD. The CD spectra for D- and L- penicillamine stabilised QDs are mirror images of each other, as one would expect for QDs modified by opposite enantiomer ligands.

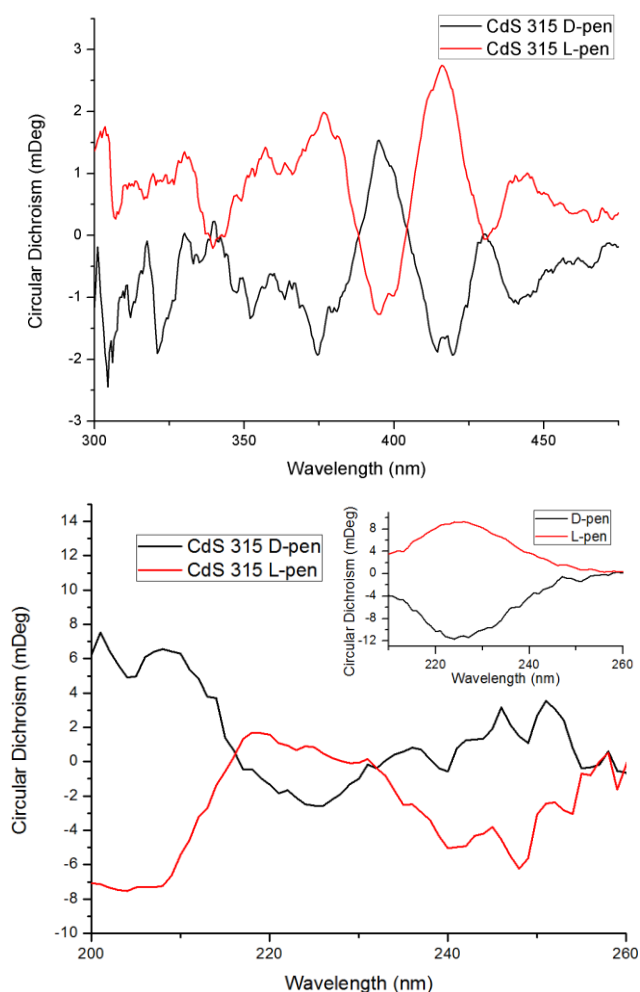


*Figure 5-5 – (A) CD spectra of L-pen and D-pen capped CdS in the nanoparticles absorption region (B) CD spectra of L-pen and D-pen capped CdS in the ligand absorption region, with the ligand own CD spectrum as inset.*

The onset of the optical activity in the CD spectra correlates with the onset of absorption visible in the UV-Vis spectra. This is characteristic of chiral QDs and demonstrates that an interaction is taking place between the chiral ligand and the achiral QD core<sup>23,24</sup>. The CD spectrum observed in the 260 – 200 nm region is also drastically different when comparing free penicillamine in solution and penicillamine conjugated QDs, further evidence of a successful ligand exchange. The CD spectra for D- and L- pen stabilised CdS have maxima located at 425nm, 400nm and 370 nm which correspond to the 3 peaks in the absorbance spectra located at the same wavelengths. The same relationship between the absorption peaks and CD peaks was observed for CdS QDs of varying different sizes.

5.3.4 Investigation of dependence of the optical activity on the size of QDs  
 Research conducted by Tohgha *et al.* on the relationship between QD size and resulting CD spectra proposed a dependence of the CD shape on the QD size for L- and D-cysteine stabilised QDs<sup>15</sup>. Therefore, similar studies were performed here using our penicillamine stabilised CdS QDs to investigate the relationship between the CD spectra and the size of the QD.

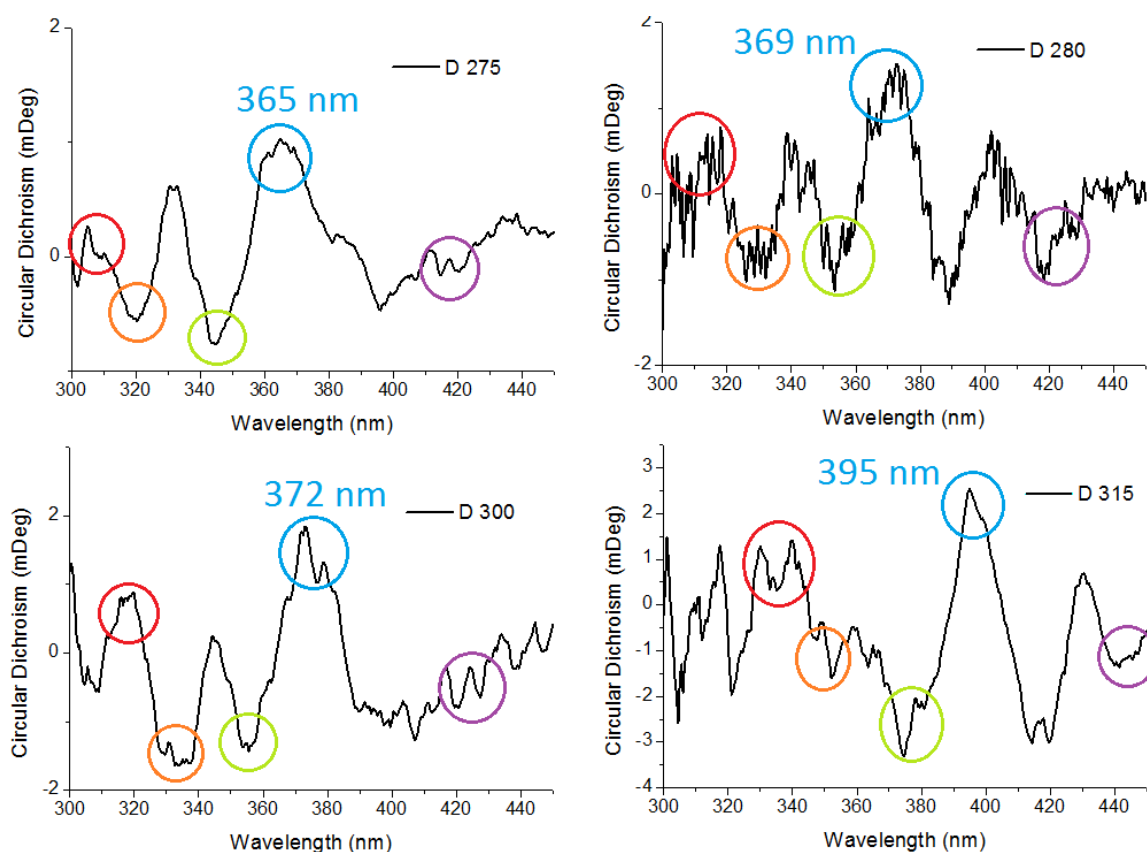


Figure 5-6 – Comparison of the CD spectra of D-pen-capped CdS QDs made at different injection temperatures.

To perform this analysis CdS QDs were synthesised at a variety of injection temperatures to give a range of QD sizes. These QDs were subsequently transferred to the aqueous phase using penicillamine and the resulting CD spectra were compared for each size of QD (Figure 5-6). Similar to the absorbance spectra for the

different sizes, the CD spectra are similar for each QD size, however the peak positions shift in accordance with the shift in absorbance peak position. In Figure 5-6 corresponding peaks have been highlighted using the same colours in each spectrum allowing us to analyse peak positions with respect to QD size. The largest peak is highlighted in blue and is the easiest to analyse. This peak position shifts from 365 nm to 395 nm as the QD size increases from 3.32 nm to 4.33 nm. It is also interesting to note that the peaks highlighted in orange and green shift in intensity relative to each other, however it is hard to separate how much of this shifting is due to noise as opposed to a photophysical phenomenon taking place.

Our results are somehow similar to Tohga as they also reported a red-shifting of CD onset with increasing QD size. Tohga also reported the appearance/changing of different peaks as QD size increased which is present in our samples also. However, due to a significant signal-to-noise ratio, a qualitative comparison is difficult.

#### 5.4 Synthesis and characterisation of aqueous CdS QDs

As an alternative method to the 2 step hot-injection + phase transfer approach for producing chiral CdS, it was decided to use a 1-step *in situ* aqueous synthesis of CdS QDs to prepare D- and L- penicillamine capped CdS chiral QDs. The synthesis was adapted from the previous report by Govan *et al*<sup>25</sup>. Originally used for the preparation of CdS tetrapods, by adjusting certain parameters, optically active CdS QDs were produced. The synthesis involves refluxing (4 hours) a mixture of a basic solution of penicillamine, cadmium nitrate and thioacetamide as a sulphur source. The resulting QDs were isolated and cleaned by precipitation with acetone followed by redispersion in water. From the results presented below it appears that the synthesis has slight issues with regards to reproducibility. The CdS produced was always luminescent and optically active however the QD sizes would vary from batch to batch. Every effort was undertaken to reduce variation in the synthesis therefore the only parameter believed to be responsible for batch variations is the inconsistent rate of heating of the hot plates. In heating up preparations of QDs, the

heating ramp rate is extremely important for controlling growth and nucleation<sup>26</sup>. Therefore, unintended differences in ramp rates may have led to a difference in nucleation and growth regimes. 25% of the time this synthesis produced a single, smaller size distribution and 75% of the time it resulted in a mixture of different larger sizes, according to analysis of the spectroscopic data. The experiment was repeated in excess of 20 times. The single, smaller size distribution (sample **A**) will be discussed first, followed by analysis of the mixed size product (sample **B**). The UV-Vis data below (Figure 5-7) represents the single, smaller sample size (Sample **A**). Sample **A** was analysed using a combination of UV-Vis, PL and CD spectroscopies below.

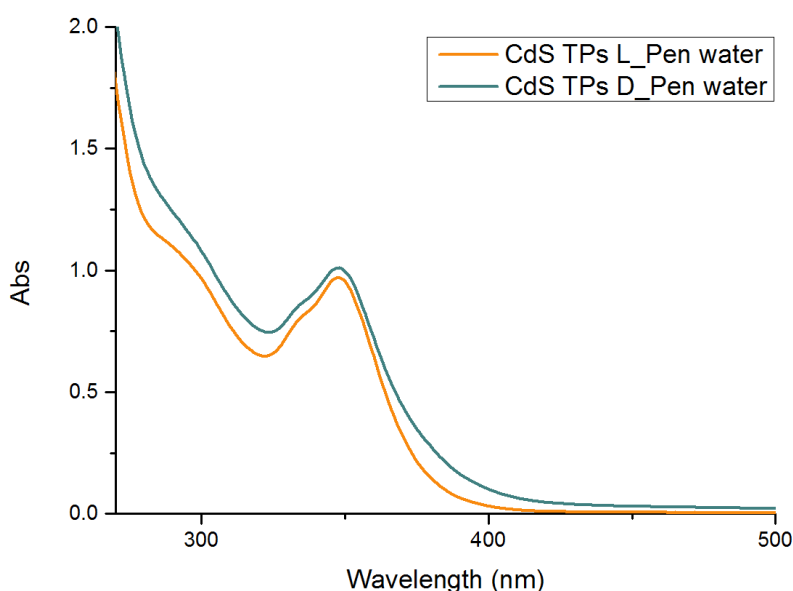


*Figure 5-7 UV-Vis spectra of CdS QDs (Sample A).*

The UV-Vis spectral shape is consistent with what you would expect for binary QDs, exhibiting a defined first exciton. The D- and the L- penicillamine capped QDs both have similar spectra with a first exciton peak located at 355 nm. It is important to note that there is no shoulder present around 385 nm which is present in Sample **B** (discussed later). The onset of absorption in both samples begins around 400 nm. Following this, circular dichroism was used to investigate the chiral properties of QDs (Figure 5-8).



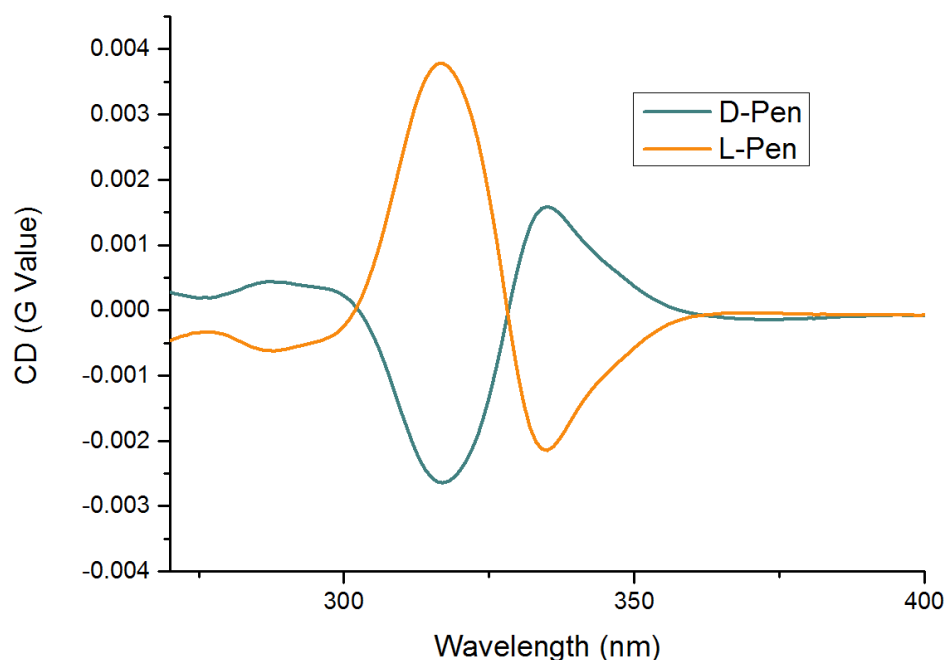


*Figure 5-8 CD spectra for CdS QDs (Sample A).*

The CD spectra above clearly demonstrate that the resultant CdS QDs display very strong optical activity. The signals for the D- and L- penicillamine stabilised QD samples are mirror images of each other with 2 primary peaks located at 317 and 335 nm. The magnitude is significantly higher than would be observed for quantum dots synthesised in the organic phase and transferred to the aqueous phase using chiral ligands. With a maximum intensity of  $4 \times 10^{-3}$ , these QDs have demonstrated optical activity orders of magnitude greater than other chiral QDs produced by other means. It also important to note that there is nearly no optical activity observed between 400 and 375 nm, which differs to Sample **B** discussed next. While these particles are luminescent, no excitonic luminescence was observed (Figure 5-9). These QDs display broad emission from 400 nm to 700 nm characteristic of defect luminescence. Defect luminescence is commonly found in quantum dots synthesised using aqueous methods as the presence of oxygen and water result in surface defects providing a large number of non-radiative decay pathways. The L- and D- pen CdS samples have their peak intensities located at 503 and 508 nm respectively. The slight red shifting of the D-Pen sample when compared to the L-

Pen sample may be due to a slightly higher size distribution of this sample, which is also reflected in the slight differences in the UV-Vis above.

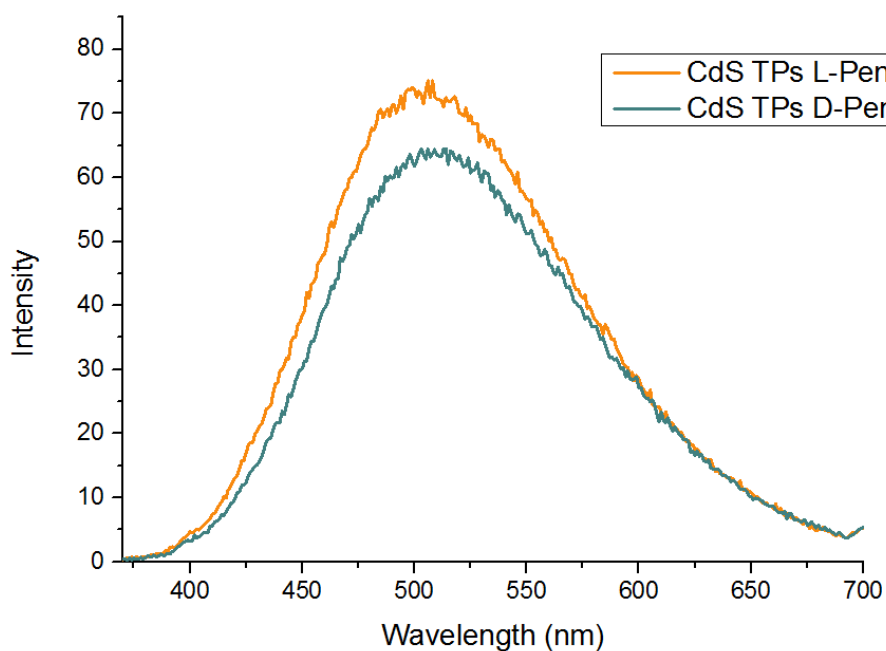


*Figure 5-9 PL spectra of CdS QDs (Sample A) (Ex.  $\lambda$  – 325 nm).*

The sample discussed up until this point (sample **A**) was the product of the synthesis about 25% of the time. The rest of the time the product (sample **B**) seems to have a much wider size distribution which is reflected in the UV-Vis (Figure 5-10) and CD spectra (Figure 5-11). It is important to note that sample **A** does not grow into sample **B** with an increased reflux time, increasing the reflux time appears to increase the intensity of the CD peaks, however it has no observable impact on the size distributions. UV-Vis data presented below show that the sample **B** product still possesses the peak located at 355 nm, but there is the introduction of a significant shoulder at 385 nm which was not present in sample **A**. As this appears to be the emergence of a new peak, rather than the red shifting of the existing exciton peak we can infer that a second, larger size distribution is being produced simultaneously.

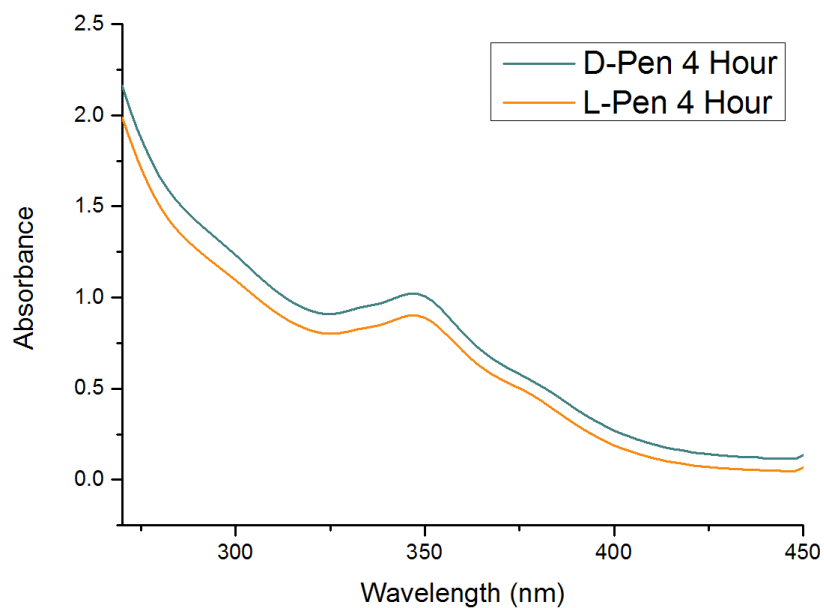


*Figure 5-10 UV-Vis spectra of CdS QDs (sample B).*

When comparing the CD spectra from sample **A** to the CD spectra from sample **B** (Figure 5-12) it is clear that both similarities and differences are present. The primary difference is the emergence of a new peak with a maximum at 385 nm which is only barely visible in the spectra for sample **A**. The CD spectra for sample **B** still contains the peaks at 317 and 335 nm, no shift in these peak positions is noted.

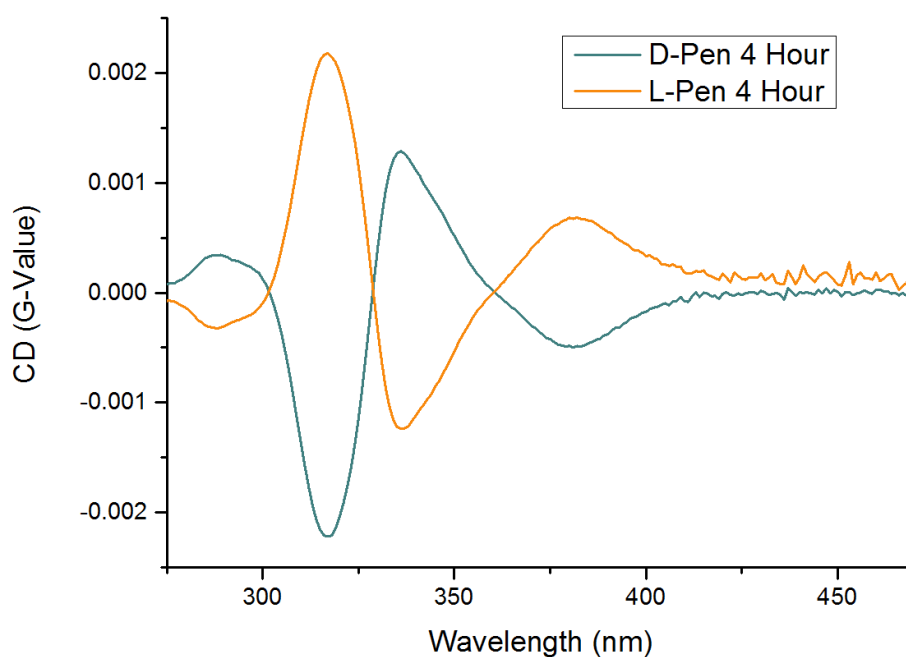


*Figure 5-11 CD spectra of sample B.*

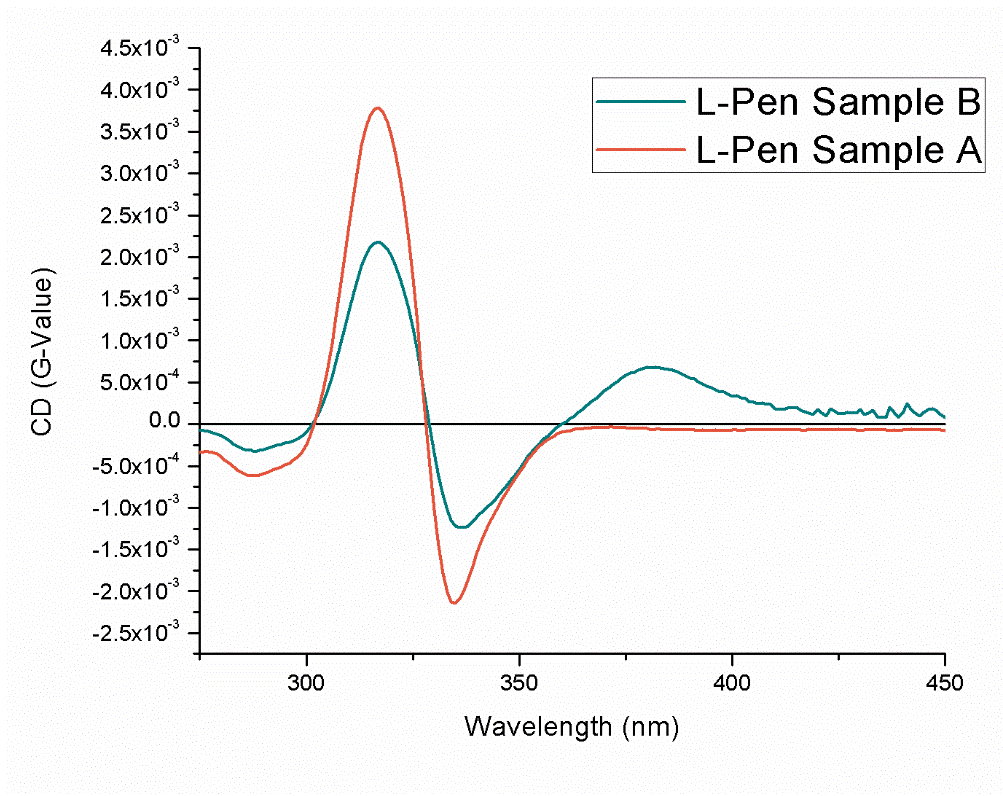


*Figure 5-12 Comparison of CD spectra for Sample A and Sample B.*

When we compare the intensities of the G-Values for the Sample **A** and Sample **B** clear differences are also present. In sample **A**, the single size sample, the intensity of the peaks is far larger when compared to sample **B**. The results are tabled below for easy comparison.

	Sample <b>A</b>	Sample <b>B</b>
Intensity at 317 nm (peak 1)	$3.7 \times 10^{-3}$	$2.1 \times 10^{-3}$
Intensity at 335 nm (peak 2)	$2.1 \times 10^{-3}$	$1.2 \times 10^{-3}$
Intensity at 385 nm (peak 3)	$3.7 \times 10^{-5}$	$6.8 \times 10^{-4}$

*Table 5-1 Relative intensities of CD peaks for CdS QDs (sample A and B).*

For the peaks at 317 nm and 335 nm, sample **A**'s intensities are nearly twice that of sample **B**'s. Conversely the intensity of the peak at 385 nm is 20 times larger in sample **B**. This would indicate that in sample **A** there exists a narrower distribution of sizes, whereas in sample **B** larger QDs are also produced. This would explain the

decrease in peaks 1 and 2 and an increase in peak 3 when comparing sample **A** and **B**.

Sample **B** was then analysed using photoluminescence to detect any differences in peak positions.

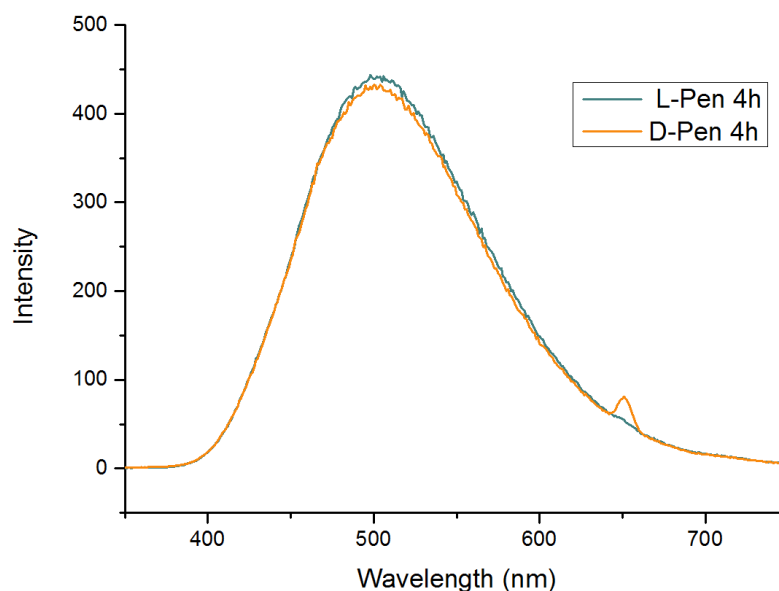


*Figure 5-13 PL spectra for D/L Pen CdS QDs (sample **B**) (Ex.  $\lambda$  – 325 nm).*

Both the D and L- penicillamine capped QDs in sample **B** have near identical PL spectra and the peak positions are closely in line with the result for sample **A**. As the emission from both sample **A** and **B** are defective in nature it is unsurprising that no observable shift in peak position occurs.

In order to investigate any differences in size, TEM analysis was performed. From analysis of the TEM images for sample **A** (Figure 5-14) and sample **B** (Figure 5-15), it is clear that the particles are spherical in both cases. From the TEM for sample **A**, it appears that a higher degree of aggregation may be present also. Using the size distribution histograms, the sizes were calculated to be  $4.36 \pm 0.47$  nm for sample **A** and  $4.48 \pm 0.86$  nm. The average sizes here would confirm what was proposed from the spectroscopic data, however the large standard deviations would infer that a slightly more detailed statistical analysis is required. By using a 2-value t-test (appendix Figure 8-9), the significance of the above results can be analysed. Using

this analysis, there is a 95% likelihood that a difference in the averages of sample **A** and sample **B** lies between -0.03 nm and 0.26 nm exists. As this confidence interval includes zero we cannot conclusively say that there is a difference, however if we lower our confidence interval to 90% the results become significant. In conclusions, we can say that sample **B** has a larger average diameter than sample **A** with 90% confidence.

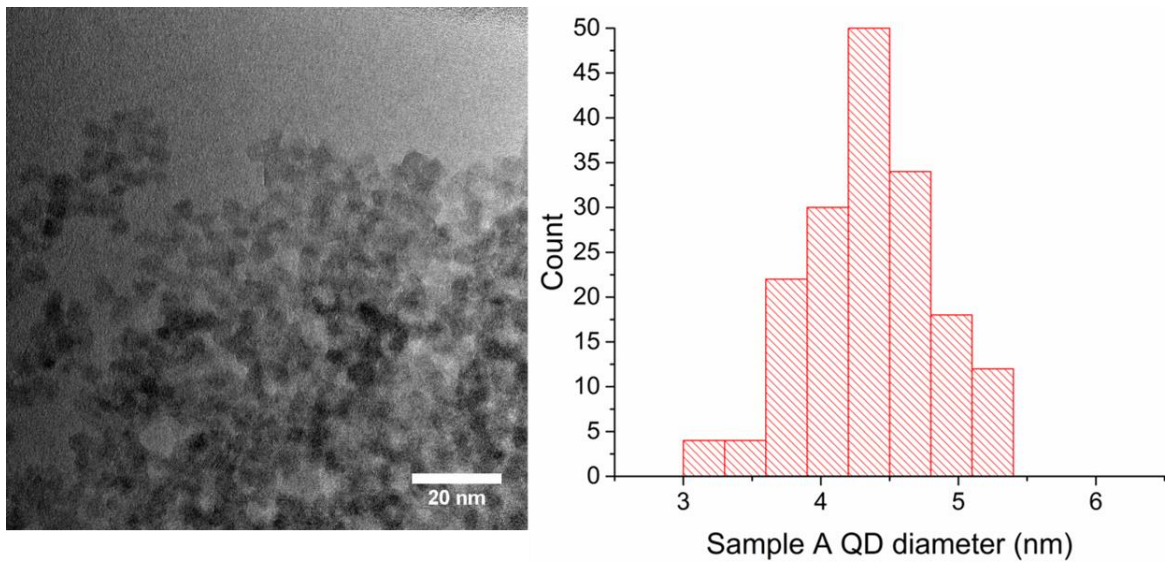


Figure 5-14 TEM image (left) and size distribution histogram (right) for D-Pen CdS Sample **A** ( $n = 150$ ).

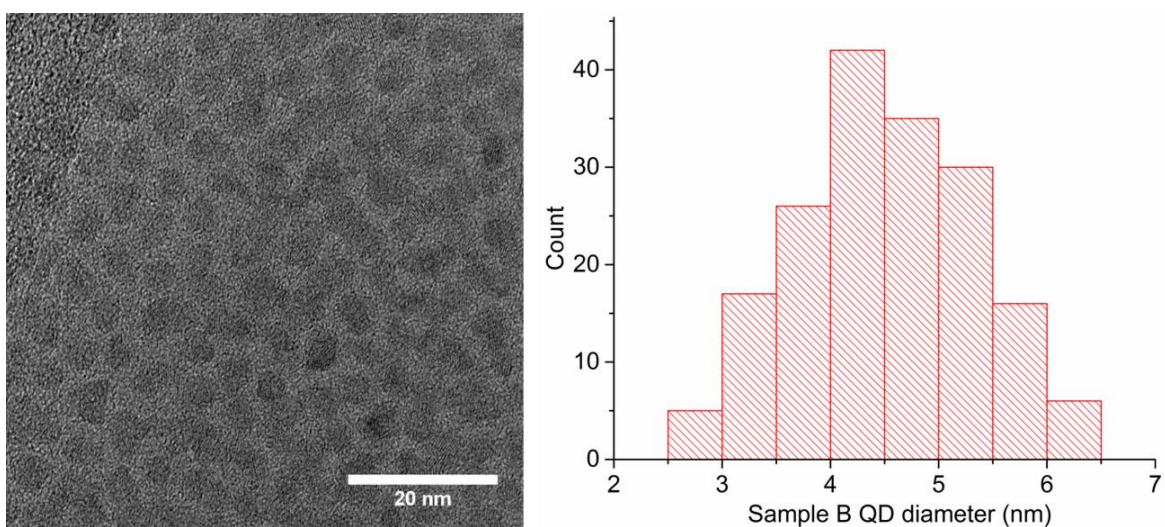
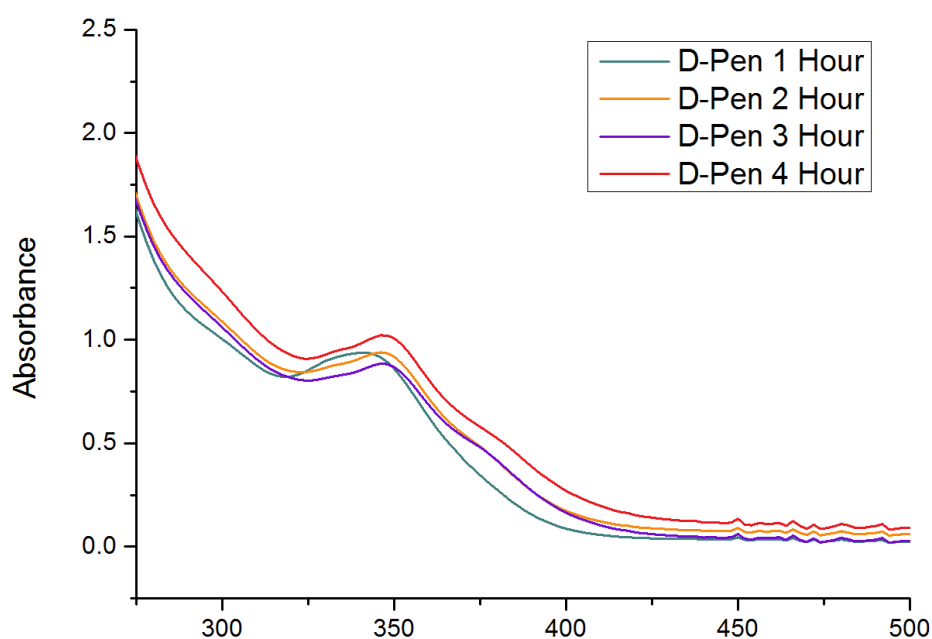


Figure 5-15 TEM image (left) and size distribution histogram (right) for D-Pen CdS Sample **B** ( $n = 150$ ).

Initially it was anticipated that sample **A** grows into sample **B** during the 4-hour reflux so in order to verify this, time resolved studies were carried out to monitor growth during the 4 hour reflux. From the subsequent results it becomes clear that this is not the case and in fact there is never a point where sample **A** resembles sample **B** in terms of UV-Vis and circular dichroism. The UV-Vis spectra below in Figure 5-16 show that the sample **B** excitonic peak is much broader than in sample **A**. Secondly, the emergence of the shoulder around 375 nm begins after 1 hour and is clearly present by the second hour of the reflux in the sample **B**, this peak never appears in sample **A**.



*Figure 5-16 UV-Vis spectra during reflux for sample B D-Pen*

Interestingly, when analysing the PL spectra (Figure 5-17), there is nearly zero change in the PL intensity throughout the reflux. There is a slight red shifting of the PL intensity from 1 to 4 hours reflux time which is to be expected however the shift is negligible (4 nm).

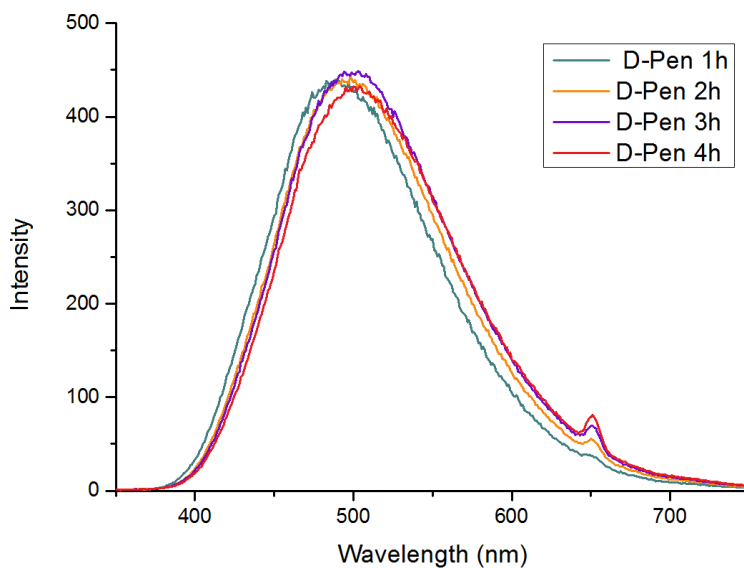


Figure 5-17 PL spectra during reflux for sample **B** (D-Pen) ( $\lambda$  ex. – 325 nm).

While the UV-Vis and PL remain roughly unchanged, the CD spectrum changes significantly as a function of reflux time. Not only do the peak intensities change, but the peak positions also shift, with the noticeable shift being the blue shifting of peak 1 over time. With regards to intensity, peak 1 and peak 2 dramatically increase in intensity after the 4-hour reflux.

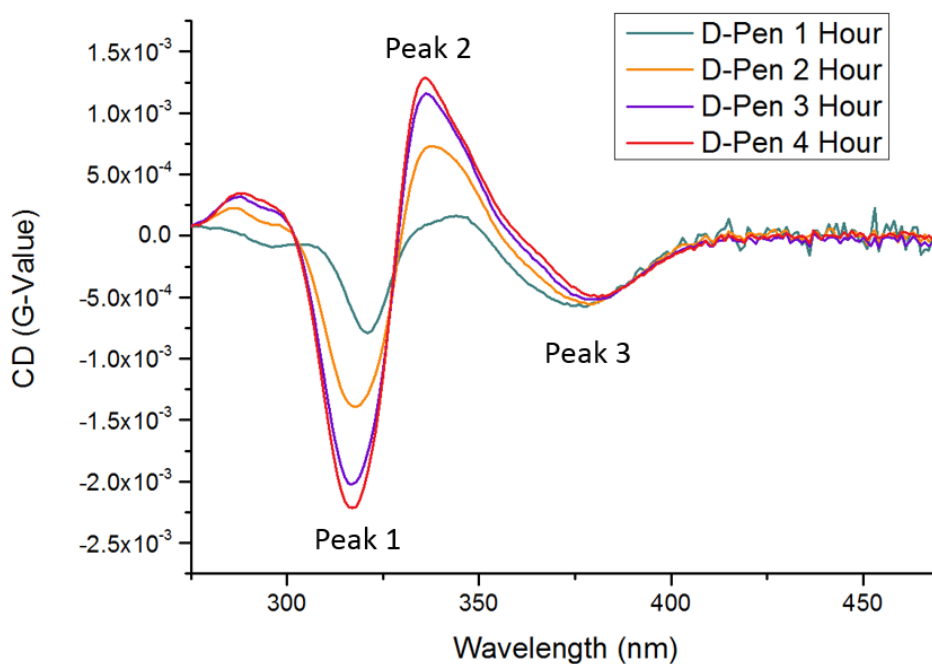
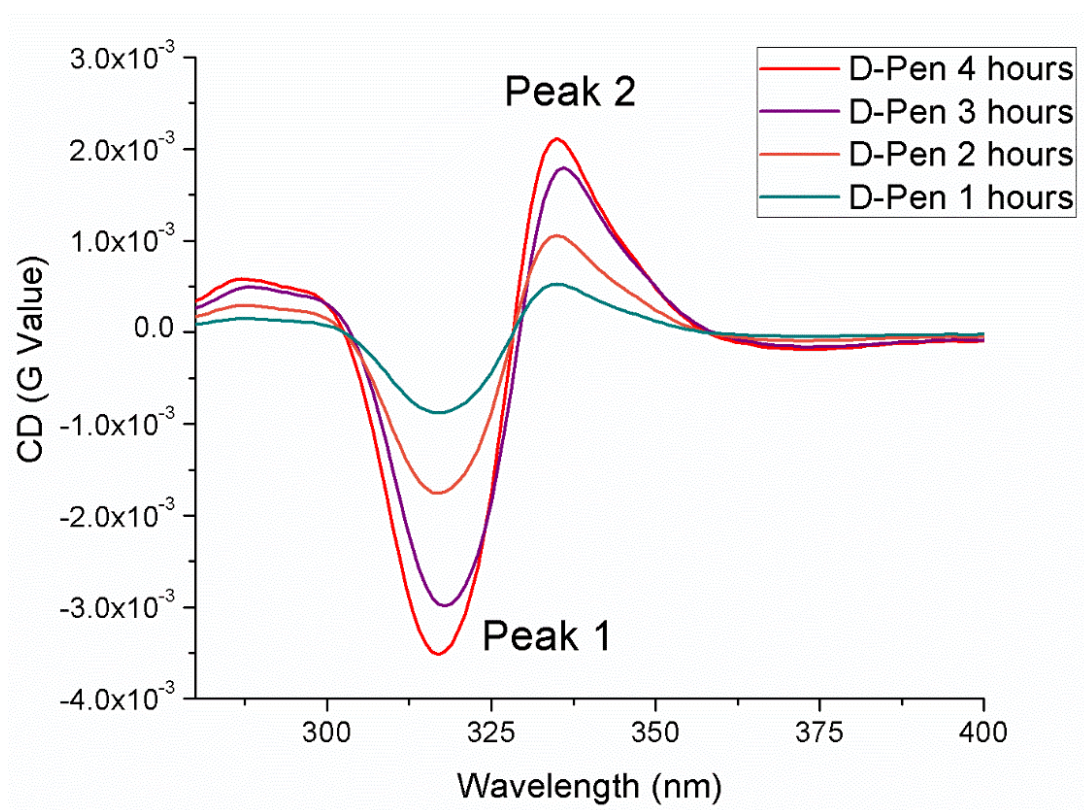


Figure 5-18 CD spectra over time for CdS QDs sample **B** (D-Pen).



It was suggested that the shifting in peak intensities with time was related to the growth of the larger population in sample **B**. However, by comparing the increase in CD intensity of peak 1 and 2 in both sample **A** (Figure 5-19) and sample **B** (Figure 5-18) it becomes evident that this isn't the case. As the intensity of peak 1 and 2 increase during the 4-hour reaction for both sample **A** and sample **B** it is believed that the development of the CD signal is a result of an increase in the concentration of smaller QDs in both samples **A** and **B**.



*Figure 5-19 CD spectra over time for CdS QDs sample A (D-Pen).*

This time resolved analysis of the CdS synthesis for sample **B** was performed for both L- and D- penicillamine samples to ensure that the results were identical for the 2 opposite enantiomers (Figure 5-20). By recording measurements at both 2 and 4 hours into the reflux, mirror image CD spectra develop at the same rate over time, confirming the synthesis works the same for both L- and D- penicillamine.

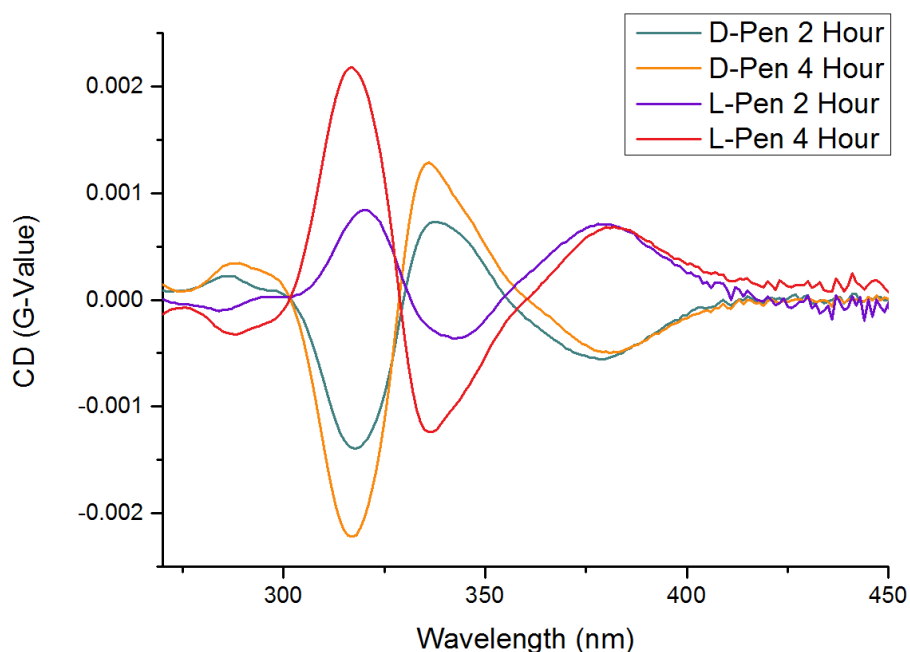


*Figure 5-20 CD spectra at t = 2 hr and t = 4 hr of reflux for CdS QDs.*

Due to the high G-value results for these CdS QDs it was decided to perform a reverse phase transfer on these QDs using dodecanethiol. The protocol for this may be found in section 2.4.5 of the experimental chapter. The process involves simple mixing of the aqueous QDs with a solution of DDT in chloroform which is allowed to stir for several minutes followed by extraction of the organic layer. Both samples have been analysed by circular dichroism spectroscopy (Figure 5-21). DDT (D-Pen) represents the results of performing the DDT phase transfer on the D-Pen stabilised CdS QDs (Sample 2) and likewise DDT (L-Pen) represents the results of performing the DDT phase transfer on the L-Pen stabilised CdS QDs (Sample 2). There is some theory on the possibility of chiral imprinting for some nanomaterials<sup>27</sup>. This theory states that in some nanomaterials, optical activity is not the result of an electronic interaction between the chiral ligand and the achiral core but rather chiral defects on the surface of the nanomaterial create optical activity. Due to the very large optical activity of our quantum dots we aimed to investigate if the origin of the CD signal was a result of the electronic interaction or a chiral imprint. If the chiral penicillamine could be replaced with the achiral DDT and optical activity still

persisted it could be concluded that the optical activity was imprinted in the QD (so called “chiral memory effect”)<sup>27</sup>.

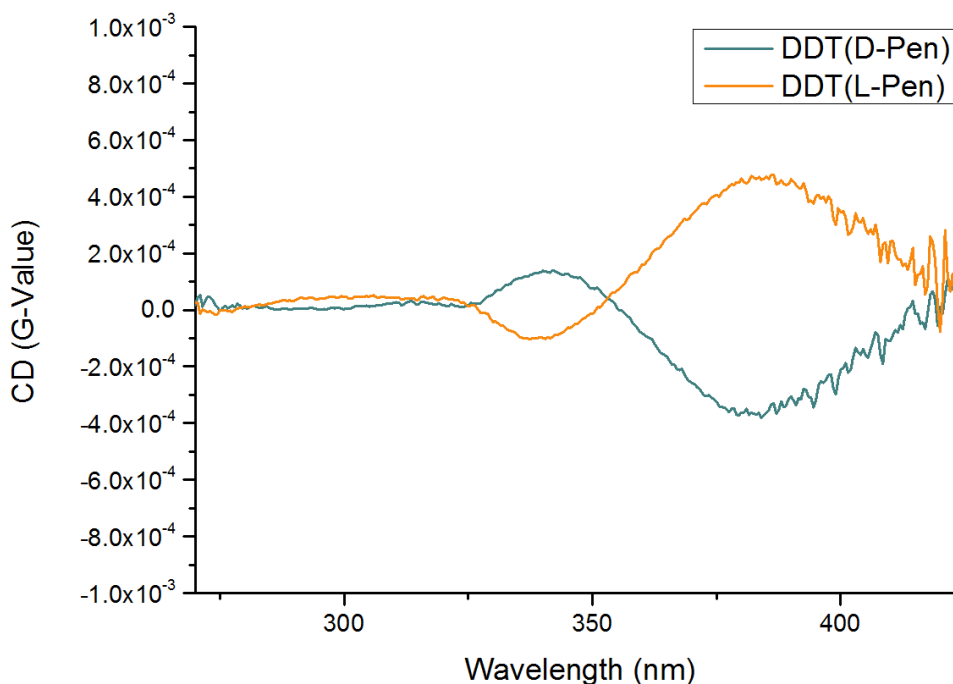


*Figure 5-21 CD spectra for DDT stabilised CdS QDs.*

The CD spectra above clearly demonstrates that optical activity is still present in the organic phase, after the penicillamine has been replaced with dodecanethiol. It is interesting to note that peak 1 (317 nm) and peak 2 (335 nm) have either diminished entirely or are drastically reduced, while peak 3 seems to remain prevalent in the organic phase. This may suggest that the origin of peaks 1 and 2 could be primarily electronic in nature whereas peak 3 may derive from a more structural feature of the QDs. Unfortunately, the QDs did not remain stable in the organic phase and so it was difficult to perform detailed analysis on the particles. UV-Vis data in Figure 5-22 was taken after CD analysis and demonstrates inconsistencies in absorption between the D and L samples which is reflected in the instability in the samples. Due to these instability issues, no further analysis was carried out.

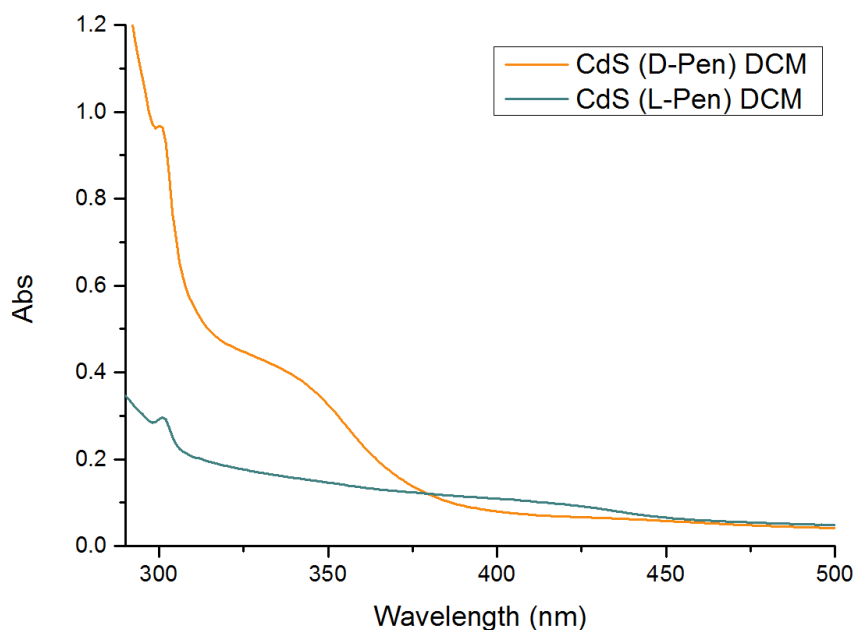


Figure 5-22 UV-Vis for DDT stabilised CdS QDs.

## 5.5 Synthesis of Cysteine capped CdS

To compare the effects of different ligands on the products the same aqueous synthesis of CdS was carried out using D- and L- cysteine ligands instead of penicillamine. The synthesis was successful and resulted in luminescent, optically active QDs, however control of the synthesis was limited and it was difficult to create D- and L- cys samples with the same absorption and luminescence with opposite optical activity. Kinetically, cysteine is more reactive than penicillamine because it does not have the 2 methyl groups adjacent to the thiol. This increased reactivity could be the cause for inconsistency in the products formation. This synthesis was carried out using a reaction time of 2 hours instead of 4 hours as performing this synthesis for 4 hours produced even more varied results when comparing the D-Cys and L-Cys samples. Figure 5-23 below demonstrates the inconsistency between the D- and L- cysteine stabilised CdS products. It may be noted that this was the closest the 2 absorption profiles would match up. It's clear that both samples demonstrate quantised absorption with broad distribution due to the relatively broad nature of the peaks. The L-Cys CdS sample would appear to have grown larger than the D-cys sample also.

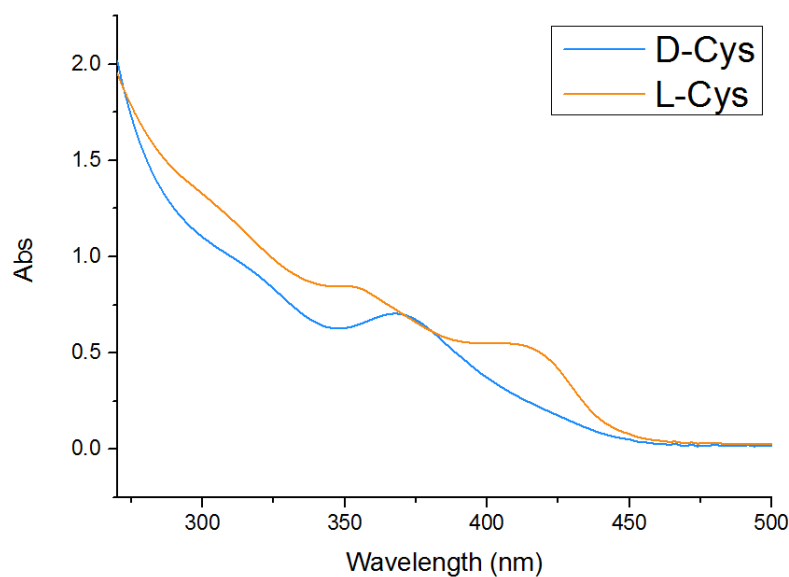


Figure 5-23 UV-Vis data for cysteine stabilised CdS QDs (2 hr reflux).

PL spectroscopy was carried out to determine if these samples are luminescent. These QDs display broad defect luminescence similar to the penicillamine stabilised QDs, however the PL intensity is not consistent in intensity between D and L cys samples. The defect luminescence was observed between 400 and 700 nm.

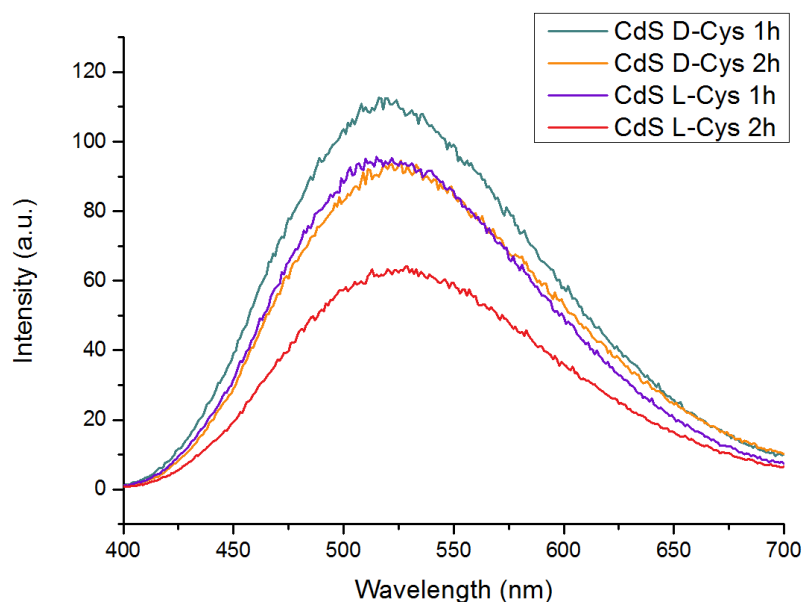


Figure 5-24 PL spectra for luminescence ( $\lambda$  ex. – 325 nm).

Finally, CD analysis was carried out to investigate the optical activity of these QDs (Figure 5-25). Both L and D cysteine stabilised QDs demonstrate optical activity in

the exciton absorption region of the spectrum, however the CD signals are not equal and opposite as would be expected for opposite enantiomers. The fact that the CD spectra are not identical and opposite is consistent with the differences in the absorption spectrum as well.

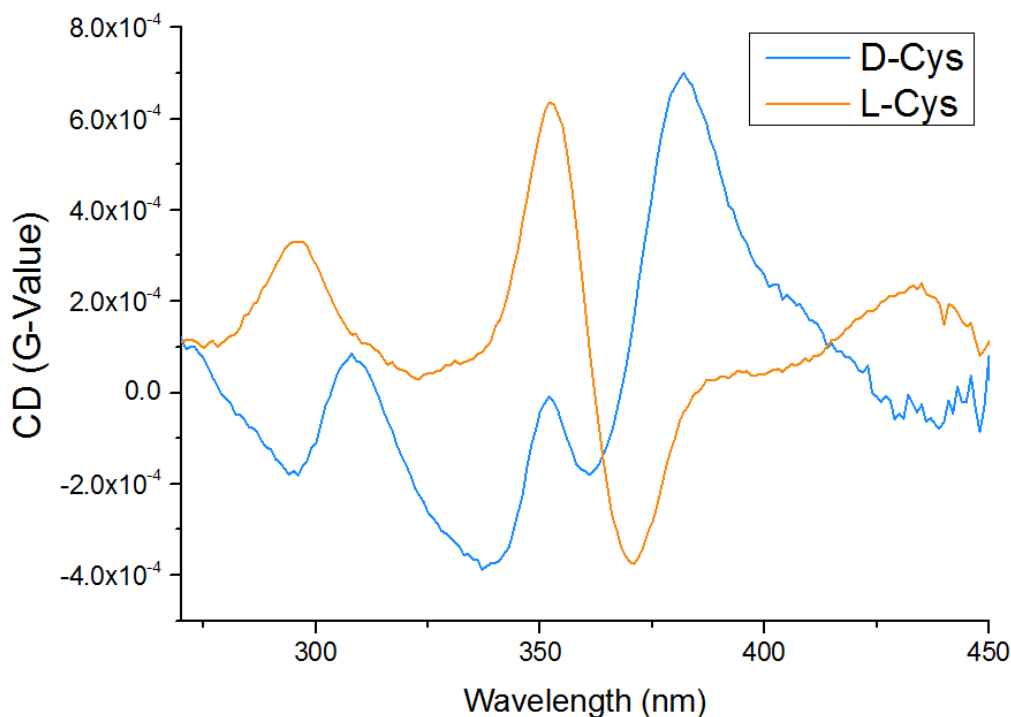


Figure 5-25 CD spectra for D and L cys stabilised CdS QDs.

Due to the significant lack of control in reproducing CdS samples capped with cysteine, no TEM was performed.

## 5.6 Synthesis of optically active CdSe QDs

Due to the higher surface to volume ratio in smaller QDs, we aimed to produce some very small CdSe QDs and investigate their chiroptical properties. To do this we aimed to synthesise small CdSe QDs in the organic phase in order to perform their phase transfers and analyse the resulting CD properties. The CdSe QDs were synthesised using a hot technique developed by Dr. Finn Purcell Milton of the Gun'ko group, the

synthesis is described in section 2.4.3 of the experimental chapter. In summary, it involves the low temperature combination of Cd(oleate), TOPSe, and CTAB under anaerobic conditions. The QDs were then transferred to the organic phase using the original phase transfer technique which was used for the ZnS:Mn QDs. Figure 5-26 below displays the UV-Vis and PL spectra for the D-Pen stabilised CdSe QDs. The UV-Vis spectra is characteristic of QDs with an onset located at 450 nm and a first exciton absorption maximum located at 385 nm. This high energy first exciton peak would indicate highly confined, very small QDs which was confirmed by TEM analysis. The PL spectra below would indicate that these QDs demonstrate defect emission with no excitonic emission present in the spectra. These QDs were synthesised at a low temperature in order to produce small QDs, however this meant that little to no annealing took place. The defective nature of the emission is unsurprising given how the QDs were prepared. It is interesting to note that nearly no loss in emission was observed when comparing the emission before and after the phase transfer, this may relate to the fact that the emission is defect emitting, as opposed to excitonic.

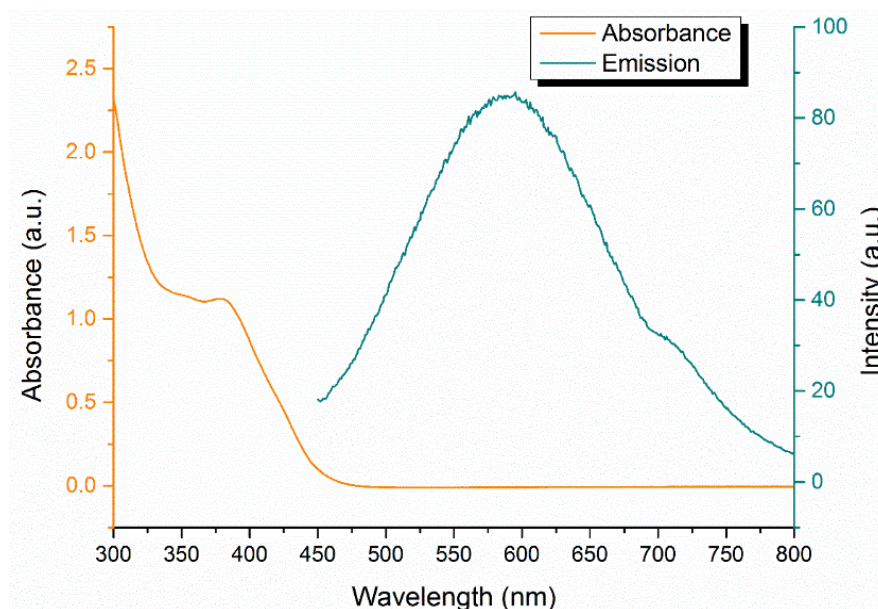


*Figure 5-26 UV-Vis and PL spectra for D-Pen stabilised CdSe QDs ( $\lambda$  ex. – 400 nm).*

Following absorbance and emission analysis the QDs were investigated using CD spectroscopy (Figure 5-27). While it was expected that the smaller QD size would

result in a larger CD signal, evidence of this is not presented in the results in Figure 5-27. However, the CD spectra do appear to be a lot less noisy than other CD spectra for chiral quantum dots. So, while the CD intensity may not be a function of size in this case, signal to noise ratio is quite low. The onset of the CD spectra corresponds with the onset of QD absorption and the CD spectra for the D- and L- penicillamine stabilised QDs are equal and opposite. Peak maxima in the CD spectra are located at 425 nm, 365 nm and 325 nm.

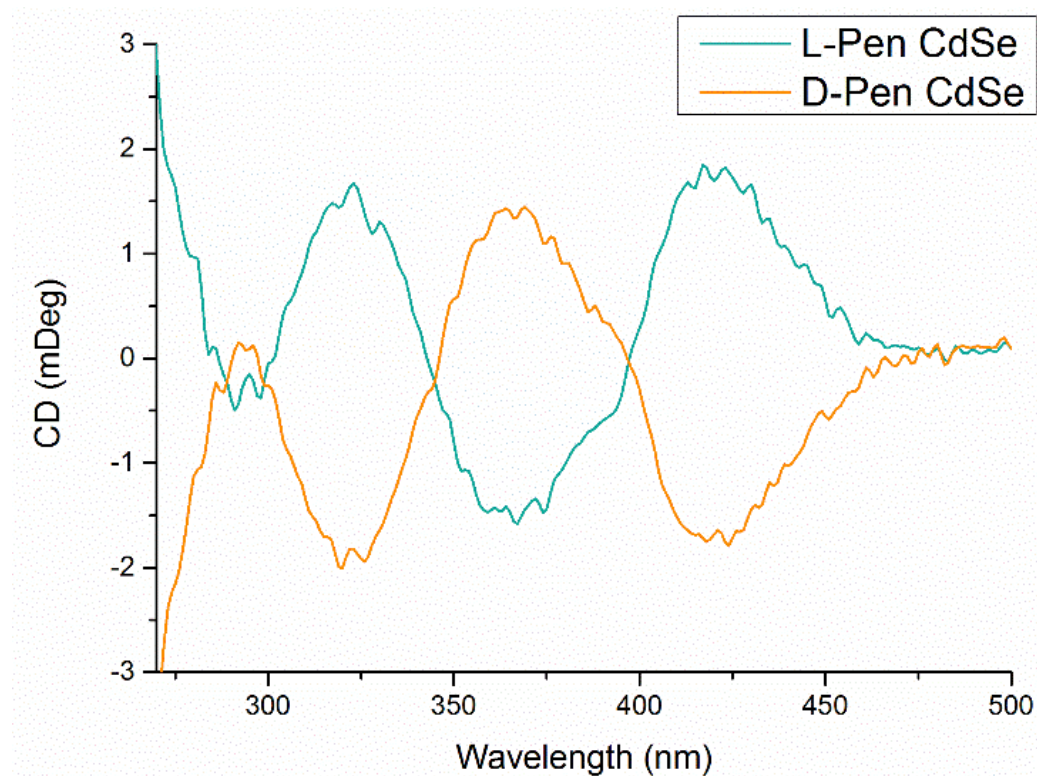


*Figure 5-27 CD spectra for D and L penicillamine stabilised CdSe QDs in H<sub>2</sub>O.*

Finally, TEM analysis was performed on the D-Pen CdSe QDs to verify their size. Due to the small size of the QDs, HRTEM was difficult to perform and lattice fringes were not visible however normal TEM was sufficient to perform size distribution analysis on the sample. The QDs appear to be roughly spherical in shape with an average size of 3.4 nm, this correlates well with the UV-Vis data for the same particles.



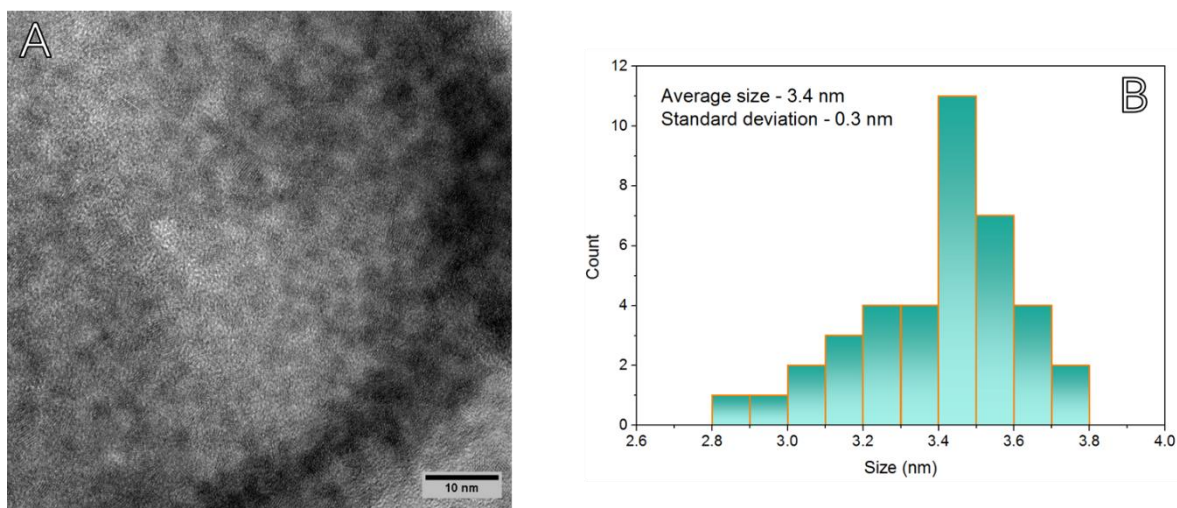
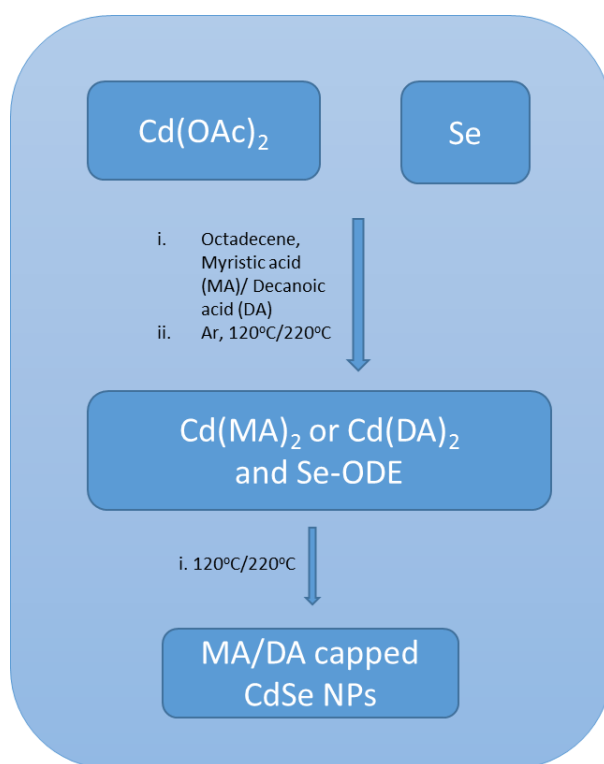


Figure 5-28 (A) TEM and (B) Size distribution for D-Pen CdSe QDs.

## 5.7 Synthesis and characterisation of CdSe nanoplatelets

In an effort to further investigate very small CdSe QDs, the synthesis of so-called “magic size” CdSe QDs<sup>28-31</sup> was attempted. Magic sized QDs are ultra-small nanoclusters whose configuration leads to a very low surface energy with respect to other closely related sizes. This leads to nanocrystals with an extremely close size distribution for any given magic size. Due to the very high surface to volume ratio, it was expected that we could induce stronger CD signals than were typically expected for larger QDs. Therefore, we aimed to synthesise a variety of “magic size” CdSe QDs, perform phase transfers on them and then analyse the resulting CD spectra. As using thiolated carbohydrates as ligands for QDs was part of our research it was planned to conjugate thiocarbohydrates to these magic sized QDs and investigate their optical properties and potential applications such as *ex vivo* imaging. These QDs samples were analysed using TEM, UV-Vis, PL and circular dichroism spectroscopy, however upon analysis of the products it became clear that the synthesis in fact resulted in CdSe nanoplatelets, confined in only 1 dimension, not “magic size” QDs. The growth of nanoplatelets of defined thickness from magic sized nanoclusters was previously documented<sup>8,32,33</sup> and appears to be greatly influenced by the counter anion present. The use of the acetate ion from cadmium

acetate in this case helps promote lateral growth of magic sized CdSe QDs into platelets. As one of the aims of this research was to investigate chirality in anisotropic nanomaterials the of CdSe nanoplatelets (NPs) presented a great interest to us and these nanomaterials have been studied in details. In our work nanoplatelets of varying sizes were synthesised using organic ligands such as myristic acid or decanoic acid, the full synthesis is provided in section 2.4.6 of the experimental section. Briefly, cadmium acetate, selenium and either myristic or decanoic acid were mixed together in octadecene and heated for several hours. Their growth was monitored by UV-Vis and a brief scheme of the reactions is presented in Figure 5-29 below.



*Figure 5-29 Scheme for the synthesis of CdSe nanoplatelets.*

Results presented below show that the synthesis temperature and acid used (decanoic or myristic) play important roles in the final size of the CdSe NPs.

Sample Number	Reaction conditions	Thickness
Sample 1	220 °C, myristic acid	1.5 nm
Sample 2	130 °C, decanoic acid	1.5 nm
Sample 3	220 °C, myristic acid, manganese doped	1.5 nm
Sample 4.1	120 °C, myristic acid	1.2 nm and 1.5 nm (mixture)
Sample 4.2	Sample 4.1 left to mature for 8 weeks	1.2 nm and 1.5 nm (mixture)
Sample 5	120 °C, decanoic acid	1.2 nm

*Figure 5-30 Table of reaction conditions for synthesis of CdSe nanoplatelets for reference*

The synthesis of NPs using myristic acid at 220 °C resulted in platelets with an average thickness of 1.5 nm (Sample 1). Similarly, the synthesis of nanoplatelets at 130 °C using decanoic acid also gave nanoplatelets with an average thickness of 1.5 nm (Sample 2). The UV-Vis and PL spectra presented below in Figure 5-31 and Figure 5-32 provide some insight into the optical properties of these nanoplatelets. The spectroscopic data would indicate that these 2 different syntheses (using myristic and decanoic acid) produce platelets of the same thickness. However, upon TEM analysis it appears the length and width for these 2 samples was quite different. Throughout our research we produced 2 different thicknesses of nanoplatelet; the 4 monolayer product with a thickness of 1.2 nm (first exciton = 398 nm) and the 5 monolayer product with a thickness of 1.5 nm (first exciton = 463 nm).

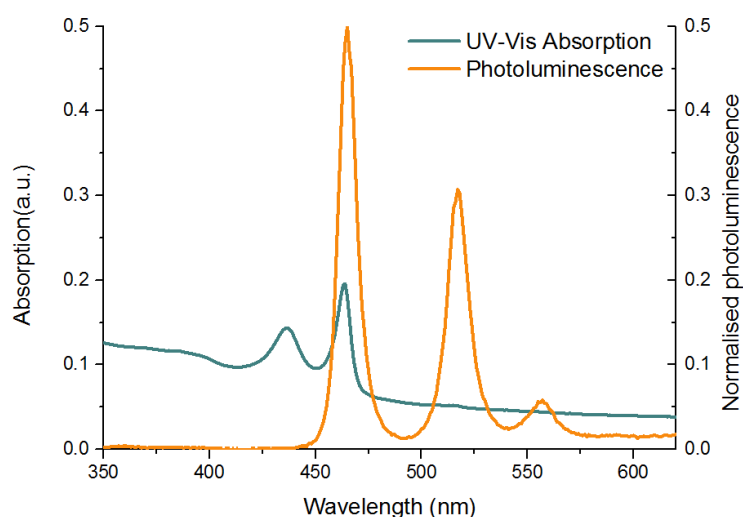


*Figure 5-31 UV-Vis and PL spectra for CdSe QPs with myristic acid, sample 1 ( $\lambda$  ex. – 420 nm).*

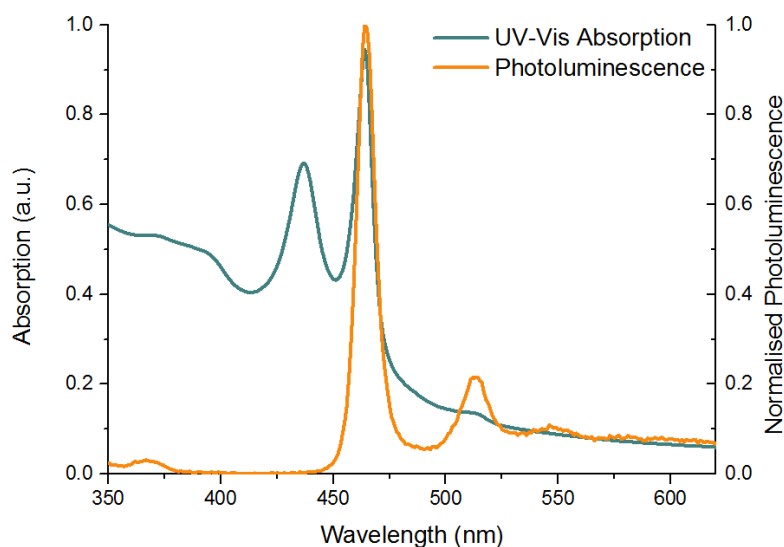


Figure 5-32 UV-Vis and PL spectra for CdSe QPs with decanoic acid, sample 2 ( $\lambda$  ex. – 420 nm).

The UV-Vis data above correlates well with literature records of CdSe nanoplatelet absorption<sup>3</sup>. Nanoplatelet absorption is slightly different than spherical QD absorption due to the presence of a double peak for the first exciton. This double peak is a result of 2 different band edge transitions taking place, relating to a heavy hole and a light hole transition<sup>34</sup>. The first exciton absorption maximum for both sample 1 and sample 2 is located at 463 nm. As confinement is only occurring in one dimension now, the exciton absorption wavelength is dependent on the thickness, so if these 2 samples have the same absorption wavelength, their thicknesses must be comparable.

While most QDs exhibit a certain amount of Stokes shift between the absorption and emission these nanoplatelets have a nearly zero Stokes shift. The first emissive wavelength occurs at 464 nm, with subsequent emission peaks located at 515 nm and 560 nm related to thicker, less abundant platelets in the sample.

TEM was used to analyse the CdSe nanoplatelets, in order to investigate their morphology and size distribution. The TEM images show a lot of rolling and scrolling of the nanoplatelets taking place which is consistent with literature<sup>35</sup>. Modification with octylamine and thioacetic acid (TAA) has been demonstrated to unroll the CdSe

nanosheets<sup>35</sup>. Using TAA as a sulfur source the CdSe nanoplatelets were coated with a CdS monolayer which flattens the nanosheets. We originally believed that the scrolling was a consequence of drying the samples for TEM, however literature offers a different explanation. XRD analysis performed by Bouet *et al.* demonstrated that the scrolling was also taking place in solution eliminating the possibility of drying effects<sup>35</sup>. They believe that the scrolling is due to an asymmetric strain between the two faces of the nanoplatelets. The cadmium atoms on the top and the bottom of the platelets are oriented at 90 degrees to each other and as a consequence the carboxylate capping agents bound to them could introduce the necessary strain for rolling and scrolling.

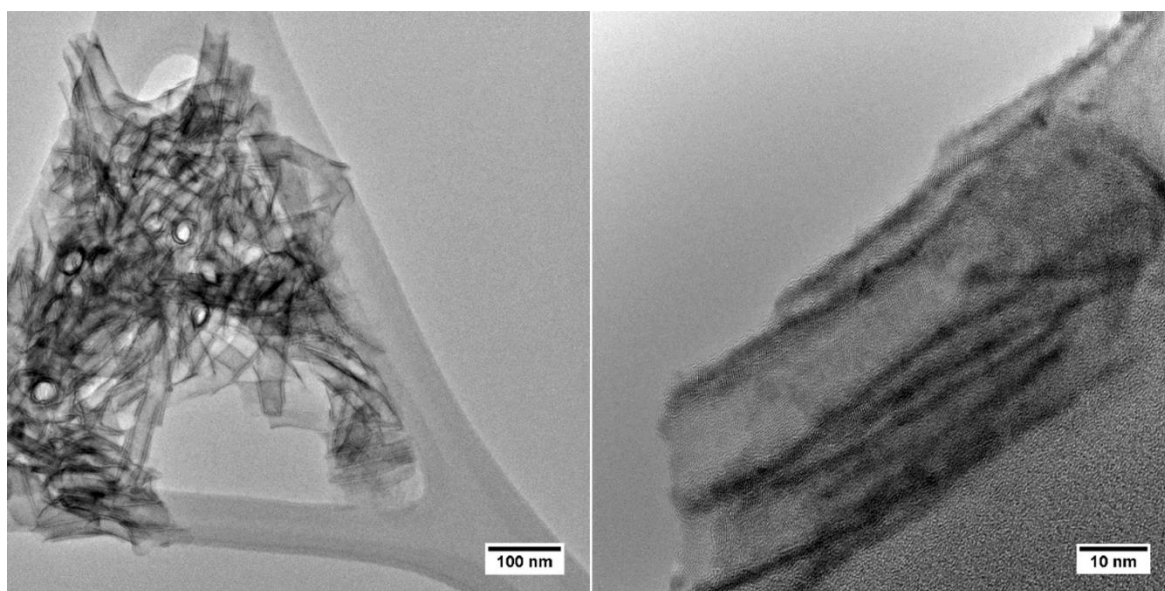


*Figure 5-33 TEM images of CdSe NPs with myristic acid as the ligand (Sample 1)*

The CdSe NPs synthesized using myristic acid as the capping ligand had an average scroll wall thickness of 1.5nm. The width and length of the scrolls were also calculated and the width of the scrolls were found to be 24nm and the scrolls were 94nm in length.

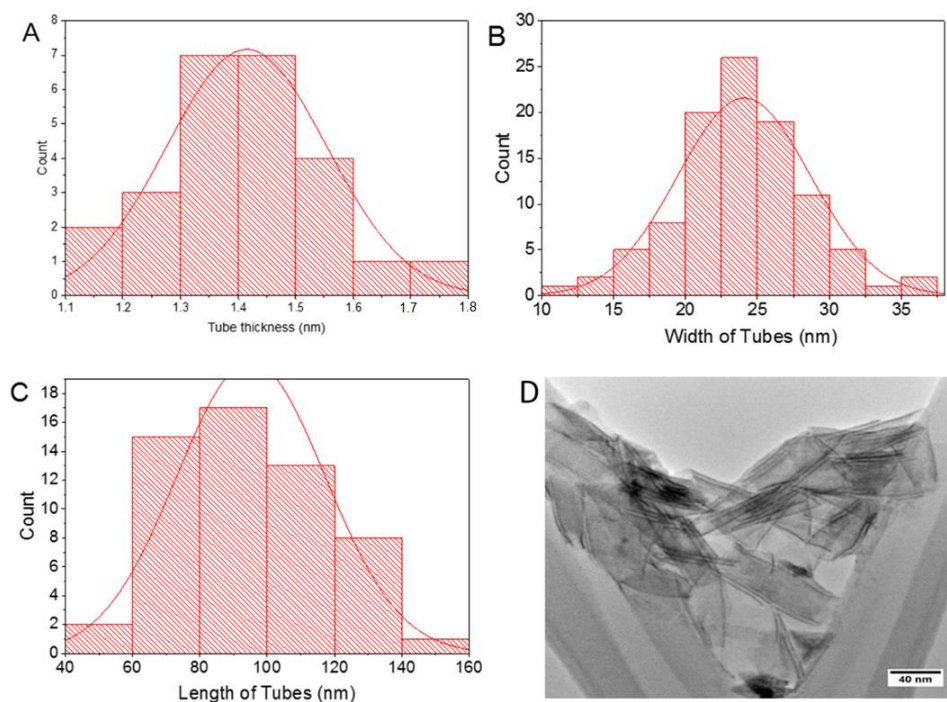


Figure 5-34 (A) CdSe QPs with myristic acid scroll thickness ( $n = 40$ ), (B) CdSe QPs with myristic acid tube width ( $n = 100$ ), (C) CdSe QPs with myristic acid scroll lengths ( $n = 100$ ), (D) TEM of size 1.5nm CdSe QPs with myristic acid.

Following this, TEM analysis was used to calculate the size of the CdSe platelets synthesised at 130 °C using decanoic acid as the capping ligand (Sample 2). From the UV-Vis it was anticipated that these platelets would have the same thickness as Sample 1 and TEM images have confirmed that.

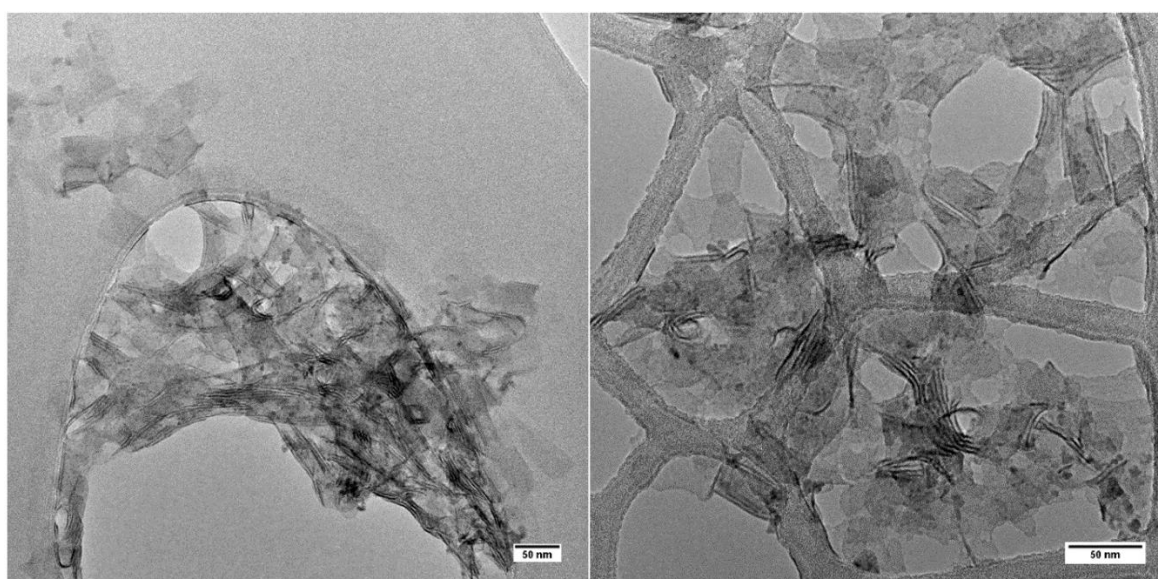


Figure 5-35 TEM images of CdSe NPs with decanoic acid as the ligand (Sample 2).

Although the CdSe NPs synthesized using decanoic acid as the capping ligand had the exact same scroll wall thickness of 1.5 nm, the width and length of the scrolls were found to be 21 nm and 57 nm respectively (Figure 5-36). So, while the thickness of the scrolls layers was the same for Sample 1 and Sample 2 the length and width of the scrolls were significantly different depending on what capping ligand was used. This may be as a result of the chain length of the capping ligand used (Decanoic acid – C10, myristic acid – C14).

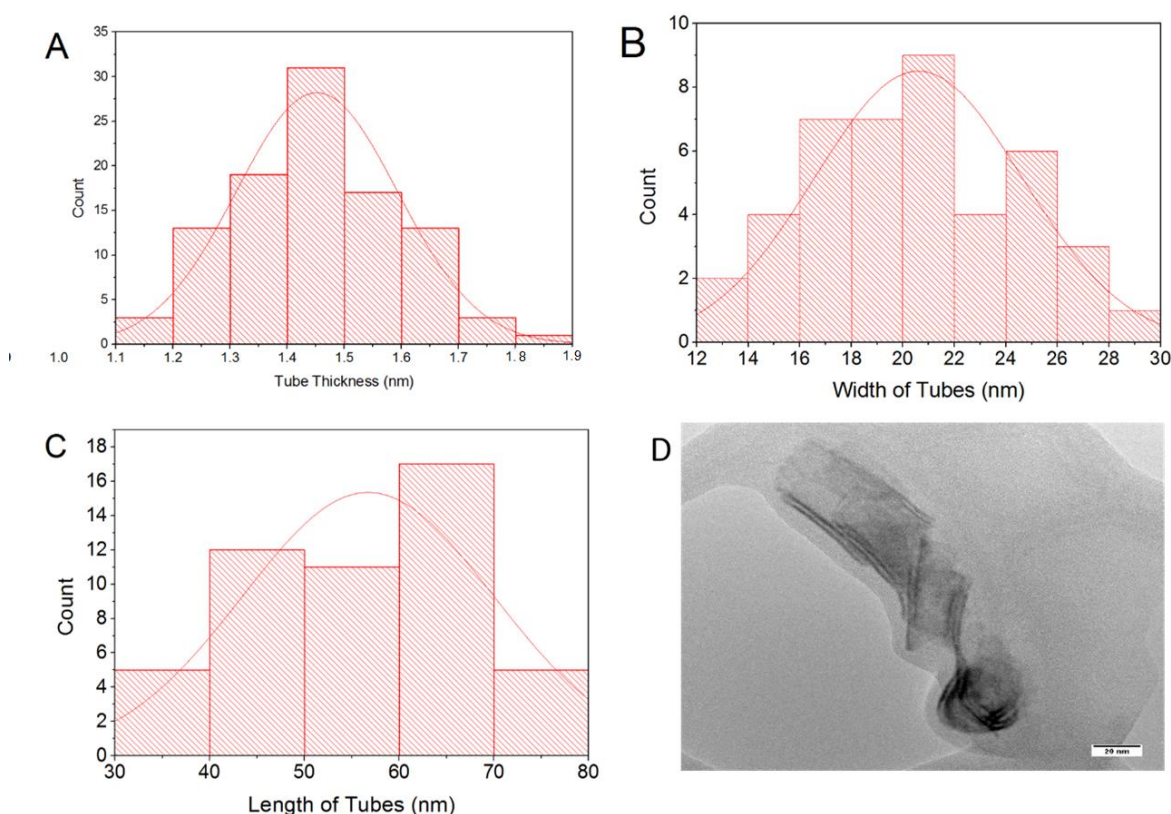
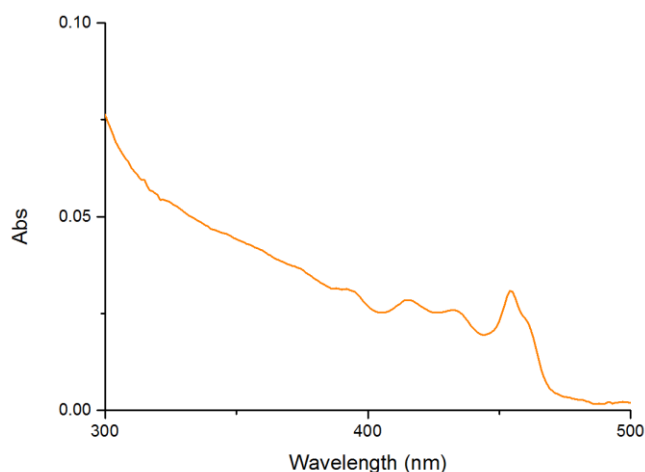


Figure 5-36 (A) Platelet thickness ( $n = 120$ ), (B) Scroll width ( $n = 60$ ), (C) Scroll length ( $n = 100$ ), (D) TEM of twisted CdSe nanoplatelets 1.5 nm (sample 2).

Following the synthesis of pure CdSe nanoplatelets with a thickness of 1.5 nm, it was also decided to synthesise CdSe nanoplatelets doped with manganese (Sample 3). Previous chapters discussed the doping of ZnS with manganese and so we were interested in the effect of doping on these CdSe platelets also. Manganese doped CdSe nanoplatelets were synthesised in a similar manner to the previous platelets,

however a small proportion of manganese acetate tetra-hydrate was added. The details of the synthesis can be found in section 2.4.10 of the Experimental section.

The manganese doped CdSe nanoplatelets were analysed using UV-Vis and PL to investigate the effect of manganese on the emission. The UV-Vis spectra in Figure 5-37 show that the manganese had an influence on the growth of these NPs. The peaks appear to be broader which would indicate less size control during the synthesis. The first exciton peaks located at 461 nm and 455 nm have broadened to the point of overlapping each other and so where you would normally expect to see 2 peaks it appears as 1 peak (455 nm) with a shoulder (461 nm). The position of the first exciton would indicate that these platelets had an average thickness of 1.5 nm.



*Figure 5-37 UV-Vis spectrum for CdSe:Mn nanoplatelets.*

These nanoplatelets were doped with manganese primarily to alter the luminescence which appears to have been successful. The introduction of manganese provides an alternative phosphorescent radiative decay pathway via a  $d \rightarrow d$  transition within the manganese. This causes a red shifting of the luminescence to 580 nm (Figure 5-38) similar to the ZnS:Mn QDs investigated in previous chapters. The peak located at 465 nm would appear to be the excitonic emission indicating that there is not 100% energy transfer from the CdSe conduction band to the  $Mn^{2+}$



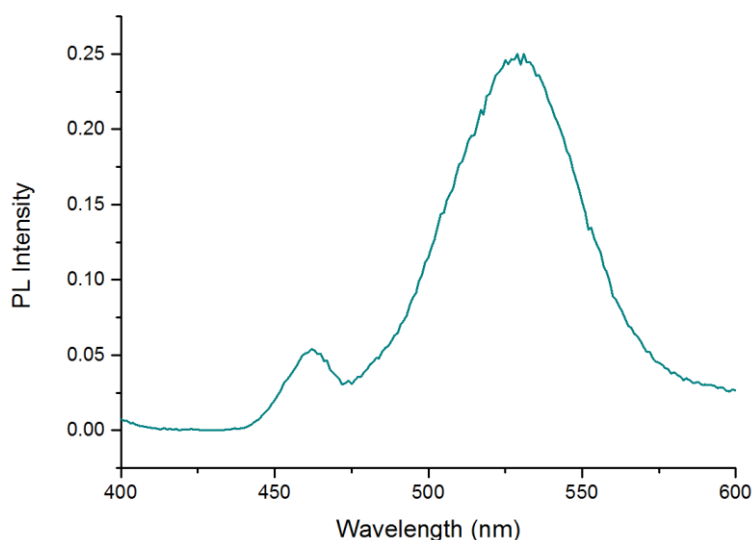


*Figure 5-38 PL spectrum of CdSe:Mn nanoplatelets (Ex.  $\lambda$  – 380 nm)*

Following this a slightly altered method for producing CdSe NPs with a thickness of 1.5 nm was performed. In this method the platelets were synthesised at 120 °C for 3 hours using myristic acid as the stabiliser (Sample **4.1**), the full protocol is described in section 2.4.8 of the Experimental section. Upon analysis of the UV-Vis spectra in Figure 5-39 it is clear that platelets with 2 distinct thicknesses have been formed due to the presence of 2 exciton peaks located at 395 nm and 478 nm. This would indicate 2 thicknesses of 1.2 nm and 1.5 nm respectively when compared to literature values<sup>7</sup>.

Stability studies were carried out on these nanoplatelets to investigate if a shift in thickness populations would occur. This was done by recording data directly after synthesis (0 weeks, sample **4.1**) and 2 months later (8 weeks, sample **4.2**) to see if a change had occurred. The data presented below describes the results of the stability experiment. Over the course of 8 weeks, the number of 1.2 nm nanoplatelets decreased and the number of 1.5 nm platelets increased which would indicate growth of the smaller sample size over time. It is interesting to note that no intermediary thickness was observed demonstrating the quantised growth of the platelets.

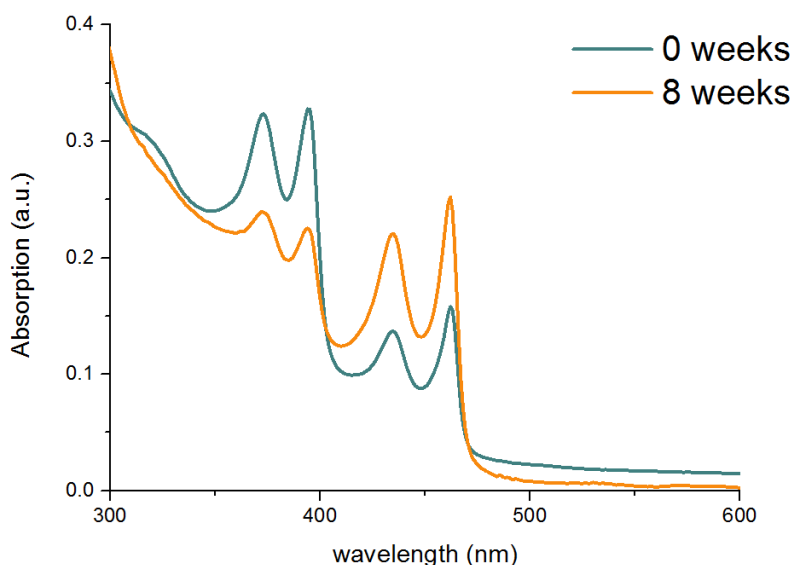


Figure 5-39 UV-Vis spectra for sample **4.1** and **4.2** (before and after storage for 8 weeks).

The photoluminescence also demonstrated growth over the same time period. The 2 excitonic peaks for the 2 sample sizes shifted from 396 nm to 418 nm and from 461 nm to 485 nm respectively. The sharpness of the peaks remains consistent between sample **4.1** and **4.2** providing further evidence of quantised growth over time.

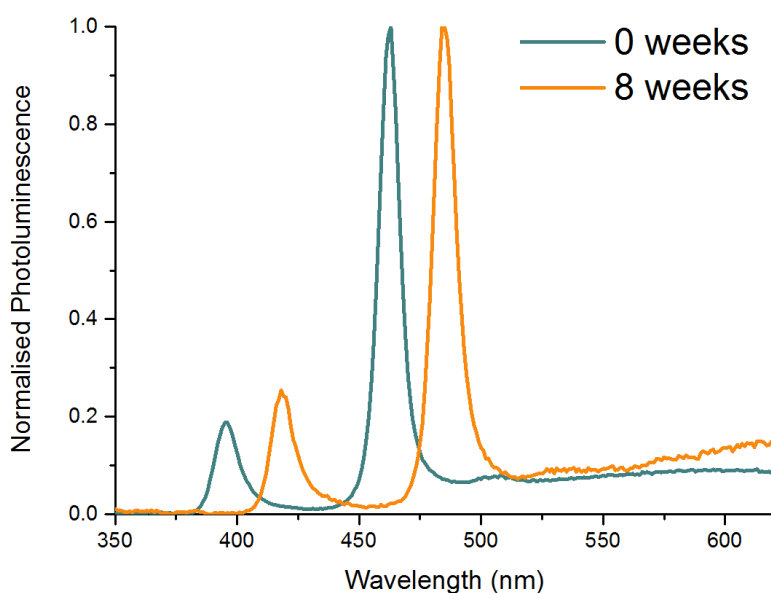
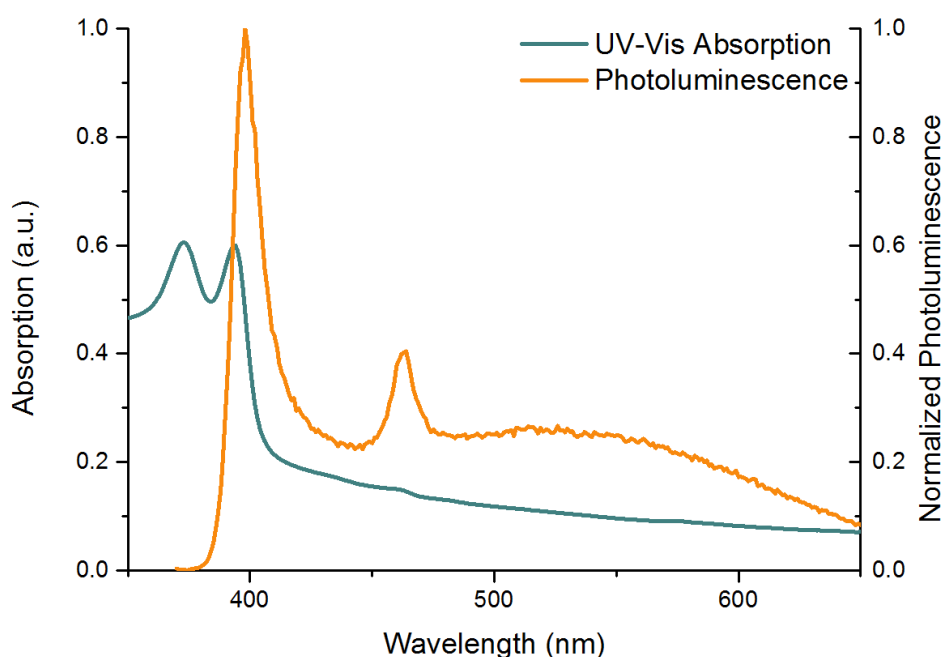


Figure 5-40 Photoluminescence spectra for sample **4.1** and **4.2** (before and after 8 weeks storage) ( $\lambda$  ex. – 350 nm).

One final synthesis of CdSe NPs was performed to produce NPs with a thickness of 1.2 nm (Sample 5). The synthesis is similar to the others however it uses a much longer reaction time. The nanoplatelets were synthesised at 120 °C for 7 days using decanoic acid as the ligand. According to the UV-Vis spectra in Figure 5-41 the first exciton is located at 392 nm corresponding to a platelet thickness of 1.2 nm (4 monolayers).



*Figure 5-41 UV-Vis and PL spectra of CdSe Sample 5 with 1.2 nm thickness ( $\lambda$  ex. – 350 nm).*

According to the emission spectra above, the excitonic peak is located at 398 nm indicating a very small Stokes shift of 6 nm which is consistent with our previous samples. Contrary to the other samples though, these platelets demonstrate broad defect luminescence between 400 and 700 nm. As the defects are surface related it makes sense that the thinnest sample should have the highest proportion of defect luminescence as it has the highest surface to volume ratio.

Following the synthesis of these CdSe nanoplatelets in the organic phase ligand exchanges were performed on a number of the samples in order to produce water

soluble, optically active nanoplatelets. The subsequent water-soluble platelets were analysed using UV-Vis, photoluminescence and circular dichroism spectroscopy.

Sample 2 (Decanoic Acid, 1.5 nm thickness) was transferred using a method identical to that used for the CdS QDs (section 2.4.11) mentioned earlier in this chapter in which an aqueous and basic solution of penicillamine was combined with the organic nanoplatelet solution and allowed to stir for 10 minutes before extraction.

The peak shapes in the UV-Vis spectrum change dramatically (Figure 5-42) after the phase transfer. The characteristic double peak has lost its resolution and instead is presented as a broad absorption peak beginning at 535 nm. This may be occurring due to an increased level of stacking and aggregation in the aqueous phase. To investigate if this was the case a brief experiment was carried out where the sample was sonicated in the presence of excess penicillamine to see if de-aggregation could be achieved however no observable difference in the UV-Vis before and after sonication was identified. The photoluminescence appears to be almost entirely quenched in these samples too (Figure 5-43). These platelets have a huge surface to volume ratio which might explain the loss of luminescence as there is a far higher proportion interacting with the water. Quantum dots typically exhibit a loss of luminescence when they are transferred from the organic to the aqueous phase due to a variety of reasons including the introduction of oxygen moieties on the surface of the nanoparticles. This loss of luminescence occurs in all of the subsequent aqueous nanoplatelet samples.

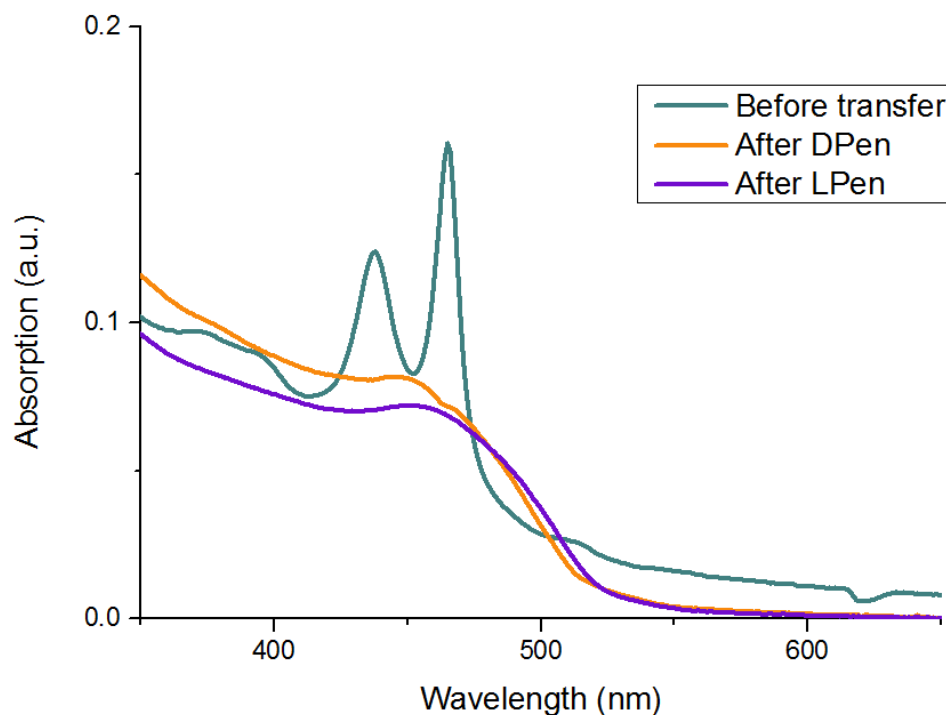


Figure 5-42 UV-Vis spectra before and after sample 2 had been transferred to water using penicillamine.

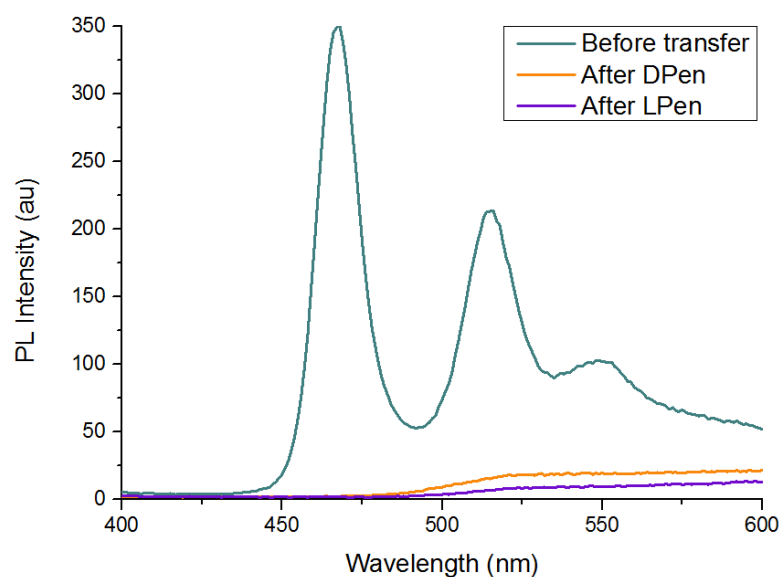
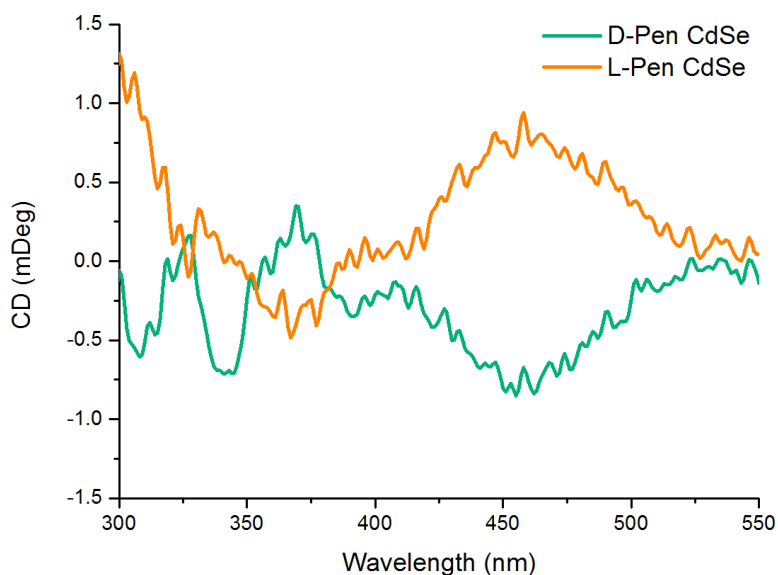


Figure 5-43 PL spectra for before and after the phase transfer (Ex.  $\lambda$  – 380 nm).

Circular dichroism is an effective technique to confirm the presence of chiral ligands on the surface of nanomaterials. In our case the achiral decanoic acid was replaced with either D- or L- penicillamine so it was expected that optical activity would be visible in the excitonic absorption region of the nanoplatelets. According to CD

spectra in Figure 5-40 below, optical activity for both the D- and L- penicillamine samples is evident. The onset of the CD spectra corresponds with the onset of absorption in the UV-Vis, around 525 nm.



*Figure 5-44 CD spectra for size 1.5 nm CdSe QPs capped with D-Pen and L-Pen*

TEM analysis was used to determine if any structural difference had taken place before and after the phase transfer. According to Figure 5-45 no appreciable difference in morphology can be observed. Therefore, we are confident that the nanoplatelet structure has remained unchanged due to the phase transfer.

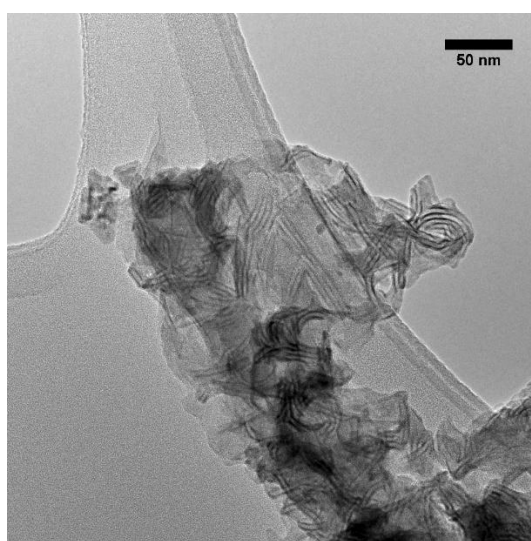


*Figure 5-45 TEM image of sample 2 after the phase transfer with D-Pen.*

Using penicillamine, the same phase transfer was carried out on sample **4.2** (Myristic acid, 120°C for 24 hours which was then left for 8 weeks). According to Figure 5-46, a similar broadening of the absorption peaks following the phase transfer has occurred. In sample 4.2 there were 2 thicknesses of nanoplatelet with first excitons beginning at 395 nm and 478 nm respectively. These 2 sets of peaks have both been smoothed into broader absorption peaks, which again may be due to stacking or aggregation in solution. Another feature of the absorption is that there is an increased absorption in the region between 525 and 475 nm which was not evident in the absorption in the organic phase. An increased in absorption in this range would suggest slight growth has taken place in the samples, this red shifting of absorption is reflected in the circular dichroism spectra below also. It is important to notice that the luminescence of sample 4.2 was entirely quenched following the phase transfer as was observed in the previous sample.

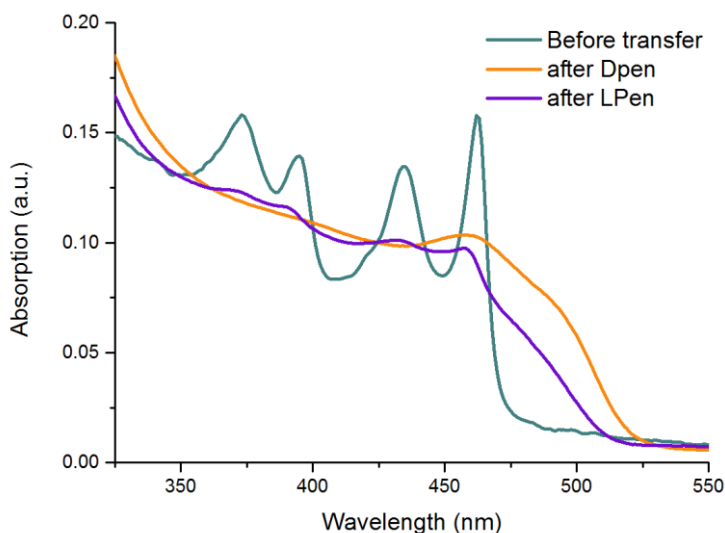


*Figure 5-46 UV-Vis spectra of sample **4.2** before and after phase transfer.*

Despite a lack of luminescence or defined absorption peaks this sample did display optical activity in the absorption region of the nanoplatelets once again. Similar to the red shifting of the absorbance of the nanoplatelets following the phase transfer, a red shifting of the CD onset also occurs. The optical activity begins around 525 nm

and the D- and L- penicillamine stabilised samples demonstrate equal intensity mirror image spectra as expected.

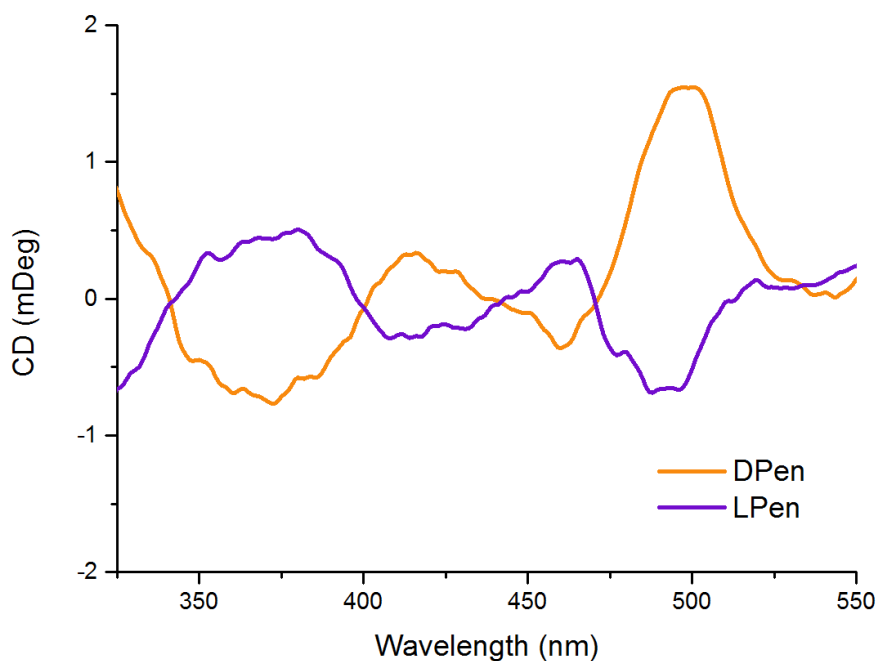


Figure 5-47 CD spectra of sample 4.2 after phase transfer.

Sample 5 (decanoic acid, 120 °C for 7 days, 1.2 nm thickness) was also used for performing phase transfers. This was the thinnest sample with the largest surface to volume ratio so it was anticipated to have the largest CD signals.

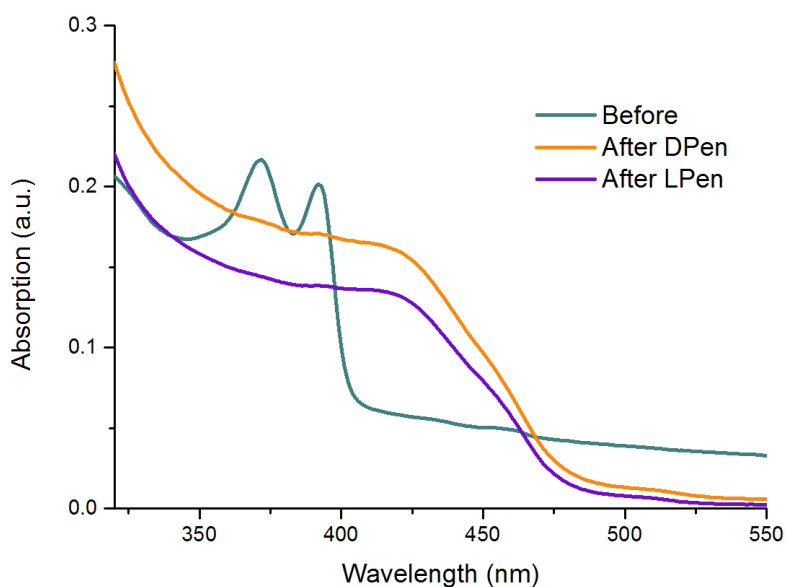
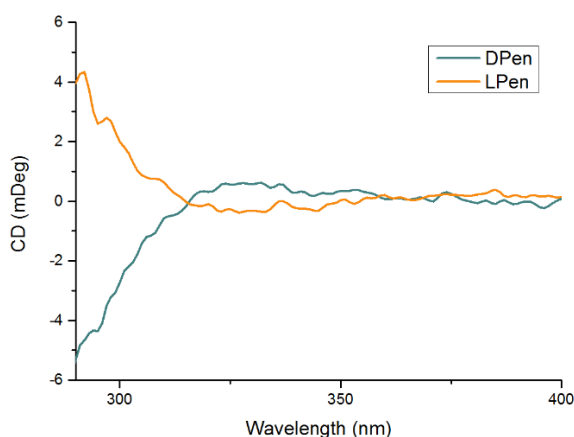


Figure 5-48 UV-Vis spectra of sample 5 before and after phase transfer.



When sample 5 was transferred using D- and L- penicillamine the same shifts in absorption that were present in previous samples were also present here. The distinct double peak exciton of the platelet has broadened. There is also an increase in absorption between 475nm and 400 nm following the phase transfer, potentially indicating nanoplatelet thickness growth. CD spectroscopy was carried out on the sample to analyse its optical activity.



*Figure 5-49 CD spectra of sample 5 after phase transfer with D/L pen.*

Figure 5-49 presents the results which are quite different from the previous samples. For the previous samples the onset of the CD corresponded with the onset of absorption, however in this case optical activity is only visible below 360 nm whereas the absorption begins around 500 nm. The stability of these samples was much less than previous samples with noticeable precipitation occurring within a week whereas the other samples were stable for months. As a consequence, it was decided to perform CD and UV-Vis on the samples after 72 hours to determine if significant sample degradation was taking place.

The UV-Vis spectra (Figure 5-50) clearly show a reduction in intensity over time. A precipitate was forming in solution and crashing out over time which explains the loss of absorption intensity over time. Despite numerous attempts to improve stability, precipitation remained an issue. It is unclear as to why this is the case and is an area of ongoing investigation.

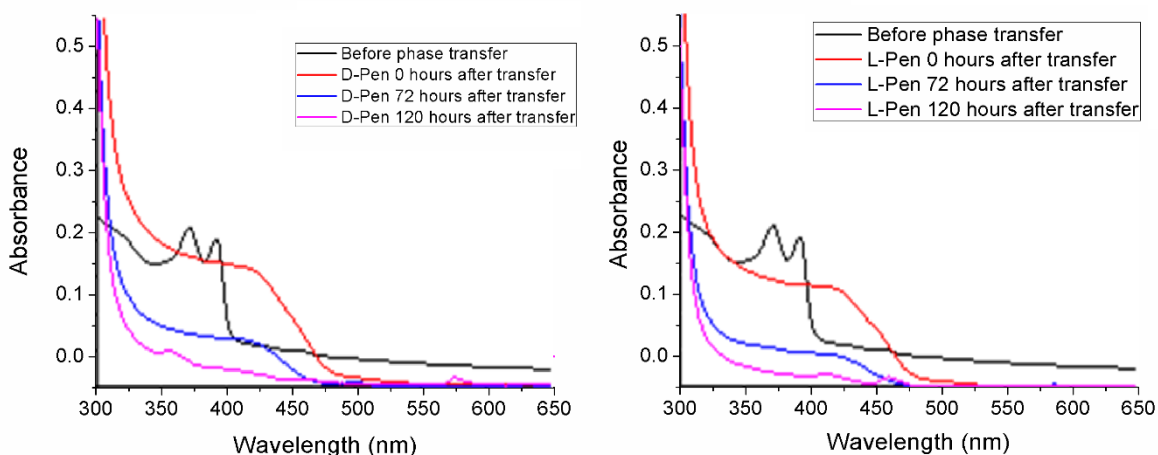


Figure 5-50 UV-Vis spectra of (A) sample 5-D and (B) sample 5-L 0 72 and 120 hours after synthesis.

A similar trend is evident in the CD spectra below in Figure 5-51. The position of the peaks in the CD do not shift, however they do decrease in intensity during the 72 hours period. It is interesting to note that sample 5 was stable in the organic phase for up to 8 weeks, however as soon as it was exchanged to the aqueous phase the stability of NPs in solution reduced dramatically. This may be due to an exchange taking place where not all of the ligands are fully exchanged and so the sample begins to precipitate rather quickly.

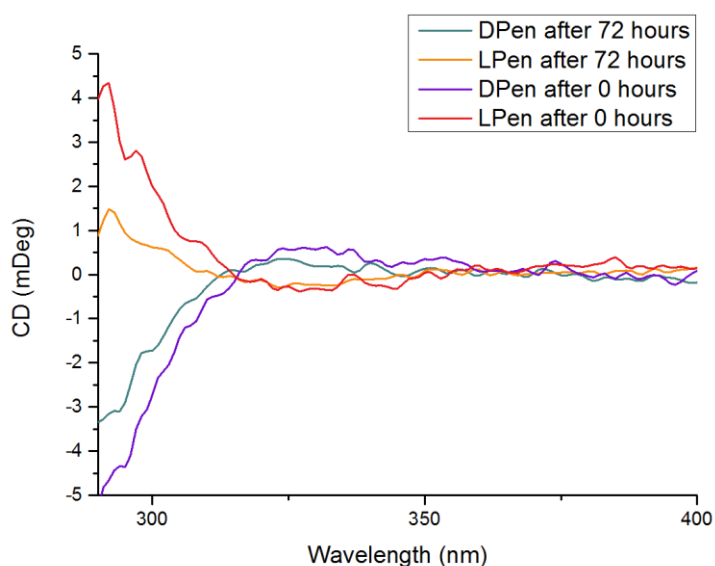
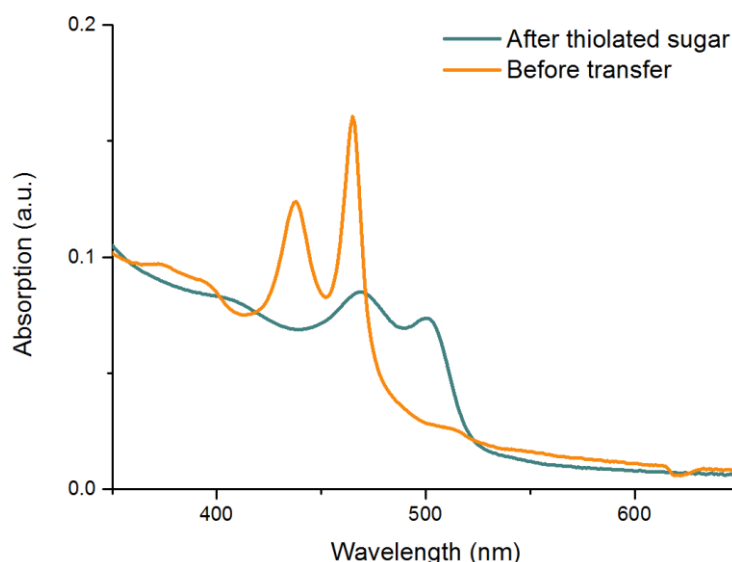


Figure 5-51 CD spectra of sample 5 after penicillamine phase transfer at 0 and 72 hours.

Finally, the same phase transfer technique that was used for the penicillamine exchange on platelet sample **2** was successfully used to conjugate thiolactose to sample **2**. This thiolated lactose derivative has been used in a variety of phase transfer experiments so it was decided to investigate its optical activity properties when conjugated to the CdSe nanoplatelets.



*Figure 5-52 UV-Vis spectra for sample 2 before and after phase transfer with thiolactose.*

The UV-Vis spectra clearly show a broadening of the peaks after the phase transfer, however compared to the other aqueous samples it retains a clear peak resolution that the other aqueous samples don't. This may be due to the bulkier thiolactose ligand preventing aggregation of NPs when compared to the other samples which used penicillamine. Without having the enantiomerically opposite thiolactose to compare it to it is difficult to analyse this information, however a large peak of activity located at 500 nm is clearly visible, corresponding to the CdSe nanoplatelet absorption onset.

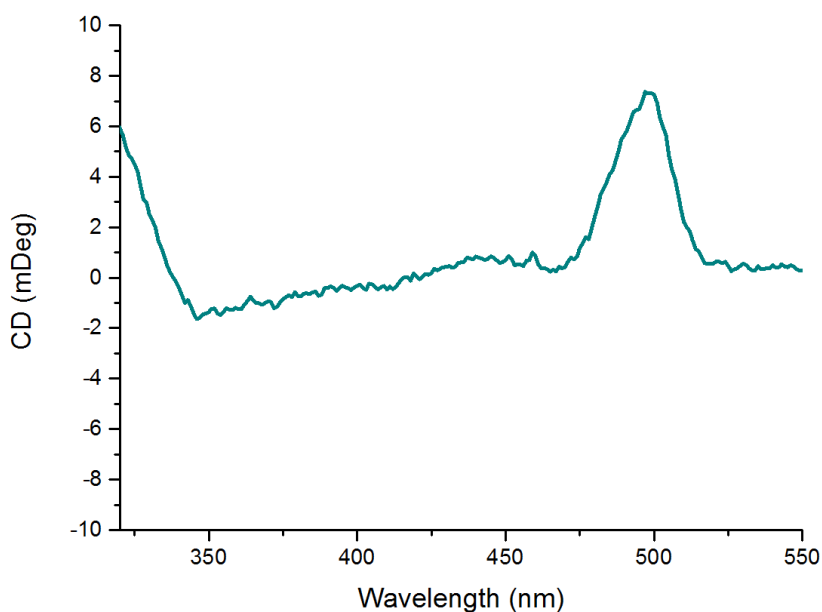


*Figure 5-53 CD spectrum for sample 2 CdSe conjugated to thiolactose.*

## 5.8 Conclusions

Our work on the development of optically active cadmium based nanomaterials has yielded a large amount of useful information. The size controlled hot injection synthesis of CdS QDs enabled us successfully produce a series of QDs of different sizes. These QDs demonstrated sharp excitonic emission in both the organic and aqueous phase, however the emission intensity in the aqueous phase was an order of magnitude smaller than in the organic phase. This result is not surprising as the particle did not possess a shell to help protect the QD luminescence throughout the ligand exchange process. By performing a ligand exchange on these particles optical activity was successfully induced in the particles, producing mirror image spectra for the D- and L- penicillamine stabilised CdS QDs respectively. After repeating this ligand exchange with the different size QDs enough information was produced to contrast optical activity of different samples as a function of QD size. Thus, we showed that the optical activity red-shifted as the QDs increased in size, which corresponds to a red shifting of the absorption. Beyond this no discernible pattern was observed between the shape of the CD spectra and the quantum dot size.

CdS QDs with a strong optical activity were also successfully synthesised by a modified aqueous synthesis under reflux in the presence of penicillamine and using thioacetamide as a sulphur source. This synthesis resulted in defect emitting particles demonstrating clear quantum confinement. While control of the synthesis was problematic at times, valuable information about CD spectra in nanomaterials was elucidated. Using dodecanethiol, a phase transfer was carried out in which the product still demonstrated residual optical activity despite on the absence of a chiral ligand. We believe further research into the properties of these organic (phase transferred) products would yield valuable information however improved stability of the product is required. By replacing penicillamine in this synthesis with cysteine optically active, defect emitting quantum dots were produced, however the increased reactivity of cysteine caused a total lack of synthetic control.

Finally, we prepared anisotropic 2D CdSe nanoplatelets and performed ligand exchanges using penicillamine, that resulted in new optically active 2D nanomaterials, which never been reported to date. These products all produced unique CD spectra however none of the samples remained luminescent following the phase transfer. This may be due to the high surface to volume ratio of the platelets allowing greater quenching from the aqueous environment. The nanoplatelets also had a tendency to scroll and roll in solution. One solution to both the quenching of the luminescence and the scrolling is to coat the CdSe nanoplatelets in a monolayer of CdS. This has been shown to prevent scrolling and by creating a core-shell style material the luminescence should remain more resistant to the ligand exchange process<sup>36</sup>. Further detailed research of new chiroptically active 2D nanomaterials is necessary in order to fully understand and optimise their properties and develop their potential applications.

## 5.9 References

- (1) Mo, Y.-m.; Tang, Y.; Gao, F.; Yang, J.; Zhang\*, Y.-m. *Industrial & Engineering Chemistry Research* **2012**, *51*, 5995.
- (2) Darbandi, M.; Urban, G.; Kruger, M. *Journal of Colloid and Interface Science* **2010**, *351*, 30.
- (3) Ithurria, S.; Tessier, M. D.; Mahler, B.; Lobo, R. P. S. M.; Dubertret, B.; Efros, A. L. *Nature materials* **2011**, *10*, 936.
- (4) Ithurria, S.; Bousquet, G.; Dubertret, B. *Journal of the American Chemical Society* **2011**, *133*, 3070.
- (5) Achtstein, A. W.; Schliwa, A.; Prudnikau, A.; Hardzei, M.; Artemyev, M. V.; Thomsen, C.; Woggon, U. *Nano Letters* **2012**, *12*, 3151.
- (6) Abecassis, B.; Tessier, M. D.; Davidson, P.; Dubertret, B. *Nano Letters* **2014**, *14*, 710.
- (7) Ithurria, S.; Dubertret, B. *Journal of the American Chemical Society* **2008**, *130*, 16504.
- (8) Wang, Y. Y.; Zhang, Y.; Wang, F. D.; Giblin, D. E.; Hoy, J.; Rohrs, H. W.; Loomis, R. A.; Buhro, W. E. *Chemistry of Materials* **2014**, *26*, 2233.
- (9) Buffard, A.; Nadal, B.; Heuclin, H.; Patriarche, G.; Dubertret, B. *New Journal of Chemistry* **2015**, *39*, 90.
- (10) Mosca, R.; Ferro, P.; Calestani, D.; Nasi, L.; Besagni, T.; Licci, F. *Crystal Research and Technology* **2011**, *46*, 818.
- (11) Sianglam, P.; Kulchat, S.; Tuntulani, T.; Ngeontae, W. *Spectrochimica Acta Part a-Molecular and Biomolecular Spectroscopy* **2017**, *183*, 408.
- (12) Ngamdee, K.; Kulchat, S.; Tuntulani, T.; Ngeontae, W. *Journal of Luminescence* **2017**, *187*, 260.
- (13) Guo, Y.; Zeng, X. Q.; Yuan, H. Y.; Huang, Y. M.; Zhao, Y. M.; Wu, H.; Yang, J. D. *Spectrochimica Acta Part a-Molecular and Biomolecular Spectroscopy* **2017**, *183*, 23.
- (14) Gao, F.; Ma, S. Y.; Xiao, X. C.; Hu, Y.; Zhao, D.; He, Z. K. *Talanta* **2017**, *163*, 102.
- (15) Tohgha, U.; Deol, K. K.; Porter, A. G.; Bartko, S. G.; Choi, J. K.; Leonard, B. M.; Varga, K.; Kubelka, J.; Muller, G.; Balaz, M. *ACS Nano* **2013**, *7*, 11094.
- (16) Purcell-Milton, F.; Visheratina, A. K.; Kuznetsova, V. A.; Ryan, A.; Orlova, A. O.; Gun'ko, Y. K. *ACS Nano* **2017**, *11*, 9207.
- (17) Gao, X.; Zhang, X.; Deng, K.; Han, B.; Zhao, L.; Wu, M.; Shi, L.; Lv, J.; Tang, Z. *Journal of the American Chemical Society* **2017**, *139*, 8734.
- (18) Mukhina, M. V.; Maslov, V. G.; Baranov, A. V.; Fedorov, A. V.; Gun'ko, Y. K.; Tanger *Nanocon 2014, 6th International Conference* **2015**, 141.
- (19) Tepliakov, N. V.; Baimuratov, A. S.; Vovk, I. A.; Leonov, M. Y.; Baranov, A. V.; Fedorov, A. V.; Rukhlenko, I. D. *Acs Nano* **2017**, *11*, 7508.
- (20) Yu, W. W.; Peng, X. *Angewandte Chemie International Edition* **2002**, *41*, 2368.
- (21) Ben-Moshe, A.; Teitelboim, A.; Oron, D.; Markovich, G. *Nano Letters* **2016**, *16*, 7467.
- (22) Yu, W. W.; Qu, L.; Guo, W.; Peng, X. *Chemistry of Materials* **2003**, *15*, 2854.
- (23) Choi, J. K.; Haynie, B. E.; Tohgha, U.; Pap, L.; Elliott, K. W.; Leonard, B. M.; Dzyuba, S. V.; Varga, K.; Kubelka, J.; Balaz, M. *ACS Nano* **2016**, *10*, 3809.
- (24) Varga, K.; Tannir, S.; Haynie, B. E.; Leonard, B. M.; Dzyuba, S. V.; Kubelka, J.; Balaz, M. *Acs Nano* **2017**, *11*, 9846.
- (25) Govan, J. E.; Jan, E.; Querejeta, A.; Kotov, N. A.; Gun'ko, Y. K. *Chemical Communications* **2010**, *46*, 6072.
- (26) Jing, L.; Kershaw, S. V.; Li, Y.; Huang, X.; Li, Y.; Rogach, A. L.; Gao, M. *Chemical Reviews* **2016**, *116*, 10623.

- (27) Nakashima, T.; Kobayashi, Y.; Kawai, T. *Journal of the American Chemical Society* **2009**, *131*, 10342.
- (28) Peng, Z. A.; Peng, X. G. *Journal of the American Chemical Society* **2002**, *124*, 3343.
- (29) Ouyang, J.; Zaman, M. B.; Yan, F. J.; Johnston, D.; Li, G.; Wu, X.; Leek, D.; Ratcliffe, C. I.; Ripmeester, J. A.; Yu, K. *Journal of Physical Chemistry C* **2008**, *112*, 13805.
- (30) Kudera, S.; Zanella, M.; Giannini, C.; Rizzo, A.; Li, Y. Q.; Gigli, G.; Cingolani, R.; Ciccarella, G.; Spahl, W.; Parak, W. J.; Manna, L. *Adv. Mater.* **2007**, *19*, 548.
- (31) Bowers, M. J.; McBride, J. R.; Rosenthal, S. J. *Journal of the American Chemical Society* **2005**, *127*, 15378.
- (32) Wang, Y. Y.; Zhou, Y.; Zhang, Y.; Buhro, W. E. *Inorganic Chemistry* **2015**, *54*, 1165.
- (33) Wang, F. D.; Wang, Y. Y.; Liu, Y. H.; Morrison, P. J.; Loomis, R. A.; Buhro, W. E. *Accounts of Chemical Research* **2015**, *48*, 13.
- (34) Flatten, L. C.; Christodoulou, S.; Patel, R. K.; Buccheri, A.; Coles, D. M.; Reid, B. P. L.; Taylor, R. A.; Moreels, I.; Smith, J. M. *Nano Letters* **2016**, *16*, 7137.
- (35) Bouet, C.; Mahler, B.; Nadal, B.; Abecassis, B.; Tessier, M. D.; Ithurria, S.; Xu, X.; Dubertret, B. *Chemistry of Materials* **2013**, *25*, 639.
- (36) Bouet, C.; Laufer, D.; Mahler, B.; Nadal, B.; Heuclin, H.; Pedetti, S.; Patriarche, G.; Dubertret, B. *Chemistry of Materials* **2014**, *26*, 3002.

## Chapter 6: Applications of chiral nanomaterials

### 6.1 Introduction

Nanoparticles have found applications in a number of biomedical fields such as drug delivery<sup>1-7</sup>, photodynamic therapy<sup>8-13</sup>, photothermal therapy<sup>14-20</sup> and cancer/tumour detection<sup>21-26</sup> in recent years. Quantum dots specifically, owing to their unique luminescence properties, have been investigated for their potential uses as imaging and diagnostic agents. Quantum dots have found uses for imaging and labelling of cancer cells<sup>27-31</sup>, optical encoding<sup>32-35</sup>, immunolabeling<sup>36-38</sup> and cell marking<sup>39,40</sup>. This chapter is focusing on some selected applications of chiral quantum nanostructures.

Work on cation exchange reactions in nanostructures has been ongoing for many years<sup>41-45</sup>, due to potential applications of this approach. Importantly, cation exchanges in nanomaterials occurs very fast compared to their bulk counterparts. As discussed in the introduction (section 1.11), the cation exchange approaches are very helpful in producing hetero-nanostructures that otherwise would not be possible. There are very interesting research reports on cation exchanges using cadmium sulphide quantum dots<sup>46-49</sup> and CdS/CdSe nanoplatelets<sup>50,51</sup> with copper, lead, and indium, there have been no studies carried out on the optical activity of products of these reactions. Also, there were no any studies on the ion exchange in chiral nanoparticles. In this chapter, we report our efforts to produce optically active Cu<sub>2</sub>S, Cu<sub>2</sub>Se, ZnS QDs and ZnSe nanoplatelets by performing a series of cation exchanges on CdS QDs and CdSe nanoplatelets respectively.

There are also several recent reports on quantum dots capped with modified carbohydrates, such as 1-β-D-thioglucose, which present a great interest due to their specific interactions within biological species. For example, glycosylated QDs have been used in such applications as bacterial detection<sup>52</sup>, investigation of protein/glycan interactions<sup>53,54</sup>, lectin detection<sup>55</sup> and cellular imaging<sup>56,57</sup>. QD



imaging using glycosylated quantum dots has been performed by Coulon *et al.* when carbohydrates were conjugated to CdTe QDs and used for yeast cell labelling<sup>58</sup>. As glycosylation plays a significant role in QD interactions *in vivo*, it was interesting to investigate the relationship between the degree of glycosylation on the surface of QDs and its imaging behaviour within cell cultures.

## 6.2 Aims of this chapter

The main goal of this chapter is to demonstrate some applications of our optically active chiral cadmium-containing materials. Firstly, we aim to perform cation exchange reactions on the optically active CdS QDs and to investigate if the subsequent optical activity in Cu<sub>2</sub>S QDs. Upon successful conversion to the copper product, we aim to convert the Cu<sub>2</sub>S into ZnS *via* cation exchange and investigate its chiroptical properties. Secondly, we aim to perform cation exchanges on CdSe:Mn nanoplatelets and to investigate the chiroptical properties and morphology of the resultant Cu<sub>2</sub>Se:Mn nanoplatelets. Once Cu<sub>2</sub>Se:Mn nanoplatelets have been produced our aim is to convert them to ZnSe:Mn nanoplatelets using another Zn cation exchange.

In addition, we aim to produce highly emissive alloyed CdZnSeS/ZnS nanoparticles and to characterise them using UV-Vis and PL spectroscopies and TEM. Following this, we aim to perform ligand exchanges on these particles to produce aqueous particles with a range of glycosylations on the surface. We plan to achieve this by varying the ratio of D-penicillamine to thio-lactose used in the phase transfer from 100:0 to 0:100. By administering our particles into cell cultures, we aim to demonstrate a difference in behaviour between the samples in terms of cellular uptake and toxicity.

## 6.3 Cation exchange experiments

As previously discussed, there is a vast amount of established procedures<sup>59-65</sup> for producing cadmium-containing quantum dots when compared to cadmium-free quantum dots. Therefore, as an alternative approach to producing non-toxic chiral

nanomaterials, it was decided to perform cation exchanges on some of our nanomaterials in an effort to replace the  $\text{Cd}^{2+}$  with  $\text{Zn}^{2+}$ . To date, no direct exchange of cadmium to zinc has been published, but it is possible by first exchanging the cadmium for copper, and subsequently exchanging the copper for zinc.

In previous chapters, a variety of cadmium-containing nanoparticles have been synthesised. However, they were primarily core-shell materials which are more complicated candidates for cation exchange reactions. Therefore, we decided to perform cation exchanges on 2 different chiral nanomaterials, CdS QDs as described at the beginning of chapter 5 and CdSe:Mn nanoplatelets described in section 5.7. These materials are both simple binary cadmium chalcogenide materials (doped and undoped) potentially allowing for more straight forwards analysis.

### 6.3.1 Cation exchange on CdS QDs

An exchange from  $\text{Cd}^{2+}$  to  $\text{Zn}^{2+}$  with  $\text{Cu}^+$  as an intermediate that retains a crystalline structure has already been documented for CdSe quantum dots and nanorods<sup>66</sup>. These methods were adapted for our CdS quantum dots as follows: a solution of  $\text{Cu}^+$  in methanol was prepared with tetrakis(acetonitrile)copper(I) hexafluorophosphate and added to the QDs as to have a  $\text{Cu}^+:\text{Cd}^{2+}$  ratio of 20:1. The very lightly coloured CdS solution instantly (<1s) turns golden-brown, the colour of the  $\text{Cu}_2\text{S}$  QDs. This reaction is very fast as methanol solvates the divalent  $\text{Cd}^{2+}$  more strongly than  $\text{Cu}^+$ , driving the exchange reaction forward. The stirring was allowed to proceed for another five minutes to be sure that the exchange is complete. The  $\text{Cu}_2\text{S}$  QDs were precipitated by the addition of methanol and centrifugation at 3500 rpm for 15 minutes and stored in toluene. Our primary focus was on performing the cation exchange in the aqueous phase, so a similar method was used to exchange  $\text{Cd}^{2+}$  for  $\text{Cu}^+$  in chiral, water-soluble, Pen-capped CdS QDs (experimental section 2.5.1).

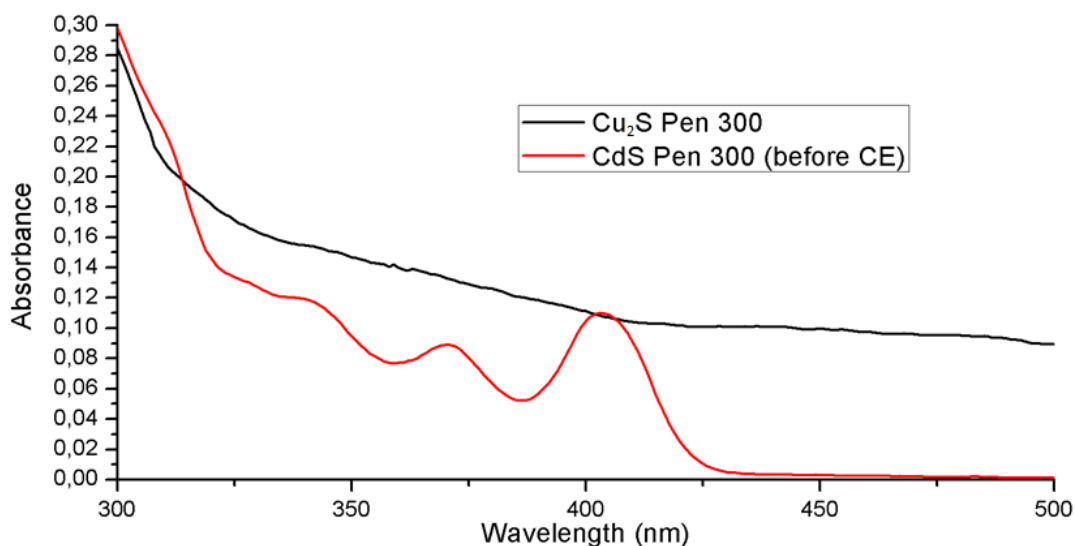


*Figure 6-1 Absorbance spectra of Pen-capped CdS before cation exchange and after (as  $Cu_2S$ ).*

After the cation exchange, all of the characteristic spectral features for CdS QDs have disappeared from the UV-Vis (Figure 6-1): this would indicate that the reaction has gone to completion and no CdS remains. The resultant spectra for  $Cu_2S$  demonstrates few interesting features and this correlates well with literature reports for  $Cu_2S$  nanoparticles<sup>67</sup>. Following UV-Vis analysis, circular dichroism was used to investigate whether chirality had been retained following the cation exchange.

The  $Cu_2S$  quantum dots display a circular dichroism signal below 400 nm, with four main maxima at 330, 270, 250 and 233 nm (Figure 6-2). Once again, below 260 nm, the CD spectrum is different from the spectra for free penicillamine in solution. By comparing the CD signals before and after the cation exchange (Figure 6-3) it is clear that significant differences in the optical activity occurred. The  $Cu_2S$  spectra contain a broader band between 400 nm and 300 nm when compared to CdS spectrum. This may be due to the broad continuous absorption of  $Cu_2S$  in this region when compared to the quantized absorbance of CdS.

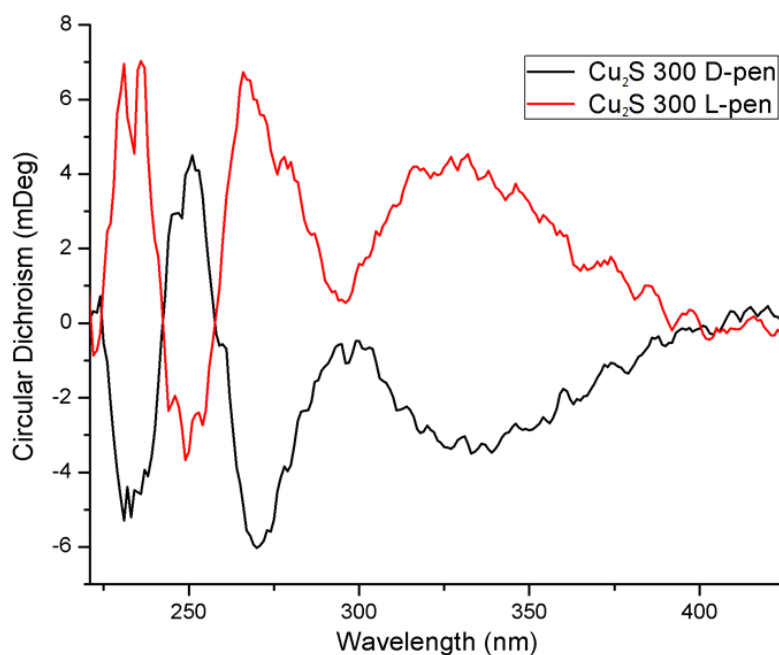


Figure 6-2 CD spectra of L-pen and D-pen  $\text{Cu}_2\text{S}$  quantum dots obtained from cation exchange from Pen-capped CdS synthesized at  $300^\circ\text{C}$ .

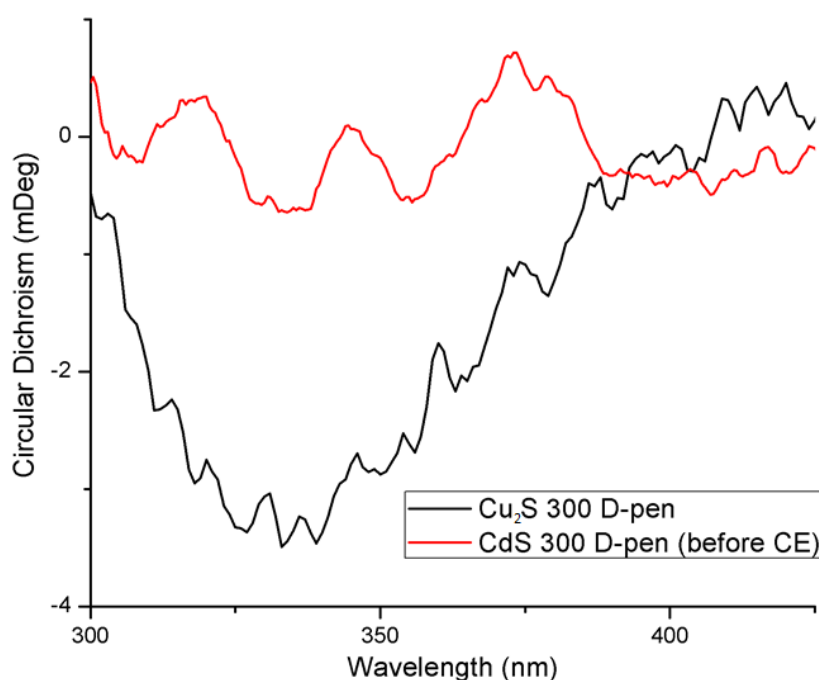


Figure 6-3 Comparison of CD spectra before and after cation exchange.

Unfortunately, the  $\text{Cu}_2\text{S}$  quantum dots were very air-sensitive and degraded quickly. This resulted in a change of colour from golden-brown to green and grey which is most likely caused by oxidation of copper (I) and subsequent degradation of the quantum dots. This post synthesis instability of the QDs prevented further analysis

from taking place. Further research must be undertaken to increase post-synthetic aqueous synthesis.

### 6.3.2 Cation exchange for CdSe nanoplatelets

Following the interesting results achieved using CdS QDs, it was decided to perform similar cation exchange reactions on our CdSe nanoplatelets. Unlike the previous cation exchange, where the CdS QDs were transferred into the aqueous phase first followed by the cation exchange, for the CdSe nanoplatelets we decided to first carry out the cation exchange in the organic phase followed by the ligand exchange. This strategy was used in order to address the instability issues of performing the cation exchange in the aqueous phase. It was expected that this methodology might lead to a more stable product for the subsequent  $\text{Cu}_2\text{Se}$  to ZnSe conversion. The cation exchange process is detailed in the experimental 2.5.2. For the cation exchange, a solution of  $\text{Cu}(\text{CH}_3\text{CN})_4\text{PF}_6$  in methanol was reacted with a solution of the CdSe:Mn nanoplatelets in chloroform. The subsequent stable  $\text{Cu}_2\text{Se}$ :Mn nanoplatelets were stored in toluene until the phase transfer. While cation exchanges were performed on a number of samples with success, the consequent ligand exchange was only successful for the nanoplatelet sample doped with manganese. It is still unclear why the phase transfer was unsuccessful for the other nanoplatelets and is an area of ongoing investigation.

While  $\text{Cu}_2\text{Se}$  is not plasmonic,  $\text{Cu}_{2-x}\text{Se}$  is<sup>68,69</sup>. So while our aim was to create  $\text{Cu}_2\text{Se}$ , the resultant data would suggest that copper deficiencies were present. This deficiency may be due to the replacement of a portion of the cadmium with manganese as CdSe:Mn nanoplatelets were used. Therefore, the presence of a clear plasmonic peak in the absorbance spectra would help confirm the successful production of  $\text{Cu}_{2-x}\text{Se}$ :Mn. UV-Vis spectra are presented below for the original CdSe nanoplatelets in the organic phase (red), the  $\text{Cu}_{2-x}\text{Se}$ :Mn platelets in the organic phase (purple) and the  $\text{Cu}_{2-x}\text{Se}$ :Mn nanoplatelets in the aqueous phase capped with D or L pen Figure 6-4 (green and orange). Upon analysis of the  $\text{Cu}_{2-x}\text{Se}$ :Mn spectra,

compared to the CdSe nanoplatelets, significant changes have occurred. The most significant feature of the new  $\text{Cu}_{2-x}\text{Se}:\text{Mn}$  platelets is the large plasmonic absorption band located between 600 nm and 800 nm with a maximum at 690 nm. The  $\text{Cu}_{2-x}\text{Se}:\text{Mn}$  platelets absorb over the entire spectral region analysed as expected for brown/ black particles. Further evidence of the morphological change is evidenced by the fact that the traditional double peak first exciton absorption of the CdSe NPs located at 463 nm has also disappeared entirely.

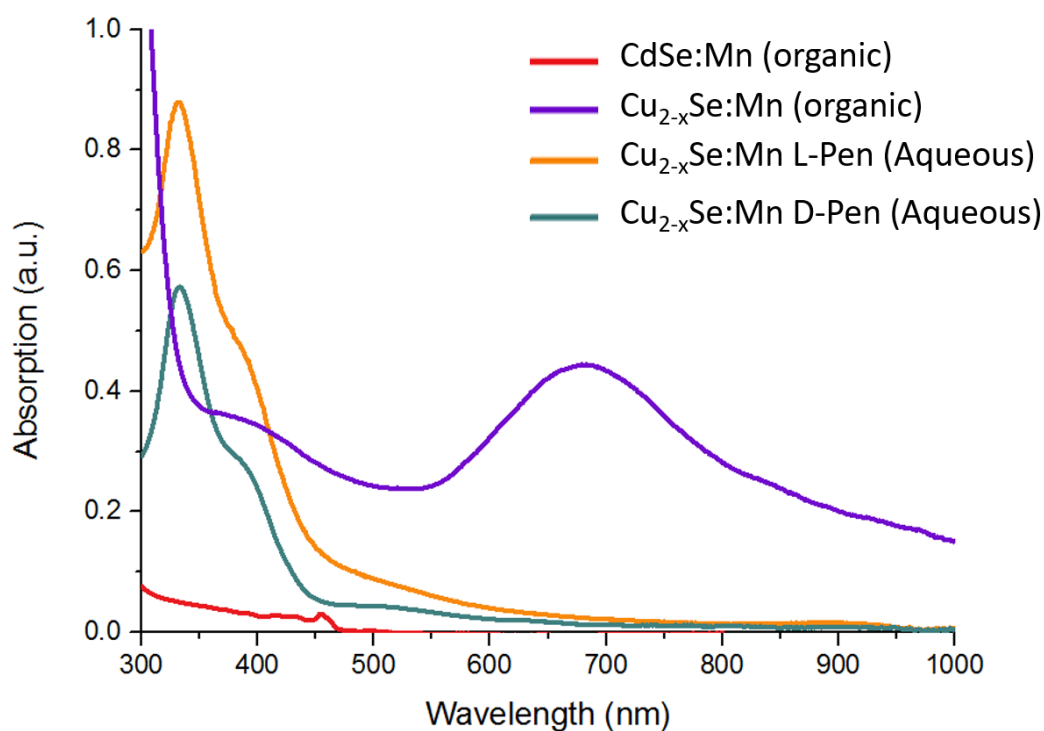


*Figure 6-4 UV-Vis spectral changes for Mn-doped CdSe QPs in chloroform before and after cation exchange and phase transfer.*

The above UV-Vis spectra also contain information about the absorbance for the  $\text{Cu}_{2-x}\text{Se}:\text{Mn}$  samples after the ligand exchange where the organic ligands were replaced with either D- or L- penicillamine. The ligand exchange procedure was exactly the same that was used for performing a ligand exchange on the CdSe:Mn nanoplatelets and is outlined in 2.4.11 of the experimental chapter. The UV-Vis data for the L and D pen  $\text{Cu}_{2-x}\text{Se}:\text{Mn}$  demonstrate a significant change in absorbance

when compared with the organic  $\text{Cu}_{2-x}\text{Se}:\text{Mn}$  samples, primarily the main plasmonic peak has disappeared entirely. These samples suffered from the same instability that our  $\text{Cu}_2\text{S}$  samples had in the aqueous phase and we believe this degradation is reflected in the UV-Vis changes. Despite the loss of the plasmonic peak, there was still a broad absorbance between 900 and 500 nm.

As the  $\text{Cu}_{2-x}\text{Se}:\text{Mn}$  was now capped with a chiral ligand, it was expected that optical activity would be present in the D- and L- penicillamine stabilised  $\text{Cu}_{2-x}\text{Se}:\text{Mn}$  samples, so CD spectroscopy was carried out (Figure 6-5).

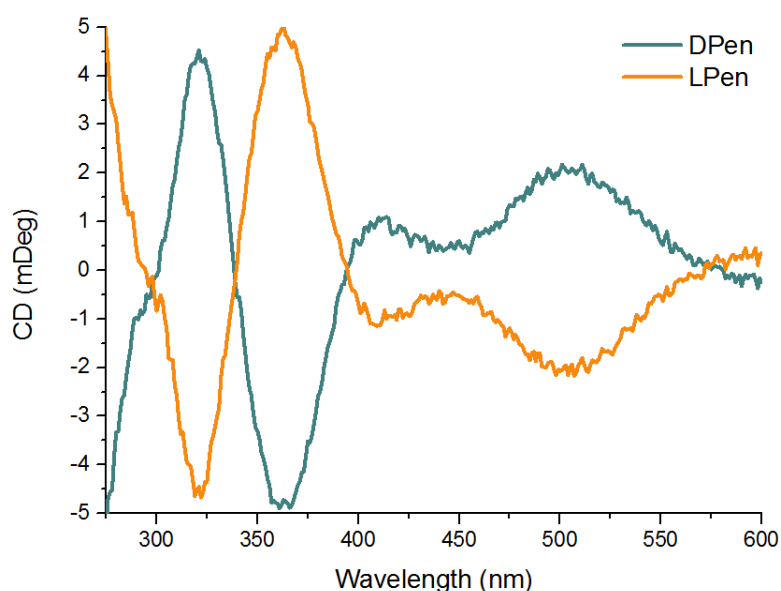


*Figure 6-5 CD spectra of resulting D/L penicillamine  $\text{Cu}_{2-x}\text{Se}:\text{Mn}$  QPs in water.*

The resultant  $\text{Cu}_{2-x}\text{Se}:\text{Mn}$  nanoplatelets demonstrate optical activity in the nanoparticle absorption region indicating the successful capping using a chiral ligand (penicillamine). The spectra are mirror images of each other and have several peaks located at 510 nm, 360 nm and 320 nm. It is interesting to note the similarities between the optical activity of this product and the CD spectra of the  $\text{Cu}_2\text{S}$  product formed from the performing a cation exchange on the CdS QDs. Most likely due to their plasmonic properties of these copper based nanomaterials, they both present signals which are typically stronger than the cadmium-containing analogues and

they both have a broad optical activity in the longer wavelength section of the spectrum followed by sharp peaks crossing the  $Y = 0$  axis multiple times.

As previously stated both the  $\text{Cu}_2\text{S}$  and  $\text{Cu}_{2-x}\text{Se}:\text{Mn}$  demonstrated a high degree of optical activity, however instability in water is a significant issue. The eventual goal of this cation exchange is to replace cadmium with zinc, *via* copper. Therefore, a stable copper intermediate product is required for the final exchange of copper for zinc. This research is currently ongoing as attempts to stabilise the Copper (I) product in water are being undertaken.

#### 6.4 Biological imaging using CdSe@ZnS-ZnS QDs in HeLa cells

As QDs have remarkable optical properties, one of our goals was to use QDs for optical imaging studies during this research. The transfer techniques were applied to a very bright CdSe@ZnS/ZnS alloyed core-shell sample to transfer the QDs in aqueous phase by capping them with penicillamine and thiolated lactose (similar to the thiolated glucose used in previous experiments) ligands for *in vitro* imaging experiments. Our objective was to produce 3 samples with varying degrees of glycosidation on the surface: 100% Lactose, 50/50 lactose/penicillamine and 100% penicillamine. By introducing our 3 different samples to HeLa cells we aimed to demonstrate a difference between how the samples interacted with the cells as a function of how much thiolactose is on the surface. The QDs were synthesised in-house by Dr Finn Purcell Milton using a method reported by Lee *et al*<sup>70</sup> and stored in chloroform. The synthesis involves the initial production of large CdSe-ZnS core-shell quantum dots using traditional hot injection techniques which then are subsequently overcoated with another layer of ZnS shell. During this overcoating, a certain amount of alloying takes place leading to a CdZnSeS-ZnS core-shell system with a high quantum yield of  $\approx 80\%$ . The thio-lactose molecule was produced by the Scanlan Group in the Trinity Biomedical Sciences Institute and used as received. The QDs were transferred into the aqueous phase using the same method used for the



ZnS:Mn QDs outlined in section 2.2.2. To prepare samples with thiolactose or a combination of thiolactose and penicillamine, equimolar solutions of both penicillamine and thiolactose in methanol are prepared and added to the QD solution in the ratio that was required (100:0, 50:50, 0:100).

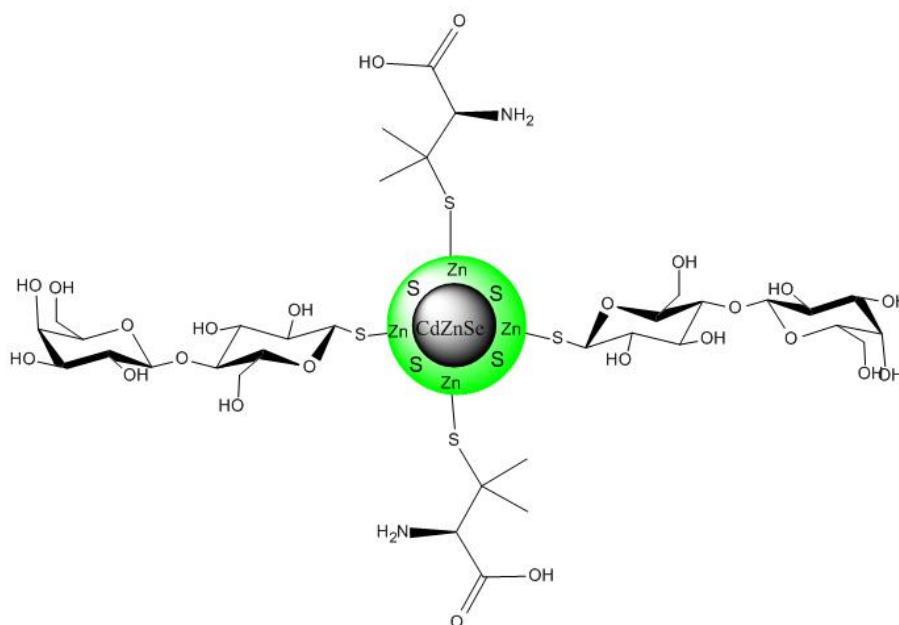


*Figure 6-6 Schematic for 50:50 penicillamine/thiolactose capped QD.*

Upon successful ligand exchange, the samples were analysed using UV-Vis, PL and TEM. UV-Vis spectra below in Figure 6-7 display the characteristic first exciton peak located between 510 nm and 517 nm that is in agreement with literature reports<sup>70</sup>. It is interesting to note the slight differences in the sharpness of the exciton peaks. These differences may be explained by a difference in scattering occurring due to the larger thiolactose ligand causing more scattering events.

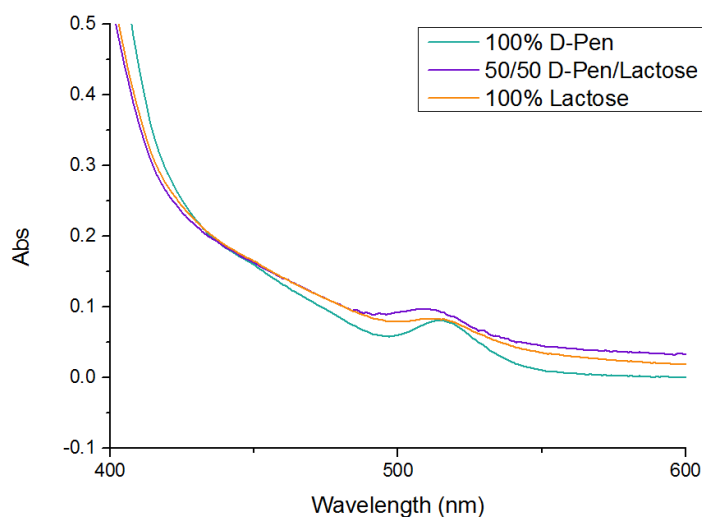


Figure 6-7 UV-Vis data for CdSe@ZnS/ZnS QDs capped with a combination of penicillamine and thiolactose.

Photoluminescence measurements were carried out to determine if significant differences in luminescence were present (Figure 6-8).

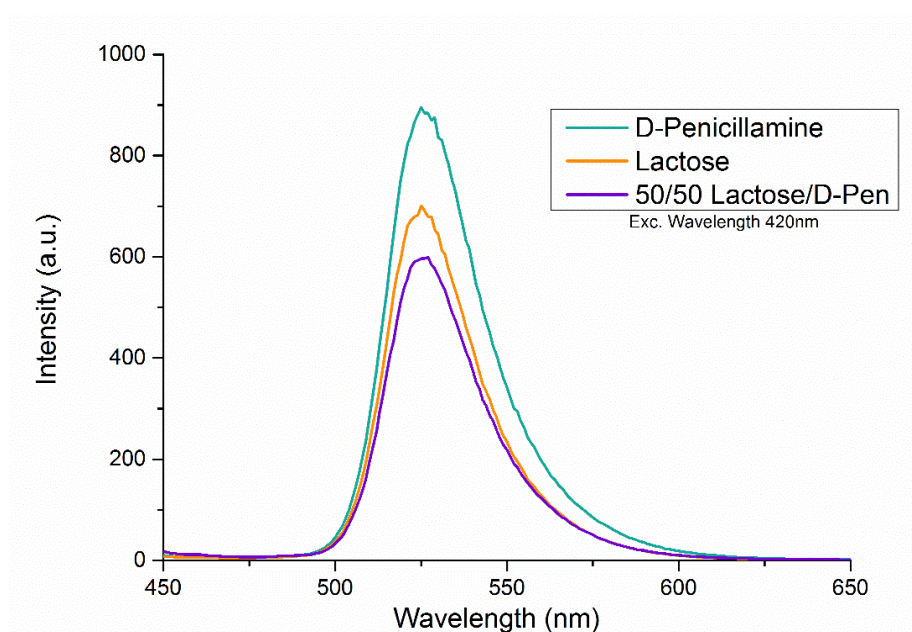
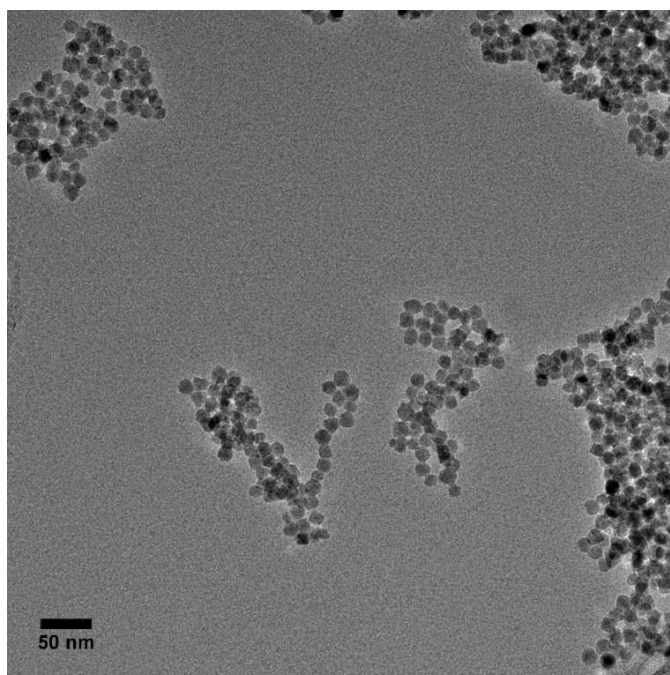


Figure 6-8 PL spectra for CdSe/ZnS@ZnS QDs stabilised with penicillamine and thiolactose.

Emission for all 3 samples had a maximum located at 520 nm and have comparable emission intensities. The sample capped with D-penicillamine only was the most luminescent, however the purely lactose capped sample and the mixed ligand capped samples demonstrated 70% and 80% percent of the luminescence of the D-

Pen only sample respectively. TEM analysis was subsequently used to indicate if any difference in size between the different samples is present. TEM analysis for the QDs capped with lactose showed that the QDs are roughly spherical with an average size of  $13.2 \pm 2.1$  nm (Figure 6-9 and Figure 6-10) which correlate well with literature values.



*Figure 6-9 TEM image of CdSe/ZnS@ZnS QDs stabilised with lactose.*

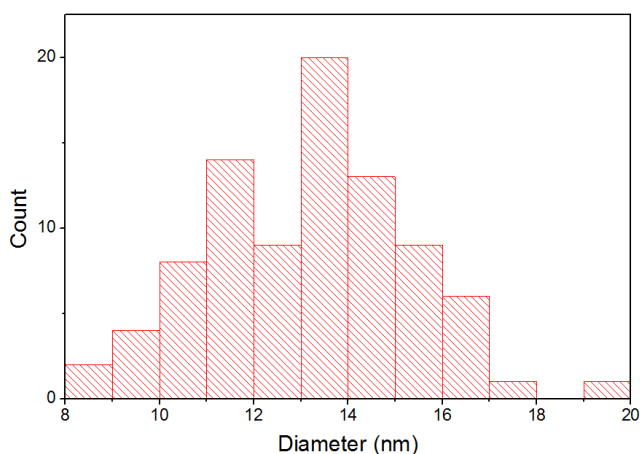


*Figure 6-10 Size distribution histogram for QDs stabilised by lactose (n = 120).*

TEM analysis of the penicillamine sample produced similar results (Figure 6-11). From the HRTEM images it is clear that the particles are spherical and crystalline.

According to the histogram presented in Figure 6-12, the QDs have an average size of  $13.4 \pm 1.5$  nm which is consistent with the previous sample and reported literature values.

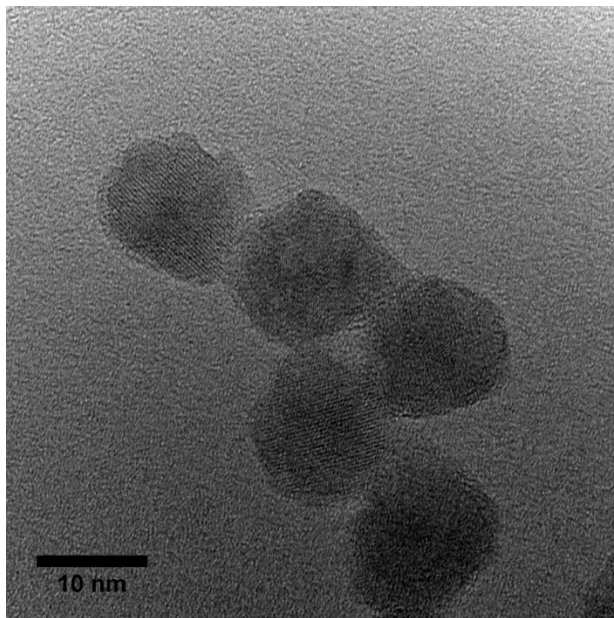


*Figure 6-11 HRTEM image of CdSe/ZnS@ZnS QDs stabilised by penicillamine.*

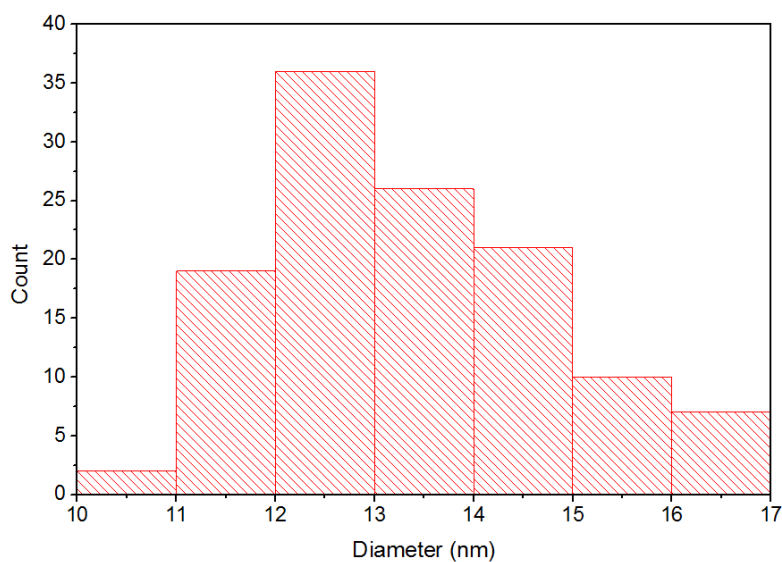


*Figure 6-12 Size distribution histogram for CdSe/ZnS@ZnS QDs stabilised by penicillamine (n = 140).*

Finally, the QDs capped with a combination of penicillamine and lactose were analysed using TEM and HRTEM. The QDs again, appear to be spherical in shape and of high crystallinity (Figure 6-14).

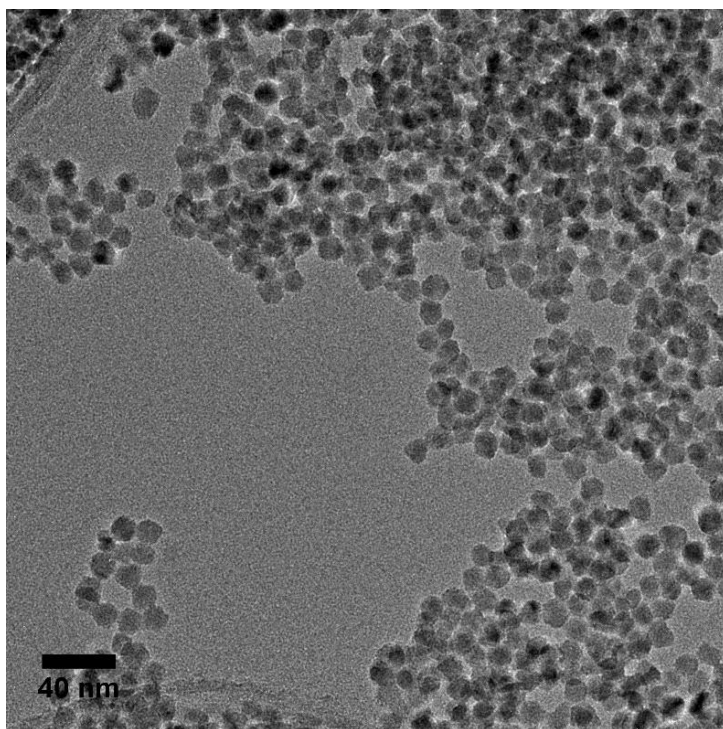


*Figure 6-13 TEM image of 50/50 lactose/penicillamine capped QDs.*

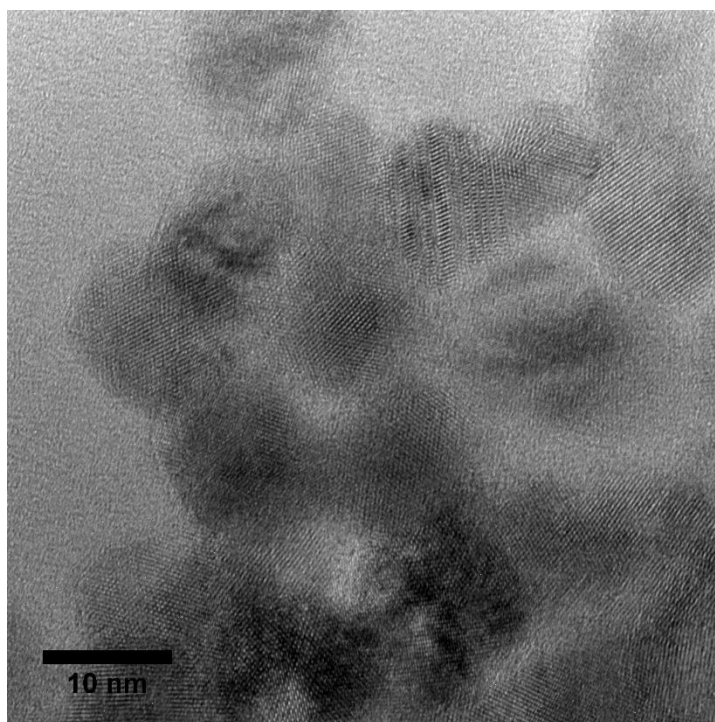


*Figure 6-14 HRTEM image of 50/50 lactose/penicillamine capped QDs.*

From the histogram below in Figure 6-15 it was determined that the QDs have an average size of  $13.1 \pm 1.5$  nm which again correlates well with previous results. For

comparison, TEMs of the organic QDs before the phase transfer are presented in Figure 8-10 of the appendix.

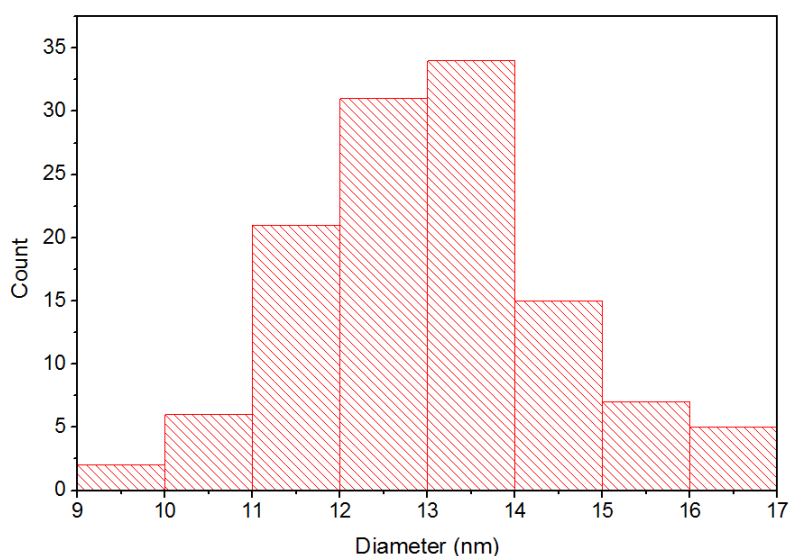


*Figure 6-15 Size distribution histogram for CdSe/ZnS@ZnS QDs stabilised by 50/50 lactose/penicillamine (n = 140).*

Once the samples were characterised, they were given to Dr Sandra Bright of the Scanlan group for *in vitro* imaging and cytotoxicity experiments. The samples were all made to the same concentration analysed using UV-Vis spectroscopy before these experiments were carried out. The QD concentration was determined using thermogravimetric analysis after these experiments were carried out. The concentration was approximated to be  $1.4 \times 10^{-5}$  M, and the calculations and TGA data are presented in Figure 8-11 of the appendix.

HeLa cells were subjected to Alamar Blue viability assays to determine if quantum dot complexes displayed any cytotoxicity towards cancer cells. Results demonstrated a potent dose-dependent reduction in cellular viability following 24 hrs of treatment with complexes (Figure 6-16). All 3 complexes induced very similar toxicities with IC<sub>50</sub> values ranging from 12 to 15.8  $\mu$ L.

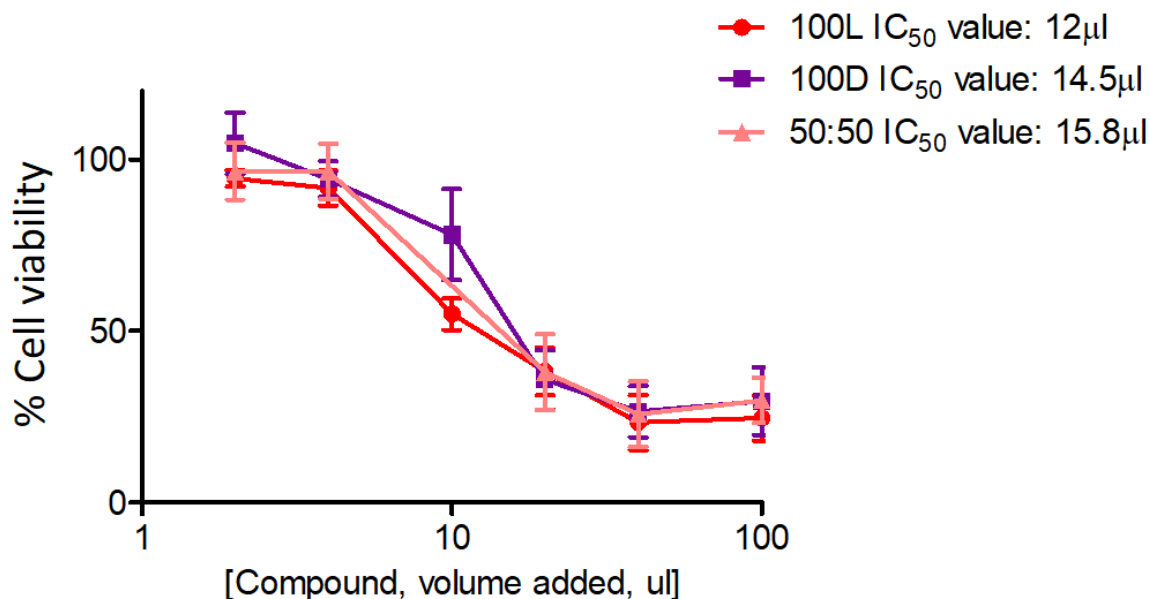
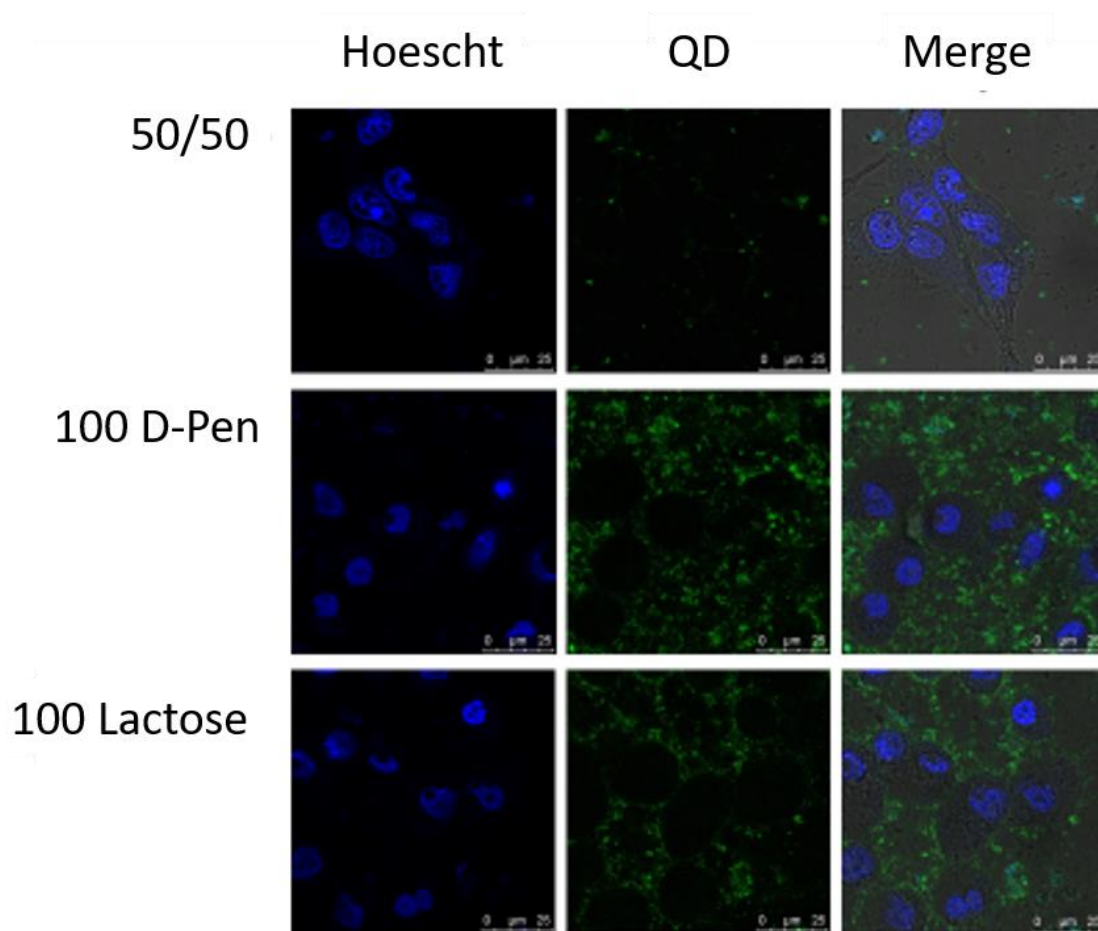


Figure 6-16 Cell viability study at high concentration as a function of capping ligand (L = lactose, D = D-Pen).

HeLa cells were treated for 24h with a range of concentrations of the indicated compounds in a 96-well plate. After the required incubation period, Alamar blue dye (20 μl) was added to each well and samples were incubated for 4h. Values represent the mean ± S.E.M. of three independent experiments performed in triplicate.

Next, live cells were studied by confocal microscopy. For preliminary studies, to determine if complexes could be easily imaged, cells were treated with 250 μl of each complex for 6 hrs. Results demonstrated that complexes were highly fluorescent (Figure 6-17). However, even with this short time-point, cells displayed evidence of toxicity such as nuclear shrinkage and cellular swelling which is typically associated with necrosis. Interestingly, while the viability data suggests complexes to be equipotent at the same treated volumes, the confocal imaging suggests a large difference in the number/concentration of quantum dots per μl with 50:50 exhibiting lowest number of dots and therefore the lowest degree of fluorescence, and 100D displaying the largest number of dots and fluorescence (Figure 6-17).



*Figure 6-17 Confocal microscopy results for samples analysed at a high concentration.*

HeLa cells were treated for 6h with 250 $\mu$ l of the indicated complexes and stained with Hoescht (blue nuclear stain). The complexes were subjected to live confocal imaging, excitation 405nm, emission 500-600nm (Leica, 63X oil immersion lens). Images are representative of two experiments performed on independent days. From the data above, it is clear that the QDs were not taken up in the HeLa cells at high concentrations and short incubation periods.

Subsequently, HeLa cells were treated with 10 $\mu$ l of each complex (a concentration below the IC50 values) for 24hrs. Cells remained healthy and viable with this treatment, and quantum dots were still clearly visible. A visible amount of quantum dots were taken up into cells under these conditions. However, a large proportion of QDs still remained outside of the cells. Again, the penicillamine capped sample



appeared to have the most number of dots per  $\mu\text{l}$ , and 50:50 the least number (Fig. 4).

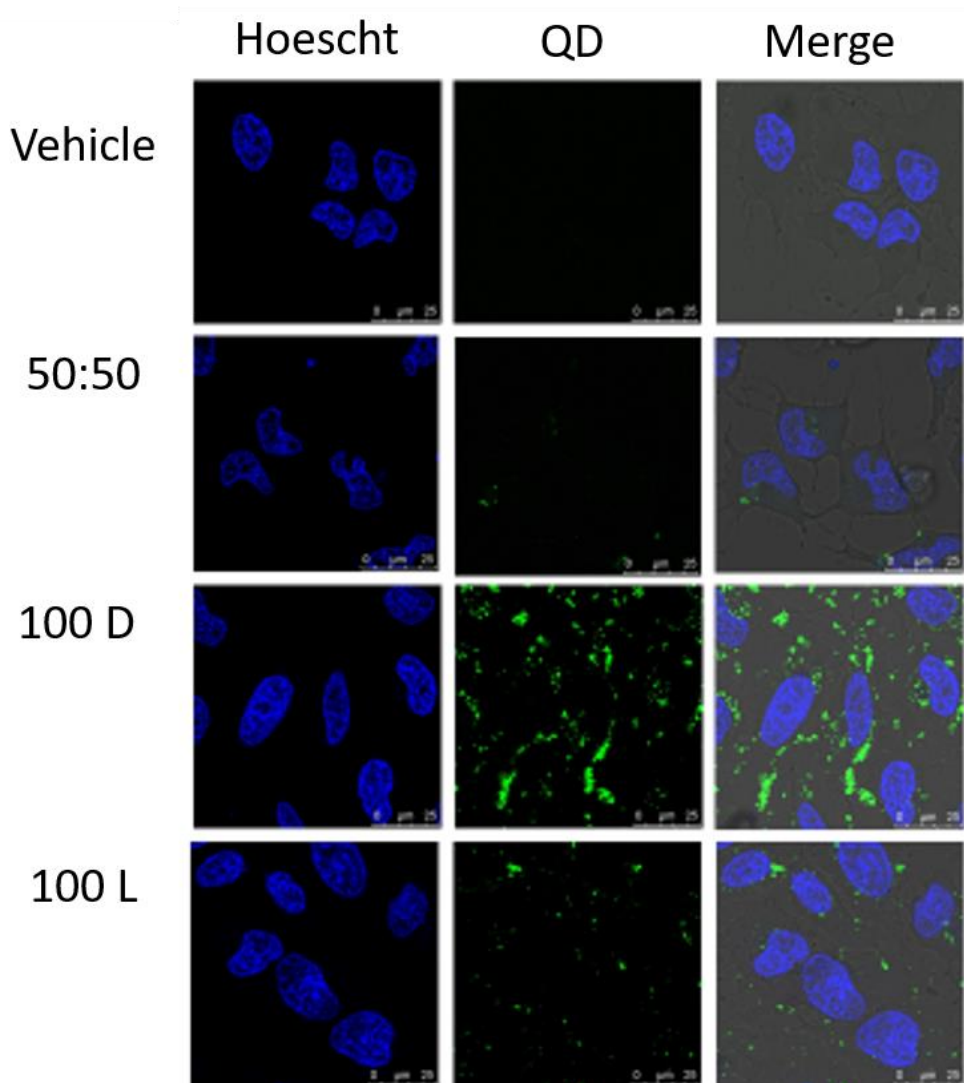


*Figure 6-18 Confocal microscopy results for samples analysed at a lower concentration. Complexes were subjected to live confocal imaging, excitation 405nm, emission 500-600nm (Leica, 63X oil immersion lens). Images are representative of three experiment performed on independent days.)*

The emission spectra of the complexes under cell culture conditions were then recorded. The emission maximum of the complexes was 520.5nm for each complex, and the range was 484 to 557nm for 50:50 and 484 to 575nm for 100D and 100L (Figure 6-19)The slight difference in emission maximum intensity correlates well with the slight differences recorded in the aqueous QD samples originally in Figure 6-8.

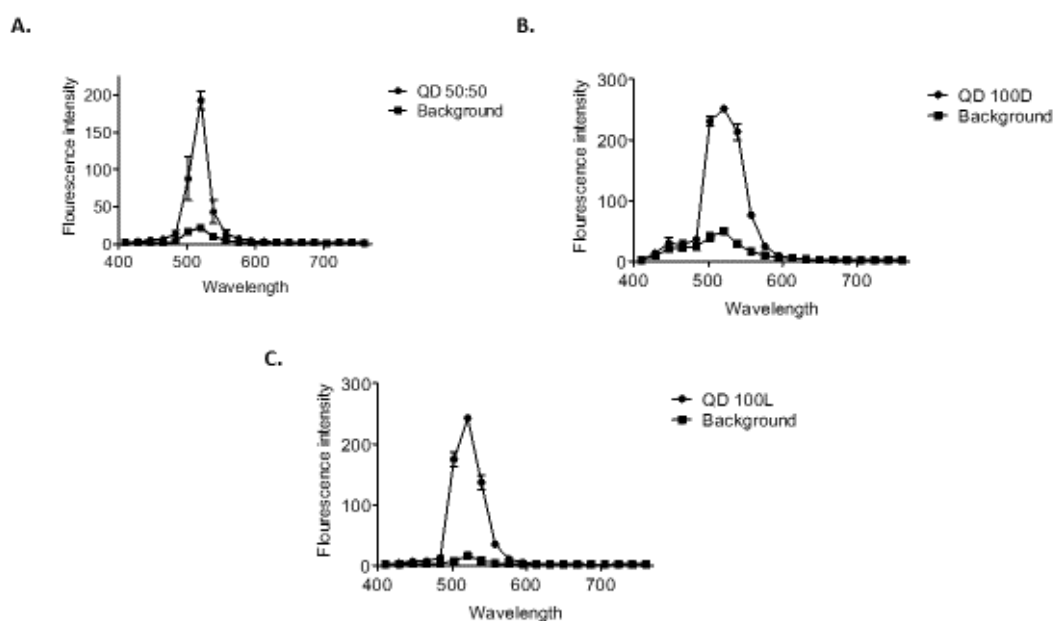


Figure 6-19 Emission spectra of the complexes under cell culture conditions (Cell medium, pH7.4, 5% CO<sub>2</sub>). HeLa cells were treated for 24h with 10 $\mu$ l of the indicated complexes and subjected to live confocal imaging, excitation 405nm, emission 410-760nm (Leica, 63X oil immersion lens). **A.** 50:50, **B.** 100D, **C.** 100L.

## 6.5 Conclusions

Therefore, several applications for our optically active QD nanomaterials have been demonstrated. Firstly, we investigated cation exchange reactions using both CdS QDs and CdSe nanoplatelets. We performed an aqueous cation exchange on our D- and L- pen stabilised CdS QDs in order to prepare optically active Cu<sub>2</sub>S QDs. This cation exchange reaction enabled us to successfully exchange the cadmium for copper and the resultant materials demonstrated significant optical activity. However, due to instability of the copper samples, we were unable to perform the subsequent exchange from copper for zinc, producing optically active ZnS QDs.

In an effort to prevent instability issues when performing a similar reaction with CdSe nanoplatelets, it was decided to alter our procedures. The cadmium-copper cation exchange took place in the organic phase this time and was successful as confirmed by UV-Vis spectroscopy. Ligand exchanges were then performed to

transfer the NPs to the aqueous phase and induce optical activity. Circular dichroism spectroscopy has confirmed that the subsequent Cu<sub>2-x</sub>Se materials are, again, optically active demonstrating large broad optical activity similar to the Cu<sub>2</sub>S QDs. These aqueous nanoplatelets suffered from similar instability issues however as degradation occurred quickly, preventing the subsequent zinc exchange from taking place.

Finally, we successfully conjugated thiolated lactose to bright CdZnSeS/ZnS alloyed core-shell quantum dots. Several samples were prepared with varying degrees of glycosylation and were characterised using TEM, UV-Vis and PL. These samples were then incubated with HeLa cells to investigate if there was a difference in toxicity or cellular uptake. All samples demonstrated similar dose dependent toxicity however cellular uptake appeared to vary with different levels of glycosylation. While no direct relationship could be established, the sample functionalised only with pure D-penicillamine and pure thiolactose exhibited the greatest uptake. The future detailed studies of the behaviour of different lactose functionalised chiral QDs in cell cultures will be necessary in order establish mechanisms of their uptake and understand how to control the biological performance of these QD based nanomaterials.

## 6.6 References

- (1) Soppimath, K. S.; Aminabhavi, T. M.; Kulkarni, A. R.; Rudzinski, W. E. *Journal of Controlled Release* **2001**, *70*, 1.
- (2) Slowing, II; Vivero-Escoto, J. L.; Wu, C. W.; Lin, V. S. Y. *Advanced Drug Delivery Reviews* **2008**, *60*, 1278.
- (3) Geng, Y.; Dalhaimer, P.; Cai, S. S.; Tsai, R.; Tewari, M.; Minko, T.; Discher, D. E. *Nature Nanotechnology* **2007**, *2*, 249.
- (4) Sun, C.; Lee, J. S. H.; Zhang, M. Q. *Advanced Drug Delivery Reviews* **2008**, *60*, 1252.
- (5) Liong, M.; Lu, J.; Kovochich, M.; Xia, T.; Ruehm, S. G.; Nel, A. E.; Tamanoi, F.; Zink, J. I. *ACS Nano* **2008**, *2*, 889.
- (6) Lai, C. Y.; Trewyn, B. G.; Jeftinija, D. M.; Jeftinija, K.; Xu, S.; Jeftinija, S.; Lin, V. S. Y. *Journal of the American Chemical Society* **2003**, *125*, 4451.
- (7) Brannon-Peppas, L.; Blanchette, J. O. *Advanced Drug Delivery Reviews* **2004**, *56*, 1649.

- (8) Wieder, M. E.; Hone, D. C.; Cook, M. J.; Handsley, M. M.; Gavrilovic, J.; Russell, D. *A. Photochemical & Photobiological Sciences* **2006**, *5*, 727.
- (9) Sheng, Y.; Nesbitt, H.; Callan, B.; Taylor, M. A.; Love, M.; McHale, A. P.; Callan, J. F. *Journal of Controlled Release* **2017**, *264*, 333.
- (10) Lin, X.; Yan, S.-Z.; Qi, S.-S.; Xu, Q.; Han, S.-S.; Guo, L.-Y.; Zhao, N.; Chen, S.-L.; Yu, S.-Q. *Frontiers in Molecular Neuroscience* **2017**, *10*.
- (11) Guo, D.; Xu, S.; Wang, N.; Jiang, H.; Huang, Y.; Jin, X.; Xue, B.; Zhang, C.; Zhu, X. *Biomaterials* **2017**, *144*, 188.
- (12) Cheng, Y.; Samia, A. C.; Meyers, J. D.; Panagopoulos, I.; Fei, B.; Burda, C. *Journal of the American Chemical Society* **2008**, *130*, 10643.
- (13) Chen, W.; Zhang, J. *Journal of Nanoscience and Nanotechnology* **2006**, *6*, 1159.
- (14) Sun, M.; Peng, D.; Hao, H.; Hu, J.; Wang, D.; Wang, K.; Liu, J.; Guo, X.; Wei, Y.; Gao, W. *Acs Applied Materials & Interfaces* **2017**, *9*, 10453.
- (15) Riley, R. S.; Day, E. S. *Wiley Interdisciplinary Reviews-Nanomedicine and Nanobiotechnology* **2017**, *9*.
- (16) Peng, H.; Tang, J.; Zheng, R.; Guo, G.; Dong, A.; Wang, Y.; Yang, W. *Advanced Healthcare Materials* **2017**, *6*.
- (17) Jang, Y.; Kim, S.; Lee, S.; Yoon, C.-M.; Lee, I.; Jang, J. *Chemistry-a European Journal* **2017**, *23*, 3719.
- (18) Gao, J.; Sanchez-Purra, M.; Huang, H.; Wang, S.; Chen, Y.; Yu, X.; Luo, Q.; Hamad-Schifferli, K.; Liu, S. *Science China-Chemistry* **2017**, *60*, 1219.
- (19) Cheng, Y.; Zhang, S.; Kang, N.; Huang, J.; Lv, X.; Wen, K.; Ye, S.; Chen, Z.; Zhou, X.; Ren, L. *Acs Applied Materials & Interfaces* **2017**, *9*, 19296.
- (20) Chen, Y.; Zhang, F.; Wang, Q.; Tong, R.; Lin, H.; Qu, F. *Dalton Transactions* **2017**, *46*, 14293.
- (21) Yezhelyev, M. V.; Gao, X.; Xing, Y.; Al-Hajj, A.; Nie, S. M.; O'Regan, R. M. *Lancet Oncology* **2006**, *7*, 657.
- (22) Lee, H. Y.; Li, Z.; Chen, K.; Hsu, A. R.; Xu, C. J.; Xie, J.; Sun, S. H.; Chen, X. Y. *Journal of Nuclear Medicine* **2008**, *49*, 1371.
- (23) Koo, Y. E. L.; Reddy, G. R.; Bhojani, M.; Schneider, R.; Philbert, M. A.; Rehemtulla, A.; Ross, B. D.; Kopelman, R. *Advanced Drug Delivery Reviews* **2006**, *58*, 1556.
- (24) Herr, J. K.; Smith, J. E.; Medley, C. D.; Shangguan, D. H.; Tan, W. H. *Analytical Chemistry* **2006**, *78*, 2918.
- (25) Benezra, M.; Penate-Medina, O.; Zanzonico, P. B.; Schaer, D.; Ow, H.; Burns, A.; DeStanchina, E.; Longo, V.; Herz, E.; Iyer, S.; Wolchok, J.; Larson, S. M.; Wiesner, U.; Bradbury, M. S. *Journal of Clinical Investigation* **2011**, *121*, 2768.
- (26) Bajaj, A.; Miranda, O. R.; Kim, I. B.; Phillips, R. L.; Jerry, D. J.; Bunz, U. H. F.; Rotello, V. M. *Proceedings of the National Academy of Sciences of the United States of America* **2009**, *106*, 10912.
- (27) Wu, X. Y.; Liu, H. J.; Liu, J. Q.; Haley, K. N.; Treadway, J. A.; Larson, J. P.; Ge, N. F.; Peale, F.; Bruchez, M. P. *Nature Biotechnology* **2003**, *21*, 41.
- (28) Smith, A. M.; Duan, H. W.; Mohs, A. M.; Nie, S. M. *Advanced Drug Delivery Reviews* **2008**, *60*, 1226.
- (29) Gao, X. H.; Cui, Y. Y.; Levenson, R. M.; Chung, L. W. K.; Nie, S. M. *Nature Biotechnology* **2004**, *22*, 969.
- (30) Cai, W. B.; Shin, D. W.; Chen, K.; Gheysens, O.; Cao, Q. Z.; Wang, S. X.; Gambhir, S. S.; Chen, X. Y. *Nano Letters* **2006**, *6*, 669.
- (31) Bagalkot, V.; Zhang, L.; Levy-Nissenbaum, E.; Jon, S.; Kantoff, P. W.; Langer, R.; Farokhzad, O. C. *Nano Letters* **2007**, *7*, 3065.
- (32) Mattheakis, L. C.; Dias, J. M.; Choi, Y. J.; Gong, J.; Bruchez, M. P.; Liu, J. Q.; Wang, E. *Analytical Biochemistry* **2004**, *327*, 200.

- (33) Han, M. Y.; Gao, X. H.; Su, J. Z.; Nie, S. *Nature Biotechnology* **2001**, *19*, 631.
- (34) Gorris, H. H.; Wolfbeis, O. S. *Angewandte Chemie-International Edition* **2013**, *52*, 3584.
- (35) Gao, X. H.; Nie, S. M. *Analytical Chemistry* **2004**, *76*, 2406.
- (36) Sukhanova, A.; Devy, M.; Venteo, L.; Kaplan, H.; Artemyev, M.; Oleinikov, V.; Klinov, D.; Pluot, M.; Cohen, J. H. M.; Nabiev, I. *Analytical Biochemistry* **2004**, *324*, 60.
- (37) Deerinck, T. J. *Toxicologic Pathology* **2008**, *36*, 112.
- (38) Alivisatos, A. P.; Gu, W. W.; Larabell, C. In *Annual Review of Biomedical Engineering* 2005; Vol. 7, p 55.
- (39) Lovric, J.; Bazzi, H. S.; Cuie, Y.; Fortin, G. R. A.; Winnik, F. M.; Maysinger, D. *Journal of Molecular Medicine-Jmm* **2005**, *83*, 377.
- (40) Fountaine, T. J.; Wincovitch, S. M.; Geho, D. H.; Garfield, S. H.; Pittaluga, S. *Modern Pathology* **2006**, *19*, 1181.
- (41) Abel, K. A.; Qiao, H. J.; Young, J. F.; van Veggel, F. *Journal of Physical Chemistry Letters* **2010**, *1*, 2334.
- (42) Neo, M. S.; Venkatram, N.; Li, G. S.; Chin, W. S.; Ji, W. *Journal of Physical Chemistry C* **2010**, *114*, 18037.
- (43) Park, J.; Kim, S. W. *Journal of Materials Chemistry* **2011**, *21*, 3745.
- (44) Smith, A. M.; Nie, S. M. *Journal of the American Chemical Society* **2011**, *133*, 24.
- (45) Zhong, X. H.; Feng, Y. Y.; Zhang, Y. L.; Gu, Z. Y.; Zou, L. *Nanotechnology* **2007**, *18*.
- (46) Luther, J. M.; Zheng, H.; Sadtler, B.; Alivisatos, A. P. *Journal of the American Chemical Society* **2009**, *131*, 16851.
- (47) Sadtler, B.; Demchenko, D. O.; Zheng, H.; Hughes, S. M.; Merkle, M. G.; Dahmen, U.; Wang, L.-W.; Alivisatos, A. P. *Journal of the American Chemical Society* **2009**, *131*, 5285.
- (48) Yu, J.; Zhang, J.; Jaroniec, M. *Green Chemistry* **2010**, *12*, 1611.
- (49) Zhao, H.; Chaker, M.; Wu, N.; Ma, D. *Journal of Materials Chemistry* **2011**, *21*, 8898.
- (50) Bouet, C.; Laufer, D.; Mahler, B.; Nadal, B.; Heuclin, H.; Pedetti, S.; Patriarche, G.; Dubertret, B. *Chemistry of Materials* **2014**, *26*, 3002.
- (51) Mu, L. J.; Wang, F. D.; Sadtler, B.; Loomis, R. A.; Buhro, W. E. *Acs Nano* **2015**, *9*, 7419.
- (52) Qi, P.; Chen, X. T.; Sun, Y.; Zhang, D. *Sens. Actuator B-Chem.* **2018**, *254*, 431.
- (53) Guo, Y.; Nehlmeier, I.; Poole, E.; Sakonsinsiri, C.; Hondow, N.; Brown, A.; Li, Q.; Li, S.; Whitworth, J.; Li, Z. J.; Yu, A. C.; Brydson, R.; Turnbull, W. B.; Pohlmann, S.; Zhou, D. J. *Journal of the American Chemical Society* **2017**, *139*, 11833.
- (54) Yang, Y.; Yu, M.; Yan, T. T.; Zhao, Z. H.; Sha, Y. L.; Li, Z. J. *Bioorganic & medicinal chemistry* **2010**, *18*, 5234.
- (55) Babu, P.; Sinha, S.; Surolia, A. *Bioconjugate Chem.* **2007**, *18*, 146.
- (56) Benito-Alifonso, D.; Tremel, S.; Hou, B.; Lockyear, H.; Mantell, J.; Fermin, D. J.; Verkade, P.; Berry, M.; Galan, M. C. *Angewandte Chemie-International Edition* **2014**, *53*, 810.
- (57) Yu, M.; Yang, Y.; Han, R. C.; Zheng, Q.; Wang, L. J.; Hong, Y. K.; Li, Z. J.; Sha, Y. L. *Langmuir* **2010**, *26*, 8534.
- (58) Coulon, J.; Thouvenin, I.; Aldeek, F.; Balan, L.; Schneider, R. *Journal of fluorescence* **2010**, *20*, 591.
- (59) Ithurria, S.; Dubertret, B. *Journal of the American Chemical Society* **2008**, *130*, 16504.
- (60) Mekis, I.; Talapin, D. V.; Kornowski, A.; Haase, M.; Weller, H. *J. Phys. Chem. B* **2003**, *107*, 7454.
- (61) Peng, X. G.; Manna, L.; Yang, W. D.; Wickham, J.; Scher, E.; Kadavanich, A.; Alivisatos, A. P. *Nature* **2000**, *404*, 59.
- (62) Qu, L. H.; Peng, Z. A.; Peng, X. G. *Nano Letters* **2001**, *1*, 333.

- (63) Rajh, T.; Micic, O. I.; Nozik, A. J. *Journal of Physical Chemistry* **1993**, *97*, 11999.
- (64) Trindade, T.; O'Brien, P.; Pickett, N. L. *Chemistry of Materials* **2001**, *13*, 3843.
- (65) Xie, R. G.; Kolb, U.; Li, J. X.; Basche, T.; Mews, A. *Journal of the American Chemical Society* **2005**, *127*, 7480.
- (66) Li, H.; Zanella, M.; Genovese, A.; Povia, M.; Falqui, A.; Giannini, C.; Manna, L. *Nano Letters* **2011**, *11*, 4964.
- (67) Zhu, Y. D.; Peng, J.; Jiang, L. P.; Zhu, J. J. *The Analyst* **2014**, *139*, 649.
- (68) Dorfs, D.; Härtling, T.; Miszta, K.; Bigall, N. C.; Kim, M. R.; Genovese, A.; Falqui, A.; Povia, M.; Manna, L. *Journal of the American Chemical Society* **2011**, *133*, 11175.
- (69) Balitskii, O. A.; Sytnyk, M.; Stangl, J.; Primetzhofer, D.; Groiss, H.; Heiss, W. *ACS Applied Materials & Interfaces* **2014**, *6*, 17770.
- (70) Lee, K.-H.; Lee, J.-H.; Kang, H.-D.; Park, B.; Kwon, Y.; Ko, H.; Lee, C.; Lee, J.; Yang, H. *ACS Nano* **2014**, *8*, 4893.

## Conclusions and future work

### 7.1 Conclusions

In this work a wide range of new optically active fluorescent nanomaterials have been synthesised and their properties have been investigated. These nanomaterials were prepared using various synthetic approaches including hot-injection and phase transfers, aqueous co-precipitation and heating up methods. These procedures enabled us to produce not only optically active spherical quantum dots produced, but also several new anisotropic materials, doped and undoped.

New optically active ZnS:Mn QDs were prepared using D/L cysteine and D/L penicillamine as a ligand. These materials were produced using an organic hot injection method followed by a variety of ligand exchange techniques. Cytotoxicity studies were performed on these QDs which resulted in a clear enantiotoxic effect with D-Cys stabilised ZnS:Mn presenting higher cytotoxicity than L-Cys stabilised ZnS:Mn. Optically active ZnSe QDs were also produced with the stabilising ligand glutathione, using an aqueous synthesis. These QDs subsequently demonstrated an enantioselective quenching response when treated with D- and L- penicillamine.

Optically active CdSe/CdS heterostructured quantum rods and tetrapods were synthesised using hot injection techniques followed by ligand exchanges using D- and L- penicillamine, D- and L- cysteine, and 1- $\beta$ -D-thioglucofucose. Chiral sensing experiments were performed using our DiRs and the chiral drug Naproxen. Enantioselective quenching of D/L cysteine stabilised CdSe/CdS DiRs was reported offering potential enantiospecific sensing applications.

A range of optically active cadmium containing dots and platelets were then prepared. Chiral CdS QDs were synthesised by hot-injection techniques followed by a ligand exchange with penicillamine. Size dependent circular dichroism responses were analysed for these QDs and a clear relationship between exciton absorption wavelength and the onset of optical activity was established. Alternatively, chiral

CdS QDs were synthesised in a 1-step aqueous reaction using D- and L- penicillamine and cysteine which demonstrated very large optical activity compared to other materials. Optically active CdSe and CdSe:Mn nanoplatelets were prepared using organic synthesis followed by ligand exchange reactions using D- and L- penicillamine as well as thioglucose. While these nanoplatelets were luminescent in the organic phase, none of the aqueous phase samples retained their luminescence despite showing optical activity.

Cation exchange reactions were carried out on both CdS QDs and CdSe nanoplatelets to replace the  $\text{Cd}^{2+}$  with  $\text{Cu}^{+1}$ , which was intended to be exchanged for  $\text{Zn}^{2+}$  subsequently. While optically active copper containing QDs and nanoplatelets were produced, further analysis was prevented due to ongoing stability issues.

Finally, our ligand exchange process was successfully implemented using thiolactose as a ligand on highly luminescent CdSe@ZnS/ZnS alloyed core-shell QDs. By varying the ratio of penicillamine to thiolactose on the surface of the QDs, the relationship between QD glycosylation and behaviour in biological media was investigated. Confocal microscopy was used to image the QDs in HeLa cells. All the samples presented similar levels of cytotoxicity but clear differences in cellular uptake were observed, however no specific relationship was verified.

In conclusion, this research has contributed to the development of the preparation and analysis of a wide variety of novel optically active fluorescent nanomaterials. It is expected that our studies will enable to further expand our knowledge and understanding of chiral fluorescent nanostructures and develop their potential applications in many areas ranging from photonics to biomedicine.

## 7.2 Future Work

Further research will include detailed studies of the photophysical properties of new Cd-free QDs (e.g. ZnS and ZnSe based) with different chiral stabilizers and the investigation of the electron transfer and energy transfer processes in these systems



in order to develop new chiroptical sensors for recognition of various enantiomeric molecules (e.g. chiral drugs). Also, antibacterial activity of the chiral nanomaterials will present a great interest and potential important applications but larger scale synthesis for chiral QDs must be developed in the near future to produce enough materials for proper antibacterial tests. Chiral anisotropic 2D quantum nanosystems (e.g. CdSe nanoplatelets deserve particular attention as this area is still unexplored. We expect that due to their unique structures, physicochemical and optical properties, 2D quantum nanostructures are very promising materials for sensing and imaging. In particular, 2D semiconducting nanomaterials can be tailored to form either fluorescent emitters or efficient fluorescence quenchers, making them powerful platforms for fabricating a series of optical biosensors to detect various targets including ions, biomolecules, nucleic acids, proteins and viruses.

In our work several potential uses of our optically active materials were explored, however there are 2 interesting directions of investigation which are necessary to continue for the near future development of applications of some of our chiral QD nanomaterials. These aspects of our future work are discussed below.

### 7.2.1 Enantioselective quenching of L- and D- cys stabilised ZnS:Mn by gold NPs

We have performed some preliminary studies into the use of gold nanoparticles as quenching agents with chiral ZnS:Mn.

Gold particles were synthesised according to procedure reported by Ock *et al*<sup>1</sup>. Briefly, the synthesis involved the reduction of a gold salt by sodium borohydride in the presence of a chiral stabiliser, in our case penicillamine. The gold nanoparticles have been characterised using UV-Vis spectroscopy, CD spectroscopy and TEM. They were then used for a series of sensing experiments involving the titration of a solution of gold nanoparticles with cysteine stabilised ZnS:Mn particles and monitoring the response by luminescence spectroscopy. UV-Vis spectra of the gold nanoparticles are presented in Figure 7-1 below.

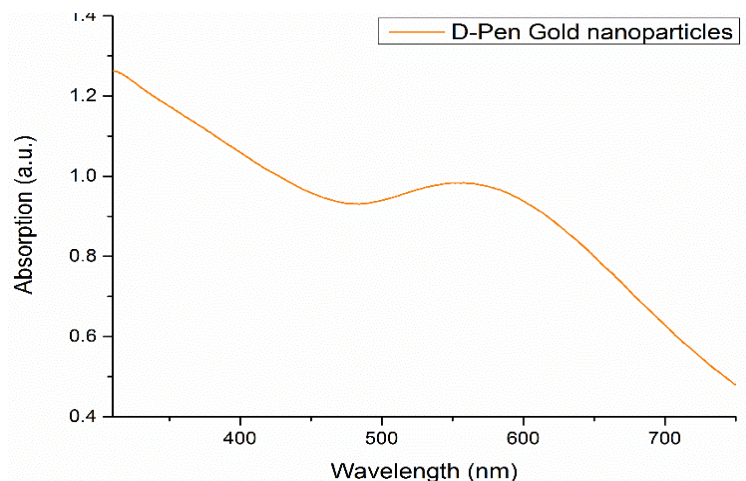


*Figure 7-1 UV-Vis spectrum for D-Pen stabilised gold nanoparticles.*

The UV-Vis presents a typical absorption spectrum for gold nanoparticles presenting a broad peak relating to the plasmonic nature of gold nanoparticles<sup>2</sup>. The large width of the peak would suggest that there is poor size control in this reaction.

Circular dichroism results (Figure 7-2) confirm that the gold nanoparticles are optically active however no activity in the plasmonic region of the gold absorbance was recorded.

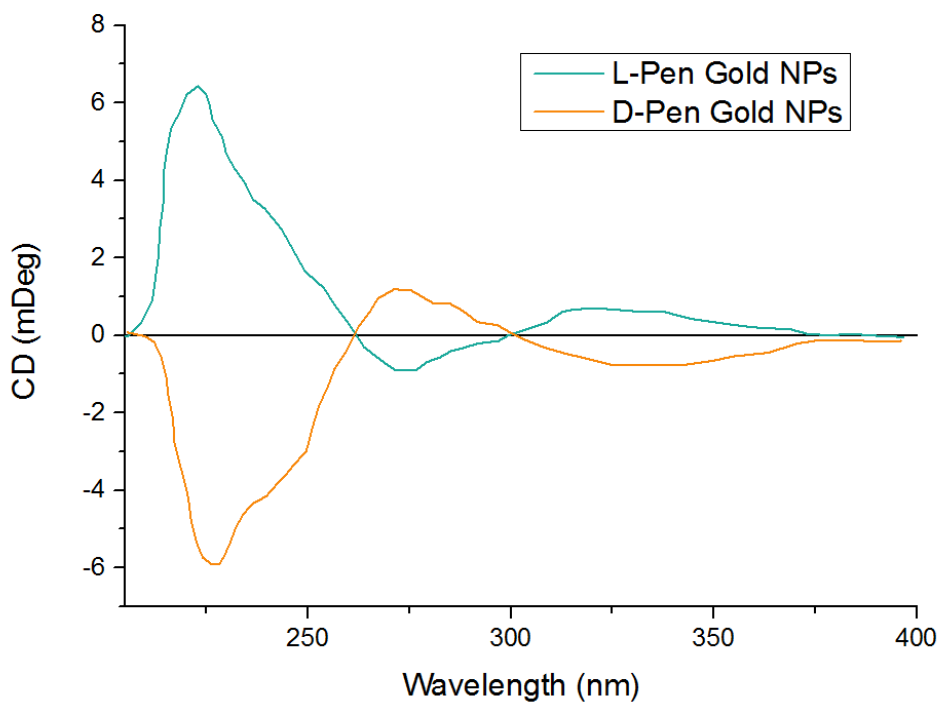


*Figure 7-2 CD spectra for D- and L- pen stabilised gold nanoparticles.*

TEM analysis (Figure 7-3) verifies that the gold nanoparticles are roughly spherical however a wide range of sizes exist. It may be noted that several very large 40nm + particles were present in the sample.

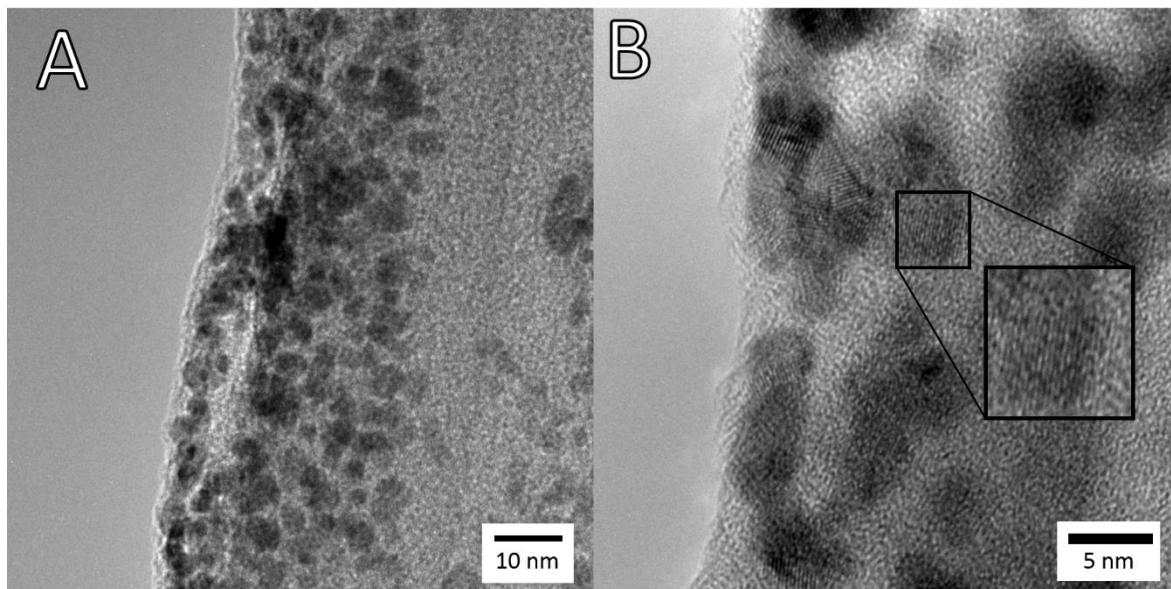


*Figure 7-3 TEM images of D-Pen stabilised QDs*

Upon successful synthesis of optically active Au nanoparticles, preliminary chiral recognition experiments were performed (Figure 7-4 Results of gold sensing using cysteineFigure 7-4). This involved titrating a solution of either D-pen or L-pen gold NPs against a solution of D-Cys stabilised ZnS:Mn QDs and monitoring the resultant quenching in luminescence of the QDs. The results below would suggest a difference in the quenching effects of D- and L- penicillamine stabilised gold NPs on the luminescence of D-Cys stabilised ZnS:Mn QDs.

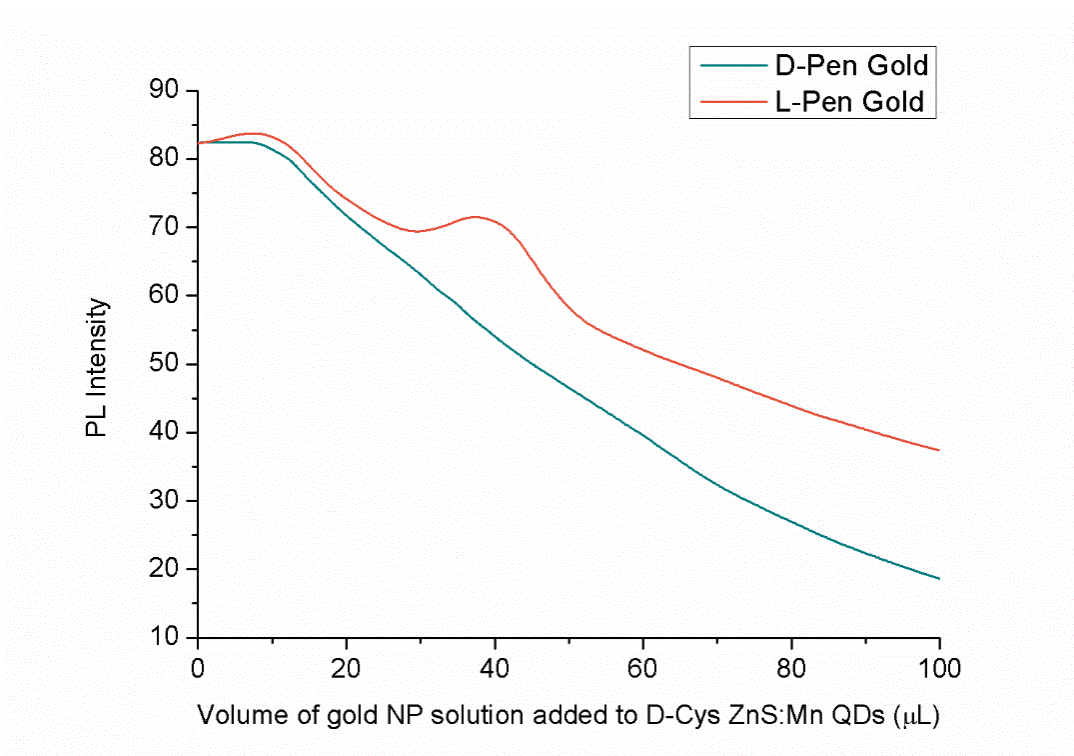


*Figure 7-4 Results of gold sensing using cysteine*

Some work has already been performed on the use of gold nanoparticles to quench QDs<sup>3-5</sup> however this work did not relate to enantioselective quenching. Therefore, we believe continuing this research is worthwhile, however much greater control of the gold NP synthesis is required for meaningful results to be attained.

### 7.2.2 Sensing of $\beta$ -Galactosidase

Following on from our research on thiocarbohydrate phase transfers processed, it will be important to investigate if either the PL or the CD responses of glycosylated QDs could be used for sensing applications. In collaboration with the Scanlan group, we attempted to do preliminary sensing of the presence of the enzyme  $\beta$ -galactosidase. B-galactosidase is responsible for the glycosylic cleavage of lactose into glucose and galactose. We prepared CdSe QDs capped with either lactose or glucose on the surface, and investigated if a difference in their spectroscopic properties existed. The small CdSe QDs mentioned in section 5.6 were used and the ligand exchange was carried out using the same method used for ZnS:Mn QDs in section 2.2.2. If a difference was confirmed, then it may be possible to combine the

lactose stabilised QDs with  $\beta$ -galactosidase and see if the optical properties change to that of the glucose stabilised QDs (Figure 7-5).

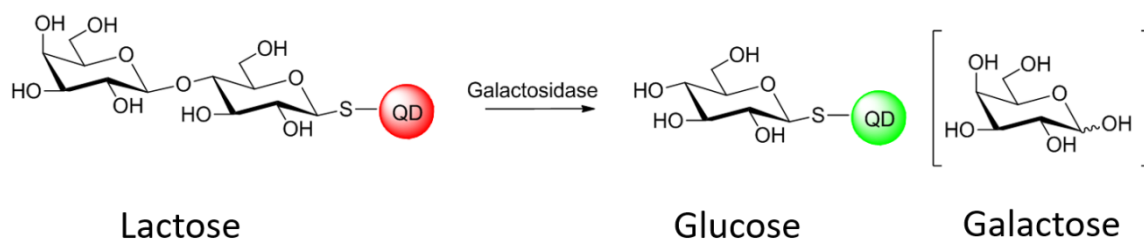


Figure 7-5 Schematic describing the sensing of  $\beta$ -galactosidase

The lactose capped and glucose capped CdSe particles were successfully synthesised and, interestingly, while no visible difference in PL was observed, a difference in the optical activity was observed (Figure 7-6).

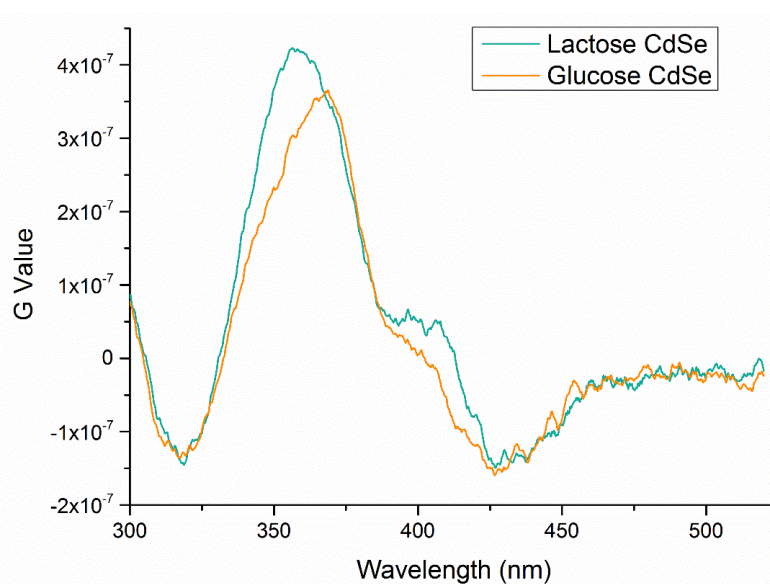


Figure 7-6 CD spectra for lactose and glucose stabilised CdSe QDs.

Due to time constraints, no more experiments were carried out however the existence of a difference would suggest that there is potential in further studies of these systems for sensing applications.

### 7.3 References

- (1) Ock, K.-S.; Dembereldorj, U.; Park, J.; Ganbold, E.-O.; Kim, S.; Shin, H.-C.; Joo, S.-W. *Spectrochimica Acta Part A: Molecular and Biomolecular Spectroscopy* **2013**, *102*, 419.
- (2) Kelly, K. L.; Coronado, E.; Zhao, L. L.; Schatz, G. C. *J. Phys. Chem. B* **2003**, *107*, 668.
- (3) Aldeek, F.; Ji, X.; Mattoussi, H. *The Journal of Physical Chemistry C* **2013**, *117*, 15429.

- (4) Liu, Y.; Loh, W. Q.; Ananthanarayanan, A.; Yang, C.; Chen, P.; Xu, C. *RSC Advances* **2014**, *4*, 35673.
- (5) Samanta, A.; Zhou, Y.; Zou, S.; Yan, H.; Liu, Y. *Nano Letters* **2014**, *14*, 5052.

## Appendix

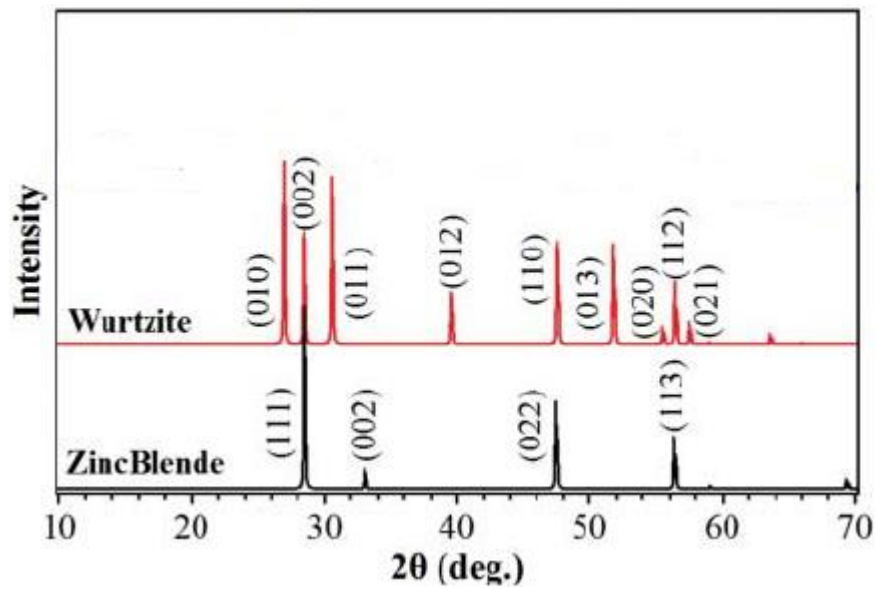


Figure 8-1 XRD patterns for both wurtzite and zinc blende ZnS (reproduced from reference<sup>1</sup>)

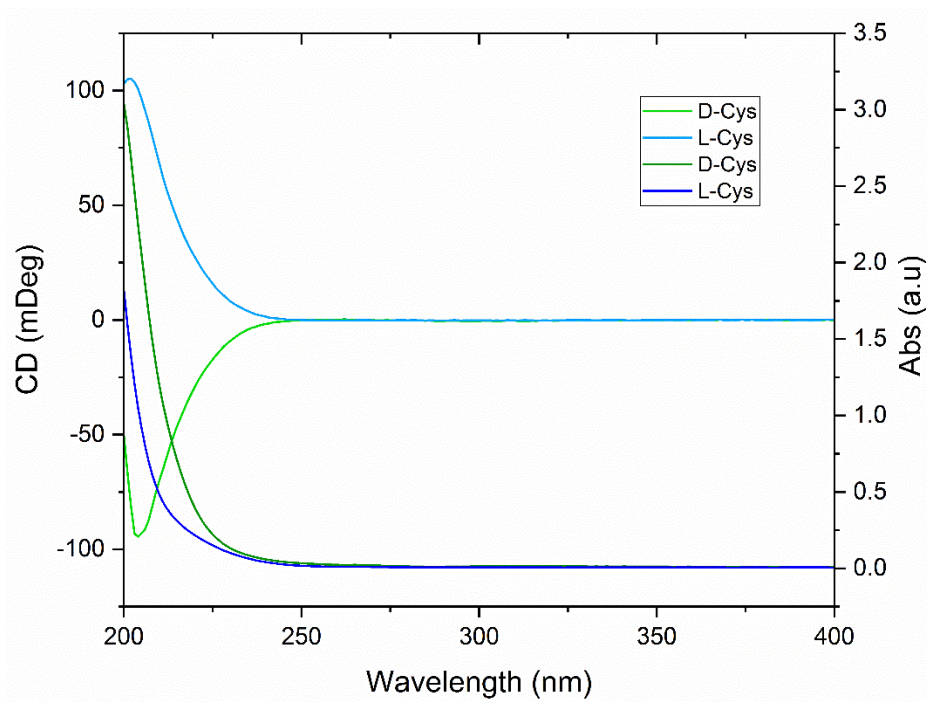


Figure 8-2 UV-Vis and CD spectra for D and L cysteine

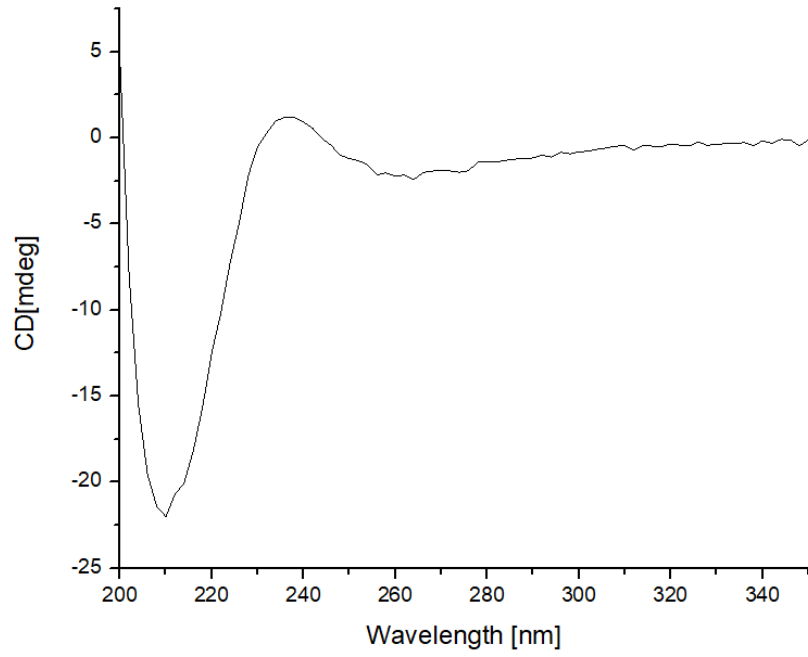


Figure 8-3 D-Pen in H<sub>2</sub>O after 48 hours at 50 °C

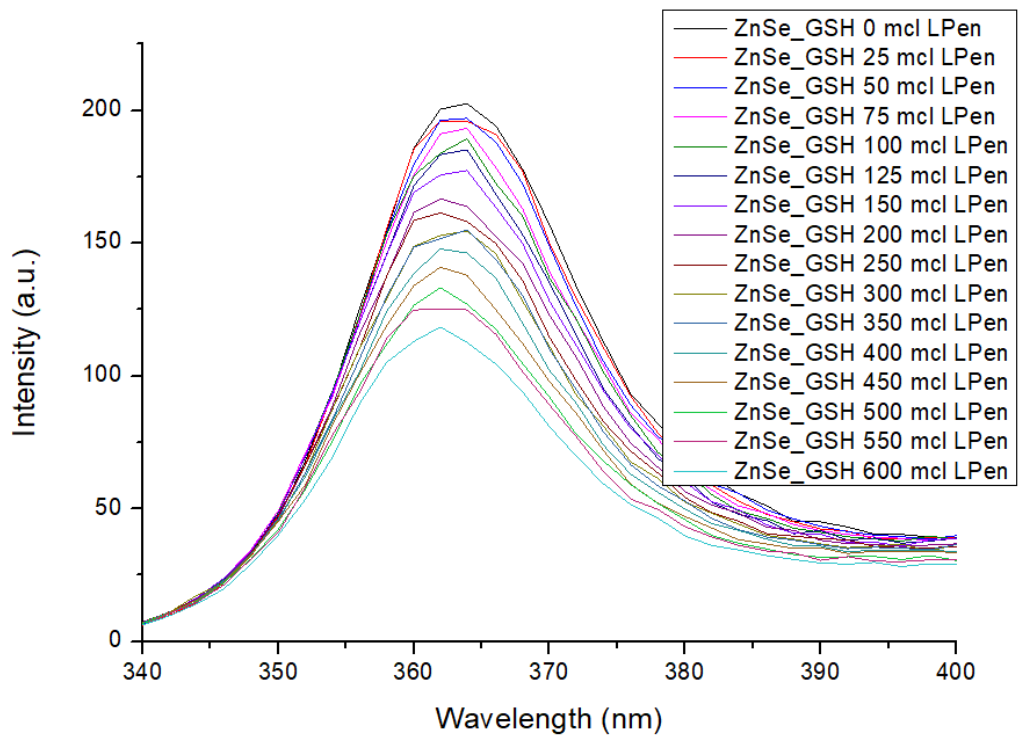


Figure 8-4 PL spectra for ZnSe quenching experiment with L-Pen



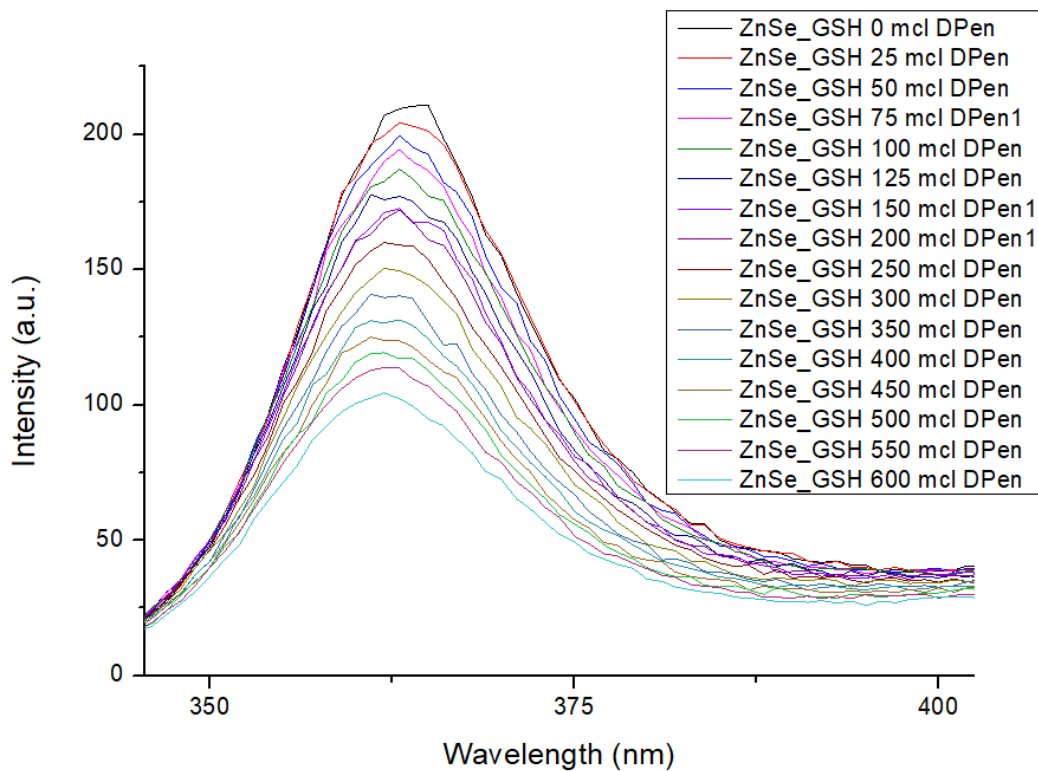


Figure 8-5 PL spectra for ZnSe quenching experiment with D-Pen

Absorbance at 350 nm	0.14
extinction co-efficient at 350 nm	2.00E+07
Path length in cm	1
concentration in moles per liter	7.00E-09
Concentration in moles per ml	7.00E-12
Rod length in nm	23.7
Rod diameter in nm	6.5
Rod radius	3.25
Rod volume in nm <sup>3</sup>	786.040125
Rod volume in cm <sup>3</sup>	7.86E-19
Rod density mg / cm <sup>3</sup>	4820
Mass of 1 rod in mg	3.78852E-15
Mass of 1 rod in g	3.78852E-18
1 mole of rods in g	2273112
Concentration in grams per ml	1.59E-05

Concentration in mg per ml	1.59E-02
Concentration in micrograms/ml	1.59E+01

Figure 8-6 Calculations for concentration of CdSe-CdS DiRs used for sensing

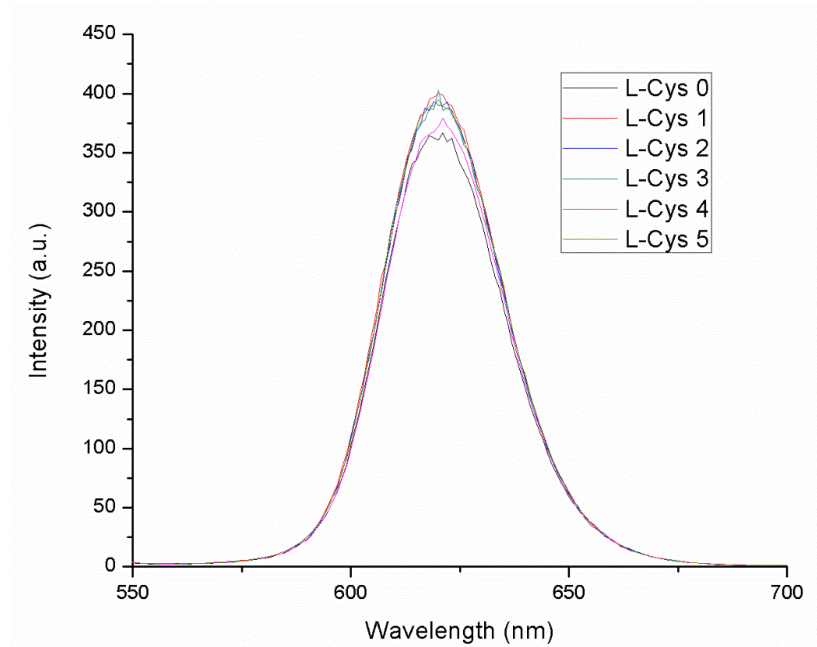


Figure 8-7 PL spectra for L-Cys CdSe-CdS DiRs vs. Naproxen

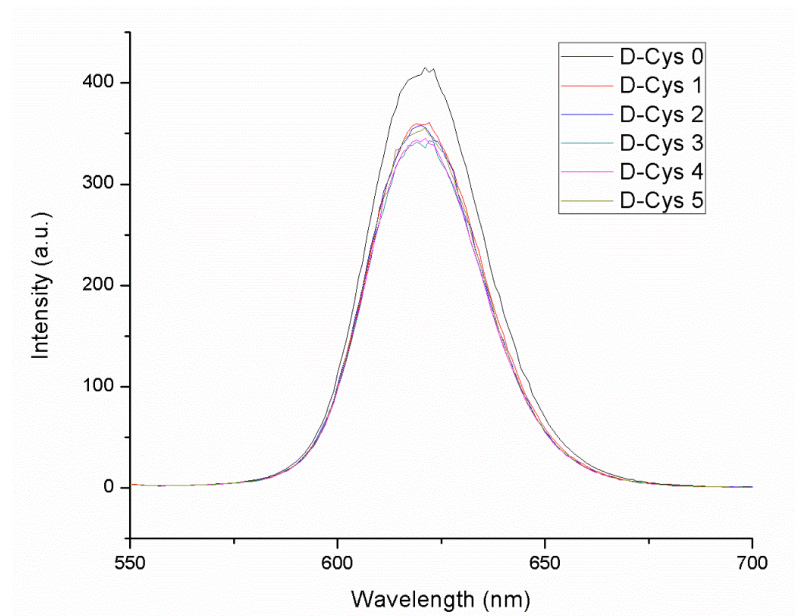


Figure 8-8 PL spectra for D-Cys CdSe-CdS DiRs vs. Naproxen

T-test

$$t = \frac{\mu_1 - \mu_2}{\sqrt{\frac{s_1^2}{n_1} + \frac{s_2^2}{n_2}}} = \frac{4.48 - 4.36}{\sqrt{\frac{0.86^2}{170} + \frac{0.47^2}{170}}} = 1.59$$

$t_c$  for 95% confidence is 1.64

$t_c$  for 90% confidence interval is 1.44

As  $t_{95} > t > t_{90}$  we can say with 90-95% confidence that there is a difference in the average size of the 2 samples.

*Figure 8-9 2 sample t-test to test for significant difference in QD means*

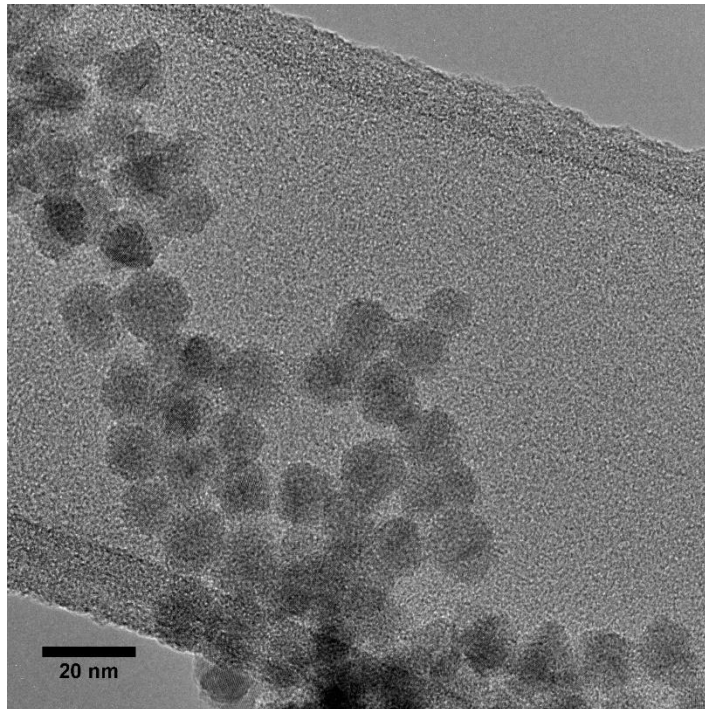


*Figure 8-10 TEM image of CdSe@ZnS/ZnS QDs in the organic phase*

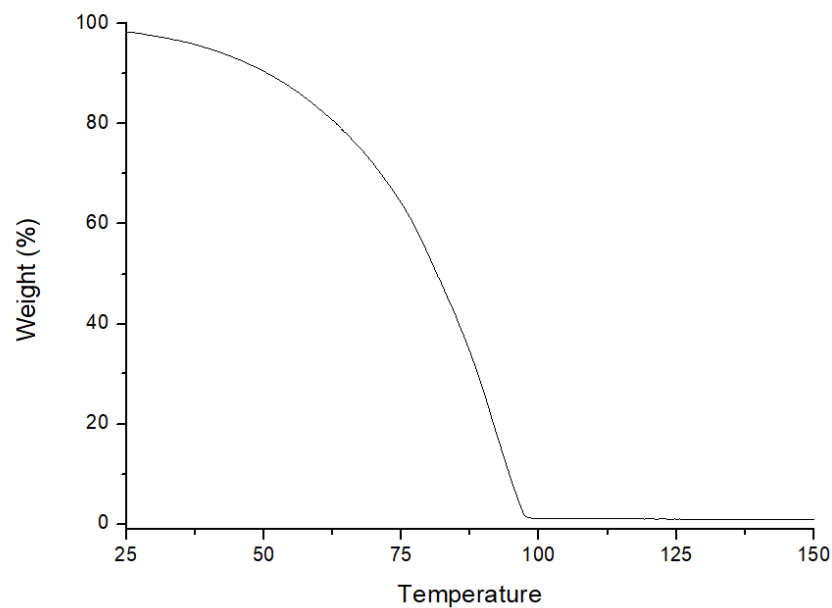


*Figure 8-11 TGA for CdSe@ZnS/ZnS*

1% by weight of the solution was left after water was evaporated. We assume that the whole remaining weight is QDs as the mass of ligands in this case is negligible compared to the large QDs. We also assume that the density of the QDs is the same as ZnS, as the majority of this material is ZnS.

## References

1. Zhao, Haofei & Liu, Wei & Zhu, Jie & Shen, Xi & Xiong, Lun & Li, Yanchun & Li, Xiaodong & Liu, Jing & Wang, Rongming & Jin, Changqing & Yu, R. C.. (2015). Structural transition behavior of ZnS nanotetrapods under high pressure. *High Pressure Research*. 35. 9-15. 10.1080/08957959.2014.996562.